3D-PRINTED STRUCTURED MEMBRANES FOR BIOMEDICAL AND TISSUE ENGINEERING APPLICATIONS

Lobat Tayebi

St Hugh's College, University of Oxford



A thesis submitted for the degree of Doctor of Philosophy

at the University of Oxford.

Michaelmas 2019

To My Parents, Shahnaz and Mohammad,

&

My Husband, Daryoosh

3D-PRINTED STRUCTURED MEMBRANES FOR BIOMEDICAL AND TISSUE ENGINEERING APPLICATIONS

Lobat Tayebi

St Hugh's College, University of Oxford

Thesis Abstract Submitted for the Degree of Doctor of Philosophy

Trinity 2019

Although biological/biomedical membranes may look like two-dimensional (2D) assemblies, depending on their functions, they may have detailed and complex configurations in their 3rd dimension. In such cases, three-dimensional (3D)-printing—as a process of layer-by-layer deposition of materials—can provide an effective and unique methodology for manufacturing of such membranes.

In this regard, 3D-printing of biocompatible hydrogels needed for fabrication of cell-free soft membranes with proper surgical handling is challenging, due to the rheological characteristics of hydrogels. This dissertation introduces and examines a newly developed generic hydrogel ink that can address such difficulties due to its several properties, including:

1) The ink is compatible with most biomedical applications in terms of the biomaterial composition and provides the appropriate cell attachment for different cell types.

2) It is easily printable without rheological complexities.

3) It is relatively inexpensive, making it appropriate for clinical use by different patients.

Using our developed printing protocol, we employed this ink for 3D-printing of structured soft thin and thick membranes for different biomedical purposes. More specifically, three applications were examined. The first application involves a structured 3D-printed membrane

with the design criteria suitable for guided tissue regeneration (GTR). Its bio-stability, mechanical strength, surgical handling and *in vitro* biocompatibility were fully characterized and successfully evaluated for GTR application.

Reconstruction of ocular surface/conjunctival defects, using the 3D-printed membrane produced by the generic ink, is the second application that was examined. Both *in vitro* and *in vivo* (rabbit model) studies were performed to evaluate the function of the 3D-printed membrane in comparison to the amniotic membrane, which is a conventional membrane used in reconstruction of ocular surface/conjunctival defects. The use of the 3D-printed membrane indicates some advantages, including predictable degradation pattern, higher goblet cell density on the healed epithelium, reduced scar tissue formation and less inflammation.

Cartilage regeneration is the third application considered for the membranes printed by this ink. For this purpose, a new knee plug was developed, and a 3D-printed membrane was fabricated with the specific design criteria for assembling in the plug. The physical analyses and the *in vitro* examinations confirm the suitability of the fabricated membrane for cartilage regeneration.

Finally, the limitations and capabilities of the produced ink for future works are discussed at the end of the thesis.

Table of Contents

Acknowledgment XI
List of Figures XII
List of Tables XIX
Table of Abbreviations XX
Chapter 1. INTRODUCTION 1
1.1. Background and Motivation 1
1.2. Aims and Objectives 4
1.3. Structure of the Thesis 5
Chapter 2. LITERATURE REVIEW 9
2.1. 3D-Printing 9
2.1.1. Direct 3D-printing/inkjet 9
2.1.2. Fused deposition modeling (FDM) 14
2.1.3. Selective laser sintering (SLS) 15
2.1.4. Stereolithography (SLA) 16
2.1.5. 3D-plotting 17
2.2. Printable Materials and 3D-Printing of Membranes 19
2.2.1. Ceramics 21
2.2.2. Synthetic polymers 23
2.2.3. Hydrogels 29
2.3. Guided Tissue Regeneration (GTR) 41
2.3.1. Non-resorbable membrane 42
2.3.2. Natural bioresorbable membrane 43
2.3.3. Synthetic bioresorbable membranes 45
2.4. Ocular Surface/Conjunctival Defect Reconstruction 47
2.4.1. Ocular surface injuries 47
2.4.2. Autologous implantation 48
2.4.3. Allograft implantation, amniotic membrane (AM) 48
2.4.5. Bioengineered grafts 49

Chapter 3. 3D-PRINTED MEMBRANE AND ITS APPLICATION FOR GUIDED TISSUE REGENERATION 58
3.0. Introduction 58
Chapter 3A. 3D-Printed Thick Structured Gelatin Membrane for Engineering of Heterogeneous Tissues 60
3A.1. Abstract 60
3A.2. Introduction 60
3A.3. Materials and methods 61
3A.4. Results and discussion 63
3A.5. Conclusion 68
Chapter 3B. 3D-Printed Membrane for Guided Tissue Regeneration 70
3B.1. Abstract 70
3B.2. Introduction 71
3B.3. Materials and methods 75
3B.3.1. Materials 75
3B.3.2. Optimizing the formulation of the bio-ink and membrane printing 75
3B.3.3. Morphology, surface roughness and thickness of the membranes 77
3B.3.4. Static and dynamic mechanical properties 77
3B.3.5. Degradation 77
3B.3.6. Tissue collection 78
3B.3.7. Cell isolation and culture 78
3B.3.8. Membrane cell seeding 78
3B.3.9. Cell vitality 79
3B.3.10. DAPI nuclei staining 79
3B.4. Results and discussion 79
3B.4.1. Ink optimization 79
3B.4.2. Morphology, surface roughness and thickness of the membranes 85
3B.4.3. Static and dynamic mechanical properties 90
3B.4.4. Degradation 92
3B.4.5. Biological evaluation in vitro 94
3B.5. Conclusion 97
Summary of Chapter 3 99

Chapter 4. 3D-PRINTED MEMBRANE AND ITS APPLICATION IN OCULAR SURFACE/CONJUNCTIVAL RECONSTRUCTION 100
4.0. Introduction 100
Chapter 4A. 3D-Printed Membrane as an Alternative to Amniotic Membrane for Ocular Surface/Conjunctival Defect Reconstruction: An In Vitro & In Vivo Study 102
4A.1. Abstract 102
4A.2. Introduction 103
4A.3. Experimental Procedure 106
4A.3.1. Ink formulation 106
4A.3.2. 3D-printing of membranes 107
4A.3.3. Morphology, line and surface roughness 108
4A.3.4. Human AM preparation and preservation 108
4A.3.5. In-vitro cell viability and attachment evaluation 108
4A.3.5.1. Human limbal epithelial cell isolation and culture 108
4A.3.5.2. Cell attachment and proliferation assays 109
4A.3.6. Mechanical properties, suturability and assessment of surgical handling of the membranes 110
4A.3.7. Conjunctival defect induction and AM/gelatin-based membrane implantation in rabbit models 110
4A.3.8. Clinical observations 111
4A.3.9. Histological staining 112
4A.3.9.1. H&E staining 113
4A.3.9.2. Periodic Acid Schiff (PAS) staining 113
4A.3.9.3. Masson's Trichrome (MT) staining 113
4A.3.9.4. Immunohistochemical staining for alpha-Smooth Muscle Actin (α-SMA) 113
4A.3.10. Statistical analysis 113
4A.4. Results 114
4A.4.1. Ink formulation and 3D-printing of the membranes 114
4A.4.2. Morphology, line and surface roughness 121
4A.4.3. In-vitro cell attachment and proliferation assays 122
4A.4.4. Mechanical properties, suturability and assessment of surgical handling of the membranes 123
4A.4.5. In-vivo conjunctival tissue reconstruction and clinical outcomes 124

4A.4.5.1. Day 12 after surgery (2nd week) 124
4A.4.5.2. Day 19 after surgery (3rd week) 125
4A.4.5.3. Day 28 (4th week) 126
4A.4.6. Histological assessment of repaired conjunctival tissue 131
4A.4.6.1. H&E staining 131
4A.4.6.2. PAS staining 133
4A.4.6.3. Masson trichrome staining 134
4A.4.6.4. Immunohistochemical staining for α-SMA 134
4A.5. Discussion 136
4A.6. Conclusions 142
Summary of Chapter 4 144
Chapter 5. 3D-PRINTED MEMBRANE AND ITS APPLICATION IN CARTILAGE REGENRATION 145
5.0. Introduction 145
Chapter 5A. Design of a New 3D-Printed Joint Plug 146
5A.1. Abstract 146
5A.2. Introduction 146
5A.3. Materials and methods 149
5A.4. Result and discussion 150
5A.4.1. Part 1: Bone portion 151
5A.4.2. Part 2: Cartilage portion 152
5A.4.3. Engagement means between the bone and cartilage portions 152
5A.4.4. Part 3: Film 153
5A.4.5. Engagement means between film and cartilage portion 153
5A.4.5. Gradient configuration 155
5A.4.6. Optional part: Barrier 157
5A.5. Conclusion 158
Competing interests The authors declare no competing interests 159
Chapter 5B. A Tri-Component Knee Plug for the 3rd Generation of Autologous Chondrocyte Implantation 161
5B.1. Abstract 161
5B.2. Introduction 161
5B.3. Materials and methods 164

5B.3.1. Design 164
5B.3.2. Materials 166
5B.3.3. 3D Printing of the Bone and Cartilage Portions 166
5B.3.4. Fabrication and surface treatment of the Film 168
5B.3.5. Characterization and biological evaluation of the Bone Portion 168
5B.3.5.1. Mechanical properties 168
5B.3.5.2. Osteoblast attachment and proliferation 168
5B.3.6. Characterization and biological evaluation of the Cartilage Portion 169
5B.3.6.1. Degradation 169
5B.3.6.2. Chondrocyte attachment and proliferation 169
5B.3.7. Characterization of the Film 170
5B.3.7.1. Scanning Electron Microscopy (SEM) 170
5B.3.7.2. Mechanical properties and suture retention strength 171
5B.3.7.3. Wettability and permeability 171
5B.4. Results and discussion 172
5B.5. Conclusion 182
Summary of Chapter 5 185
Chapter 6. DISCUSSION AND CONCLUSION 186
6.1. Summary of Key Findings 186
6.2. Limitations and Future Works 187
6.2.1. Modifying and enabling the ink for cell-laden printing 187
6.2.2. Loading membranes with drugs/growth factors 189
6.2.3. Improving the mechanical properties and exploring other applications 190
6.2.4. In vivo examinations 191
Appendices 193
Supplementary Information 1 (SI1): Composition of Initial Solutions (Appendix of Chapter 3B) 193
Supplementary Information 2 (SI2): Detailed Analyses of the 3D Printed Gelatin/Elastin/Sodium-Hyaluronate Membrane (Appendix of Chapter 4A) 194
SI2.1. Background 194
SI2.2. Gelation temperature of various formulations 197
SI2.3. Cross-linking and mechanical properties of the membranes 199
SI2.4. Degradation rate of the gelatin-based membranes 201

SI2.5. In-vitro cell culture 202
SI2.6. Grading criteria for clinical inflammation 202
SI2.7. Discussion 203
Supplementary Information 3 (SI3): Optimizing the Paste to Print the Bone Portion (Appendix of Chapter 5B) 207
SI3.1. Purpose 207
SI3.2. Materials and method 207
SI3.2.1. Preparation of the Pastes 207
SI3.2.2. Rheological analysis 207
SI3.2.3. 3D-Printing and sintering 208
SI3.2.4. Mechanical testing and degradation analysis 208
SI3.3. Results and discussion 208
SI3.4. Conclusion 213
Bibliography 214

ACKNOWLEDGMENT

I would like to thank my supervisors Professors Hua Ye and Zhanfeng Cui for their continuous support, help, encouragement, and tolerance throughout this DPhil. I truly enjoyed being their student.

I would also like to thank the late Professor James Richardson from The Robert Jones & Agnes Hunt Orthopaedic Hospital (RJAH) for his valuable contribution in designing the knee plug (Chapter 5). It was extremely sad losing him. We had very happy and fruitful memories of working with him during this DPhil study.

Thanks should also go to all of our group members at Institute of Biomedical Engineering (IBME) at University of Oxford.

This DPhil has been funded by China Regenerative Medicine International Limited (CRMI).

LIST OF FIGURES

Figure 1.1: Some beneficial biomedical applications of membranes are presented in this figure. Among those, 3D-printing has already been thoroughly researched for skin reconstruction and would dressing by other investigators. This dissertation aims to study the use of cell-free 3D-printed membranes for GTR (Chapter 3), reconstruction of ocular surface/conjunctival defects (Chapter 4) and cartilage regeneration (Chapter 5), by employing a generic ink developed in this thesis. 2
Figure 2.1: Schematics of A) Direct 3D-Printing/Powder-Binder inkje), B) Fused Deposition Modeling (FDM), C) Selective Laser Sintering (SLS), D) Stereolithography (SLA) and E) 3D-Plotting. The schematics are obtained from reference [41] with permission. 13
Figure 2.2: Example of a 3D-printed ceramic construct. (a-b) The image of the 3D-printed scaffold made with 50 wt% HA. (c) A pore channel, (d) Strut of the 3D-printed scaffold, (e–f) Surface of the scaffold. This figure is obtained from reference [116] with permission..... 23
Figure 2.3: Examples of PLA-based 3D-printed constructs. Scanning electron microscopy (SEM) of 3D-printed scaffolds of (a) PLA/PEG - top view, (b) PLA/PEG/G5 - top view, (c) PLA/PEG - cross-sectional view, (d) PLA/PEG/G5 - cross-sectional view. This figure is obtained from reference [92] with permission. 24
Figure 2.4: 3D-printed complex structures are possible to be made by PCL. PEG was used as the sacrificial material. Panels (a-c) present an overhanging assembly with the sized of 2x1x0.6 cm; (a) CAD design, (b) 3D-printed construct with PCL and PEG, (c) Final structure of the overhanging shape. Panels (d-f) demonstrate a hollowed hemisphere shape with the diameter of 1 cm; (d) CAD design, (e) 3D-printed constructs before removing PEG, (f) Final structure after removing PEG. Panels (g-i) illustrate a framework of an ear, (g) 3D-printed structure with PCL and PEG, (h) The ear-shaped framework after removing the PEG, (i) A demonstration of the flexibility of the construct. Images are obtained from various figures in reference [93] with permission. 26
Figure 2.5: 3D-printed PLGA construct: Structure of the 3D-printed scaffold (left) and an individual filament (right) using SEM imaging. The figure is obtained from reference [146] with permission 27
Figure 2.6: 3D-printed membrane made by alginate–BFP1 (right) and the 3D-printing machine used for its fabrication (left). This figure is obtained from reference [98] with permission..... 32
Figure 2.7: A 3D-printed gelatin membrane with five layers and homogamous distribution of pore. Insert presents the same membrane with higher magnification. The membrane is cross-linked by EDC/NHS. Scale bar is 250 mm. This figure is obtained from reference [194] which is licensed under a Creative Commons Attribution 4.0 International License, and no permission is required. 33
Figure 2.8: Gelatin 3D-printed membrane/construct in various repetitive geometries. (A) Interior pattern of the 3D-printed models. (B) The photo of the 3D-printed gelatin structure with the nozzle diameter of 0.2 mm, scale bars = 1 mm. (C) Cross-linked structure of the 3D-printed gelatin (diameter is 6 mm). The figure is obtained from reference [99] with permission. 34

Figure 2.9: A 3-layered 3D-printed membrane made of 5% PGC hydrogels. Scale bars are 5 mm. This figure is obtained from reference [204], which is licensed under a Creative Commons Attribution 4.0 International License, and no permission is needed. 36
Figure 2.10: This schematic presents the carboxyl-to-amine cross-linking reaction of EDC and Sulfo-NHS (water-soluble analog of NHS). Inclusion of NHS leads to formation of amine-reactive intermediate, which is dry-stable and, therefore, can enhance the final efficacy. 41
Figure 2.11: (a) 3D-printed PCL/PLGA/β-TCP GBR membrane (2) A display of the membrane flexibility. The figure is obtained from reference [322] with permission. 46
Figure 2.12: Attachment of corneal epithelial cells in the scaffolds made by (a) unmodified PLGA, (b) PLGA/collagen, (c) PLGA /collagen/ hyaluronic acid, (d) PLGA/collagen/AM, (e) PLGA/collagen/AM/ hyaluronic acid, after one day culture of corneal epithelial cells. They are SEM images with 200 times magnification. The arrows pointed out the examples of the attached cells. The PLGA/collagen/ hyaluronic acid scaffold was ultimately selected for the in vivo study of conjunctival reconstruction in rabbits' eyes. The figure is obtained from reference [372] with permission. 51
Figure 2.13: Procedure for making the collagen-based conjunctival equivalent for ocular surface reconstruction. (A) Isolating and harvesting of rabbit conjunctival epithelial cells (rCjECs). (B) Cultivation of rCjECs on collagen vitrigel, considering particular goblet cell phenotype. (C) The conjunctival equivalent to reconstruct the conjunctival defect. (D, E) Transmission electron microscopy (TEM) images of fibrillar density and assembly of normal collagen gel and optimal collagen vitrigel, respectively. The arrow indicates the bending of collagen fibril. Scale bar is 500 nm. The figure is obtained from reference [373] with permission. 52
Figure 2.14: Biphasic osteochondral scaffolds made of fibrin/PCL (left) and PCL/PCL-TCP (right). The figure is obtained from reference [412] with permission. 55
Figure 2.15: (A) A biphasic osteochondral scaffold made of agarose gel and decellularized bone for the cartilage and bone parts, respectively. The figure is obtained from reference [414]with permission. (B) A multiphasic osteochondral scaffold made of collagen type I/glycosaminoglycan/calcium phosphate (CGCaP) for the bone part and collagen type II/glycosaminoglycan (CG) for the cartilage part (Micro-CT image). The scale bar is 1 mm. The figure is obtained from reference [417] with permission. 56
Figure 3A.1: 3D-printer set up (A). Macroscopic images of fabricated 3D-printed scaffold immediately after printing (B), and after crosslinking (C, D). As can be seen in the images, the scaffolds are bendable with easy-handling properties. 62
Figure 3A.2: Rheological and flow characterization of Gelatin 15% (w/v) aqueous solution as the ink for printing; sol-gel transition detection through oscillatory sweep measurements (A); shear stress and shear viscosity as a function of shear rate (B, C); complex viscosity as a function of angular frequency (D); flow rate as a function of applied pressure (E); complex viscosity change over time when cooling the solution from 37℃ (F), 35℃ (G), 33℃ (H) or 31℃ (I) to 22℃ with maximum cooling rate; and the required time for the complex viscosity of the ink to reach 10 Pa.s as a function of surface to volume ratio (J). 66
Figure 3A.3 : Examples of the first and last layers of the gradient membrane are shown in panel (A) and (B). The smaller pore size can be easily achieved by altering the angels of strands in the printing process (C). Panel (D) shows an SEM image of the printed membrane. 68
Figure 3B.1: Loss tangent vs. temperature plotted in different frequencies for (A) gelatin 15%, (B) gelatin 15% elastin 2% sodium hyaluronate 0.5%, and (C) gelatin 8% elastin 2% sodium hyaluronate 0.5% 83

Figure 3B.2: Viscosity vs. shear rate plotted in different temperatures for (A) gelatin 15%, (B) gelatin 15% elastin 2% sodium hyaluronate 0.5%, and (C) gelatin 8% elastin 2% sodium hyaluronate 0.5%..... 85
Figure 3B.3: (A-C): Schematic of our design. Each membrane is composed of 6 layers. The strand angels from the first layer to the last layer are: 45, 135, 0, 90, 0, 90°. Distances between strands (from the middle of one strand to the middle of the adjacent one) are set to 0.6 mm for the layers 1-4 and 0.9 mm for layers 5-6. (D-E): The macroscopic view of the 3D-printed gradient membranes of gelatin/elastin/sodium hyaluronate. The membranes are completely flexible and bendable. The surgical handling of the membrane is easy. The thickness is approximately 150 µm. 87
Figure 3B.4: Confocal laser scanning (label-free) of the scaffolds from both sides of the sample composing of gelatin 8%, elastin 2% and sodium hyaluronate 0.5%. (A1, B1): imaging of the small-pore-side and large-pore-side in a completely swelled state. (A2, B2) the height profile and surface morphology of the images in panel A1 and B1. The Red area. Small-pore-side has smoother surface than the large-pore-side. The color coding indicates the height in µm. (C). Both sides of the membrane can be visualized under the 3D Lase Measuring Microscope after drying the sample by 30 minutes keeping a fully swelled membrane under room conditions (C). 89
Figure 3B.5: (A) The lable-free 3D confocal laser imaging of the membranes to confirm the thickness of the membranes measured by the Electronic Digital Micrometer. (B) The height profile of the edge of the membrane. (C) The line height scan of the blue line in panel A. The edge of the membrane is a bit higher than the actual surface as the printer was set to do the contouring after each layer of printing. 90
Figure 3B.6: Static mechanical testing revealed elastic modulus of 1.95 ± 0.55 Mpa (black); dynamic storage modulus vs. frequency for printed membranes (red). The measured dynamic storage modulus was 314 ± 50 kPa and had not been significantly altered by increasing the frequency (Although the values presented in the text were obtained out of four measurements from four different samples (n=4), the figure only illustrates the result of the experiment from one sample.)..... 91
Figure 3B.7: Degradation rate of the membranes crosslinked using EDC/NHS for 0.5 h (A), 1.5 h (B) and 2 h (C). The membranes were soaked in PBS at 37℃ for this experiment. Four different samples in each condition were examined (n=4)..... 93
Figure 3B.8: Histological sections of paraffin wax-embedded constructs cultured at submerged condition for 4 days followed by air-liquid interface culture for 12 days. (A) acellular 3D-printed membrane; (B) the epithelial side of the 3D-printed scaffold with cultured NOK forming multilayers at the surface of the membrane without invading deeper into the membrane and (C) the connective tissue side of the scaffold with cultured NOF showing abundance of fibroblast cells nicely separated from the epithelial layer by the GTR membrane. Hematoxylin and Eosin staining, original magnification ×100. Vertical lines are due to folding of the sections..... 94
Figure 3B.9: Viability of the membranes seeded with oral fibroblasts and keratinocytes at different culture intervals as assessed by the prestoblue PB assay (assay has been performed after seeding of both cell types i.e. 2 days, 10 days and 20 days). Four different samples in each condition were examined (n=4) and GraphPad Prism 7 was employed to conduct the statistic. The P-value< 0.05 is considered statistically significant difference using the one-way ANOVA test. 96
Figure 3B.10: DAPI-stained image of the frozen sectioned construct cultured at submerged condition for 4 days followed by air-liquid interface culture for an additional 12 days showing

the nuclei of the cells cultured on the 3D-printed membrane forming multilayers at the surface and absence of any cell nuclei within the membrane confirming its desirable barrier function. 96
Figure 4A.1: Induction of conjunctival defect and implantation of membranes. (A) The final defect, (B) Gelatin-based membrane, (C) AM cut into an 8-mm round piece, (D) Representative eye implanted with Gelatin-based membrane, (E) Representative eye grafted with AM. 112
Figure 4A.2: A diagram to explain the ink flow and the thermal model used in this study: For successful 3D-printing, we need to adjust the printing parameters to have appropriate cartridge temperature, needle diameter, temperature difference between the bottom and top of the needle, and the platform temperature as four main challenges.
Challenge 1 (cartridge temperature): Needle obstruction affected by ink gelation can be controlled by adjusting the ink gel point and cartridge temperature. The ink gel point is shown in Figures SI2.1 and SI2.2, and the suitable cartridge temperature are found by creep and recovery test, as explained in Figure 4A.3. 32°C is found to be the suitable temperature for cartridge using the ink of this study.
Challenge 2 (needle diameter): The appropriate needle diameter is found by simulating the needle of the printer using the parallel plates of the rheometer while the “Gap” between the plates is half of the needle dimeter (D) to have the same ratio of surface to volume for two systems (Gap=D/2). The appropriate needle dimeter found in Figure 4A.4 D is 250 μm to have the most secure ink flow.
Challenge 3 (temperature difference between the bottom and top of the needle): The bottom of the needle is at the room temperature, while the temperature of top of the needle is equal to the cartridge temperature. Thus, there is a gradient of temperature between the bottom and top of the needle, which influences the viscosity of the ink. This temperature difference can be minimized by making the ink formulation in a way to have the gel point temperature—and, in turn, the cartridge temperature—closer to room temperature. Challenge 4 (platform temperature):The proper platform temperature for suitable hardening of the ink is explained and found in figure 4A.4E (12 ^{o}C). 114
Figure 4A.3: Creep and recovery tests performed at (A) 20 °C, (B) 24 °C, (C) 28 °C and (D) 32 °C for G8 and G8E2H0.5 samples. 117
Figure 4A.4: The shear viscosity of (A) G4E2H0.5, (B) G8E2H0.5, (C) G16E2H0.5 as a function of shear rate at different temperatures. (D) The mass flow rate of G8E2H0.5 as a function 3D-printer actual pressure, dispensing needle gauge and temperature. (E) The complex shear modulus of G8E2H0.5 as a function of time, gap distance, final temperature and cooling rate when the formulation is cooled between the rheometer parallel plates; the initial temperature was 32 °C and the material was cooled down to 12, 18 or 24 °C with a cooling rate of 10, 8 or 4 °C/min, respectively. (F) The printing procedure on petri-dishes and the obtained 3D-printed membranes. 120
Figure 4A.5: (A) Line roughness of the printed membrane measured in 4 different directions, surface roughness of the strands and the whole membrane and the average pore size in both dehydrated and hydrated states along with the morphology and height profile of the surface of the membrane as well as the histograms in all the specified directions for both (B) dehydrated and (C) hydrated states were obtained using laser microscopy..... 122
Figure 4A.6: In vitro study of the samples. (A) MTT test absorption values at 24, 48 and 72 h. (B) SEM image illustrating partial gelatin-based membrane degradation and epithelial cell adhesion to the surface, 48 h after cultivation. 123
Figure 4A.7: Clinical observation at day 28. (A-C) AM transplanted eyes. Gross conjunctival remodeling and inflammation can be observed. Inflammation is more abundant at the wound

edges. (A & B) Non-degraded AM was observed in eyes showing yellowish discoloration under the repaired conjunctivae. (A′-C′) Gelatin-based membrane grafted eyes. Less inflammation and conjunctival remodeling was observed compared to AM grafted eyes. (A′) Remnant membrane pieces can be seen under the conjunctiva (arrowhead) with no significant adjacent inflammation. (C′) White debris clinging onto a suture in a gelatin-based membrane grafted eye. The trend of clinical observations is shown in Figure 4A.8. 127
Figure 4A.8: (A) Clinical Observations of the defect size at 1st , 12th , 19th and 28th days post-implantation: GM and AM samples presented significantly higher defect sizes compared to the ungrafted sample (p=0.00078) only at day 12, but not in any other time points. The p-values between other samples in different time points are as follows: p=0.05203 for AM/GM at day 12; p=0.40081 for both Ungrafted/AM and Ungrafted/GM at day 19; p=0.91636 for AM/GM at day 19. The values are same for all samples at day 28 and thus p-value is 1. 130
(B) the inflammation score at 1st , 12th , 19th and 28th days post-implantation: Significant differences in the inflammation score can be observed between Ungrafted and AM (p=0.00078), and Ungrafted and GM (p=0.00078) at day 12, and between Ungrafted and AM at day 19 (p=0.01172) and day 28 (p=0.00328). Moreover, the inflammation is significantly less in GM samples compared to AM ones at the end of the experiment at day 28 (p=0.03132). The p-values between other samples in different time points are as follows: p=0.08312 for AM/GM at day 12; p=0.09289 for Ungrafted/GM at day 19; p=0.29362 for AM/GM at day 19; p= 0.20758 for Ungrafted/GM at day 28. 130
Note: Non-parametric one-way ANOVA (Kruskal Wallace) has been used to measure the p-values and the results are considered significant at $p < .05$ 130
Figure 4A.9: H&E staining; (A & A′) gelatin-based membrane grafted eyes: 3-5 layers of epithelial cells (yellow double arrow) are seen in the repaired epithelium with normal cellular morphology. (B & B′) Amniotic membrane grafted eyes: 3-5 layers of epithelial cells (yellow double arrow). (B) Squamous metaplasia of epithelium (large cells with increased nuclear to cytoplasmic ratio) and remnant AM can be seen in sub-epithelial stroma (yellow arrowhead) with adjacent inflammatory reaction. (B′) Severe inflammatory reaction in site of transplantation. (C & C′) Ungrafted eyes: thin epithelium with non-satisfactory flattening of epithelial cells, especially in C′. 131
Figure 4A.10: H&E staining; (A & A′ & A″) Macrophages (green arrow) are digesting the gelatin-based membrane without an adjacent significant inflammatory response (green asterisk). (B & B′ & B″) Multiple giant cells (red arrow) along with a severe inflammatory response (red asterisk) composed of monocyte, macrophage and mast cells are seen around the remaining AM. 133
Figure 4A.11: PAS staining: (A&A′&A″) Amniotic membrane grafted eyes: Less than 10 goblet cells (orange arrows) per 100 cells are seen along the repaired epithelium. Remnant amniotic membrane (yellow arrowhead) is seen in the sub-epithelial area with adjacent inflammatory cells and fibrosis. (B&B′&B″) Gelatin-based membrane grafted eyes: 10 or more goblet cells per 100 cells are seen in the repaired epithelium. The sub-epithelial stoma shows no abundant inflammatory cell infiltration. 133
Figure 4A.12: Masson trichrome staining and IHC for α-SMA: (A&A′) gelatin-based membrane grafted eyes showed random alignment of collagen fibers (green asterisk) while (B&B′) AM grafted eyes showed parallel deposition of collagen (green arrow) along the AM remnant (red arrowhead). (C&C′) A thick layer of densely packed collagen fibers was seen in both ungrafted eyes. (D&D′) Gelatin-based membrane grafted eyes exhibited no α-SMA-positive cells while (E&E′) AM grafted eyes exhibited numerous elongated α-SMA-positive cells. 135

Figure 5A.1: Different designs of the plug that can be used based on the surgery needs: (A) Fully assembled, (B) Adhered Cartilage and Bone Portions, (C) Adhered Film and Cartilage Portion, (D) Unattached form. 151
Figure 5A.2: (A) Photographs of the Bone Portion made of TCP/HA (80:20), Cartilage Portion made of gelatin/elastin/sodium-hyaluronate (8:2:0.5) and Film made of PCL and sacrificial material of PEG (PCL/PEG 3:2), (B) Assembled plug with three parts of Film, Cartilage and Bone Portions (C) Florescence image of Bone Portion of the plug with attached human osteoblasts, (D) Fluorescent image of the Cartilage Portion with attached normal human chondrocytes, (E) SEM image of the PCL Film. 154
Figure 5A.3: Various engagement means that can be used between the Film and Cartilage Portion: (A) Mechanical engagements, such as suturing/stitching of the two parts, which can be used when the materials of the Film and Cartilage Portion are suturable. (B) Aminolysis treatment of the Film, which usually can be used when the Film is made of some polymers (such as PCL) in which aminolysis can create amine functional groups on the surface of polyesters, which can react with the NH_2 groups of the Cartilage Portion (which is made of hydrogel materials) via aldehyde coupling. (C) Enhancing the wettability of one side of the Film in a way to have the hydrophilic surface facing the Cartilage Portion (to enhance the cell attachment), while the hydrophobic surface faces outside of the plug (to prevent departure of cells). In our case (PCL Film), NaOH treatment could make such hydrophilic/hydrophobic surfaces. 155
Figure 5A.4: (A) The Cartilage and/or the Bone Portion of the plug may have gradient configuration to enhance the cell seeding efficiency and to prevent the chondrocytes from dropping deep into the Bone Portion, all while maintaining the contact between chondrocytes and osteoblasts. The suggested pore sizes in different areas of the Bone and Cartilage Portions are indicated in this schematic. (B) The Barrier is an optional part of the plug to substantially avoid fall of chondrocytes to the Bone Portion. A distance (250-500 μm) between the Barrier and the bottom of the Cartilage Portion is necessary to provide a space for communication of osteoblasts and chondrocytes to modulate their phenotypic reactions. Barrier and gradient configuration can be used together in a design, as well. 156
Figure 5B.1: A schematic view of the tri-component knee plug. 166
Figure 5B.2: The experimental setup for monitoring the diffusion of the model probe, i.e. fluorescein sodium salt through the PCL Film. 172
Figure 5B.3: (A) 3D confocal laser scanning images of a 3D printed hard scaffold (TCP/HA 80:20) to be used for the Bone Portion of the Plug. (B)The proliferation rate of human osteoblasts on the scaffolds, as well as the standard cell culture plate (control group). Four samples were examined at each time point/condition (n=4). N0: Initial number of the cells, N: Number of cells at each time point. Statistical significance *: $p<0.05$, **: $p<0.01$, P-values in Day 3: 0.006, Day 7: 0.011, Day 14: 0.006 and Day 21: 0.023. (C-F) The fluorescence images of the attached osteoblasts on the scaffolds after (C) 3, (D) 7, (E) 14 and (F) 21 days. 174
Figure 5B.4: SEM images of the attached osteoblasts on the scaffolds of the Bone Portion after A) 3, (B) 7, (C) 14 and (D) 21 days. 175
Figure 5B.5: (A) 3D printed construct of the Cartilage Portion (gelatin/elastin/sodium hyaluronate soft membrane). The knobs on the 3D printed membrane are constructed to mechanically interlock the Cartilage Portion to the Bone one. (B) Degradation kinetics of the Cartilage Portion—the weight of the sample at each time point has been normalized to the initial weight of the sample and exploited as an indicator for degradation magnitude. (C-F)

Chondrocyte attachment on the gelatin/elastin/sodium-hyaluronate construct one day after seeding. The magnification of SEM images increases from panel C to F 177
Figure 5B.6: The proliferation rate of normal human chondrocytes on the cartilage (gelatin/elastin/sodium hyaluronate) constructs. The experiments were performed on four samples at each time point (n=4). N: Number of cells at each time point, N_0: Initial number of the cells. 177
Figure 5B.7: (A1-A3) Chondrocyte attachment, growth and ECM secretion on gelatin/elastin/sodium hyaluronate scaffolds after (A1) 7, (A2) 14 and (A3) 21 days post-seeding. The samples were stained with Eosin/Hematoxylin using standard histology protocols and the images were taken using a 3D confocal laser scanning microscope (label-free). (B1-B3) Fluorescence images of the chondrocytes growing on the gelatin/elastin/sodium-hyaluronate construct after (B1) 7, (B2) 14 and (B3) 21 days. 178
Figure 5B.8: SEM images of both sides (top and bottom) of PCL membranes prepared by addition of different amount of PEG. PEG/PCL w/w ratio is 0(A), 1:5(B), 2:5(C), 1:1(D) and 3:2(E). Only the ratio of 3:2 PEG/PCL formed pores in both sides, which is selected to be used as the Film in the knee plug. The average size of the formed pores in the Film is 10 μm..... 181
Figure 5B.9: (A) The effect of treatment with NaOH on the wettability and contact angle of the PCL Film. (B) The diffusion kinetics of the model probe (i.e. fluorescein sodium salt) through the Film (C: concentration , C_{eq}: Concentration at equilibrium). 182
Figure SI2.1: Damping factor (tanδ) as a function of temperature at different oscillation frequencies for (A) G4, (B) G8, (C) G16, (D) G4E2, (E) G8E2, (F) G16E2, (G) G4E2H0.5, (H) G8E2H0.5 and (I) G16E2H0.5 formulations. The green bar displays the estimated gelation temperature for each formulation defined as the frequency-independent value of the damping factor (tanδ). 198
Figure SI2.2: The frequency dependence of G' and G" at different temperatures could be used to calculate the relaxation exponents and, consequently, the critical gelation temperature for (A-C) G8 and (D-F) G8E2H0.5 formulations..... 198
Figure SI2.3: The effect of cross-linker concentration on the cross-linking kinetics of G8E2H0.5 represented by the variation of (A) storage (G') and loss (G") moduli as well as (B) complex modulus (G*) measured at 5 Hz and 20 °C. (C) The schematic representation of the effect of cross-linking time on the Young's modulus and ultimate strength of the membranes along with the obtained data for G8E2H0.5 membranes cross-linked by 6 mg/ml EDC and 0.75 mg/ml NHS for 0.5 or 1.5 h. 201
Figure SI2.4: The degradation profile of gelatin-based membranes 201
Figure SI3.1: Microscopic images of the 3D printed scaffolds with the TCP/HA ratio of: (A) 100:0 [formulation 1], (B) 80:20 [formulation 2], (C) 70:30 [formulation 3] and (D) 50:50 [formulation 4]. 209
Figure SI3.2: Shear stress versus shear rate and shear viscosity versus shear rate at various temperatures for the pates with the TCP/HA ratio of: (A1,A2) 100:0 [formulation 1], (B1,B2) 80:20 [formulation 2], (C1,C2) 70:30 [formulation 3] and (D1,D2) 50:50 [formulation 4]..... 211
Figure SI3.3: Mechanical properties (Young modulus and compressive strength) and degradation of the printed scaffolds using the ink composed of TCP/HA ratio of: 1) 100:0, 2) 80:20, 3) 70:30 and 4) 50:50 were measured immediately after preparation and storage in SBF for 4, 8 and 12 weeks. The values of Young modulus and compressive strength are obtained after three repetitions on three separate samples. All scaffolds were in the shape of a disc with 6 mm diameter, 3 mm thickness, porosity of 41.9 ± 2.5% and the inner structure as shown in Figure SI3.2. 212

LIST OF TABLES

Table 2.1: Different 3D-printing methods and their advantages and disadvantages..... 14
Table 2.2: Information regarding the main printable material groups (excluding metals) to conclude their appropriateness to be employed in fabrication of flexible and soft 3D-printed membranes with appropriate mechanical property and surgical handling for biomedical and tissue engineering applications..... 19
Table 2.3: Summarized information about different types of GTR/GBR membranes. 46
Table 2.4: Summary of the treatment options for reconstruction of conjunctival reconstruction and their advantages/disadvantages..... 53
Table 3B.1: Sample specification for the primary rheometry experiment. The w/v refers to the weight of the materials in DI water. 76
Table 4A.1: Detailed composition of various formulations used for rheological measurements. 106
Table 4A.2: Clinical Outcomes for 2nd Week 128
Table 4A.3: Clinical Outcomes for 3rd Week..... 129
Table 4A.4: Clinical Outcomes for 4th Week..... 129
Table 4A.5: Comparison of healed epithelium characteristics between gelatin-based membrane, AM and ungrafted eyes 135
Table 4A.6: Comparison of inflammation (severity and type) and characteristics of the healed stroma between gelatin-based membrane, AM and ungrafted eyes (for details about grading criteria, see SI2)..... 135
Table 5B.1: Parameters used in 3D printing of the Bone Portion of the plug..... 167
Table 5B.2: Applied parameters to 3D print the Cartilage Portion of the plug. 167
Table 5B.3: The mechanical properties and suture retention strength of porous PCL Film compared to a solid PCL membrane. 181
Table SI1.1: Initial solution composition. The w/v refers to the weight of the materials in DI water. G: Gelatin, E: Elastin, H: Sodium hyaluronate, CL: Crosslinking Time 193

TABLE OF ABBREVIATIONS

2D ----------Two-dimensional
3D ----------Three-dimensional
ABS----------Acrylonitrile butadiene styrene
ACI ----------Autologous chondrocyte implantation
ACECM----------Articular cartilage ECM
ACI-C---------- Autologous chondrocyte implantation-collagen
ACI-P----------Autologous chondrocyte implantation-periosteum
ALI----------Air liquid interface
AM----------Amniotic membrane
α-SMA----------Alpha-Smooth Muscle Actin
BFP1----------Bone formation peptide-1
BMSC----------Bone marrow stem cell
CAD---------- Computer-aided design
CALT----------Conjunctiva-associated lymphoid tissue
CaP----------Calcium phosphate
CG----------Collagen/glycosaminoglycan
CGCaP----------Collagen type I/glycosaminoglycan/calcium phosphate
CLIP----------Continuous liquid interface production
CMC ----------Caboxymethyle cellulose
CRMI----------China Regenerative Medicine International Limited
DAPI----------4′,6-diamidino-2-phenylindole
DI----------Deionized
DMA----------Dynamic mechanical analyzer
DMEM----------Dulbecco Modified Eagle Medium
DMSO----------Dimethyl sulfoxide
ePTFE----------expanded polytetrafluorethylene
ECM----------Extracellular matrix
EDC----------1-ethyl-3-(3-dimethylaminopropyl)carbodiimide hydrochloride
EGF----------Epidermal growth factor
FBS----------Fetal bovine serum
FDA----------Food and Drug Administration
FDM----------Fused deposition modeling
GBR----------Guided bone regeneration
GelMA----------Gelatin methacrylate
GRAS----------Generally-regarded-as-safe
GTR----------Guided tissue regeneration
HA----------Hydroxyapatite
hADSC----------Human adipose-derived stem cell
H&E----------Hematoxylin and Eosin
HBSS----------Hank’s balanced salt solution
HC----------Heavy chain
HOB----------Human osteoblasts
HUVEC----------Human umbilical vein endothelial cell
IL----------Interleukin
LEPC----------Limbal epithelial progenitor cell
min----------Minute
MACT----------Matrix-assisted autologous chondrocyte transplantation
MIT----------Massachusetts Institute of Technology
MSC----------Mesenchymal stem cell
MT----------Masson’s Trichrome
NHS----------N-hydroxysuccinimide esters

NOF----------Normal oral fibroblasts
NOK----------Normal oral keratinocytes
PAS----------Periodic Acid Schiff
PB----------Prestoblue
pBMPC----------porcine bone marrow progenitor cell
PBS----------Phosphate buffered saline
PBT----------Poly(butylene terephthalate)
PC----------Polycarbonate
PCL----------Polycaprolactone
PDLLA----------Poly(D,L-lactide)
PEEK----------Polyether ether ketone
PEG----------Polyethylene glycol
PEO----------Poly(ethylene oxide)
PGA----------Poly(glycolides)
PGC----------Polyelectrolyte gelatin-chitosan
PHBV----------Poly(hydroxybutyrate-co-hydroxyvalerate)
pHiso----------pH over the isoelectric point
PLA----------Poly(lactic acid)
PLGA----------Poly Lactic-co-Glycolic Acid
PLLA----------Poly(l- lactic acid)
PPF----------Polypropylene fumarate
PPSF----------Polyphenylsulfone
PTFE----------Polytetrafluorethylene
PTX3----------Pentraxin 3
RGD----------Arginine-glycine-aspartic
rCjEC----------Rabbit conjunctival epithelial cell
SEM----------Scanning electron microscopy
SHEM----------Supplemental hormonal epithelial medium
SFF----------Solid free-form fabrication
SI----------Supplementary Information
SLA----------Stereolithography
SLS----------Selective laser sintering
SPSS----------Statistical Product and Service Solutions
TCP----------Tricalcium phosphate
TEM----------Transmission electron microscopy
TGF----------Transforming Growth Factor
TMC----------Trimethylane carbonate
TMP----------Trimethylolpropane
TPP----------Sodium tripolyphosphate
UTM----------Universal testing machine
UV----------Ultraviolet
VEGF----------Vascularized Endothelium Growth Factor

CHAPTER 1. INTRODUCTION

1.1. Background and Motivation

During the last few decades, the technology of printing evolved from two-dimensional (2D) to three-dimensional (3D)-printing. The 3D-printing method begins from a computer-aided design (CAD) of a 3D model sliced into discrete layers, in which a 3D object will be fabricated through layer-by-layer deposition of materials [1]. Not all materials can be printed, but scientists are investigating to make various types of materials printable for different applications. Current accessible printable materials include several ceramics [2], some metals [3], graphene-based materials [4], some polymers (especially the thermoplastic ones) [5] and also, to a lesser extent, some hydrogels [6].

Other than biomedicine, many areas including art [7], education [8, 9], manufacturing and engineering [10, 11] are now employing 3D-printing technology. Interestingly, many of these fields have recently found that 3D-printing of membranes can be quite useful and efficient [12]. For example, we are observing the progress in 3D-printing of ion exchange membranes [13], separation membranes [14], patterned thin-film composite membranes [15], and filters [16, 17].

Membranes may appear to be 2D structures; however, they often need to have an intricate pattern in their third dimension, especially for biomedical applications. Using layer-by-layer assembly, 3D-printing may offer a versatile and practical approach for the fabrication of such models.

Membranes have different applications in biomedicine, including the reconstruction of skin, ocular surface/conjunctival defect and cartilage or being used for guided tissue regeneration (GTR) or wound dressing (Figure 1.1). For example, 3D-printed membranes have already been used in skin reconstruction [18] and wound dressing [19]. However, the capabilities of 3D-printed membranes have not been examined in many other biomedical applications. This thesis aims to help filling this gap in the field.

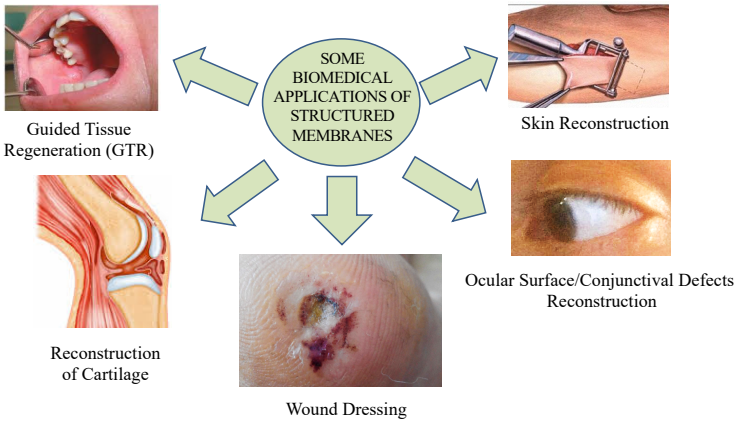

Figure 1.1: Some beneficial biomedical applications of membranes are presented in this figure. Among those, 3D-printing has already been thoroughly researched for skin reconstruction and would dressing by other investigators. This dissertation aims to study the use of cell-free 3D-printed membranes for GTR (Chapter 3), reconstruction of ocular surface/conjunctival defects (Chapter 4) and cartilage regeneration (Chapter 5), by employing a generic ink developed in this thesis.

The Merriam-Webster dictionary defines a membrane as "a thin soft pliable sheet or layer especially of animal or plant origin" [20]. Hence, flexibility and softness must be among the desired characteristics we pursue for producing 3D-printed structured membranes. On the other hand, since this thesis is in search of a generic construct to be used in biomedical applications, biocompatibility and secure surgical handling (mechanical integrity) are also vital characteristics that the favorable membrane must have.

Among various groups of material, hydrogels have soft texture and supple morphology with decent degree of flexibility. Since hydrogels are gels swelled by water, the can hold good amount of water, and thus mimic the tissues of the body as a hydrated construct, while remaining insoluble and maintaining their 3D-printed shape. Therefore, they have the potential qualities that we are looking for in this thesis to be used for making 3D-printed structured membranes for biomedical and tissue engineering applications.

Although 3D-printing is currently being intensely studied, as many other methods in their early developmental path, it presents its own challenge [21]. A key challenge is related to the printing of hydrogels [22, 23]. However, due to their rheological complexities, many of the soft 3D-printed

membranes made by hydrogels cannot be practically used for biomedical applications that require safe surgical handling [22].

This thesis offers a reproducible approach to overcome such difficulties by introducing a specific composition of hydrogels that can be employed as an appropriate generic 3D-printing ink for production of soft cell-free membranes to be used in biomedical applications.

More specifically, the final ink produced in this thesis for this purpose is composed of gelatin, elastin and sodium hyaluronate. The rationale behind focusing on these three components is the fact that gelatin is low-cost and can act as a cell-attractant for almost any cell type [24]. Elastin has long-term stability, elasticity and biological activity [25], while sodium hyaluronate facilitates chemical signaling among cells [26]. After performing the rheological analyses on many different compositions of these three components, we selected a specific composition of 8% gelatin, 2% elastin and 0.5% sodium hyaluronate (w/v) in aqueous solution as the most suitable and printable ink, which resulted in membranes with appropriate biocompatibility, flexibility, mechanical integrity and secure surgical handling.

The protocol and printing parameters of this ink are established in an experimental approach with the assist of rheological analyses of the composition. The printability of this composition allows fabrication of membranes with various porosity, pore size, thickness, and configurations which we termed ‘structured membrane’ in this thesis. Although the ink composition and printing parameters are similar for preparation of different membranes, the design of the membrane (e.g., configuration of setting the different layers on top of each other, thickness, pore size, etc.) can be adjusted based on the desired applications.

We hypothesize that the 3D-printed membranes made by this ink can be used for various biomedical applications. To examine this hypothesis, we have studied three different applications of the membrane including GTR, ocular surface/conjunctival reconstruction and cartilage regeneration. We have shown that the produced membranes have presented stable physical and chemical properties, suitable biological characteristics (*in vitro* and/or *in vivo*), and proper functionality for their anticipated applications.

1.2. Aims and Objectives

Based on the background and motivations described above, the final aims and objectives (steps toward achieving the aims) of the thesis are listed as follows:

Aim 1. Preparation of a generic biocompatible hydrogel ink and developing a 3D-printing protocol to fabricate soft structured membranes.

To achieve this aim, we will follow two below objectives:

Objective 1) Synthesis of a biocompatible hydrogel ink with the following characteristics:

A) Compatible to most biomedical applications in terms of the biomaterial composition to be cell-attractant for different cell types.

B) Relatively low-cost to make it appropriate for future clinical use by different patients.

C) Easily printable without the rheological complexities, which is common in hydrogels.

Objective 2) Development of the 3D-printing protocols by identifying all microextrusion printing parameters, including:

A) Formulation and rheology of the ink, B) Material container temperature, C) Platform temperatures, D) Dispensing needle diameter, E) Pressure, F) Printing speed and G) Pre- and post-flow delays

Aim 2. Filling the gaps in using the capacities of 3D-printing technique to fabricate membranes suitable for specific biomedical applications by employing the generic hydrogel ink developed in Aim 1.

To achieve this aim, we follow the three below objectives:

Objective 1) Developing the design criteria, fabrication, and characterization of a structured membrane to be used for GTR application.

Objective 2) Examining the application of the produced 3D-printed membrane in ocular surface/conjunctival defect reconstruction.

Objective 3) Designing and preparing a 3D-printed membrane to be used for cartilage regeneration as part of a newly developed joint plug.

It should be noted that although cell-laden 3D-printing (or 3D-bioprinting) using bioinks—a composition of cells and biomaterials—has drawn the attention of many scientists recently [27, 28], it is not within the scope and methodology of this thesis. We believe, considering the above aims, it may not be a suitable strategy for our purpose owing to three significant drawbacks:

1) The formulations of hydrogels that can be used for cell-laden printing need to meet specific criteria regarding their speed of gelation, viscosity and cross-linking, which limit the potential materials that can be used for cell-laden printing [29].

2) It may not provide a safe environment for cells in terms of keeping them alive for the long-term. There are problems with the growth of the cells in cell-laden constructs such as slow proliferation and possible immobilization within the hydrogels, which hinder their migration [30].

3) Cell-laden constructs are often too soft without secure surgical handling (they collapse when held by hand). The mechanical resistance and stiffness of cell-laden constructs are much lower than the mechanical property values of most living tissues [31].

Since the vision of this thesis was aimed toward commercialization and practical clinical applications, we avoided compromising the quality of our membranes by including cells into our ink. As the pore size of a construct is adjustable in 3D-printing approach, various type of cells can always be added after preparation of the membrane with the optional use of bioreactor for specific applications.

1.3. Structure of the Thesis

This thesis is organized into six chapters. Chapter 1 is the introduction, which briefly describes the background, motivation of the study, and the gaps to be filled in the field. This chapter also lists the specific aims of the thesis and the steps to achieve the aims, which are described as objectives of the study.

Chapter 2 includes the literature review of the scientific subjects of the thesis. More specifically, this chapter first reviews the literature about 3D-printing technique to describe the most popular 3D-printing methods including direct 3D-printing/inkjet, fused deposition modeling (FDM), selective laser sintering (SLS), stereolithography (SLA) and 3D-plotting. After discussing about

each method, we concluded that, 3D-plotting method is a suitable technique for the purpose of our study in this thesis. This chapter also reviews the produced 3D-printed membranes by other investigators, and discusses the suitability of different materials for preparation of membranes to be used for biomedical applications. We concluded that hydrogels can be the most appropriate group of materials for this purpose. Reviewing literature about GTR, reconstruction of ocular surface/conjunctival defects and cartilage regeneration, and the scaffolds and membranes previously made by different methods for these applications, are also included in Chapter 2.

Chapter 3 begins with a study about 3D-printing of pure gelatin. Section A of this chapter presents a study entitled "3D-printed thick structured gelatin membrane for engineering of heterogeneous tissues." This section mainly describes the initial attempt to perform the first objective of Aim 1, i.e., "synthesizing a generic biocompatible hydrogel ink". The reason that gelatin has been selected as the first attempt is the fact that it is compatible to most biomedical applications (Objective 1A of Aim 1) and is relatively low-cost (Objective 1B of Aim 1). However, it does not fulfill the Objective 1C of Aim 1, as there are many rheological complexities involved in 3D-printing of pure gelatin. Such rheological complications have been eliminated by modifying this gelatin ink after incorporation of the right amount of elastin and sodium hyaluronate in Section B of Chapter 3. This comprehensive study produces the optimized ink (composed of 8% gelatin, 2% elastin and 0.5% sodium hyaluronate (w/v)) that has been used in the remaining parts of the thesis for different applications. This ink is prepared after examining 17 various compositions of gelatin, elastin and sodium hyaluronate. This ink does not have the previous problems involved in printing of pure gelatin and meets all the three criteria described in Objective 1 of Aim 1. Objective 2 of Aim 1 has also been considered in Section B of Chapter 3, in which a 3D-printing protocol has been developed by identifying all microextrusion printing parameters. This section has gone further into Objective 1 of Aim 2 and used the produced generic ink to fabricate a thin structured membrane to be employed for GTR application. Full design criteria, characterization, *in vitro* examinations of this 3D-printed GTR membrane are presented in this section.

While the produced membrane demonstrates excellent mechanical properties and surgical handling in terms of suturability, it exhibits the barrier function of a typical GTR membrane by nicely separating the oral epithelial layer from the underlying tissues. To the best of our knowledge, this is the first report in fabrication of 3D-printed hydrogel GTR membrane as a soft tissue barrier construct. Therefore, it is in line with Aim 2 regarding filling gaps in using the capabilities of 3D-printing for preparation of membranes to be employed in biomedical applications.

Chapter 4 of this thesis is dedicated to fulfilling the Objective 2 of Aim 2, in which the application of the produced structured 3D-printed membrane is examined for the reconstruction of ocular surface/conjunctival defects, by using the generic ink developed in Aim 1. More specifically, this chapter presents a study "3D-printed membrane as an alternative to amniotic membrane for ocular surface/conjunctival defect reconstruction: an *in vitro* & *in vivo* study". This study further analyzes the rheological properties of the ink and characterizes the produced 3D-printed membrane. It then evaluates the surgical handling and clinical applicability of the membrane for conjunctival reconstruction in comprehensive *in vitro* and *in vivo* (rabbit model) analyses and compares its functionality with amniotic membrane (AM). AM is the conventional membrane used for treatment of ocular surface/conjunctival defects.

The results show that the produced 3D-printed membrane has proper surgical handling and appropriate mechanical properties to be used for conjunctival reconstruction. In comparison with the functionality of AM, the 3D-printed membrane presents better outcomes in terms of having more predictable degradation pattern, higher goblet cell density on the healed epithelium, less inflammation and reduced scar tissue formation. To the best of our knowledge, this is the first study on using cell-free 3D-printed membranes for reconstruction of ocular surface/conjunctival defects, which is in line with Aim 2 of this thesis.

Objective 3 of Aim 2 is the subject of Chapter 5, in which design the criteria, fabrication, and characterization of a thick 3D-printed membrane are presented to be used for cartilage regeneration as a part of a newly developed joint plug. For this purpose, the design of a kit of

parts as a new 3D-printed joint plug is presented in Section A of this chapter. The focus of this section is introducing the various aspects of this design, such as configuration options for surgery and implantation in the body, along with the cooperative function of the components as a joint plug.

Section B of Chapter 5 shows how the 3D-printed membrane, made by the generic ink developed in Aim 1, can be used as a part of the newly developed knee plug and facilitated the cartilage regeneration. This section presents a study entitled "A tri-component knee plug for the 3rd generation of autologous chondrocyte implantation". The 3D-printed membrane for the cartilage portion of this knee plug is relatively thick (2 mm) with large pores to accommodate chondrocytes. It contains specific 3D-printed knobs to be interlocked on top of a 3D-printed bone scaffold. A stitchable permeable membrane secures the cartilage portion of the plug in place. This design has been filed for patent as an achievement of this thesis.

The final chapter, Chapter 6, presents a brief conclusion of the thesis and suggests the future works, for example enabling the ink for cell-laden printing, loading relevant biological agents to the membrane, improving the mechanical property of the membrane by inclusion of support layers to the construct, exploring other applications for the membrane and performing *in vivo* examinations for the described applications in Chapters 3 and 5.

CHAPTER 2. LITERATURE REVIEW

2.1. 3D-Printing

Various techniques are being utilized for the production of 3D constructs in biomedical and tissue engineering applications [32, 33]. The methods that are usually used for fabrication of tissue engineering scaffolds include freeze-drying [34], 3D-printing (rapid prototyping) [21], freeze casting [35], salt leaching [36], electrospinning [37], gas foaming [38], blending-pressing-sintering [39] and microsphere fusion techniques [40]. Among these methods, one of the most advanced technique is 3D-printing, as it offers perfect control over the detailed arrangement of the construct [41]. 3D-printing is currently being intensely studied by a diverse set of applications, including the development of bioengineered tissues, as well as the production of functional biomedical materials and devices for regenerative medicine applications [21].

3D-printing is defined as layer-by-layer deposition of materials, usually through an automated procedure. It is alternatively referred to as rapid prototyping. In much literature, solid free-form fabrication (SFF) and 3D-printing are also used as synonyms [41].

During the last few decades, various types of 3D-printing have been developed, which will be described in this section (summarized in Table 2.1). As it will be explained at the end of the section, the 3D-plotting technique is the suitable method to manufacture the desired 3D-printed structured membranes based on the aims and objectives of this thesis.

2.1.1. Direct 3D-printing/inkjet

In 1993, scientists from the Massachusetts Institute of Technology (MIT) reported the development of the first 3D-printer using the techniques of a traditional 2D inkjet printer [42]. The difference between a 2D-printer and a 3D one is the movement of the nozzles. In a 2D inkjet printer, the nozzle moves the ink in *x* (length) and *y* (width) directions on the surface of a paper, while in a 3D-printer, the nozzle also moves in *z* (height) direction to provide the third dimension to the printed objects [43]. In the 3D-printer developed by the MIT group, rather than the ink, a liquid binder was used, and instead of the paper, a powder bed has been employed. In this method

of printing, which is called direct 3D-printing or powder-binder inkjet that uses a computer-aided design (CAD), the nozzle deposits the binder on specific locations of the powder in a leveled platform. Then, the excess materials (powder) are blown off. The process is continued and repeated by lowering the platform and spreading of a fresh sheet of powder followed by deposition of the liquid binder until the ultimate 3D construct is achieved (Figure 2.1(A)) [22].

A wide range of powder and binders can be used in this method, which is considered as an advantage of this technique. Another advantage is the possibility of using two or more types/compositions of binders and powder beds in one construct. This allows having a scaffold with different properties in different areas of the scaffold. For example, a construct with a larger pore size in the middle and smaller pore size on the surface can be made using this technique [41].

Many groups have used this method of 3D-printing for different applications, such as fabrication of tissue engineering scaffolds. For example, Tan el. al in 2014 fabricated an alginate scaffold in which the cross-linker of $CaCl_2$ was used as the liquid binder [44]. For this purpose, they used a Palmetto 3D-printer manufactured by Clemson University and Medical University of South Carolina [44].

Chavanne *et al*. in 2013 used this method of 3D-printing to fabricate tissue engineering scaffolds made of chitosan and HA with the binder solution of lactic acid (40 wt%) [45]. They employed a Spectrum 510 3D-printer made by Z-Corp to perform this study [45]. The authors attempted to print both nonporous and porous scaffolds in a cylindrical shape. While in tissue engineering, porosity of construct is necessary, the authors were not successful in making an acceptable porous scaffold because of the post-hardening process. This process required the use of concentrated solvent, which eventually caused the failure of the porous scaffolds [45]. It can be concluded that the need for post-processing—such as heat treatment—to provide stability for the scaffold is an important drawback of this 3D-printing method [46].

Many binders might be toxic and, if not thoroughly removed from the scaffold, can negatively influence the growth of cells and tissues [41]. For example, when the organic solvent is used in

powdered polymers, such removal is challenging. Thus, the possible toxicity of binder is considered as another disadvantage of this method [41].

Drop-on-demand printers are also known as thermal [47] or acoustic [48-50] inkjet 3D-printers, which can be used for printing thin membranes with fine structures. In a thermal inkjet 3D-printer, the printhead temperature is electrically adjusted to make air-pressure pulses. These pulses push the droplets of the ink to move out of the needle for deposition on the platform. An acoustic inkjet 3D-printer uses a similar approach, with the exception that the pulses are made by piezoelectric or ultrasound pressure [27]. In thermal inkjet printers, the produced droplets usually do not have uniform size, and the directionality of the droplets are low [27]. This printer can expose the ink to thermal and mechanical stress [27]. Moreover, frequent needle clogging has been reported in this kind of printer [27].

Acoustic inkjet printers can better control the size and ejection direction of droplets [51-53]. Exposure of the ink to heat and pressure stress is lower [51-53], and the needle clogging is less frequent in acoustic inkjet printing [27, 54].

Both thermal and acoustic inkjet printers are more popular in cell-laden printing rather than the cell-free scaffold fabrication, since such printers work better with low-viscous materials. Ejection of materials with high viscosity (usually higher than 10 centipoise) requires high force, which is not easily accessible for these printers [27]. Moreover, droplet formation in acoustic and thermal inkjet printers is only possible for liquid inks [27]. Even for cell-laden printing, inks with low cell density must be used [55], otherwise droplet formation, controlling of the shear stress, and frequent needle clogging will be challenging [52]. Post-processing—such as pH, chemical or ultraviolet (UV) crosslinking—is often required for thermal/acoustic inkjet printing [6, 56].

Among the advantages of thermal and acoustic inkjet 3D-printers, their low-cost, high speed and good resolution printing capabilities are highlighted [27]. Moreover, wide range of biological materials are compatible for 3D-printing using these inkjet printers [27]. Some good examples of thermal/acoustic inkjet printing for membrane fabrication include cell-laden printing of skin [57] and layered cartilage constructs [58].

In this thesis, we have not employed this type of printing for producing the 3D-printed membranes due to the limitation of this technique to thin membrane applications and also the fact that only low-viscous ink can be used in this method. As we will discuss in Section 2.1.5, 3D-bioplotting provides us with more flexible options and less limitations for printing cell-free hydrogel membranes.

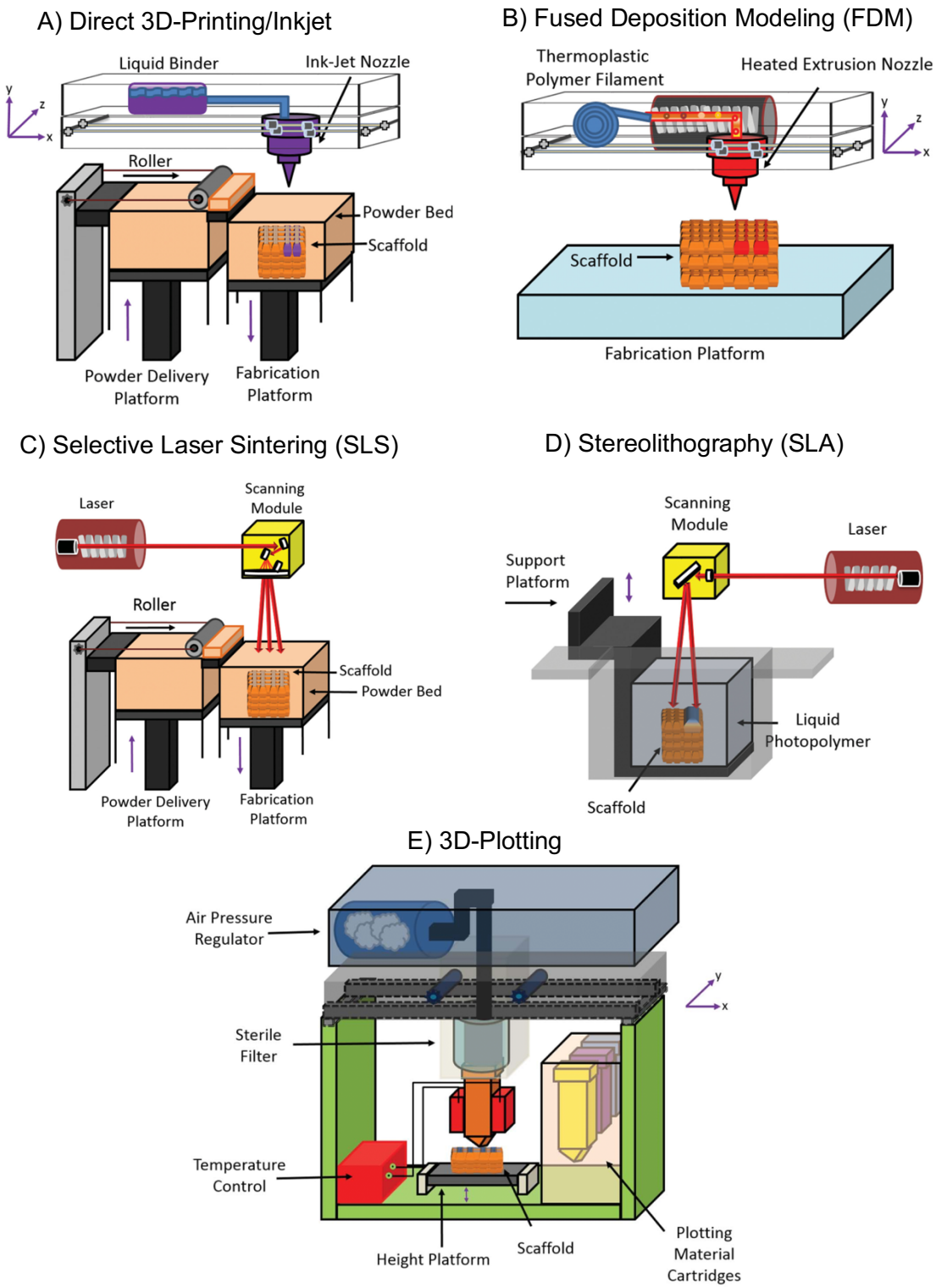

Figure 2.1: Schematics of A) Direct 3D-Printing/Powder-Binder inkje), B) Fused Deposition Modeling (FDM), C) Selective Laser Sintering (SLS), D) Stereolithography (SLA) and E) 3D-Plotting. The schematics are obtained from reference [41] with permission.

Table 2.1: Different 3D-printing methods and their advantages and disadvantages.

Direct 3D-Printing/Inkjet [27, 41, 46]	
Advantages	• Use of a wide range of materials • Possibility of using two or more kinds/compositions of binders and powder beds in one construct to make complex and heterogenous structures in poweder-binder inkjet printers • High speed, low cost and good resolution • Capability of cell-laden printing in thermal and acoustic inkjet printers
Disadvantages	• Need for post-processing • Toxicity of many ordinary binders in poweder-binder inkjet printers • Possible frequent needle clogging especially in thermal inkjet printers • Limitation in viscosity of inks in in thermal and acoustic inkjet printers • Limited to thin membrane applications (in thermal and acoustic inkjet printing)
Fused Deposition Modeling (FDM) [59-64]	
Advantages	• No use of solvent material
Disadvantages	• Limitation of the number of eligible materials (only some thermoplastic materials)
Selective Laser Sintering (SLS) [65, 66]	
Advantages	• Possibility to fabricate scaffolds with high mechanical strength and low porosity
Disadvantages	• Limitation of the number of eligible materials (only materials can be used that can withstand both laser heat and the shrinkage) • Need for pre- and post-heating treatments of the powdered material
Stereolithography (SLA) [67-72]	
Advantages	• High resolution
Disadvantages	• Limitation of the number of eligible materials (only photopolymers can used that employ photoinitiators, which often generate a toxic derivative, and thus, usually not suitable for biomedical applications) • Slow procedure for fabricating constructs with high resolution
3D-Plotting [73-75]	
Advantages	• Material flexibility • Possible room temperature processing • Capability of printing hydrogels • Capability of cell-laden printing
Disadvantages	• Negative influence of the shear stress on the cell viability during the extrusion • Possible collapse of hydrogel constructs during and after printing

2.1.2. Fused deposition modeling (FDM)

FDM is a method of 3D-printing that employs deposition of thermoresponsive materials that are molten (warmed above their glass transition temperatures) on a solid surface of a fabrication platform using a heated extrusion nozzle. As seen in Figure 2.1(B), a coiled thermoplastic

polymer filament is the input of the 3D-printer. Although the material is molten during the process, it will be hardened and set upon reaching the fabrication platform.

The fact that no solvent material is used in this process prevents any possible toxicity that can occur by the use of a usual solvent to solubilize some polymers (e.g., dichloromethane for Poly Lactic-co-Glycolic Acid (PLGA) solubilization) [59]. The disadvantage of this method is the limited number of materials that can be 3D-printed in this technique, as they must be thermoplastic. For example, this FDM mostly accepts acrylonitrile butadiene styrene (ABS) and a few more polymers, such as polyphenylsulfone (PPSF), polycarbonate (PC) and polyetherimide (PEI) [60]. Unfortunately, these materials can mostly be used to build ordinary object (such as toys) and are not suitable for biomedical and tissue engineering applications. To use FDM method in tissue engineering, there is research regarding use of other thermoplastic materials, including polyester, polycaprolactone (PCL) [61] and compositions of PCL, such as PCL-tricalcium phosphate (TCP) [62, 63], PCL-hydroxyapatite (HA) [64] and PCL-PLGA [59].

Combination of FDM and electrospinning allows for more used of FDM for tissue engineering applications. For example, Costa *et al*. produced a biphasic multi-tissue scaffold made of PCL and TCP, in which one phase (bone compartment) is produced using FDM, and another phase (periodontal compartment) is fabricated using electrospinning method [76]. They used an in-house customized melt electrospinning machine to build this scaffold. They showed that combination of FDM and electrospinning is helpful in designing appropriate scaffolds for regeneration of the complicated hierarchical periodontal assembly [76].

2.1.3. Selective laser sintering (SLS)

Selective laser sintering (SLS) is another method of 3D-printing used for scaffold fabrication, in which there is a layer of powder particles that are sintered using a laser beam to make a specific pattern. The process is performed in a layer-by-layer fashion, in which one layer is processed on top of the previously made layer (Figure 2.1(C)). The laser used for SLS is usually a CO_2 one. Various polymers have been 3D-printed using SLS, including polyvinyl alcohol, polyetheretherketone, poly(lactic acid) (PLA) and PCL [77]. SLS is very suitable to make

mechanically robust scaffolds with low porosity. For example, Liu *et al*. presented an SLS scaffold made of HA, silica sol and sodium tripolyphosphate, with a mechanical strength at approximately 43.26 MPa and low porosity [65]. In other studies, PCL [78] and PCL-HA [79] scaffolds have been produced by SLS technique for application in bone tissue engineering, in which the compression moduli were approximately 52-67 MPa.

The materials used in SLS must be able to resist the high temperature of the laser (usually up to 1400 ºC), which is a key limitation of SLS method [65]. Another significant disadvantage of this method is the need for pre- and post-heating treatments of the powdered material. To decrease the laser-induced shrinkage of the constructs, the procedure must be done at a temperature between the crystallization and glass transition or the melting points of the materials [66]. Basically, only materials that can be used in SLS are those that can endure both laser heat and the shrinkage.

It is known that quality of SLS scaffolds is very much dependent on the parameters of SLS procedures that must be optimized [80, 81]. These parameters include laser power, powdered material, scan spacing and speed, layer thickness, roller speed and part bed temperature [80, 81]. For example, Duan *et al*. carefully adjusted laser power, scan spacing and laser thickness to fabricate scaffolds consisting of poly(hydroxybutyrate-co-hydroxyvalerate)(PHBV) and calcium phosphate/PHBV with optimized mechanical/compressive properties, accuracy and stability [80].

2.1.4. Stereolithography (SLA)

In stereolithography (SLA), a liquid photocurable polymer on a surface medium is exposed to the UV light (300-400 nm) in a layer-by-layer manner to make scaffolds by light-facilitated chemical reaction (Figure 2.1(D)).

SLA is a method of 3D-printing with high resolution [67]; however, a key drawback of SLS involves the limitation of the eligible materials, which must be photopolymers that employ photoinitiators. These materials usually generate a toxic derivative and, hence, are not suitable for tissue engineering applications [68, 69]. One of the materials employed in the SLA method to fabricate scaffolds for tissue engineering is polypropylene fumarate (PPF) with the photoinitiator,

Irgacure 819. [70]. An SLA 250/40 stereolithograph machine was used for this purpose, and the results were scaffolds with a porosity of 90% and pore size of 150-800 μm [70].

In another experiment, Elomaa *et al*. employed the SLA method to make scaffolds with a porosity of ~70.5% and pore size of ~465 μm using photo-cross-linkable PCL macromers and Irgracure 369 as the photoinitiator [71]. EnvisionTEC's Perfactory Mini Multi Lens SLA instrument was used in this experiment, and supplementary solvents were necessary for the printing procedure. No material shrinkage was observed in this study [71].

Fabrication of a high-resolution product with SLA is a lengthy procedure. It has been demonstrated that a continuous liquid interface production (CLIP) technique can help to significantly reduce the time of production in the SLA method, although the resolution will be dropped [72].

2.1.5. 3D-plotting

3D-plotting was first developed in 2000 at the Freiburg Materials Research Center, mainly for use in soft material printing [82]. This method of 3D-printing works by extruding ink through a nozzle in a layer-by-layer manner (Figure 2.1(E)). The ink can be a viscous liquid solution, paste or dispersion, which are usually thermally or chemically treated. Different inks may be used in fabrication of different layers. A pneumatic pressurized system is usually installed in a 3D-plotting machine to extrude the viscous ink on the platform surface.

While FDM and 3D-plotting methods are similar in terms of extrusion of materials from a nozzle, 3D-plotting does not have the limitation of FDM in working only with thermoplastic materials [21]. In 3D-plotting, the extruded material can be structured in the form of continuous strands or individual dots using various categories of materials, including ceramics, polymers or hydrogels [82]. While limitations and processing conditions of many 3D-printing methods do not allow printing of hydrogels, the capability of 3D-plotting in hydrogel printing is considered as a significant advantage of this method and is highly useful for printing soft membranes, such as the ones we need in this thesis.

However, one should consider the challenges to prevent the hydrogel constructs from collapsing during and after the printing process [21].

The capability of hydrogel printing using 3D-plotting leads to another capacity of this method, which is printing of cell-laden constructs [74, 75]. It should be noted that, cell viability can be inversely influenced by the shear stress that occurs during the extrusion process [73].

Similar to the incorporation of cells into the inks of 3D-plotters, other biological agents—such as growth factors—can be mixed with the hydrogel inks, as well. For example, Poldervaart *et al*. incorporated vascularized endothelium growth factor (VEGF) into the ink of 3D-printed Matrigel-alginate scaffold to induce vascularization [83]. The bioactivity of growth factors or other biological agents must be thoroughly examined in such cases to make sure that shear stress during the printing procedure does not damage/denature the molecules.

Depending on the materials to be printed, the ink cartridges of 3D-plotters are usually at room or high temperatures, while the platforms are at room or low temperature. The possible high temperature of the cartridges aids in melting the material, and the range of lower temperature of the platform acts to harden it.

3D-plotting is primarily useful for printing simple constructs. Production of the complicated shapes can be highly challenging as printing of complex configurations with overhangs requires the use of support structures, such as sacrificial material [21].

In 3D-plotting, the extruded materials can be deposited either on a regular dry platform or into a wet container holding relevant cross-linkers or liquid reactants. For example, Pataky *et al*. extruded hydrogel into a Ca^{2+} solution for microvasculature [84].

Among all 3D-printing techniques introduced in this section, we have selected 3D-plotting for printing the membranes in this thesis, due to the capabilities of this method in printing hydrogels, which are a class of material necessary for the fabrication of soft membranes. Various commercial 3D-plotter machines have been developed and used by investigators to fabricate tissue engineering scaffolds, including NovoGen MMX Bioprinter from Organovo [85], 3Dn-300 by

Sciperio/nScrypt [86] and 3D-Bioplotter from EnvisionTEC [87-89]. The latter is the one used in this thesis.

2.2. Printable Materials and 3D-Printing of Membranes

Based on the Merriam-Webster dictionary, a membrane is "a thin soft pliable sheet or layer especially of animal or plant origin" [20]. Thus, the main characteristics of 3D-printed membranes that we are considering in this thesis are flexibility and softness. Moreover, since this dissertation pursues membranes for application in tissue engineering and biomedical purposes, the appropriate mechanical integrity and easy surgical handlings of the membranes are also highly desired.

To make a 3D-printed construct (including membranes), appropriate printable materials with acceptable reproducibility—both in the printing procedure and the ultimate printed object—is necessary.

The mechanical properties of metals hardly allow their use in 3D-printing of soft flexible membranes. Thus, we do not consider metals in our study. Other than metals, there are three main groups of materials that are available to produce printable inks for biomedical and tissue engineering applications [41]: ceramics, synthetic polymers, and hydrogels. In this section, we review and discuss each group to determine the materials suitable for 3D-printing membranes to be used in biomedical and tissue engineering applications. Table 2.2 summarizes the information regarding the primary printable materials in each group, their highlighted characteristics and their appropriateness to be employed for production of 3D-printed membranes.

Table 2.2: Information regarding the main printable material groups (excluding metals) to conclude their appropriateness to be employed in fabrication of flexible and soft 3D-printed membranes with appropriate mechanical property and surgical handling for biomedical and tissue engineering applications.

Ceramics	
Examples of Main Printable Materials	• Hydroxyapatite [90] • Tricalcium phosphates [91]
Highlighted Characteristics	• High stiffness • Brittleness • Bioactivity
Appropriateness for Fabrication of the Desired	• Not appropriate

3D-Printed Membranes	
Synthetic Polymers	
Examples of Main Printable Materials	• Poly(lactic acid) (PLA) [92] • Poly(caprolactone) (PCL) [93] • Poly (D,L-lactic-co-glycolic acid) (PLGA) [94] • Polyether Ether Ketone (PEEK) [95] • Acrylonitrile Butadiene Styrene (ABS) [96] • Poly(butylene terephthalate) (PBT) [97]
Highlighted Characteristics	• **PLA**: Brittleness, Releasing of acidic byproducts, Low-cost, Poor cell integration • **PCL**: Low-cost, Slow degradation, High hydrophobicity, Flexibility, Biocompatible but not very good cell integration • **PLGA**: Build-up of acidic oligomers, Wide range of degradability and properties based on the molecular weight ratio of LA:GA, Not very good cell attachment • **PEEK**: Mechanical strength, Heat resistance, Inertness, Risk of triggering foreign body reaction, High-cost, Bio-inert, Radiolucent, Very high melting point (~350 ºC) • **ABS**: Good toughness (not as brittle as polyesters), Mechanical strength, Non-degradability, Very poor cell integration • **PBT**: Similar to PCL and PLA but with higher melting point (225 ºC), Poor cell integration • **All synthetic polymers**: Low biological activity and poor cell attachment as a result of intrinsic hydrophobicity
Appropriateness for Fabrication of the Desired 3D-Printed Membranes	• Among synthetic polymers, PCL can be more appropriate, as its property allows 3D-printing in a flexible membrane shape; however, its slow degradation time, hydrophobicity and low biological activity hinder the acceptable appropriateness
Hydrogels	
Examples of Main Printable Materials	• Alginate [98] • Gelatin [99] • GelMA [100] • Hyaluronan [101] • Collagen [102] • Others (Silk [103], Fibrin [6], Decellularized extracellular matrix [104], Naturally derived Matrigel [105], Elastin [106] and Decellularized adipose tissue [107])
Highlighted Characteristics	• **Alginate**: Non-toxic cross-linking by positively charged ions (such as Ca^{2+} or Ba^{2+} or Mg^{2+}) and possibility of *in situe* cross-linking, Mechanical strength, Flexibility, Possible deformation of the final printed construct, Popular in cell-laden printing, Poor cell attachment (Although alginate has many desired characteristics, its biological cell-integration is not as good as some other hydrogels, such as gelatin) • **Gelatin**: Generally-regarded-as-safe (GRAS) material, Low-cost, Good attachment to any cell type (highly biocompatible), Good matrix material, Suitable speed of degradation, Low antigenicity, Soft but relatively durable mechanical properties • **GelMA:** Photocurable (the UV cross-linked GelMA membrane is not mechanically as strong as a chemically crosslinked gelatin membrane),

	Good attachment to various cell types, Appropriate for cell-laden printing while inherit many good properties of geltain • **Hyaluronan:** Highly viscous (can be printable in modified form or in combination with other printable hydrogels), Has favorable characters in regulating the functions of cells/tissues and cell signaling • **Collagen:** Highly biocompatible, Important constituent of the ECM Low-immunogenic, Poor mechanical properties, Challenging sterilization, Easily shrinkable/contractable, High-cost, Extended crosslinking time, Thermosensitive (causing complications in the sterilization) • **All hydrogels**: Good degree of flexibility, Soft texture and supple morphology, Capability of holding good amount of water (as opposed to the hydrophobic property of polymers) while staying insoluble and keeping their 3D-printed configuration
Appropriateness for Fabrication of the Desired 3D-Printed Membranes	• Appropriate

2.2.1. Ceramics

High stiffness and bioactivity are the two essential characteristics of ceramics that have made them attractive for biomedical applications [108, 109]. Many ceramics are biocompatible and can provide a natural and osteoinductive environment appropriate for hard tissue growth [110, 111]. Thus, they are mostly used in dentistry/craniomaxillofacial [112] and orthopedics [113] applications. HA [90], TCP [91] and HA- or TCP-based composite materials [114, 115] are the main printable ceramics, described further here:

- **Hydroxyapatite (HA):** Mimicking the configuration, mineral and mechanical properties of natural bone are the main subject of investigations on 3D-printed ceramic constructs. Thus, HA, which is chemically similar to the mineral phase of bone, is one of the important ceramics used for this purpose (Figure 2.2) [90, 116, 117].

For example, bone tissue engineering scaffolds were made by Michna *et al*. using an extremely concentrated HA ink by direct 3D-printing [118]. The viscosity and composition of the ink were carefully adjusted in this study to 3D-print self-supporting HA scaffolds with very low organic content (<1 wt %) [118].

- **Tricalcium phosphates (TCP) and composites:** After HA, TCP (composed of α- and β-TCP) are the second most common calcium phosphate phase in natural bone, and thus has been a focus in 3D-printing scaffolds for bone repair [91, 119].

While the degradability of HA is slow, TCP can degrade faster and is often used in combination with HA to adjust the degradation [120]. The mechanical strength of TCP is low; thus, pure TCP is not appropriate for making 3D constructs. It is desired to use other elements to improve the mechanical properties of TCP by making composite materials [114]. For example, Tarafdar *et al*. showed that inclusion of strontium and magnesium oxide to the 3D-printed TCP scaffold can considerably improve its mechanical properties [115].

Using polymer additives with HA and TCP to make 3D-printed constructs with enhanced binding property is also typical [121]. For example, in various studies, PCL as a polymer additive has been used with β-TCP to enhance the interlayer binding in 3D-printing procedure, resulting in constructs with improved mechanical properties [122, 123].

In another study, alginate has been mixed with TCP to fabricate 3D-printed scaffolds with decreased brittleness and enhanced mechanical strength [124]. Phosphoric acid has been used as the binding solvent in this construct. Compared to the pure TCP 3D-printed construct (the control sample), the inclusion of alginate as a natural polymer not only enhanced the mechanical property of the 3D-printed construct, but also improved the biocompatibility of the scaffolds, evidenced by increased proliferation of MG63 osteoblastic cell [124]. Collagen is another natural polymer that has been mixed with TCP to improve the properties of constructs for use as osteochondral scaffolds [125].

Due to the mechanical characteristics of ceramics, including high stiffness and brittleness, along with their bioactive properties, 3D-printed constructs produced by this group of materials are appropriate for bone tissue engineering but are not flexible enough to be used for 3D-printing of membranes.

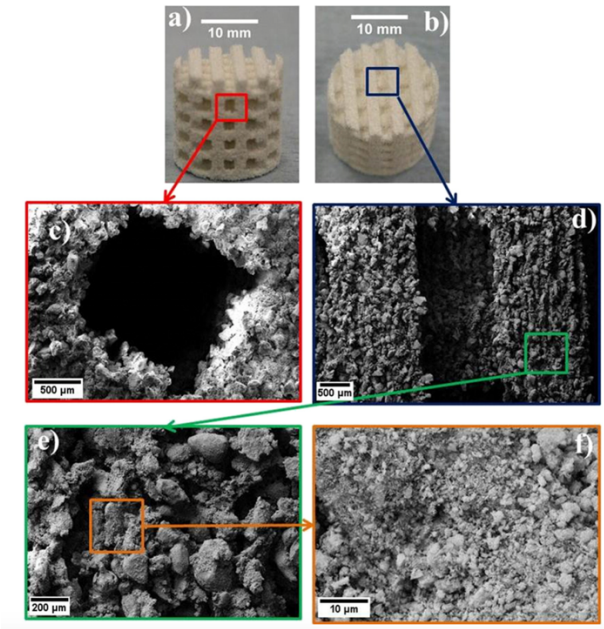

Figure 2.2: Example of a 3D-printed ceramic construct. (a-b) The image of the 3D-printed scaffold made with 50 wt% HA. (c) A pore channel, (d) Strut of the 3D-printed scaffold, (e–f) Surface of the scaffold. This figure is obtained from reference [116] with permission.

2.2.2. Synthetic polymers

Man-made polymers in three common categories of thermoplastics, elastomers, and synthetic fibers are known as synthetic polymers [126]. Various structures with different properties can be assumed for synthetic polymers to be used for a wide range of functions in biomedicine, including applications in therapeutics, drug delivery, diagnostics, and tissue engineering [126].

Synthetic polymers are an important group of materials for 3D-printing in general, not specifically just for biomedical applications. This is attributed to their excellent mechanical properties, low-cost and possible degradability [127, 128]. They can be used in the form of filaments in FDM method, solutions in SLA technique and beads or powders in SLS and 3D-plotting methods [129]. Main printable synthetic polymers include PLA [92], PCL [93], PLGA [94], polyether ether ketone (PEEK) [95], poly(butylene terephthalate) (PBT) and acrylonitrile butadiene styrene (ABS).

- **Poly (lactic acid) (PLA):** The melting temperature of PLA is around 175°C, and thus, it is appropriate for the use in melt-based 3D-printing procedures. More specifically, making filaments out of this polymer for the use in the FDM method is relatively easy. Such filaments can be extruded around 200-230°C.

There are two significant problems with PLA that make it unsuitable for 3D-printing membranes for use in delicate biomedical applications:

1) Release of acidic degradation byproducts is an important drawback of PLA, which can cause inflammation in tissues and necrosis of cells [130]. Since the degradation happens over ester bond hydrolysis, it creates a localized decrease in physiological pH through lactic acid release.

2) Although PLA is known as a material with excellent mechanical properties among synthetic polymers, it is relatively brittle and does not have the expected flexibility needed for membrane fabrication.

Serra *et al*. had used the direct-printing method to 3D-print various PLA-based 3D-printed scaffolds [92]. To improve its mechanical property and bioactivity, a calcium phosphate (CaP) glass, as an inorganic phase with molar composition of 44.5P2O5–44.5Ca2- O–6Na2O–5TiO2 coded G5, and polyethylene glycol (PEG) had been combined with PLA. Figure 2.3 presents its configuration. Due to its bioactive and mechanical characteristics, this construct is appropriate for bone tissue engineering [92], and not a good option for making flexible membrane.

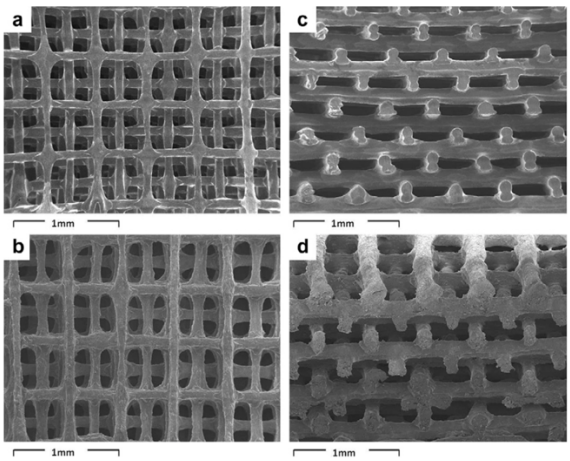

Figure 2.3: Examples of PLA-based 3D-printed constructs. Scanning electron microscopy (SEM) of 3D-printed scaffolds of (a) PLA/PEG - top view, (b) PLA/PEG/G5 - top view, (c) PLA/PEG - cross-sectional view, (d) PLA/PEG/G5 - cross-sectional view. This figure is obtained from reference [92] with permission.

- **Poly(caprolactone) (PCL):** PCL is a biodegradable, biocompatible polyester which is low-cost, and thus, FDM technology takes advantage of its use by making abundant PCL filaments for 3D-printing [131-133]. In fact, tissue engineering and 3D-printing have an effective role in making this polymer accessible and popular for biomedical applications [131].

PCL works very well in melt-based extrusion printing due to its rheological and viscoelastic characteristics and appropriate melting temperature. However, its slow degradability and stiffness make it mostly applicable for bone tissue engineering [129]. 3D-printed PCL constructs can be utilized as a support material during tissue repair, as it can stay stably and non-toxically for more than 6 months in the body and be fully resorbed in approximately 3 years [129].

PCL is one of the critical materials in SLS method and is being employed as 10−100 μm bead [78, 134]. This technique can result in a porous scaffold with interconnected pores, good roughness and a mechanical property comparable to the properties of bone [78]. There are many studies that indicated the successful use of 3D-printed PCL for treatment of bony defects [135, 136]. In some studies, PCL is combined with ceramics. For example, in an *in vivo* study, Konopnicki *et al*. made a 3D-printed scaffold with combined PCL and β-TCP, then seeded it with porcine bone marrow progenitor cells (pBMPCs) and implanted in the 2×2 cm defects of minipigs' mandible. The results indicated good bone penetration depth [137].

The mechanical property of PCL allows its 3D-printing in a flexible membrane shape; however, its long degradation time is not a positive factor in biomedical applications of membranes. Moreover, PCL is highly hydrophobic and is not suitable for cell adhesion [138, 139]. This is an important problem with most of the synthetic polymers, which results in reduced proliferation and differentiation [140]. Also, like many other synthetic polymers, it does not have good biological activity to facilitate tissue regeneration compared to naturally derived extracellular matrix (ECM) polymers.

Synthetic polymers, and specifically PCL, are suitable to be used for 3D-printing of complex shapes, such as ears and nose [93, 141]. Using a sacrificial material is very common in such cases. For example, Lee *et al*. printed the complex configuration such as human ear using PCL (Figure 2.4) [93]. In this work, PEG was employed as the sacrificial material and was stacked at the same level of the PCL 3D-printed layers. After completing the fabrication, PEG was simply removed from the construct by dissolving in distilled water (in an incubator for 40 min) [93].

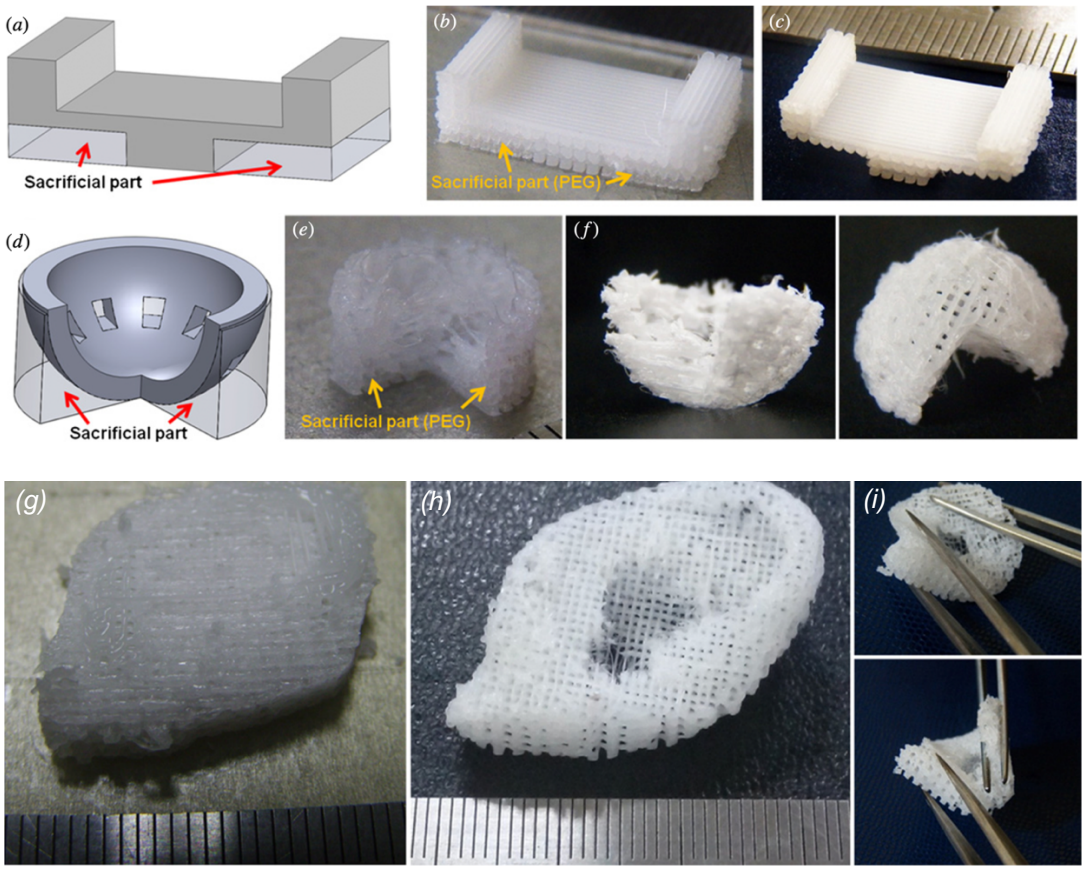

Figure 2.4: 3D-printed complex structures are possible to be made by PCL. PEG was used as the sacrificial material. Panels (a-c) present an overhanging assembly with the sized of 2x1x0.6 cm; (a) CAD design, (b) 3D-printed construct with PCL and PEG, (c) Final structure of the overhanging shape. Panels (d-f) demonstrate a hollowed hemisphere shape with the diameter of 1 cm; (d) CAD design, (e) 3D-printed constructs before removing PEG, (f) Final structure after removing PEG. Panels (g-i) illustrate a framework of an ear, (g) 3D-printed structure with PCL and PEG, (h) The ear-shaped framework after removing the PEG, (i) A demonstration of the flexibility of the construct. Images are obtained from various figures in reference [93] with permission.

- **Poly (D,L-lactic-co-glycolic acid) (PLGA):** PLGA is a biocompatible copolymer of PLA and poly(glycolides) (PGA) [142]. The primary use of PLGA in biomedical applications is its suitable function as a carrier for controlled drug delivery [142]. The degradation of PLGA can be varied from 24 hours to several years, depending on the molecular mass distribution and crystallinity of these elements, along with the molecular weight ratio of lactic acid:glycolic acid (LA:GA) [143].

Different PLGA compositions have been 3D-printed by various methods [5, 144, 145]. For example, Mironov *et al*. 3D-printed PLGA constructs by extrusion of the PLGA solution in

tetraglycol of specific viscosity (Figure 2.5) [146]. Cultures of line NIH 3T3 mouse fibroblasts, mesenchymal stem cells of human adipose tissue and floating islet cultures were used to observe the *in vitro* cytotoxicity and cytocompatibility of this scaffold, and positive results were achieved [146].

In an extensive recent study by Guo *et al*., 3D-printed PLGA constructs with a different molecular weight ratio of LA:GA (with no additional ingredients) were fabricated by employing a direct 3D-printing technique [94]. The dependency of the printing parameters to the PLGA compositions, the effect of the compositions on water adsorption, mechanical properties, and degradation of the 3D-printed scaffolds were thoroughly examined in this study [94].

The major disadvantage of PLGA, which is highly unfavorable for its possible use in delicate biomedical membranes, is having the potential trigger for build-up of acidic oligomers, leading to inflammatory responses in the tissues [147]. Although inflammation is important in regeneration of tissues, it is vital to control the inflammatory responses [148]. Excessive inflammation can cause fibrosis, which may distract the function of tissues or may lead to rejection of the implanted materials. This is because the inflammatory response, which is related to the immune system, can stimulate cells—such as neutrophils and monocytes—to move into the injured region of the body [149].

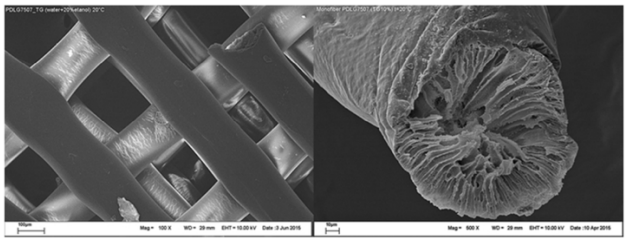

Figure 2.5: 3D-printed PLGA construct: Structure of the 3D-printed scaffold (left) and an individual filament (right) using SEM imaging. The figure is obtained from reference [146] with permission.

- **Polyether Ether Ketone (PEEK):** PEEK is known as a semicrystalline polymer [150], which can be utilized to 3D-print customized craniofacial implants [151]. PEEK is usually used for bone replacement, as it is bioinert, radiolucent, biocompatible and robust with the mechanical property similar to cortical bone [129]. It has a very high melting point (~350°C) [152], and thus

cannot be printed with usual extrusion-based printing, such as 3D-plotting, used in this thesis. Only the SLS method is popular for 3D-printing this material [151, 153, 154]; however, there are limited reports about using FDM method to 3D-print PEEK [155, 156]. PEEK has excellent heat resistance, and therefore, steam sterilization can be applied to it [157]. Due to the lack of ability to integrate with body tissues, the risk of triggering foreign body reaction—such as dislodging, encapsulation and extrusion—is very high for PEEK [129]. 3D-printed PEEK implants are also more expensive than other polymer constructs [129].

The above disadvantages of PEEK make it inappropriate to be used in the fabrication of 3D-printed membranes for biomedical and tissue engineering applications.

- **Acrylonitrile Butadiene Styrene (ABS):** ABS is a triblock and petrochemical-based copolymer with meting point of 105°C. As it is composed of acrylonitrile and butadiene elements, its mechanical strength is outstanding [158, 159]. While polyester synthetic polymers suffer from brittleness, ABS possesses good toughness due to its styrene units [158]. It has been shown that blending poly (l-lactide)(PLLA) with ABS can increase the toughness of PLLA [160].

FDM and SLA 3D-printing systems take advantage of this synthetic polymer [158, 159, 161, 162]. However, since ABS is non-degradable and very poor in cell integration, it is not often being used as scaffold or membrane materials for biomedical applications. There are limited reports of using this material in tissue engineering of bone, cartilage, and other tissues [96, 163, 164].

- **Poly(butylene terephthalate) (PBT):** PBT, as a thermoplastic polyester, is very similar to PLA and PCL [129]. Although it is as biocompatible as PLA and PCL, its melting point is very high (225°C), which is a significant drawback of its use in 3D-printing [129]. More specifically, since it does not seem to have an advantage over these two polyesters (PCL and PLA), its higher melting point makes it not very popular in biomedical applications.

PBT can be used in FDM 3D-printing systems. Tellis *et al*. reported the use of 3D-printed PBT scaffold, made by FDM method, for bone tissue engineering of canine trabecular bones [97]. The

fabricated 3D-printed scaffold matched well with the trabecular bone in terms of porosity; however, its biocompatibility with cells was not examined in this study [97].

PBT has also been utilized as coatings for scaffolds. For example, PBT-coated CaP scaffolds were appropriate for bone regeneration in a canine knee model [165]. Coating of a combination of PBT and poly(ethylene oxide) (PEO) on titanium alloy implants has also demonstrated effectiveness in bone binding [166], although it is not clear if the positive effects are achieved because of the coating itself or the combination of coating and scaffold materials.

- **Regarding all synthetic polymers:** Low biological activity and poor cell attachment, as a result of intrinsic hydrophobicity, are the disadvantages of all synthetic polymers that hinder their use in delicate biomedical applications, such as the ones we intended in this thesis.

Among all the synthetic polymers we introduced above, only PCL may have the required characteristics to make thin and flexible 3D-printed constructs. However, due to the disadvantage of PCL, including its slow degradation and stiffness, its use is limited. As we will suggest in Chapter 6, as a future work of the study in this thesis, the PCL layer can be used as a support layer in the hydrogel membranes to improve their mechanical properties.

2.2.3. Hydrogels

As discussed at the beginning of this section, membranes are considered as thin and flexible constructs. Non-toxic hydrogels are the most popular material being used to make 3D-printed membranes for actual biomedical applications due to two significant characteristics [167]:

1) Hydrogels are made of 3D polymer networks with a reasonable degree of flexibility, soft texture and supple morphology, which are beneficial characteristics to produce a flexible membrane.

2) Hydrogels are known as gels with water as their swelling agent. Thus, they are capable of maintaining a right amount of water, while staying insoluble and maintaining their 3D-printed configuration, which allows them to closely mimic body tissues in term of being hydrated constructs (in opposite to the hydrophobic property of polymers).

Therefore, in this thesis we focus on hydrogels to create the desired 3D-printed membranes for biomedical applications.

3D-plotting and, to a lesser extent, SLA are known as the major methods of 3D-printing hydrogels [129]. An important step in maintaining the integrity of 3D-printed hydrogel constructs is cross-linking. Constructs made by chains of natural or synthetic polymer networks in hydrogels can be cross-linked chemically (e.g., covalent bonds), physically (e.g., hydrogen bonds, hydrophobic/hydrophilic associations or ionic complexation) or by mixed chemical and physical cross-linking mechanisms [167, 168].

The major printable hydrogels are explained below:

- **Alginate:** As a plentiful natural polymer in nature, alginate can be extracted from marine brown algae (Phaeophyceae) [169]. As a structure-forming element in the brown algae and its gel matrix, it provides the plant with both flexibility and mechanical strength [170], characteristics that are desired in making suitable biomedical membranes.

Alginate, as an anionic polysaccharide, can absorb water to the extent of 200-300 times its weight [171]. Moreover, alginate is chemically similar to the ECM, and thus nutrients and metabolites can quickly diffuse into it. While sodium alginate is water-soluble in water, calcium alginate does not dissolve in water; thus, it is possible to have sodium alginate extruded from a 3D-printing nozzle to a solution of calcium ion solution [171]. Basically, the most exciting characteristic of alginate as a polycation is the capability of being crosslinked using positively charged ions, such as Ca^{2+} in $CaCl_2$ [171] or Ba^{2+} [172] or Mg^{2+} [173]. This is why the use of alginate is prevalent in cell-laden printing or any 3D-printing method/construct in which cell encapsulated hydrogel is somehow involved.

There are numerous reports about how various cells are encapsulated in hydrogels and used in 3D-printed constructs. In some reports, the scaffolds are made with different materials, and then, cell encapsulated alginate was incorporated to the 3D-printed scaffolds [174-176]. For example, chondrocyte-encapsulated alginate was incorporated in a specific SLS 3D-printed scaffold made

with acrylated trimethylane carbonate/trimethylolpropane (TMC/TMP) and implanted in mice [174].

In many other reports, alginate has been used in cell-laden printing to regenerate different tissues [177]. For example, using inkjet 3D-printing method, Huang *et al*. made zig-zag tubes with a combination of alginate and cells for use in tissue engineering of blood vessels [178]. Alginate has been used for bioprinting of blood vessels by other investigators, as well [179-181].

Alginate has also been employed for skin bioprinting [182], or in cell-laden printing with chondrocytes for cartilage tissue engineering application [183]. Although in all of the above applications, the constructs may look like a membrane, they are mostly made to hold the designated cell for the limited time of the experiment (rather than storage for future use). Such cell-laden printed membranes are not mechanically strong enough for surgical handling [182, 183].

On the other hand, while alginate is suitable for cell-laden printing among the hydrogels, due to its non-toxic cross-linking procedure, the cell attachments of many other hydrogels—such as gelatin—is much better than alginate. This is why cell-free alginate membrane is not a perfect choice for offering prolonged cell attachment and growth [184].

Moreover, in our experimental work, we realized that alginate, even at high concentrations, tends to flow once printed on the platform. This characteristic causes deformation of the final printed object. Such deformation may not be necessary for cell-laden printing but is not favorable for having a robust cell-free membrane to be used for generic biomedical applications, as we intended in this thesis.

Most of the studies on alginate suggest *in situ* cross-linking while the object is being printed [98]. Our experience indicated that care must be taken not to cross-link the last printed layer before printing the next one on top of it, since it abolishes the adhesion between layers and, consequently, damages the object coherence. To address such problem, *in situ* cross-linking is carried out by precise control of cross-linker diffusion throughout a grid used as the platform. Such a strategy

requires very complicated designs. Additives can be used to adjust the viscosity and donate a liquid-solid transition to such inks for addressing this issue.

In a recent study performed by Heo *et al*., the membrane of alginate conjugated to bone formation peptide-1 (BFP1) was 3D-printed (Figure 2.6) [98]. The *in vitro* and *in vivo* studies were conducted on the 3D-printed constructs to demonstrate that the scaffold could safely accommodate human adipose-derived stem cells (hADSCs) and is appropriate for bone regeneration [98].

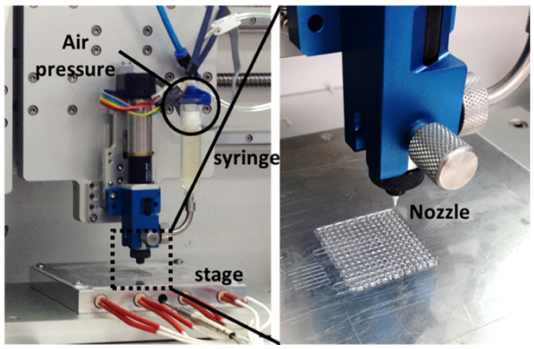

Figure 2.6: 3D-printed membrane made by alginate–BFP1 (right) and the 3D-printing machine used for its fabrication (left). This figure is obtained from reference [98] with permission.

- **Gelatin:** Gelatin is a denatured form of collagen and is achieved by hydrolyzing collagen from the animal using acid or alkaline. Gelatin is one of the safest and most reasonably priced biomaterials to be used in pharmaceuticals, medical/food products and cosmetics [24, 185]. United States Food and Drug Administration (FDA) considers gelatin as a generally-regarded-as-safe (GRAS) material [186].

Among the many advantages of gelatin, the ones that are important for the purpose of making a generic biomedical membrane include:

1) It is biocompatible and low-cost with reasonable speed of degradability [24, 185].

2) Chains of gelatin are rich in motifs, such as arginine-glycine-aspartic (RGD) sequences, which can modulate cell attachment. It can effectively attach to all cell types and is very appropriate for generic use. This is an essential advantage of gelatin compared to many other materials without cell-recognition sites, such as polymers [187].

3) Gelatin can act as a suitable matrix material, which is critical for applications in tissue engineering. Basically, cell adhesion can be supported by gelatin without involving cell phenotypes [187-189]; while as a porogenic element, gelatin offers structural support when combined with other material components [190].

4) Since gelatin is a denatured product, it is less antigenic than collagen [186].

5) Gelatin has soft but durable mechanical properties [191].

All these advantages make gelatin a favorable candidate for use in fabrication of a generic biomedical membrane.

For 3D-printing of gelatin, the dependency of its so-gel transition to temperature is the crucial player in the entire procedure of printing. Premature gelation of gelatin during printing can be the reason for the challenging 3D-printing route, as this material can cause fabrication of low-quality constructs [192]. Combining gelatin with other polymers can make the printing procedure much easier [181, 193]. While it can be costly and not be applicable for all 3D-printing machines to 3D-print the pure or modified gelatin, it is recommended to conduct specific adaptations on the 3D-printer to improve the handling of gelatin hydrogels [100].

Laronda *et al*. have recently reported the 3D-printing of microporous hydrogel scaffolds to examine how the pore geometry—changed by altering the angle between layers—influences the ovarian follicles (Figure 2.7) [194]. They chemically cross-linked the scaffolds using 1-ethyl-3-(3-dimethylaminopropyl)carbodiimide hydrochloride (EDC)/N-hydroxysuccinimide esters (NHS).

Shortly after this report, Lewis *et al*. reported 3D-printing of gelatin in the various repetitive geometries (Figure 2.8) [99]. They studied the effect of different pore geometry on the biological response of seeded undifferentiated hepatocyte cell line (HUH7) as a model hepatocyte system [99].

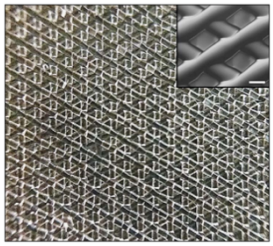

Figure 2.7: A 3D-printed gelatin membrane with five layers and homogamous distribution of pore. Insert presents the same membrane with higher magnification. The membrane is cross-linked by EDC/NHS. Scale bar is 250 mm. This figure is obtained from reference [194] which is licensed under a Creative Commons Attribution 4.0 International License, and no permission is required.

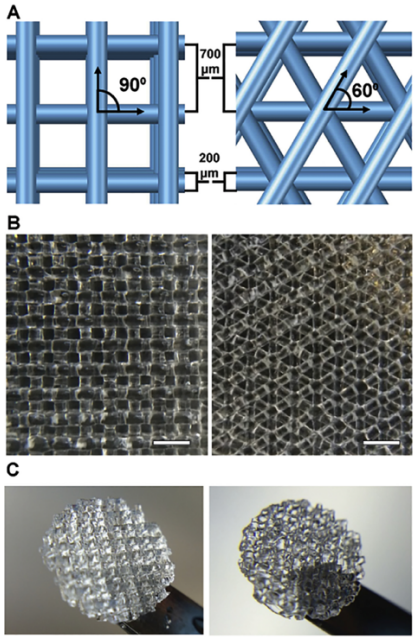

Figure 2.8: Gelatin 3D-printed membrane/construct in various repetitive geometries. (A) Interior pattern of the 3D-printed models. (B) The photo of the 3D-printed gelatin structure with the nozzle diameter of 0.2 mm, scale bars = 1 mm. (C) Cross-linked structure of the 3D-printed gelatin (diameter is 6 mm). The figure is obtained from reference [99] with permission.

Cell-laden printing with gelatin has also been reported by using microbial transglutaminase (mTgase) as a cross-linker [195]. However, most investigators prefer to use photocurable methacrylated gelatin for cell-laden printing instead of gelatin itself, so they can employ UV for cross-linking, which is safer than other methods for cells [85].

In summary, the thermoreversible gelation of gelatin must be exploited to obtain a solid object after printing. The printed object must then be cross-linked to permanently fix the final shape. Various additives to the gelatin matrix can control different characteristics of the ink and the printed object. These additive options include:

1) **Thickeners**: A particular concentration of this group of materials can assist not only in adjusting the viscosity of the ink but also in modulating the gelation temperature of gelatin. Carboxymethylcellulose is an example of such additives [196].

2) **Filler to improve mechanical properties**: Various micro and nanoparticles can be added to gelatin to enhance the mechanical properties of the final products. HA and TCP are examples of such fillers. Many organic/inorganic fillers have been used to improve biological, mechanical and/or degradation behavior of hydrogel scaffolds *in vitro* and *in vivo* by preparing hydrogel-

based composites [197], among which calcium phosphates are an important group. This group of fillers may improve bone bonding [198, 199] and in some studies reported to enhance mechanical properties [200].

3) **Other materials, proteins, and biomolecules to improve biological response**: Gelatin itself generally represents ideal cell attachment and biological response. However, different proteins, could be added to the gelatin matrix to improve biological response. It becomes more highlighted when the cells of the target tissue are considered responsive to a specific protein. For example, elastin-derived motifs have been used as non-integrin adhesion ligands in tissue engineered hydrogels [201].

It should be noted that one or more additive could be included in the formulation simultaneously, and a single additive might have one or more functions. For example, as it will be seen in following chapters, the inclusion of hyaluronic acid to gelatin in our formulation adjusted the viscosity and improved mechanical and biological characteristics of the gelatin ink [202].

As another example, in a study performed by Shi et a., silk fibroin and bone marrow stem cells (BMSC)-specific-affinity peptide were added to gelatin to improve the 3D-printed scaffold both structurally and functionally to be used for cartilage tissue regeneration [203].

To make an appropriate 3D-printed membrane for skin tissue engineering, chitosan was incorporated to gelatin to take advantage of the antimicrobial property of chitosan and its capability to trigger hemostasis [204]. About the interaction between chitosan and gelatin, it should be considered that gelatin is negatively charged at the pH over the isoelectric point (pHiso = 4.7) [205]. This leads to creation of a polyelectrolyte complex due to the reaction of ammonium ions of chitosan (positively charged) with the carboxylate groups from the ampholytic gelatin. Hence, in this study, gelatin was improved with chitosan to make polyelectrolyte gelatin-chitosan (PGC) hydrogels, which were used in 3D-printing of membranes suitable for skin regeneration and wound healing (Figure 2.9) [204]. The 3D-printed membranes exhibited good configurational integrity and acceptable biocompatibility using fibroblast skin cells [204].

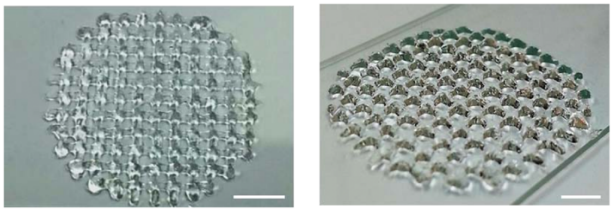

Figure 2.9: A 3-layered 3D-printed membrane made of 5% PGC hydrogels. Scale bars are 5 mm. This figure is obtained from reference [204], which is licensed under a Creative Commons Attribution 4.0 International License, and no permission is needed.

- **Gelatin Methacrylate (GelMA):** The peptide chains of gelatin contain lysine, and this lysine terminal amino group has the ability to interact with methacrylamide and make a methacrylate group [206]. This modified version of gelatin is known as gelatin methacrylate (GelMA), which is a photocurable hydrogel that can be cross-linked with UV, rather than the usual chemical cross-linkers, such as EDC/NHS [206]. Thus, GelMA is appropriate for cell-laden printing, as cells cannot tolerate the chemical cross-linkers. However, it should be noted that the UV cross-linking is not as strong as chemical cross-linking, and thus, the 3D-printed membranes made with GelMA are not mechanically as strong as the gelatin membranes and do not have secure surgical handling property. They do, however, still inherit the valuable properties of gelatin, such as biocompatibility, perfect attachment to various cell types and biodegradability (can be absorbed *in vivo* in about 2 months) [171, 207]. As an example of GelMA 3D-printing, Billiet *et al*. pre-seeded the HepG2 (liver hepatocellular carcinoma) cell line into GelMA and 3D-printed the hydrogel/cell mixture by extruding it through a nozzle [100]. Short after printing, the 3D-printed membrane was cured using the UV light. In such printing, the viability of cells under the extrusion pressure is an important concern, which was discussed in this study [100]. They showed that conical needles were more appropriate than cylindrical ones for such cell-laden printing [100].
- **Hyaluronan:** Hyaluronan (or hyaluronic acid), as an ECM material, can be found in any connective tissues of our body. This natural glycosaminoglycan is highly compatible for biomedical and tissue engineering applications, and has already been used in clinic for a long period of time [208, 209]. The importance of hyaluronan is related to its involvement in regulating

cells and tissue functions, such as cell differentiation, migration, angiogenesis and proliferation [208].

However, unmodified hyaluronan can be highly viscous and not easily printable (or not stable after possible printing) [101]. But, due to its favorable characters in regulating cells, it has been used in compositions with other printable hydrogels, such as GelMA [210], photocurable dextran [211], and via conjugation with thermoresponsive poly(N-isopropylacrylamide) [212]. The other approach of using this hydrogel in 3D-printing is chemically modifying it [208, 213].

For example, methacrylated hyaluronan, which is photocurable, was used as one element of a multi-component ink for a 3D-printing process [214-216].

Skardal *et al*., in a series of papers, showed the ability to use different modified hyaluronan in 3D-printing inks, such as using methacrylated hyaluronan with gelatin in a two-step bioprinting [216], using a composition of poly(ethylene glycol) and thiolated hyaluronan for 3D-bioprinting of vessel-like constructs [217], and using gold nanoparticle-cross-linked hyaluronan-gelatin composite in a bioprinting ink [218].

In another study by Ouyang *et al*., the authors introduced a new hyaluronan-based ink that meets the criteria for printability in an extrusion-based 3D-printing method [101]. More specifically, they coupled adamantane (Ad, guest) and β-cyclodextrin (CD, host) moieties to make a guest-host bonding, resulting in a supramolecular assembly of two hydrogel-precursors [101]. Photo-cross-linkable methacrylate groups have also been used in the macromers. The authors investigated how different types of cross-linking—including guest-host, photo-cross-linking or a grouping of these two—can affect the printability of hyaluronan to fabricate multilayer membranes [101].

- **Collagen:** Collagen is the important constituent of the ECM and one of the most plentiful proteins in the body [219]. About 25% of our dry weight is composed of collagen [219, 220]. Although more than 20 different types of collagen exist, fibril forming collagen type I is the more frequently used collagen in biomedical and tissue engineering applications, which can be extracted from rat tail, tendons, bovine and pork skin [219].

Collagen is biocompatible, low-immunogenic and can be degraded by collagenases [219-221]. However, if no extra cross-linking applies to collagen, its mechanical properties will be very poor. For example, 1-5 mg/ml collagen gel type I (extracted from a rat tail) at 37ºC has a storage modulus below 100 Pa [222]. To improve its mechanical properties, collagen can be cross-linked, either chemically or enzymatically, or blended with other polymers to make double networks [223]. Some cross-linking strategies induce cytotoxic challenges for collagen to be used in biomedical applications [223]. There are also complications regarding the sterilization of collagen because of its thermosensitivity and degradation, as temperature can change the fibrillar form of collagen [219]. Moreover, shrinkage/contraction is frequently reported in collagen scaffolds after cell activity [224-226].

Despite the shear-thinning properties of collagen, its gelation temperature and pH-dependency make it an interesting hydrogel for 3D-printing. Due to its poor mechanical property, it is usually printed in preformed molds, such as 3D freeform fabrication, or as support inside various biomaterials [102, 227, 228]. It also must go through additional crosslinking after the 3D-printing procedures [228-232]. 3D-printing of collagen with other materials is very common, and many investigators reported such compositions for 3D-printing [6, 57, 58, 227, 233-241].

High-cost of collagen is a barrier in using this material in 3D-printter with large-capability cartridge (e.g. 30 ml). For example, we found it very difficult and expensive to use EnvisionTEC® 3D-bioplotter employed in this thesis, for collagen printing, especially for fabricating large constructs or membranes. However, its use in cell-laden printing and/or in combination with other materials is reasonable [232, 238]. Various applications are considered for the 3D constructs/membranes composed of collagen. Examples include mimicking skins and grafts [229, 232], making scaffolds for regeneration of bone [227, 242], neural tissue engineering [230, 243], examining materials for the new printing techniques [231, 234, 244-246], making models for *in vitro* analyses in a 3D environment, drug examining, tissue assays, disease modeling [229, 232, 236] and other various tissue engineering applications [228, 247].

- **Others:** Among other relevant 3D-printing hydrogels, one may refer to silk [103], fibrin [6], decellularized ECM [104], naturally derived Matrigel [105] and decellularized adipose tissue [107], all of which are mostly used for cell-laden printing. Elastin is also a main ECM protein in arteries [248]. However, we hardly found any report of 3D-printing of this material for biomedical applications, other than the gelatin/elastin/sodium hyaluronate membranes reported in this thesis [106]. Elastin is usually used for fabrication of engineered tissues in combination with collagen [249].

Silk and fibrin, as important structural proteins, are used more often than the above mentioned materials [250]. Regarding the 3D-printing of silk, long term of solution precipitation is one of the major issues in printing native silk fibroin [251, 252]. Moreover, the metastable state of silk is highly problematic in its printing [251, 252], and addition of some additives can be helpful to resolve this issue [251, 253-255]. Making recombinant silk for 3D-printing is also effective in terms of printability due to its shear-thinning behavior [252]. 3D-printed inks composed of silk material have been examined in different applications, including cartilage regeneration [103], optical waveguides [256], testing cell-matrix interactions [257], small scale catalytic motors [258], biosensors [251], strain gauges for biological use [259] and general tissue engineering [103, 257, 260].

Fibrin is an expensive FDA-approved material. The gels of fibrin have low viscosity, quick gelation and well-behaved cross-linking procedure, however, the accuracy of 3D-printing with fibrin is reported to be low (~52%) [6]. Since it has a quick gelation time and high rate of degradation, the inks made based on fibrin are often blended with other materials, such as gelatin [261] or gelatin/alginate [262-264].

Matrigel is a commercialized blend of proteins extracted from mouse sarcoma cells and composed of laminin, collagen, entactin, heparan sulfate proteoglycans, and some growth factors [265]. The compositions of decellularized ECM depend on the living tissues they are extracted from, as well as the use of the decellularization protocol [266]. However, they usually contain structural proteins, polysaccharides, glycosaminoglycans and biofunctional factors [266].

Although Matrigel and decellularized ECM are similar to the natural matrix [104], their use in 3D-printing or cell-laden printing is limited. This is mostly due the challenges in decellularization processes and standardization of extraction materials caused by batch variability, which highly influence the reproducibility and controllability of printing [250].

Since using EDC/NHS is a common and popular method of cross-linking in many hydrogel constructs—including 3D-printed hydrogel membranes—and is also the approach that has been used in this thesis, here we explain the mechanism of EDC/NHS cross-linking.

As shown in Figure 2.10, during the cross-linking procedure, when EDC is included in the hydrogel solutions, it first reacts with the groups of carboxylic acid and makes an amine reactive O-acylisourea intermediate, which is as unstable element [267, 268]. This compound impulsively reacts with primary amines and makes an amide bond and a by-product as a soluble urea derivative. Due to the instability of O-acylisourea intermediate, if it does not react with an amine, hydrolysis of the intermediate and regeneration of carboxyls can occur, and N-substituted urea will be released. Thus, quenching the EDC activation reaction by a thiol-containing compound, such as 2-mercaptoethanol, is essential [267].

Here, the role of NHS or Sulfo-NHS (water-soluble analog of NHS) is important. EDC links NHS to carboxyls, making an NHS ester that is stable and allows the effective conjugation to primary amines when the pH is appropriate (physiologic pH) [267].

EDC is known as a zero-length carboxyl-to-amine crosslinkers, because it can make a direct conjugation of carboxylates to primary amines [268, 269]. More specifically, after the cross-linking procedure, ECD will not be a portion of the final amide bond among the conjugated molecules [268]. EDC and its by-product, isourea, are water soluble and dissolve in the aqueous solution. This helps the purification of the final cross-linked products [267].

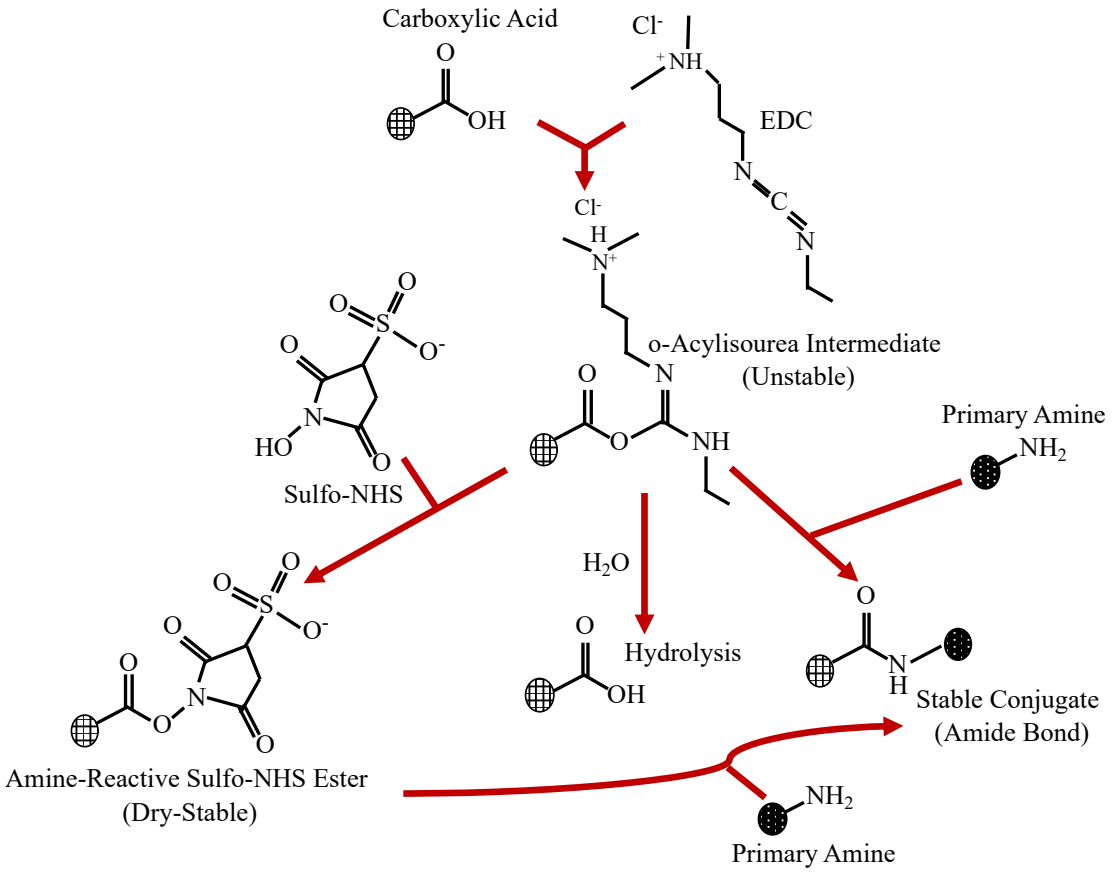

Figure 2.10: This schematic presents the carboxyl-to-amine cross-linking reaction of EDC and Sulfo-NHS (water-soluble analog of NHS). Inclusion of NHS leads to formation of amine-reactive intermediate, which is dry-stable and, therefore, can enhance the final efficacy.

2.3. Guided Tissue Regeneration (GTR)

The concept of guided tissue/bone regeneration (GTR/GBR) was initially introduced in 1959 [270] and then recapped more clearly in 1984 [271]. In GTR and GBR techniques, a barrier membrane prevents the migration of cells from the connective tissue or epithelium to the underlaying tissues.

GBR and GTR, as barrier membranes, share similar concepts and sometimes are used interchangeably, however, GTR typically involves soft tissues and is mostly applies for regeneration of periodontal soft defects [272], while in GBR, the goal is growth of healthy bone in a way that no fibroblast or other interfering cells penetrate into the bony region [273, 274].

A good GTR/GBR membrane must: 1) be biocompatible without prompting inflammatory response, 2) have appropriate configuration and pore size in each side to accommodate relevant

and different cell types in different sides of the barrier and to prevent penetration of cells while allowing the nutrient delivery and neovascularization, 3) have proper degradation (if resorbable), 4) have appropriate mechanical properties for secure and easy surgical handling, preventing the membrane collapse and also maintaining the space (for specific applications) [275, 276].

As summarized in Table 2.3, we can categorize the GTR/GBR membranes into two groups of non-resorbable and bioabsorbable membranes. Bioresorbable membranes can be made either by natural or synthetic materials.

2.3.1. Non-resorbable membrane

The gold standard material for many non-resorbable biomedical membranes is expanded polytetrafluorethylene (ePTFE), which is the porous form of polytetrafluorethylene (PTFE) [277]. PTFE is made of fluorocarbon polymer and is a fully inert and biocompatible material that makes minimal inflammatory reaction in human body [278, 279]. However, since PTFE is nonporous, it prevents tissue ingrowth, thus ePTFE is manufactured with the aim of supplying porosity to the body of PTFE [280, 281]. The structure of the pores in ePTFE has the shape of solid nodes and fibrils, which are formed by expanding the PTFE in a way to create a microporous configuration [280, 282]. The porosity in in ePTFE can be variable based on the fabrication condition and parameters . Gore-Tex® is the very first commercialized non-resorbable membrane, which took advantage of this characteristic of ePTFE. In an innovative configuration, Gore-Tex® membranes are made with a bilayer configuration, in which each layer has a different porosity (90% and 30%) to deliver a certain function. More specifically, the Gore-Tex® membrane is composed of:

1) A membrane with the thickness of 1 mm that is 90% porous. It does not allow the migration of apical epithelium cells and facilitates the ingrowth of connective tissue. It is placed coronally, and effectively helps the stability of wound [280].
2) A membrane with the thickness of 0.15 mm which is 30% porous. This part maintains the required spaced for regeneration (a space maintainer). The structural stability of Gore-Tex® comes from this part, which acts as a barrier near the gingival flap [280].

The bilayer configuration of Gore-Tex® membrane, with different porosity in each layer, established the principle of pore size anisotropy of a GTR membrane, which inspired the design of the GTR membrane developed in this thesis.

The outcomes of using ePTFE membranes were generally successful in different clinical studies [283-285]. Although some investigation indicated that the membrane could act similar to conventional flap surgery [286], there are other studies that exhibited its capability to considerably facilitate the periodontal regeneration after 3 months [287]. Some studies also reported observation of new cementum formation with inserting fibers [288]. There are also reports indicating other complications such as swelling and pain [289].

Integration of titanium reinforcements between the two layers of the Gore-Tex® membrane have made it a better construct in terms of space maintenance and mechanical properties [288, 290]. Although some clinical studies reported that the incorporation of titanium reinforcements could not make much difference in the final clinical outcomes [283].

Other examples of non-resorbable membranes include TefGen-FD® made of dense non-porous PTFE [291], Cytoplast TXT-200® made of high-density PTFE [292], and Cytoplast Ti-250® made of titanium enforced high-density PTFE [293].

Since non-resorbable membranes do not degrade in the body, they have to be surgically removed in the follow up phases of treatments. The second surgery can cause additional trauma in which the membrane removal interferes with the growth of new regenerated tissue [294]. Moreover, the second surgery is not favorable for patients in terms of additional cost, pain and therapy period [294]. Thus, bioresorbable materials, made of synthetic or natural materials, became very popular.

2.3.2. Natural bioresorbable membrane

Collagen is one of the main natural materials in production of resorbable GTR membranes due to its low immunogenicity, hemostatic, potential capability to augment the thickness of tissues, and the capability to interact with different cell types including gingival fibroblast cells and periodontal ligament [295, 296].

In a comparison study between collagen and PTFE, it was shown that while PTFE may inhibit the DNA synthesis of gingival fibroblasts and significantly decrease the synthesis of ECM, collagen could facilitate the gingival fibroblast proliferation [297]. The superior attachment capability of collagen membrane to osteoblasts has also been verified [298]

Animal studies showed that it took 8 weeks for BioGide® as a bovine collagen membrane to be degraded in the body, while this degradation time for a rat-tail collagen membrane was 4 weeks [299, 300]. However, both membranes facilitated the periodontal regeneration. Although there were signs of chronic inflammation adjacent to the membranes, the signs were vanished after full degradation of the membranes [299, 300].

BioMend® as a bovine Achilles tendon type I collagen membrane with the pore size of 0.004 μm can also degrade in 4-8 weeks [301]. Good clinical results were reported regarding the use of this membrane [302-304]. However, since it does not have the capability of maintaining space, the clinical effectiveness of the membranes depend of the size of the defects [302-304].

Using Avitene® GTR membranes, made of microfibrillar hemostatic bovine corium type I collagen, some investigators reported the difficulty in surgical handling and also comparable effectivity of this membrane to the control group, evidenced by histological evaluations [305]. Similar results of non-effectivity were also reported using Collistat® hemostatic membrane made of bovine dermis collagen, in which rapid degradation (7 days) was another concern [306].

Among the non-collagen natural materials, chitosan showed good results to be used in resorbable membranes. For example, Kuo *et al*. examined chitosan membranes for GTR applications by preparing the membranes using thermally induced phase separation method and examined its function in the critical sized skull defects of rats [307].

Combination of gelatin and HA were also used for GTR/GBR applications [308]. More specifically matrix of HA precipitate and gelatin were first lyophilized and dissolved in an organic solution, and then went through the electrospinning procedure to make the membrane [308].

Many of other natural materials have also been examined to be used for GTR application. Some of them such as oxydized cellulose [309], dura mater [310, 311], and laminar bone [312] were not successful.

2.3.3. Synthetic bioresorbable membranes

The disadvantages of natural membranes including their high-cost, inadequate toughness and incapability to act as a space maintenance [295], made investigators to continuously look for synthetic materials to make resorbable GTR/GBR membranes.

Aliphatic polyesters are the main group of materials used for fabrication of synthetic resorbable membranes [277]. More specifically, PCL, PLA, poly(hydroxyl butyric acid), PGA, poly(hydroxyl valeric acid), and their copolymers play the important role in in such membranes [277].

The degradation products of these materials can cause unfavorable inflammatory response of living tissues [277, 313]. There are reports that showed using PLA and PGA membranes can cause a reduced defect fill compare to ePTFE membranes [314, 315].

The membranes made by synthetic materials are not as biologically active as the ones made by natural materials [316]. However, they have advantages such as controllable biodegradability, low rigidity, good surgical handling and manageability, the ability to encapsulate drugs and processability [314, 317-319].

Guidor® Matrix Barrier, a bi-layered membrane made by combination of poly(D,L-lactide) (PDLLA) and PLLA which is doped with acetyl tri-n-butyl citrate, is known as the first commercially available synthetic GTR membranes [320, 321]. The degradation time of this membrane is 13 months, and it can hold its barrier characteristics for approximately 6 weeks [320].

Shim *et al*., fabricated a 3D-printed GBR membranes using a combination of PCL, PLGA and β-TCP as shown in Figure 2.11 [322]. This membrane was loaded by rhBMP-2 and used to reconstruct calvaria defects in rabbits. The result showed that the membrane has good space making ability and could heal the calvaria defects within 8 weeks [322].

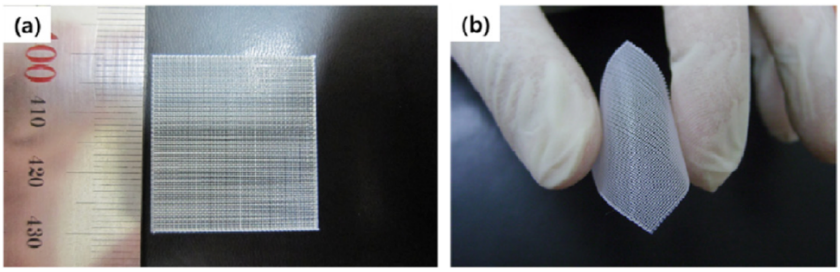

Figure 2.11: (a) 3D-printed PCL/PLGA/β-TCP GBR membrane (2) A display of the membrane flexibility. The figure is obtained from reference [322] with permission.

The same research group evaluated this 3D-printed PCL/PLGA/β-TCP membrane in a beagle implant model and compared its function with the function of a collagen membrane [323]. They concluded that this 3D-printed membrane can maintain its reliability and structure better than the collagen membrane and thus more appropriate for GBR applications [323].

Some other examples of synthetic GTR/GBR membranes are listed in Table 2.3.

Table 2.3: Summarized information about different types of GTR/GBR membranes.

Non-resorbable membranes	
Examples	• GoreTex® made of expanded PTFE (ePTFE) [324] • TefGen-FD® made of non-porous PTFE [325] • Cytoplast TXT-200 ® made of high-density PTFE [326] • Cytoplast Ti-250® made of Titanium enforced high-density PTFE [293]
Advantages	• Excellent surgical handling, • Effective clinical outcome
Disadvantages	• The need for the second surgery to remove the membrane
Natural bioresorbable membranes	
Examples	• BioGide® (Geistlich Biomaterials) made of bovine collagen [327] • BioMend® made of bovine Achilles tendon type I collagen [328] • Avitene ® made of microfibrillar hemostatic bovine corium type I collagen [329] • Collistat® made of bovine dermis collagen [330] • Oxydized cellulose membrane [309] • Dura mater membrane [310, 311] • Laminar bone membrane [312] • Chitosan-based membrane[307] • Gelatin-based membrane [308]
Advantages	• Low immunogenicity • Potential capability to augment the thickness of tissues • Hemostatic • Good interaction with different cell types including gingival fibroblast cells and periodontal ligament
Disadvantages	• Inadequate toughness • Low space maintenance • Relatively high-cost • Difficult surgical handling • Possible rapid resorption

Synthetic bioresorbable membranes	
Examples	• GUIDOR® Matrix Barrier made of PDLLA and PLLA doped with acetyl tri-n-butyl citrate [321] • Resolut Adapt® made of PLGA [324] • Epi-Guide® made of PDLLA [331] • Vivosorb® made of Poly(D,L-lactide-ε-caprolactone) [332] • 3D-printed PCL/PLGA/β-TCP membrane [323]
Advantages	• Controllable biodegradability • Low rigidity • Good surgical handling and manageability • Ability to encapsulate drugs • Processability • Possible good space maintainer
Disadvantages	• Unfavorable degradation product • Possible inflammatory response • Low biological activity

2.4. Ocular Surface/Conjunctival Defect Reconstruction

2.4.1. Ocular surface injuries

The interface between the surface of our eye and outside environment is called the ocular surface [333]. Conjunctival epithelium, a protective thin and transparent film that lines the white part of eyes, is an integral part of the ocular surface [333]. The functions of conjunctiva are as follows:

1) Facilitates the proper performance of the ocular refractive surface.
2) Protects the cornea through the composition of the tear film by discharging aqueous, lipid and mucin [334].
3) Shields the eye from infections by functioning as a mechanical blockade and comprising conjunctiva-associated lymphoid tissue (CALT) [335].

There are several reasons for ocular surface injuries, including autoimmune diseases [336, 337] and chemical or thermal burns [338]. Moreover, during surgeries such as pterygium surgery, in which conjunctival excision is needed, occurrence of injuries at the ocular surface is very common [339]. Conjunctival tumor removal is another reason for damages in ocular surface [340].

It is known that in case of such damages, ocular surface re-epithelization initiates naturally [341-343]. However, it is essential to consider that any delay in having a restored epithelium has significant adverse effects on the function of eyes and may even cause eventual blindness. Such delays in re-epithelization can quickly happen by development of scars and contracture or the

decreased goblet cell density [342, 344, 345]. Damage in the ocular epithelium leads to reduction in the density of goblet cells and mucin layer thickness of the tear film [342, 344], which are essential for keeping the ocular surface wet and clearing debris [345]. Fornix foreshortening and ultimate symblepharon development and entropion in the eye can also occur in cases of conjunctival contracture and decreased surface area of the injured conjunctiva [346, 347].

2.4.2. Autologous implantation

Autologous implantation to treat the injured conjunctiva showed successful outcomes [347-349]. Examples of such autologous implantations include oral mucosa uransplantation [350] and nasal floor mucosa transplantation [351]. However, there are three limitations in regards to this treatment method: 1) lack of goblet cells, 2) limited source of healthy conjunctiva in autoimmune diseases, and 3) cosmetic problems [335].

Due to these practical limitations, allografts implantations—including pericardium [343] and amniotic membrane (AM) [352, 353]—became popular.

2.4.3. Allograft implantation, amniotic membrane (AM)

Among the allografts, AM is known as the most common graft used to treat injured conjunctiva and is actively being used in fornix reconstruction, pterygium surgery, conjunctivochalasis, symblepharon lysis and tumor resections [354].

There are reports indicating the absence of immunogenicity for AM and also other favorable properties, such as anti-inflammatory and anti-fibrotic features [355, 356]. Basically, AM can effectively assist a healthy re-epithelization and produce basement membrane and stroma similar to natural conjunctiva [336, 347, 357, 358].

Although AM treatment exhibits good outcomes in ophthalmic applications [352, 353], there are also reports against its use. For example, enhanced inflammatory responses were reported in some cases of treating the conjunctival injuries by AM, through histological evidence of the grafted tissues [343, 359-361]. It should be noted that there are also numerous reports that indicate the anti-inflammatory effect of AM [336, 338, 347, 356, 357, 362-364]. In another example that questioned the use of AM, Yang *et al*. in 2015 reported deficient goblet density and poor epithelial

stratification during the re-epithelization facilitated by AM for the conjunctival reconstruction [365]. Apart from these unfavorable reports regarding AM, it should be considered that, as an allogenic tissue, risk of disease transmission is always a concern [352].

In an investigation of 326 patients, the infection rate after transplanting AM was 3.4% [366]. Thus, another complication in treatments using AM is the possibility of undesirable host response and infections due to the absence of standardized and sterile preparations of AM. Other disadvantages regarding the use of AM are related to the challenging surgical handling and extensive incidents in the graft site [346, 359, 360], and site opacification [367].

2.4.5. Bioengineered grafts

Due to the above issues with allograft treatment of ocular surface reconstruction, investigators have studied the possibility of using alternatives, such as bioengineered grafts that can facilitate the ocular epithelialization.

Several bioengineered grafts have been designed and examined in animals [341, 342, 344, 361, 368]. For example, in a study by Hsu *et al*., porous collagen-glycosaminoglycan (CG) copolymer matrix was used as a graft material to treat conjunctival defects [369]. The freeze-drying method was used to prepare the porous membrane of CG copolymer matrix with a thickness of 2 mm and 95% pore volume fraction [369]. It went through the crosslinking procedure by dehydrothermal treatment, in which the construct was exposed to the vacuum condition at 105°C for 24 hours. It was further cross-linked by glutaraldehyde treatment [369].

The same membrane was previously made for skin regeneration [370, 371], and the authors examined its function for inhibition of conjunctival scarring [369]. For this purpose, they implanted the graft (membrane with 8 mm diameter and 2 mm thickness) to the lesions of the bulbar conjunctiva in rabbit eyes and compared the results with the ungrafted wounds. They concluded that using the membrane reduced the contraction and improved the development of normal subconjunctival stroma, although the myofibroblasts present at the margin of the wound in both groups of grafted and ungrafted lesions indicated active wound contraction [369]. It should

be noted that the membrane thickness of 2 mm may not be suitable for this study, and a thinner membrane is more desirable for such treatment.

In another study performed by Lee *et al*., scaffolds of modified PLGA (LA:GA of 50:50) with a thickness of 700 μm were fabricated to reconstruct injured conjunctiva [372]. In this study, the scaffolds were made by a solvent-casting particulate-leaching method using NaCl followed by modification with collagen, hyaluronic acid or/and components of AM.

The *in vitro* study was performed on various modified scaffolds using human stromal fibroblasts and corneal epithelial cells. The unmodified scaffolds showed the poorest *in vitro* results, while the scaffolds modified by all components—including collagen, hyaluronic acid and AM, along with the scaffold modified by collagen and hyaluronic acid—presented better results than the scaffolds modified by collagen and AM or only collagen (Figure 2.12). Based on the *in vitro* results, the PLGA scaffold modified by collagen and hyaluronic acid was selected to be implanted in the conjunctival defects of rabbits to assess the ocular surface regeneration in a 4-week study [372].

The results showed that although both the ungrafted and the modified PLGA grafted wounds went through good epithelialization, the contraction in the grafted defects was much lower than the ungrafted ones (6% in the grafted vs. 25% in the ungrafted wounds) [372]. Moreover, random array of the collagen fibers (similar to natural conjunctiva) was formed in the PLGA scaffold, while an aligned array of dense collagen fibers was observed in the ungrafted conjunctival defect. These results indicated the positive effect of synthetic scaffolds on the reconstruction of conjunctival defects in terms of scar formation, regeneration, and contraction [372]. The possible negative influence of PLGA, in terms of acidic oligomers build-up, was not discussed in this study.

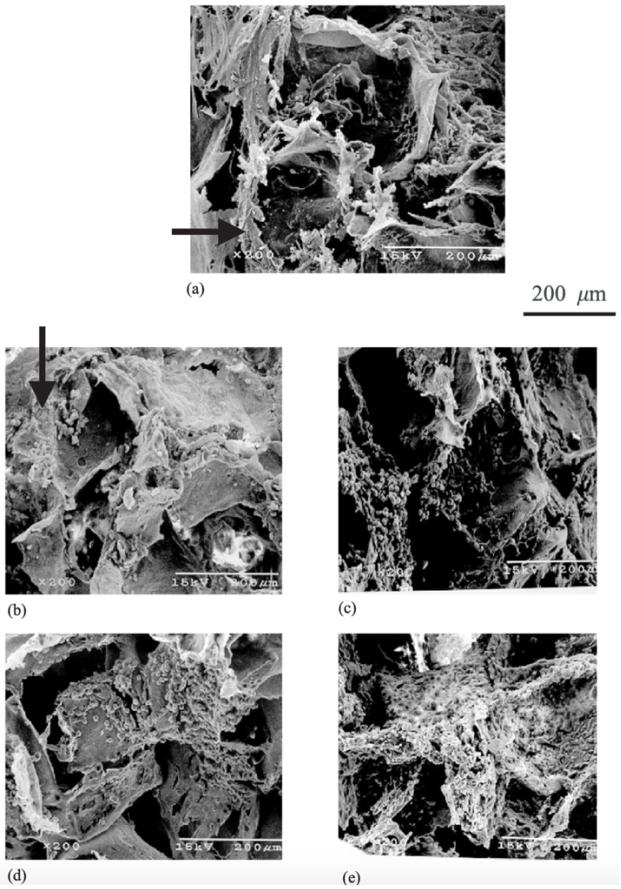

Figure 2.12: Attachment of corneal epithelial cells in the scaffolds made by (a) unmodified PLGA, (b) PLGA/collagen, (c) PLGA /collagen/ hyaluronic acid, (d) PLGA/collagen/AM, (e) PLGA/collagen/AM/ hyaluronic acid, after one day culture of corneal epithelial cells. They are SEM images with 200 times magnification. The arrows pointed out the examples of the attached cells. The PLGA/collagen/ hyaluronic acid scaffold was ultimately selected for the in vivo study of conjunctival reconstruction in rabbits' eyes. The figure is obtained from reference [372] with permission.

As another example of bioengineered grafts, Zhou *et al*. used vitrified collagen to make a conjunctival equivalent for the reconstruction of ocular surface [373]. To make a collagen vitrigel, collagen type 1 went through three steps of gelation, vitrification, and rehydration [374, 375]. The procedure that the study followed to make the conjunctival equivalent is presented in Figure 2.13. Vitrified collagen was implanted in rabbit eyes with promising results in terms of fast re-epithelization, adequate repopulation of goblet cells, proper conjunctival regeneration, and reduced fibrosis and defect contracture [373]. Surgical handling of vitrified collagen membrane was not discussed in this paper.

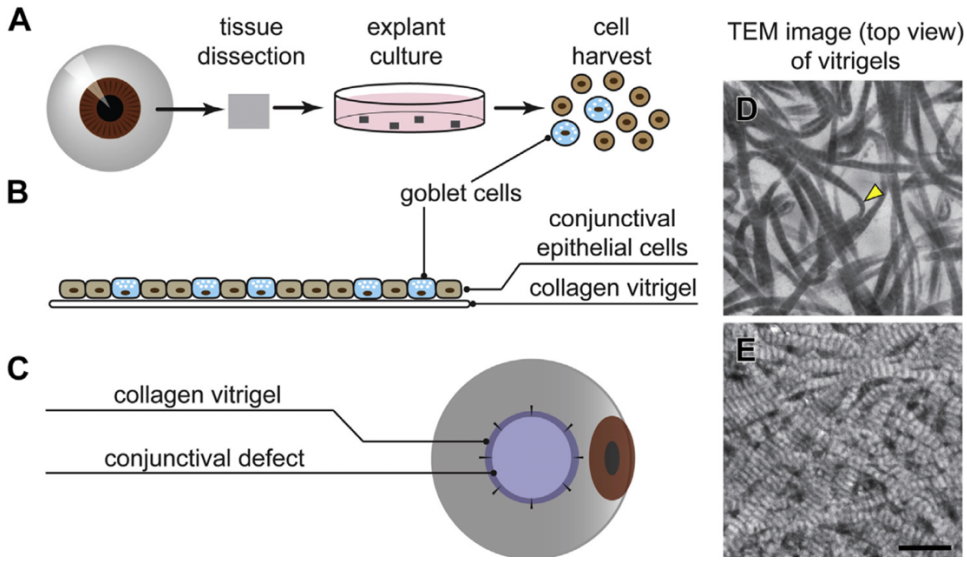

Figure 2.13: Procedure for making the collagen-based conjunctival equivalent for ocular surface reconstruction. (A) Isolating and harvesting of rabbit conjunctival epithelial cells (rCjECs). (B) Cultivation of rCjECs on collagen vitrigel, considering particular goblet cell phenotype. (C) The conjunctival equivalent to reconstruct the conjunctival defect. (D, E) Transmission electron microscopy (TEM) images of fibrillar density and assembly of normal collagen gel and optimal collagen vitrigel, respectively. The arrow indicates the bending of collagen fibril. Scale bar is 500 nm. The figure is obtained from reference [373] with permission.

As seen in the above examples, many of the designed bioengineered grafts have been encouraging in regards to reducing scar development and fornix foreshortening, as well as re-epithelialization [346, 357, 358]. Nevertheless, there are still many disadvantages associated with their use, such as unfavorable thickness, transparency, and elasticity [341-343]. Moreover, possible difficulty in surgical handling and issues with goblet population were not considered in many designs and studies [341, 342, 376]. Table 2.4 summarizes the options for ocular surface/conjunctival defect reconstruction along with the examples and advantage/disadvantages of the treatment options.

Table 2.4: Summary of the treatment options for reconstruction of conjunctival reconstruction and their advantages/disadvantages.

Treatment method	**Autograft**
Examples	• Oral mucosa transplantation [350] • Nasal nloor mucosa transplantation [351]
Advantages	• Reports of favorable outcome in facilitating the re-epithelization
Disadvantages	• Absence of goblets, • Limited source of healthy conjunctiva in autoimmune diseases • Cosmetic problems
Treatment method	**Allograft**
Examples	• Amniotic membrane (AM) [354]
Advantages	• Non-immunogenic • Anti-inflammatory • Anti-fibrotic • Assisting a healthy re-epithelization
Disadvantages	• Reports of deficient goblet density and poor epithelial stratification • Reports of increased inflammatory responses • Risk of disease transmission • Possibility of undesirable host response and infections • Challenging surgical handling • Site opacification
Treatment method	**Bioengineered Graft**
Examples	• Membrane of porous collagen-glycosaminoglycan (CG) copolymer matrix (thickness of 2 mm) (preparation method: freeze-drying) [369] • Scaffold of porous modified PLGA (thickness of 700 μm) (preparation method: solvent-casting particulate-leaching method using NaCl) [372] • Vitrified collagen-based conjunctival equivalent [373]
Advantages	• No risk of transmitting allogenic-associated diseases • Reports of effective re-epithelialization, reducing scar development and fornix foreshortening
Disadvantages	• Possible unfavorable thickness elasticity and transparency • Possible difficulty in surgical handling and inadequate goblet population

2.5. Cartilage Regeneration

Cartilage damage can be prompted by many reasons, including aging, chronic repetitive micro-trauma and traumatic injuries [377]. Cartilage injuries easily spread to the underlying bones, causing osteochondral defects and disturbing the mechanical instability of the joint [378-380]. Since cartilage tissue is not able to restore itself, it is very important to consider an appropriate strategy for its regeneration. Some strategies include palliation, repair and restoration [381].

Palliation can be useful for minor to moderate cartilage abrasions. Arthroscopic chondroplasty and debridement are examples of palliation [382-385]. Repair is usually considered a minimally-invasive and outpatient treatment. Microfracture drilling is an example of this strategy [386-388]. Restoration is a strategy to treat severe cartilage damages [389]. Osteochondral autograft and allograft, as well as autologous chondrocyte implantation (ACI), are the main methods in this strategy.

Patient's own tissue or a donor's body are used for osteochondral autograft and allograft, respectively [390-392]. Due to the limitation of tissues from a patient's body, osteochondral autograft is not a good method for treatment of large defects [393, 394]. Risks of immune rejection, as well as possible transmission of disease, are important disadvantages of treatment involving osteochondral allografts [395, 396].

In the ACI method, introduced in 1994 [397], a small portion of cartilage from the patient's joint is removed and its chondrocytes are extracted and expanded in the laboratory for a few weeks. The expanded cells are returned to the patient's body at the area of the cartilage damage in an open surgical procedure [398-401]. ACI method began with ACI-P (1st generation of ACI), in which the expanded chondrocytes were used as a liquid suspension and transferred into the area of cartilage damage, followed by covering the injured region with periosteum. ACI-P ('P' refers to periosteum) has two main disadvantages including the difficulties of harvesting patients' periosteum [402] and the challenging hypertrophy or ossification of the periosteum [403].

Periosteum is replaced by a collagen cover in the 2nd generation of ACI (ACI-C). Liquid suspension of cells is still used in this generation. Retention of these cells is a major challenge in both 1st and 2nd generations of ACI [402]. To overcome this challenge, the 3rd generation of ACI is developed, in which a 3D environment or object—such as scaffolds—are used to accommodate the cells and allowing their retention [404, 405]. Such scaffolds not only protect the cells, but also can distribute them more homogeneously, help their re-differentiation and make the surgical procedure easier [404, 405]. Here the scaffolds made for tissue engineering applications,

especially the osteochondral scaffolds, have become very useful. Three types of biomaterial-based scaffolds can be used for this purpose [406]:

1) Monophasic scaffolds, in which one material with homogenous porosity is used.

2) Biphasic scaffolds, in which either two different materials or one material consisting of two parts with different porosities are used.

3) Triphasic or multiphasic scaffolds, are scaffolds with three or more materials, or one material consisting of three or more parts with different porosities are employed [406].

Biphasic and multiphasic osteochondral scaffolds are more effective for cartilage regeneration and can be made with both natural and synthetic materials [406-410]. The materials selected for different phases of the osteochondral constructs depend on the fabrication method of the construct [411]. The other factor in material selection is the approach for incorporating the cells into the scaffolds [411]. For example, if the intended approach is encapsulation of cells within the scaffolds during the fabrication, the material selection is different than a scenario in which the cells are seeded into the scaffolds after fabrication [411].

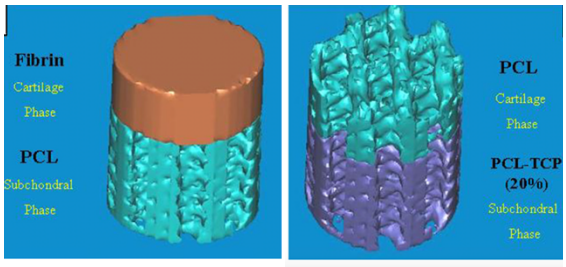

Figure 2.14: Biphasic osteochondral scaffolds made of fibrin/PCL (left) and PCL/PCL-TCP (right). The figure is obtained from reference [412] with permission.

One of the approaches in making such bi/multiphasic osteochondral scaffolds is fabricating separate bone and cartilage parts, then connecting them together by different methods, such as press fitting, suturing or using a glue [413]. For example, in scaffolds made of two phases of fibrin/PCL or PCL/PCL-TCP (Figure 2.14), fibrin glue was used to connect the phases after seeding them separately in chondrogenic (for cartilage regeneration) and osteogenic (for developing bone) media [412, 414]. There are reports indicating that such methods can result in poor connection between cartilage and bone parts and ultimately lead to dissociation [415].

In another biphasic scaffold, agarose gel and decellularized bone were used to make the cartilage and bone parts, respectively (Figure 2.15(A)) [414]. Agarose provided the good mechanical property for immature chondrocytes [414, 416], while the decellularized bone was helpful in terms of making osteoinductive construct with mechanical properties and biochemical composition similar to bone [414]. 500 µm of agarose layer penetrated into the bone portion and solidified at room temperature to form an interface between the two cartilage and bone segments. However, the ultimate interfacial tissue after incubation in an osteochondral bioreactor was distinctive from the interfaces of a native tissue [414].

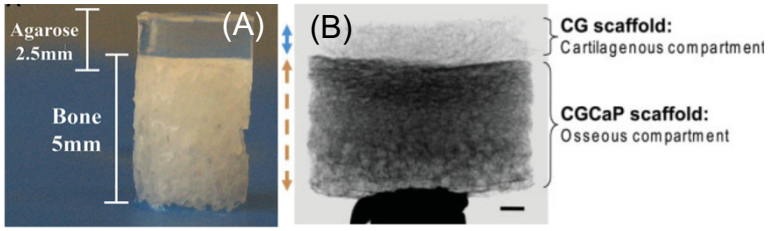

Figure 2.15: (A) A biphasic osteochondral scaffold made of agarose gel and decellularized bone for the cartilage and bone parts, respectively. The figure is obtained from reference [414]with permission. (B) A multiphasic osteochondral scaffold made of collagen type I/glycosaminoglycan/calcium phosphate (CGCaP) for the bone part and collagen type II/glycosaminoglycan (CG) for the cartilage part (Micro-CT image). The scale bar is 1 mm. The figure is obtained from reference [417] with permission.

Attempting to make multiphasic osteochondral scaffolds, Harley *et al*. used sequences of collagen type I/glycosaminoglycan/calcium phosphate (CGCaP) in scaffolds fabricated by employing the freeze-drying technique [418]. In another study by the same research group, they made a specific multiphasic scaffold using a mineralized CGCaP and an unmineralized collagen type II/ glycosaminoglycan (CG) suspensions for osteochondral regeneration (Figure 2.15(B)) [417]. In this scaffold, the interface of the two parts were formed by interdiffusion amongst the suspensions of each layer before freeze-drying [417]. The authors did not investigate the cell proliferation in the fabricated scaffolds.

The method of interfusion to form an interface between phases of an scaffolds was also used by Wang *et al*., where they employed articular cartilage ECM (ACECM) for cartilage regeneration and HA for bone regeneration in a biphasic osteochondral scaffold [419]. It was evident that the cartilage portion could accommodate the rabbit chondrocytes well, yet not many cells were

observed at the interfacial region. The fact that no chondrocytes migrated into the bony portion demonstrated the barrier characteristics of the interface [419].

A grouping of ß-TCP blocks and scaffold-free sheet of mesenchymal stem cell (MSCs) was used by Miyagi *et al.* for osteochondral applications [420]. In a similar strategy, centrifuged chondrocyte cell sheets were employed by Niyama *et al*. [421]. However, it was found that using such cell-sheet method has some technical difficulties and limitations, which are mostly related to the use of one kind of cell culture medium in a cell-sheet construct to stimulate the differentiation of both osteoblasts and chondrocytes [420, 421].

Tuan *et al*. fabricated a biphasic scaffold in which the PCL and PCL/TCP were used for the cartilage and bone parts, respectively [422]. To make this scaffold, a combination of FDM 3D-printing method and electrospinning was used. The investigators have implanted this scaffold in pigs and achieved successful cartilage regeneration. However, it was found that not only the scaffold design affected the results, but also the implantation site had considerable influence (e.g., medial condyle against patellar groove) [422].

A multiphasic scaffold was produced by Jeon *et al*., in which one part was composed of 2% alginate and the other part was a biphasic scaffold made of PCL [423]. A combination of FDM 3D-printing method and electrospinning was used to fabricate this construct [423]. The two phases were press-fitted to allow the alginate to infiltrate into the PCL part. The scaffold was implanted in rats, and the histological analysis showed separation of some alginate from PCL, indicating the failure of the interface [423].

Another biphasic scaffold was developed using freeze-drying technique, in which the cartilage part was made of chitosan/collagen, while the bone part was composed of ß-TCP [424]. A glue composed of cross-linked 1.2 % (w/v) sodium alginate and calcium chloride formed the connection between the two parts [424].

Among other bi/multiphasic osteochondral scaffolds, we can refer to PCL/alginate construct [425], tri-layered PEG-based scaffold with varying ECM composition [426], and bi-layered chitosan/gelatin construct [427].

CHAPTER 3. 3D-PRINTED MEMBRANE AND ITS APPLICATION FOR GUIDED TISSUE REGENERATION

3.0. Introduction

Aim 1 of this thesis is defined as "preparation of a generic biocompatible hydrogel ink and developing 3D-printing protocol to fabricate soft structured membranes". To reach this aim, two major objectives have been planned. The first objective is synthesis of a generic biocompatible hydrogel ink with below characteristics:

A) Compatible to most biomedical applications in terms of the biomaterial composition to be cell-attractant for different cell types.

B) Relatively low-cost to make it appropriate for clinical use by different patients.

C) Easily printable without the rheological complexities, which is common in hydrogels.

Chapter 3 is going to achieve the Aim 1 by starting with production of a pure gelatin ink, which is presented in Section A of this chapter entitled "3D-printed thick structured gelatin membrane for engineering of heterogeneous tissues". Gelatin is known as a low-cost material that is highly biocompatible and can be attached to any cell type [24]. These characteristics of gelatin fulfill parts A and B of Objective 1, and justifie its use as the first attempt in producing the generic biocompatible hydrogel ink described in Aim 1. However, as shown in Section A of this chapter, pure gelatin is not easily printable due to its rheologic properties, and thus, does not match with part C of Objective 1. Hence, Section B of this chapter modifies this pure gelatin ink by addition of elastin and sodium hyaluronate. This section demonstrates how addition of proper amount of these two materials can improve the properties of the ink in a way to fulfill all three parts described in Objective 1 of Aim 1. More specifically, in this section, 17 different compositions of gelatin, elastin and sodium hyaluronate have been examined and the blend of 8% gelatin, 2% elastin and 0.5% sodium hyaluronate (w/v) is selected as the generic biocompatible hydrogel, which will be used in the rest of this thesis for different applications.

Objective 2 of Aim 1, "development of the 3D-printing protocols by identifying all microextrusion printing parameters" has also been studied in Section B of this chapter and all the required parameters are carefully optimized for reproducible printing. Moreover, in this section we hypothesize that a 3D-printed membrane can be designed and produced using the developed ink with the functionality of a GTR membrane. Thus, this section goes further to fulfill Objective 1 of Aim 2, in which the target is "developing the design criteria, fabrication, and characterization of a structured membrane to be used for GTR application." The 150 μm thick 3D-printed membrane—which is designed and fabricated in this section—could robustly separate two cell types of epithelial and connective tissue, which successfully indicates the function of a GTR membrane. To the best of our knowledge, this is the first report of producing a soft hydrogel GTR 3D-printed membrane, which is in accordance with Aim 2 of the thesis to "fill the gaps in using the capacities of 3D-printing technique to fabricate membranes suitable for specific biomedical applications by employing the generic hydrogel ink developed in Aim 1".

Chapter 3A. 3D-Printed Thick Structured Gelatin Membrane for Engineering of Heterogeneous Tissues

Attributed paper: Lobat Tayebi, Morteza Rasoulianboroujeni, Zhanfeng Cui, and Hua Ye. "3D-printed thick structured gelatin membrane for engineering of heterogeneous tissues." Materials Letters, 217 (2018): 39-43.

3A.1. Abstract

Although biological membranes may look like a 2D assembly, they often have complex structures in their 3rd dimension. Using layer-by-layer assembly, 3D-printing can offer an advanced and unique approach for the fabrication of such models. However, printing of some widely used hydrogels, such as gelatin, encounters experimental difficulties due to their rheological properties. In this study, we (a) discuss the complexities involved in printing gelatin, (b) offer a reproducible approach to overcome such difficulties, and (c) present the detailed design criteria and the production process of such 3D-printed gelatin membranes by exemplifying scaffolds suitable for growth of full-thickness oral mucosa as a heterogeneous tissue.

3A.2. Introduction

3D-printing has revolutionized research in the area of organ regeneration and tissue engineering through layer-by-layer deposition of biomaterials. However, whilst hard tissue printing has been achieved with various materials, 3D-printing of soft tissue remains a challenge in many cases [27, 428, 429]. Using such a layered assembly, we have produced a thick structured membrane with different porosity and assembly in the different layers/sides for concurrent growth of dissimilar cell types on each side.

Although alginate is known as the major component of hydrogel inks due to its perfect printability and gelation induced by divalent cations [129], it is not a preferred biomaterial for hosting cells due to the relatively poor cell-material interaction [430]. Gelatin is known as a fibroblast-attractant and macrophage activator biomaterial, which promotes epithelialization and granulation tissue formation. The final engineered construct can be obtained through either post-fabrication cell seeding or cell encapsulation strategies producing cell-laden prototyped scaffolds [100, 181, 195]. The latter could be achieved using gelatin methacrylamide [100] or enzymatic protein crosslinking [195]. Either strategy used, the temperature-dependent sol–gel transition of gelatin plays a critical

role in printing procedure. Challenging printing procedure of gelatin-based inks due to premature gelation of this biopolymer, may result in low quality parts [192]. While gelatin could be blended with other polymers [181, 193] to improve printability, for pure gelatin/modified gelatin, performing adaptations on the 3D-printer has been suggested to ameliorate the processing of gelatin hydrogels [100]. However, such strategy might lead to extra cost and might not be applicable to every device.

This study presents the detailed method of printing gelatin as well as the specific design criteria used for producing the membranes suitable for engineering of heterogeneous tissues. The rheological properties of gelatin have been examined. The 3D-printer machine employed in this study was EnvisionTEC 3D-Bioplotter® which uses a pneumatic control for applying pressure. The advantages of a pneumatic control are its low-cost and cleanness, as well as being safe and easy to operate [431]. The disadvantages of such a system include the deficiency of precision controls, high sensitivity to vibrations and being loud and noisy [431].

The present study is expected to increase the fundamental understanding of the effect of rheological parameters on the 3D-printing procedure of gelatin. The outcome of optimization is a 3D-printed construct with potential applications in tissue engineering of different membrane-shaped organs such as oral mucosa, skin and eye conjunctiva.

3A.3. Materials and methods

Gelatin (Type A, from porcine skin, Bioreagent grade, Gel strength ~300 g Bloom) was purchased from Sigma-Aldrich, (St. Louis, MO, USA). 1-Ethyl-3-(3-dimethylaminopropyl)carbodiimide (EDC) and N-Hydroxysuccinimide (NHS) were obtained from Alfa Aesar (Haverhill, MA, USA) EnvisionTEC 3D-Bioplotter® (Manufacturer Series, Germany) was used for the 3D-printing of scaffolds.

The low magnification images of the scaffolds were taken using a Dino-lite Digital Camera. The high magnification imaging of the scaffolds was performed using a JEOL-JSM-6510 Scanning Electron Microscope (SEM, Japan). The samples were dehydrated by immersing in 50, 70 and 90 %v/v ascending ethanol series for 20 minutes each. Then they were air-dried overnight, and

sputter coated with gold before SEM imaging. Rheological properties of the ink were measured using a shear rheometer (Kinexus, Malvern, UK).

To print any material, seven parameters had to be systematically adjusted: 1) Formulation and rheology of the ink, 2) Material container temperature, 3) Platform temperatures, 4) Dispensing needle diameter, 5) Pressure, 6) Printing speed, and 7) Pre- and post-flow delays.

In our experiment, a 15% (w/v) solution of gelatin in deionized (DI) water was prepared for printing. Gelatin solution was printed at a material container temperature of 37°C and a platform temperature of 22°C using a 250 µm-diameter needle (25G). Nordson EFD Optimum® general purpose disposable stainless steel blunt end dispensing tips (1/2 inch) were used in this study.

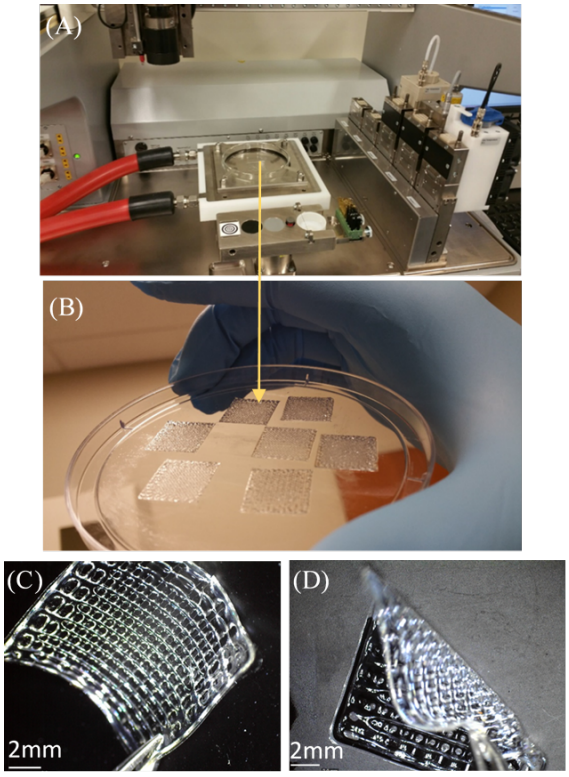

Figure 3A.1: 3D-printer set up (A). Macroscopic images of fabricated 3D-printed scaffold immediately after printing (B), and after crosslinking (C, D). As can be seen in the images, the scaffolds are bendable with easy-handling properties.

Printing pressure and speed were adjusted to 0.6 bar and 15 mm/s, respectively. Pre- and post-flow delays were zero. The reasons for selecting the above printing parameters are described in the "Results and discussion" section. The ink was solidified on the platform through sol-gel transition.

The scaffolds were cross-linked by soaking in a 12mg/ml EDC and 1.5mg/ml NHS in 90% ethanol solution for 4 hours. To remove the toxic cross-linking agent, the scaffolds were soaked in one liter of DI water which was replaced every hour for 3 hours and before finally rinsing with DI water. After dehydration using 50, 70 and 90 %v/v ethanol, the scaffolds were stored in 90 %v/v ethanol in a -20℃ freezer until used when they were rehydrated and washed carefully as described above. The printing process and macroscopic view of the printed membrane can be seen in Figure 3A.1.

3A.4. Results and discussion

Printing Criteria: To describe the difficulties in finding the optimal gelatin printing parameters, rheological analysis has been performed.

Figure 3A.1 presents the macroscopic images of the fabricated gelatin 3D-printed scaffold. To print successfully, the temperature of 1) the cartridge where the ink is kept, 2) the platform and 3) the dispensing needle are all of great importance. While the first two points can be adjusted precisely, the latter is dictated by heat transfer principles. The temperature of the cartridge must be set above the sol-gel transition temperature and the temperature of the platform needs to be set below this temperature.

The gel point of the ink was determined using oscillatory sweep measurements. The gelation temperature can be defined by observation of a frequency-independent value of damping factor (tanδ) obtained from a multi-frequency plot for a temperature sweep measurement [432]. The sol-gel transition temperature of gelatin solution was found to be between 27℃ and 29℃ (Figure 3A. 2(A)). Therefore, the cartridge and platform temperatures needed to be above 29℃ and below 27℃, respectively.

The shear stress and shear viscosity of the ink as a function of shear rate is demonstrated in Figures 3A.2(B) and 3A.2(C) for different temperatures. The high shear stress and viscosity at 19-28°C was because the measurements were conducted below the gel point. At these temperatures, the ink showed a shear thinning behavior as a result of disruption in physical network formed by hydrogen bonding between helices. It may come to mind that this apparent flow could be an artefact of delamination of the gel from the rotating plate. This assumption could be declined through

considering oscillation data where complex viscosity vs. angular frequency shows the same trend (Figure 3A.2(D)). It should be noted that the shear stress, and consequently the pressure required to create a certain deformation and subsequently flow, is extremely higher when the ink temperature is below the gel point. As can be seen in Figure 3A.2, viscosity could be decreased by increasing the temperature from 31°C to 40°C. The ink indicated Newtonian behavior (coefficient of determination, R^2, greater than 0.99) at temperatures higher than 28 °C. Figure 3A.2(E) displays the flow rate-pressure diagram for two standard dispensing needles at 37℃. The relationship between the flow rate and pressure was nearly linear (coefficient of determination, R^2, greater than 0.95) for pressures between 0 and 1.5 bar and two dispensing needles of 250 and 400 µm in diameter. Since the ink represents Newtonian behavior at 37℃, the Hagen- pressure and the flow rate are related by: $Q = \frac{\pi R^4 \Delta P}{8 \mu l}$, in which Q is the flow rate, R is the radius of the pipe, P is pressure, µ is dynamic viscosity and l is the length of the pipe. The linear relationship between the pressure and flow rate, as well as the ratio of the slopes of the lines $((R_2/R_1)^4$, R_2=400 µm, R_1=250 µm), suggests that the flow of the ink through the needle followed the Hagen-Poiseuille's equation.

As can be seen in Figure 3A.2(C), the viscosity remained almost constant for the temperatures between 34-40℃. It comes to mind that there should be no significant difference when any temperature in this range is selected. One should note, however, that the dispensing needle temperature is dictated by the balance between cartridge, room and platform temperature. When the printer is in standby mode (i.e. not printing and no material flows), the temperature of the remaining material in the dispensing needle starts to decrease and eventually drops below the gel point because of contact with room temperature. This results in obstruction of the dispensing needle and interruption of printing. However, this phenomenon does not occur instantaneously and there is a certain lag time between the standby and the onset of obstruction. This period is referred to as the "the golden time" in this study. To investigate the effect of cartridge temperature (i.e. the initial temperature of the material in the dispensing needle), as well as the effect of dispensing needle diameter on the golden time, rheological assessment with a plate-plate geometry was employed. The ink was loaded between the plates with various gap distances (0.2-0.5 mm) at

different temperatures ranging from 37℃ to 31℃. The maximum cooling rate of the instrument was used to cool down the ink to 22℃ while measuring the complex viscosity as a function of time in oscillatory mode at shear strain of 1% and frequency of 5 Hz. The results are shown in Figure 3A.2(F-I). Each gap distance is expected to resemble a certain needle diameter; if contact surface to volume ratio (A/V) is taken into the account, the gap distance of 0.2 mm resembles the blue needle (D = 400 μm) characteristics (A/V = 10 mm^{-1}). However, this ratio is relatively big for the red needle (D = 250 μm, A/V = 16 mm^{-1}) making it difficult to run the experiment with the resembled gap distance. By taking the time required to reach the target temperature by the rheometer into consideration, the period in which the complex viscosity remained unchanged analogizes the golden time though not precisely equal to it and the time at which the complex viscosity starts to ascend resembles the onset of needle obstruction. The delay of the rheometer was found to be in the range of 20-30 s as shown in Figure 3A.2(F-I). Furthermore, the temperature of the rheometer platform is not necessarily equal to the material temperature as there is also a lag time to reach the equilibrium temperature applied by the rheometer. Such limitations cause the golden time measured using the rheometer to be longer than its actual value. As can be seen in Figure 3A.2, the golden time was found to around 40, 35, 25 and 20 s for cartridge temperatures of 37, 35, 33, 31 °C, respectively. Increasing the temperature from 31℃ to 37℃ can approximately double the golden time. On the other hand, the needle diameter does not seem to have had a significant effect on the golden time or the onset of obstruction at least up to A/V = 10 but it did influence the speed of viscosity increase; the larger the gap (diameter), the slower the complete obstruction. Figure 3A.2(J) represents the length of time required to reach the complex viscosity of 10 Pa.s (including the delay time of the rheometer) as a function of contact surface to volume ratio (A/V). The significance of the effect of cartridge temperature compared to the contact surface to volume ratio on the golden time is again perceptible.

With regard to the effect of temperature on viscosity and golden time, 37℃ was selected as the cartridge temperature. A 250 μm needle was utilized since it was assumed not to have a significant effect on the golden time, it regulated flow rate variations caused by pressure fluctuation and yielded a better resolution because of lower strand thickness. The platform temperature was set at

22℃ which was well below the gel point and very close to room temperature to avoid accelerated needle obstruction upon contact. The platform temperature affects the gelation time which in turn may influence the shape fidelity of the strands. Further investigation is required to optimize the

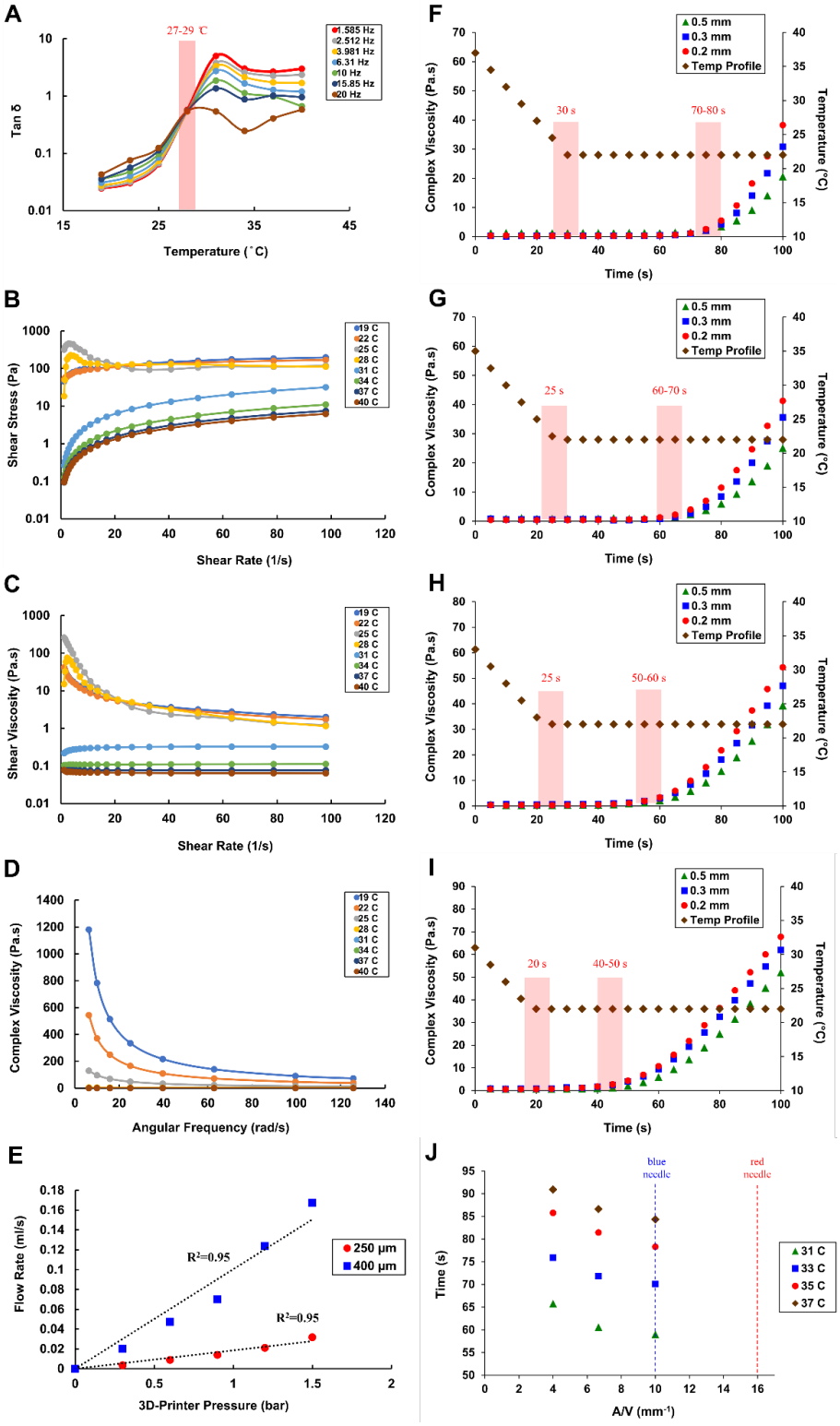

Figure 3A.2: Rheological and flow characterization of Gelatin 15% (w/v) aqueous solution as the ink for printing; sol-gel transition detection through oscillatory sweep measurements (A);

shear stress and shear viscosity as a function of shear rate (B, C); complex viscosity as a function of angular frequency (D); flow rate as a function of applied pressure (E); complex viscosity change over time when cooling the solution from 37℃ (F), 35℃ (G), 33℃ (H) or 31℃ (I) to 22℃ with maximum cooling rate; and the required time for the complex viscosity of the ink to reach 10 Pa.s as a function of surface to volume ratio (J).

platform temperature so that the shape of the strands is kept flawlessly while the printing is not disrupted because of needle obstruction.

To print an appropriate scaffold for oral mucosa as an example of heterogeneous tissue, the design criteria were as follows:

1. An appropriate thickness for oral mucosa scaffold ranges from 0.2 mm to 2 mm.

2. In a novel model in oral mucosa scaffold designs, we printed the membrane in gradient shape with a large pore size on one side for the growth and penetration of connective tissue (i.e. fibroblasts) and a small pore size on the other side to accommodate keratinocytes (i.e. the epithelial layer). It is worth mentioning that the membrane in this study has been designed for post-fabrication cell seeding. If cell encapsulation is desired, gelatin methacrylamide or enzymatic protein crosslinking can be used.

3. The keratinocytes side needed to be permeable (i.e. no zero pore size) to allow nutrient diffusion and avoid reduced epithelial growth and differentiation.

Considering the above criteria and using the presented protocol, we printed our main scaffold by the following configurations: Using a 250μm-diameter needle, six layers were printed while the distance between strands at each layer was set to approximately 300 μm, 300 μm, 450 μm, 450 μm, 600 μm and 600 μm from the bottom to the top to achieve a gradient in pore size. The first and last layers' pore sizes are approximately 100 and 400 μm (see Figure 3A.3 (A-B)). The angles of strand-printing were selected to be 0º and 90º degrees on every other layer. The thickness of this membrane was initially 500 μm and after cross-linking it shrunk to 300 μm. Such a low thickness might be a result of possible shape infidelity, stretching of the strand because of high printing speed and water evaporation from the sample.

If required, smaller pore size on the epithelial side of the scaffolds can be achieved by changing the angle of the strand-printing on the last two layers to 45 º and 135 º instead of 0 º and 90 º (see

Figure 3A.3(C)). The pore size can be reduced significantly by changing the angle of strands in various combinations. Figure 3A.3(D) demonstrates the SEM images of the membrane.

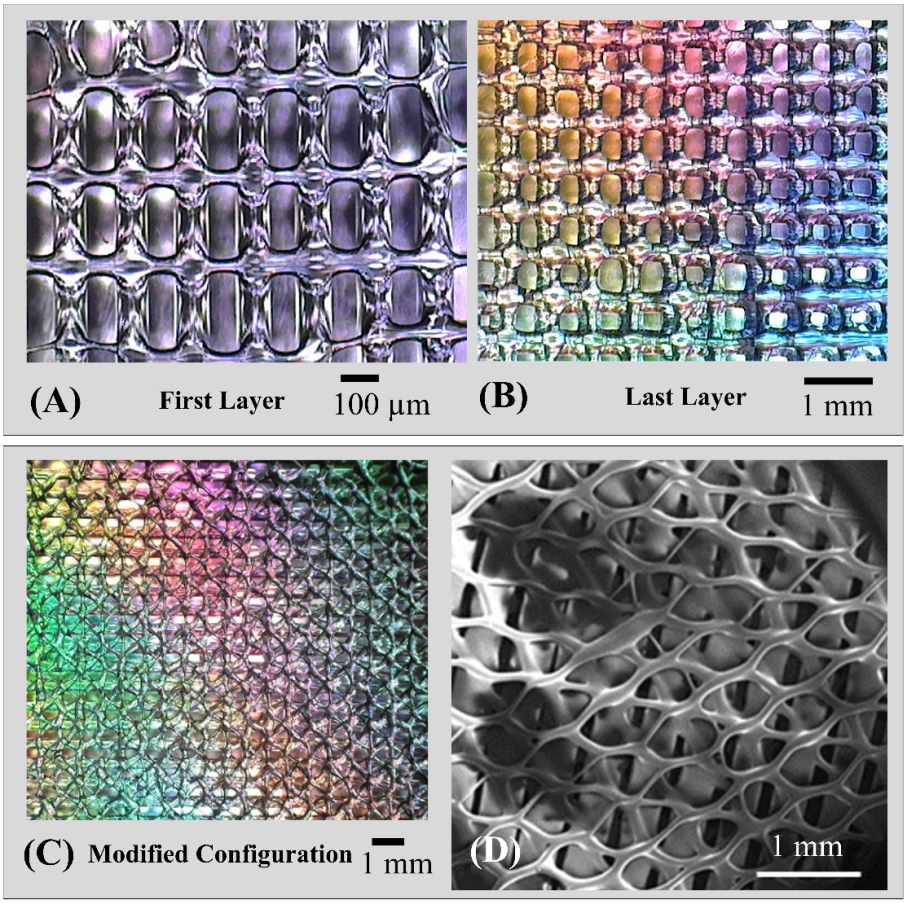

Figure 3A.3 : Examples of the first and last layers of the gradient membrane are shown in panel (A) and (B). The smaller pore size can be easily achieved by altering the angels of strands in the printing process (C). Panel (D) shows an SEM image of the printed membrane.

3A.5. Conclusion

Employing a 3D-printing technique and using gelatin as the ink, we have introduced a novel scaffold design with potential application for tissue engineering of heterogeneous membrane-shape organs. The detailed printing process for gelatin, after consideration of its rheological characteristics is presented in this study.

As a particular example, the design criteria described in this study have been used to produce a membrane that could be potentially used for oral mucosa tissue engineering.

Acknowledgment:

This work was supported by China Regenerative Medicine International Limited (CRMI).

Statement of Authorship for joint/multi-authored papers for PGR thesis

To appear at the end of each thesis chapter submitted as an article/paper

The statement shall describe the candidate's and co-authors' independent research contributions in the thesis publications. For each publication there should exist a complete statement that is to be filled out and signed by the candidate and supervisor **(only required where there isn't already a statement of contribution within the paper itself).**

Title of Paper	3D-Printed Thick Structured Gelatin Membrane for Engineering of Heterogeneous Tissues
Publication Status	■Published □ Accepted for Publication □Submitted for Publication □Unpublished and □Unsubmitted work written in a manuscript style
Publication Details	Lobat Tayebi, Morteza Rasoulianboroujeni, Zhanfeng Cui, and Hua Ye. "3D-printed thick structured gelatin membrane for engineering of heterogeneous tissues." Materials Letters, 217 (2018): 39-43. https://doi.org/10.1016/j.matlet.2018.01.032

Student Confirmation

Student Name:	Lobat Tayebi		
Contribution to the Paper	Contribution in: developing the idea, planning the experiment, performing analysis on samples, interpreting the data, preparing the manuscript		
Signature 		Date	16/09/2019

Supervisor Confirmation

By signing the Statement of Authorship, you are certifying that the candidate made a substantial contribution to the publication, and that the description described above is accurate.

Supervisor name and title: Hua Ye, DPhil, Associate Professor, Institute of Biomedical Engineering Department of Engineering Science, University of Oxford Zhanfeng Cui, Professor, Institute of Biomedical Engineering Department of Engineering Science, University of Oxford		
Supervisor comments		
Signature 	Date	25 Sep, 2019

This completed form should be included in the thesis, at the end of the relevant chapter.

Chapter 3B. 3D-Printed Membrane for Guided Tissue Regeneration

Attributed paper: Lobat Tayebi, Morteza Rasoulianboroujeni, Keyvan Moharamzadeh, Thafar KD Almela, Zhanfeng Cui, and Hua Ye. "3D-printed membrane for guided tissue regeneration." Materials Science and Engineering: C, 84 (2018): 148-158.

3B.1. Abstract

Three-dimensional (3D) printing is currently being intensely studied for a diverse set of applications, including the development of bioengineered tissues, as well as the production of functional biomedical materials and devices for dental and orthopedic applications. The aim of this study was to develop and characterize a 3D-printed hybrid construct that can be potentially suitable for guided tissue regeneration (GTR). For this purpose, the rheology analyses have been performed on different bioinks and a specific solution comprising 8% gelatin, 2% elastin and 0.5% sodium hyaluronate has been selected as the most suitable composition for printing a structured membrane for GTR application. Each membrane is composed of 6 layers with strand angles from the first layer to the last layer of 45, 135, 0, 90, 0 and 90°. Confirmed by 3D Laser Measuring imaging, the membrane has small pores on one side and large pores on the other to be able to accommodate different cells like osteoblasts, fibroblasts and keratinocytes on different sides. The ultimate cross-linked product is a 150 μm thick flexible and bendable membrane with easy surgical handling. Static and dynamic mechanical testing revealed static tensile modules of 1.95 ± 0.55 MPa and a dynamic tensile storage modulus of 314 ± 50 kPa. Through seeding the membranes with fibroblast and keratinocyte cells, the results of *in vitro* tests, including histological analysis, tissue viability examinations and DAPI staining, indicated that the membrane has desirable *in vitro* biocompatibility. The membrane has demonstrated the barrier function of a GTR membrane by thorough separation of the oral epithelial layer from the underlying tissues. In conclusion, we have characterized a biocompatible and bio-resorbable 3D-printed structured gelatin/elastin/sodium hyaluronate membrane with optimal biostability, mechanical strength and surgical handling characteristics in terms of suturability for potential application in GTR procedures.

3B.2. Introduction

Barrier biomaterials have been developed over the past decades for guided tissue regeneration (GTR) which have a wide range of applications in medicine and dentistry.

GTR is a surgical procedure that uses barrier membranes to direct the growth of new tissues at sites with insufficient volumes or dimensions of tissue for proper function, aesthetics or prosthetic restoration [433-435]. While GTR mostly deals with soft tissue, guided bone regeneration (GBR) focuses on separation of bone from the connective tissue [275, 436].

Intraoral applications include regeneration of periodontal bone defects, ridge augmentation prior to dental implant placement in atrophic bone and management of bone defects following trauma, surgical resection of cancer, and repair of cleft palate [434, 437]. Extra-oral applications include orbital floor reconstruction following traumatic fracture of the orbital floor, spinal fusion surgery, orthopedic applications for repair and regeneration of radial bone, rib and femoral bone defects, and neurosurgical applications such as prevention of cerebrospinal fluid leakage from dura mater sites [438].

In addition to favorable biocompatibility and biodegradability, a GTR membrane should have suitable pore size to prevent excessive penetration of oral keratinocytes into the bone defect from one side but allow neovascularization and bone formation from the connective tissue side of the membrane. The three-dimensional topography of the membrane with interconnecting pores and channels is also important to achieve its intended function. Furthermore, the membrane should have good mechanical and handling properties and sufficient tear strength to be able to be sutured and stabilized in place to allow the infiltrated bone cells to differentiate into bone without being disturbed during normal oral function [439]. Mechanical stability facilitates the attachment since it allows additional fixation to be applied to the flexible membranes [440], thereby inhibiting the development of fibrous tissue between the bone and the membrane [441, 442]. It has been observed that bone formation is significantly enhanced when the resorbable membrane is tightly attached and immobilized to the bone surface [443]. Other characteristics of the membrane such as architecture, pore size and permeability can also affect its efficiency. Pore size of a construct has been reported to influence cell adhesion [444, 445] which in turn facilitates coronal migration

of the progenitor cells from periodontium in case of barrier membranes since anchorage dependent cells need to adhere to a substrate prior to begin proliferation, migration, differentiation, and maturation [446]. For example, the presence of connective tissue cells on the inner surface of the retrieved membrane has been reported to be predictive of enhanced periodontal tissue regeneration [447]. Cell attachment to the barrier may not only help clot formation and wound stabilization [448], but also stabilize the barrier to diminish membrane micromovement and prevent the disruption of newly formed attachments [449]. Besides, it has been shown that the use of semi-permeable membranes (made of ePTFE) results in a relatively greater speed and quantity of osseous replacement compared to the high-density non-permeable ones. Such a difference has been attributed to the capability of the membranes to exclude cells lacking osteogenic potential and to allow free diffusion of nutrients and growth factors [450].

Non-resorbable membranes initially developed for GTR included expanded polytetrafluoroethylene (e-PTFE) (Gore-Tex® Periodontal Material), titanium reinforced ePTFE (Cytoplast™), high-density-PTFE (TefGen-FD®), or titanium mesh. The main disadvantage of these non-resorbable membranes was the need for a second surgery to remove the membrane. Bio-resorbable membranes were then developed to obviate the need for the second surgery. In addition, such membranes also allow imaging because of their radiolucency as well as reduce stress shielding of the newly formed bone [451]. The most commonly used GTR membranes are made of natural materials. Most of the commercialized bio-resorbable GTR/GBR membranes are made of collagen, such as BioGide® (Geistlich Biomaterials) made of bovine collagen [327], BioMend® made of bovine Achilles tendon type I collagen [328], Avitene® made of microfibrillar hemostatic bovine corium type I collagen [329], and Collistat® made of bovine dermis collagen [330]. Due to the recognition of collagen membranes in clinical GTR/GBR applications, it is a reasonable reference material for any GTR membrane made of natural materials. Thus, in this study, we consider collagen membrane—and more specifically the BioGide® membrane (Geistlich Biomaterials)—as a reference material and will compare the mechanical and degradation characteristics of our membranes with its properties using the values described in the relevant literatures.

There are several limitations associated with the use of collagen-based membranes. These include fast resorption rate and premature loss of material, poor handling characteristics and mechanical strength and risk of disease transmission from animal products and autoimmunization. Synthetic membranes made of various polymers such as poly glycolic acid (PGA), poly lactic acid (PLA), and polycaprolactone (PCL), have been developed to address these issues. However, synthetic bio-resorbable membranes also suffer from lack of control over the resorption rate dictated by factors like local pH and lack of inertness because of unfavorable reactions during degradation [452]. Gelatin-based membranes could be considered as an alternative to collagen ones as gelatin reduces the concerns of immunogenicity and pathogen transmission associated with collagen while provides integrin binding sites for cell adhesion [453]. Other biopolymers and proteins could be added to improve the properties of the membrane. For example, addition of elastin, an extracellular matrix protein, improves elasticity, self-assembly, long-term stability, and biological activity of biomaterials [454] while addition of hyaluronic acid, an essential component of the ECM, may facilitate cellular signaling, wound repair, morphogenesis, and matrix organization [455].

Various techniques are being used for making 3D constructs for specific applications [40, 456, 457]. Amongst all of the additive manufacturing methods such as stereolithography (SLA), fused deposition modeling (FDM), and selective laser sintering (SLS) are the most advanced ones, however, the pressure-assisted FDM process is one of the most popular for tissue engineering and bioprinting applications [61, 458-460]. Advances in 3D printing technology have permitted optimization of multiple characteristics of biomaterials for their intended clinical application. Biomaterials, including (i) polymers and ceramics, (ii) natural and synthetic bioplastics, (iii) hydrogels in combination with living cells and/or growth factors, and (iv) proteins and biomolecules, as well as their hybrid structures, can all be printed using these processes [6, 461-463].

For printing biomaterials using pressure-assisted FDM process, the bioink is essentially a material/composite of the appropriate viscosity that is capable of being extruded under pressure through a micro-scale nozzle orifice or a micro-needle [84]. The mechanical integrity of the

extruded structures can be controlled through thermal or chemical crosslinking, or multi-material channel approaches post-deposition [464-466]. During the process, the biomaterial is contained in a temperature-controlled cartridge inside a three axis robotic print head with a nozzle or micro-needle. Deposition takes place by pneumatic pressure, plunger or screw-based extrusion of the material as a continuous filament through the nozzle or micro-needle orifice onto a substrate. The substrate can be a solid (e.g., a culture dish), a liquid (e.g., growth media), or a gel-based substrate material. The substrate, as well as the deposition setup, can be contained within a sterile and climate-controlled environment, further enabling the use of temperature sensitive biomaterials. The print head trajectory is guided by layered data obtained from the digital model of the construct to be laid out. The rheological properties of the biomaterial, extrusion temperature, and nozzle type used and the applied pressure are the critical parameters that affect the physical and biological characteristics of the printed construct [465, 467, 468].

Bioinks are an integral part of bioprinting technology [30, 84, 469]. It is not the bioprinting process parameters alone that are important, but also the material-process interactions that govern the viability and success of the resultant constructs. Hence, developing appropriate bioinks and comprehensively characterizing their rheological behavior as well as mechanical, and biological characteristics of the printed construct out of them is critical to the success of bioprinting. It is accepted that this development and characterization will have to be process specific [84, 462].

After developing an appropriate bioink, we characterized a biocompatible and bio-resorbable 3D-printed structured gelatin/elastin/sodium hyaluronate membrane. It is known that gelatin is biocompatible, low-cost and cell-attractant, and sodium hyaluronate improves chemical signaling among cells [470-472]. Elastin may also benefit long-term stability, elasticity, and biological activity of the membrane [470]. The optimal biostability, mechanical strength, surgical handling characteristics and *in vitro* biocompatibility to be used for GTR surgical procedures have been explored in this study.

In sum, the aim of this study is to print a structured membrane with optimal physical and biological properties for GTR application. More specifically, the key target property of the 3D-printed construct fabricated in this study is the capability of separating epithelial layers from the connective

tissue, while having the reasonable physical properties comparable to the properties of widely used collagen membranes for GTR applications. Moreover, according to the aims and objectives of this thesis, it is expected that the materials by which this membrane is fabricated have these two target properties: being low-cost to make it appropriate for clinical use by different patients, and being easily printable without the rheological complexities.

3B.3. Materials and methods

3B.3.1. Materials

Elastin with molecular weight 60KDa (Elastin-Soluble, No. ES12) was purchased from Elastin Products Company, Inc. (USA). Sodium hyaluronate (Research Grade, 500KDa-749KDa) and gelatin (Type A, from porcine skin, Bioreagent grade, Gel strength ~300 g Bloom) were obtained from Lifecore Biomedical (USA) and Sigma-Aldrich (USA), respectively. 1-Ethyl-3-(3-dimethylaminopropyl) carbodiimide (EDC) and N-Hydroxysuccinimide (NHS) were purchased from Alfa Aesar (USA).

Penicillin, streptomycin, amphotericin B, complete Dulbecco's Modified Eagle Medium (cDMEM) and ascorbic acid were purchased from Sigma-Aldrich (UK). Collagenase type I solution was obtained from Gibco (USA) and prestoblue (PB) assay was purchased from Invitrogen (UK).

3B.3.2. Optimizing the formulation of the bio-ink and membrane printing

To select the most suitable composition of materials, different aqueous solutions of gelatin, elastin and sodium hyaluronate were prepared. Each solution was molded into a 24 well plate dish (150 µl in each well). After crossing linking with 6 mg/ml EDC and 0.75 mg/ml NHS in 70% ethanol for 0.5-2 hour, molded thin membranes with the approximate thickness of 200 µm were obtained and washed with a large amount of deionized (DI) water. After primary screening, seventeen different memebranes (described in Supplementary Information 1 (SI1) sent to the surgeons for their evaluation.

Three solutions with the compositions described in Table 3B.1 were selected for the rheology analyses.

Table 3B.1: Sample specification for the primary rheometry experiment. The w/v refers to the weight of the materials in DI water.

	Gelatin concentration (w/v)	Elastin concentration (w/v)	Sodium hyaluronate concentration (w/v)
Sample 1	15	-	-
Sample 2	15	2	0.5
Sample 3	8	2	0.5

The gel point of different solutions was measured using a Malvern Kinexus rheometer with disc (D=20 mm) and parallel plate geometry. The distance between the disc and plate was adjusted to be 0.3 mm. Oscillation and viscometry experiments were conducted at different temperature ranging from 20 to 40ºC. Oscillatory shear measurements were performed in the linear viscoelastic regime (shear strain 2%) where the storage and loss modulus are independent of the strain amplitude. Scanning from high temperatures to low temperatures, different frequencies were scanned at each temperature. The sample with the closest gel point to room temperature was selected as the bio-ink to be printed. The rest of the experiment was carried out for the constructs printed using selected bio-ink.

After optimizing the ink composition, EnvisionTEC 3D-Bioplotter® (Manufacturer Series, Germany) was employed for the 3D printing of scaffolds. The camera of the 3D-Bioplotter® was utilized for the imaging of each layer during the process.

The selected solution was printed at material container temperature of 30-32 °C, platform temperature of 11 °C, printing pressure of 0.6-1.2 bar, speed of 20 mm/s using a 250 µm-diameter needle. Pre- and post-flow delays were set to zero. Each membrane contained 6 layers with strand angels of 45, 135, 0, 90, 0, 90° for layers 1 to 6, respectively. Distances between strands were set to 0.6 mm for the first 4 layers and 0.9 mm for the last 2 layers. Hardening of the ink happened almost immediately after being dispensed from the needle and touching the platform through the capability of the solution to form a solid gel at lower temperatures. The 3D-printed membranes were cross-linked by soaking them in 6 mg/ml EDC and 0.75mg/ml NHS in 70% ethanol for 0.5-2 h. To remove the residual cross-linker, the membranes were washed carefully through soaking them in a large amount of DI water (500 ml) for 1.5 h. The water was replaced with fresh water

every 0.5 h. The prepared membranes were stored in 100% ethanol inside a -20 °C freezer to be used after rehydration when needed.

3B.3.3. Morphology, surface roughness and thickness of the membranes

A Dino-lite digital microscope camera was employed to obtain low magnification photos of the membranes after complete preparation. LEXT OLS4000 3D Confocal Laser Scanning Microscopy (Olympus, Japan) was used for imaging of the membranes. Moreover, the surface morphology and roughness were analyzed using the 3D Laser Measuring Microscopy. The thickness of the membranes was measured using a Marathon Electronic Digital Micrometer. The thickness values were confirmed by scanning the edge of the membrane using the 3D Laser Measuring Microscope.

3B.3.4. Static and dynamic mechanical properties

Static tensile properties of the membrane were measured using a universal tester (AGS-X 5kN, Shimadzu). For this purpose, the samples cross-linked for 0.5 h were fixed into screw flat tensile grip and underwent tensile test using a 1 kN load cell and crosshead speed of 1 mm/min. Dynamic mechanical analyser (DMA 8000, Perkin Elmer) was used to measure the dynamic tensile storage modulus of the printed membranes after cross-linking for 0.5 h. The samples were sized into small pieces appropriate for the DMA analysis (approximately 5.0 mm × 5.0 mm). The samples were anlyzed in tension mode while soaked in a fluid bath. The frequeny sweep from 0.1 to 25 Hz was conducted at a dynamic displacement of 0.05 mm.

3B.3.5. Degradation

The degradation rate of the samples (15 mm × 15 mm) with different cross-linking times (i.e. 0.5, 1.5, 2 h) were measured through immersing the samples in 10 ml Phosphate-buffered saline (PBS) each and storing them in a shaking incubator at 37℃. First, the intial weights of the samples were recorded. Then, at cartain time intervals, samples were taken out and their weights were recorded after excess water was removed. The ratio of the weight of each sample at that time point to the initial weight of the sample was reported against the time of immersion (weight loss). The measurements were performed until complete collapse of the samples.

3B.3.6. Tissue collection

Keratinized gingival biopsies (5×5 mm) were obtained from patients undergoing oral surgery with their informed written consent at the Charles Clifford Dental Hospital, Sheffield under ethical approval granted by the Sheffield Research Ethics Committee (15/LO/0116, STH Research Department: STH18551). The specimens were collected in sterile PBS and transported on the same day to the laboratory for processing.

3B.3.7. Cell isolation and culture

Tissues were rinsed and disinfected three times with PBS supplemented with 50 $U.ml^{-1}$ penicillin, 50 $U.ml^{-1}$ streptomycin and 625 $ng.ml^{-1}$ amphotericin B. Normal oral fibroblasts (NOF) and normal oral keratinocytes (NOK) were enzymatically isolated from oral biopsies as previously described [473]. Briefly, NOK were isolated by incubating the tissues in trypsin in PBS (1:250) for 1 hour at 4°C and then 2 hours at 37°C. The epithelial layer was scraped and the tiny pieces were plated in a T-25 tissue culture flask, allowed to adhere for 15 minutes, and then cultured in Green's medium [474] at 37°C in a humidified and 5% CO_2/95% air atmosphere. The medium was changed every two days until the cells were 90% confluent. The cells were then sub-cultured as mentioned above and used after the first passage.

NOF were isolated from the connective tissue layer of the remaining oral mucosa biopsy by incubation in 0.05% (w/v) collagenase type I solution in cDMEM at 37 °C overnight. Digested tissue was centrifuged at 200 rpm for 5 minutes and the pellet was re-suspended in cDMEM and cultured in a T-75 cell culture flask. The medium was changed 2-3 times a week until the cells were 90% confluent when they were sub-cultured and used following the second passage.

3B.3.8. Membrane cell seeding

Membranes sized 15mm × 15mm (N=6) were washed 3 times with PBS prior to the experiment and each scaffold was placed in 3 cm diameter hanged cell culture inserts. Then, NOF 0.5×10^6 cells/ scaffold were seeded onto the large pore-size side and after 4 hours NOK 10^6 cells/scaffold were seeded onto the small-pore size surface. The culture media used was cDMEM supplemented with 50 µg/ml ascorbic acid in the outside of the insert (2 ml) and Green's M inside the insert (2 ml). The medium was changed every other day. After 4 days, the constructs were lifted to the air

liquid interface (ALI) and following 12 days at ALI, two of the constructs were fixed in 10 % formalin and paraffin embedded sections were prepared for histological examination. The remaining constructs were further cultured for another 4 days for tissue viability assay as described below.

3B.3.9. Cell vitality

Cell vitality was assessed after 2, 10, and 20 days of culture (after initial cell seeding) using PB assay. At each time point, the constructs were washed 3 times with PBS before 900 µl of serum free medium with 100 µl of PB reagent added to each insert. After 3 hours of incubation, 200 µl in triplicate were aspirated from each model for fluorescent reading using a spectrophotometric plate reader (Infinite® M200,TECAN, USA) at 560 nm excitation and 590 nm emission. The statistic was performed using GraphPad Prism 7. The difference was considered significant at P-value< 0.05 using the one-way ANOVA test.

3B.3.10. DAPI nuclei staining

Frozen sections (8 µm) of the membranes with cells were prepared and the slides were washed with PBS 3 times and mounted using mounting medium containing 4,6-diamidino-2-phenylindole (DAPI) stain (Sigma Chemical Co.) and assessed under a fluorescence microscope (BX51, Olympus, Tokyo, Japan).

3B.4. Results and discussion

3B.4.1. Ink optimization

To make the appropriate composition of the ink for this study, we began with pure gelatin solutions. The reason for selecting gelatin as the main material of the ink was its advantageous properties that matches the required characteristics described in Aim 1 of the thesis. More specifically, gelatin is highly biocompatible (can attach to all cell types), inexpensive and degradable [24, 185]. It is a soft hydrogel with low antigenicity [186] and relatively durable mechanical properties [191].

Molded gelatin membranes with gelatin concentration of 4%, 8%, 10% and 15% (w/v) and thickness of ~200 µm were first made, as described in Section 3B.3.2. Manipulation by hands and visual observation of the prepared samples clearly indicated the lack of elasticity in all samples,

while the 15% gelatin sample were firmer than the others. To increase the elasticity, elastin was added in the gelatin solution (0.5-2%). While 0.5 and 1% elastin components were not adequate, including 2% elastin to the solution with various gelatin concentrations (4%, 8%, 10% and 15%) provided membranes with the desired improvement in terms of elasticity, which could be observed by manipulation of the gelatin/elastin membranes and comparing them with the pure gelatin ones. To keep gelatin as the main component of the membrane, we did not increase the elastin concentration further.

As explained above, gelatin has the preferred characteristics to be used as the matrix material. It is known as a material that is able to provide perfect structural support, while other components can be added to it for improving specific capabilities [190]. One of these components that we would like to have in our composition was sodium hyaluronate, due to its enhanced biological properties to facilitate signaling among cells and regulate cells/tissue functions [208]. It is also an ECM material, existing in any connective tissues of the human body and, thus, reasonable to be included in our membrane. However, the limiting factor regarding sodium hyaluronate to be included in a 3D-printing ink is its high molecular weight (500-749 KDa). Planning to include 0.25-1% sodium hyaluronate, we realized that increasing the sodium hyaluronate to more than 0.5% in both pure gelatin and gelatin/elastin solutions dramatically decreased the fluidity, which could be visually observed (viscosity is also measured in Figure 3D.2, which indicates an order of magnitude viscosity rise by addition of 0.5% sodium hyaluronate; please note that elastin with molecular weight of 60 KDa did not significantly influence the viscosity). Highly viscous solutions are not appropriate for printing and should be avoided; our experience showed that the viscosity over 10 Pa.s makes the printing difficult and hardly reproducible. In order to have reasonable viscosity and acceptable fluidity, increasing the sodium hyaluronate more than 0.5% required significant decrease of gelatin concentration, which was not favorable, as we wanted to keep gelatin as the main material in our composition.

This initial screening of various above-mentioned combinations allowed us to select membranes with seventeen different combination of gelatin, elastin and sodium hyaluronate (as listed in Table SI1.1), which had acceptable visual configuration, shape and handling properties. The criteria to

select these seventeen membranes were: 1)firmness, and 2) ease of manipulation (more specifically not collapsing upon manipulating by hand).

These membranes were then tested three different surgeons. The samples were completely blind for them to avoid any assessment bias. They examined: 1) the suturability of membranes, 2) cutting with surgical forceps and scissors, and 3) rigidity in terms of ability of the membrane to lie on the tissue. Among the three selections of the three surgeons, two were 8% gelatin/2% elastin/0.5% sodium hyaluronate and one was 15% gelatin/2% elastin/0.5% sodium. As will be shown by detailed rheological analyses in this and next chapter, the ink with the composition of 8% gelatin/2% elastin/0.5% sodium hyaluronate offers the best rheological properties for the purpose of our study.

For thermoreversible gels, the gel point can be defined as the temperature at which the loss tangent (dissipation factor, Tan δ) is independent of frequency [432]. Therefore, the gelation temperature of a solution can be acquired through a multi-frequency plot for a temperature sweep measurement. Loss tangent (Tan δ) of gels of different compositions against temperature has been plotted at different frequencies in Figure 3B.1.

The gel point of the gelatin-containing solutions is important in the printing process. For fused deposition modeling of such solutions, it is necessary to have them in sol (liquid) state in the cartridge and needle while a sol-gel transition is required to maintain the shape on the platform after printing. The transition should be fast enough to prevent any flow after the material is printed on the platform. To do this, the cartridge containing the ink could be heated above the gel point while the platform temperature is kept below the gel point. In this case, the closer the cartridge temperature to the gel point and the further the platform temperature is away from the gel point, the faster the gelation process will be. However, there are some key issues in practice that need to be addressed for successful printing:

- The needle is in contact with room temperature when the printer is in stand-by mode. Therefore, there is always a temperature gradient between the cartridge and the needle. In this case, if the needle temperature falls below the gel point, the needle will be clogged through gelation and the material can’t be printed.

- If the cartridge temperature is increased far above the gel point in order to manage the temperature gradient mentioned earlier, two possible problems may occur; firstly, the high temperature of the sol postpones the gelation on the platform; secondly, the pressure that should be used to initiate the ink flow is too high for printing because of the difference between the needle and cartridge temperatures. At the beginning, the pressure should be high enough to overcome the needle-contained ink resistance to flow but once the flow is achieved, such pressure is too high to be used for printing the strands. This happens because the viscosity of the solution highly depends on the temperature as shown in Figure 3B.2. Lower temperature of the needle results in higher viscosity and the need to use higher pressure to start. However, as the needle content is completely printed, such high pressure is no longer required, and it may cause overflow onto the platform.

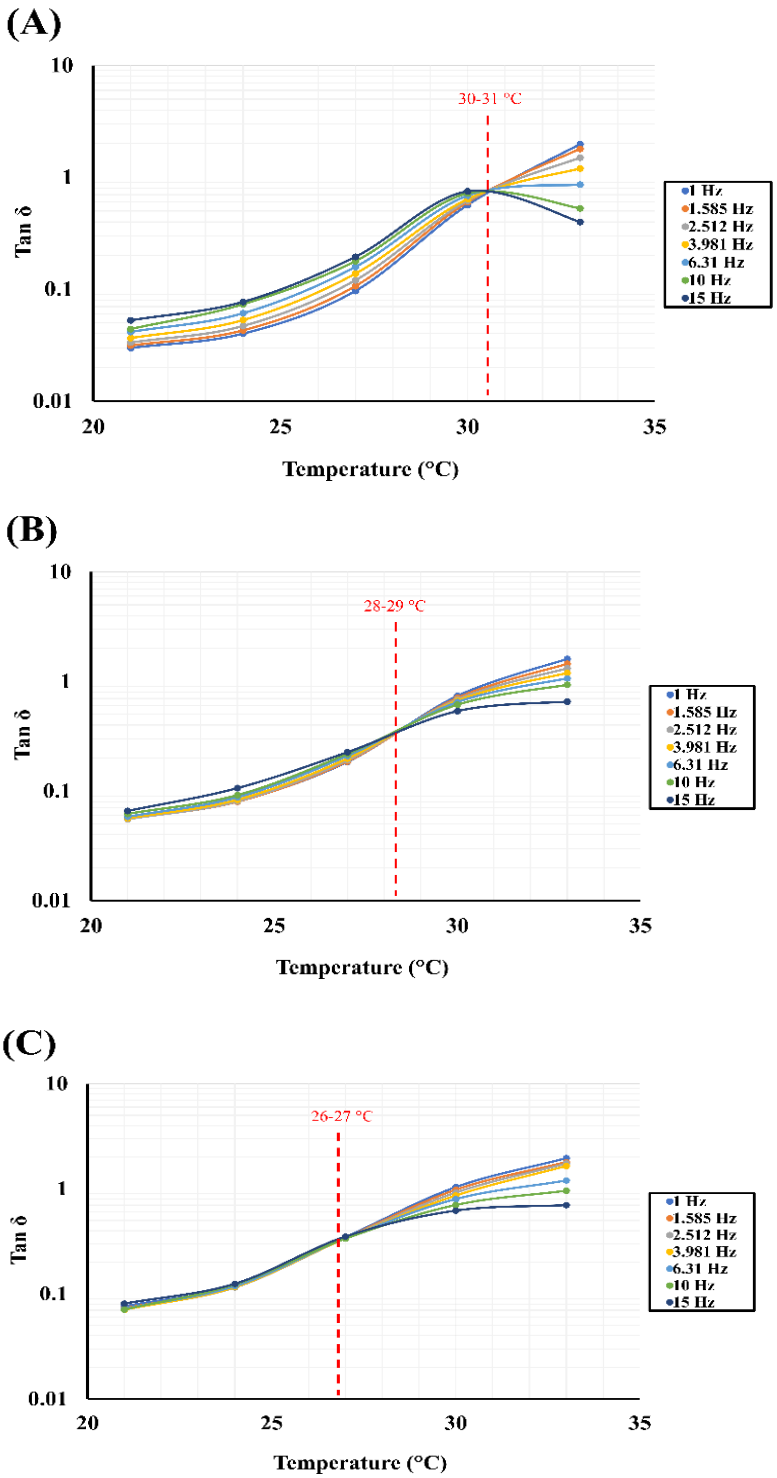

Figure 3B.1: Loss tangent vs. temperature plotted in different frequencies for (A) gelatin 15%, (B) gelatin 15% elastin 2% sodium hyaluronate 0.5%, and (C) gelatin 8% elastin 2% sodium hyaluronate 0.5%

- As the printing is in progress, the needle is in contact with the material printed on the platform in previous cycles. In this case, the needle temperature may drop below the gel point which causes the needle to be clogged in the middle of the printing process.

Minimizing the temperature gradient between the material in the cartridge and the needle was found to be an effective strategy to eliminate such problems. It can be performed by adjusting the gel point to be close to room temperature to prevent gelation in the needle. Changing the concentration of gelatin as the main component of the formulation and addition of elastin and sodium hyaluronate was found to be effective for adjusting the gel point.

As can be seen in Figure 3B.1, the gel point of 15% gelatin solution was found to be between 30-31℃. Addition of elastin and sodium hyaluronate to 15% gelatin solution resulted in a decrease of the gel point to 28-29℃. The gel point was further decreased by reducing the concentration of gelatin to 8% while keeping the concentration of elastin and sodium hyaluronate constant. It was decreased to 26-27℃ (Figure 3B.1) which is close enough to room temperature for printing. This gave us a good reason for choosing 8% gelatin/ 2% elastin/ 0.5% sodium hyaluronate as the ink for the 3D printing.

Viscosity of the ink is an important parameter for reproducing the printing process and determining the printing variables such as pressure and speed. Very low or high viscosity makes the solution unprintable. Figure 3B.2 presents the values of viscosity for our solutions**.** As can be seen in the figure, gelatin-based solutions represent a shear-thinning behavior in sol state. The viscosity highly depends on the temperature especially in temperatures closer to the gel point which shows the importance of the temperature of the cartridge in the printing process.

At a specific temperature, addition of 2% elastin and 0.5% sodium hyaluronate to 15% gelatin solution results in a significant increase in viscosity. On the other hand, decreasing the gelatin concentration from 15% to 8% causes a decrease in viscosity. In the printing procedure, the cartridge temperature was set to 30-32℃ that corresponded to viscosity values between 1-10 Pa.s. A solution with such viscosity can be printed using the applied pressure, speed and platform temperature to yield a reproducible well-ordered membrane.

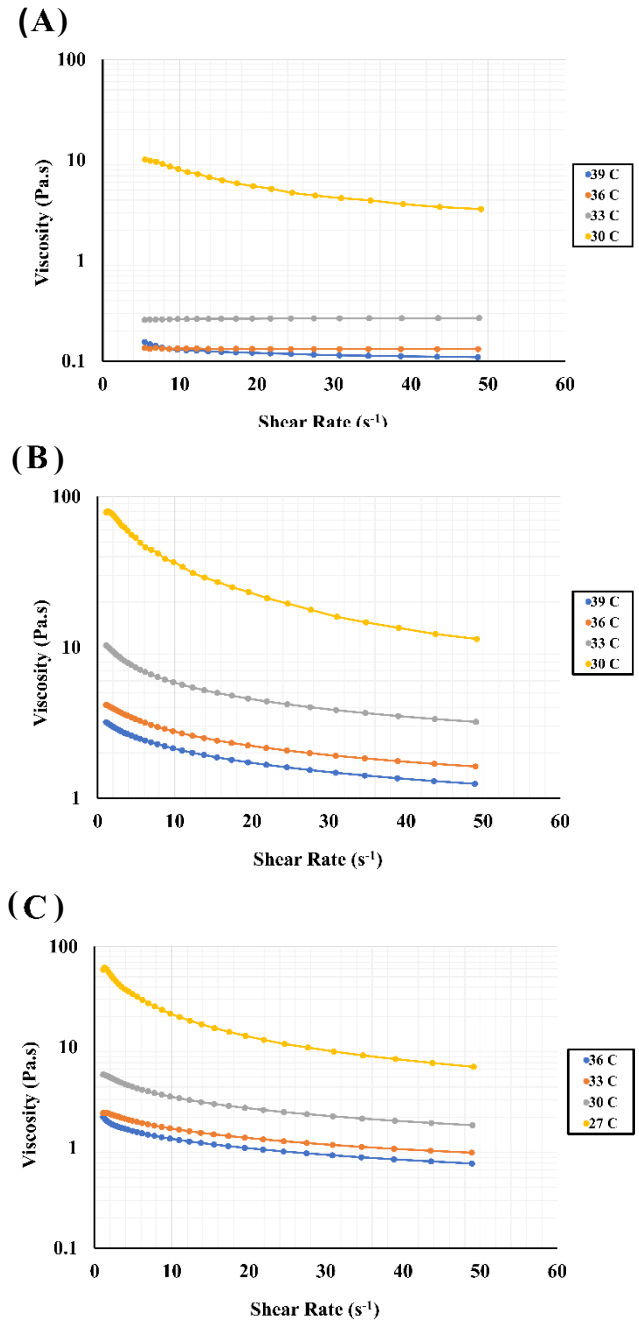

Figure 3B.2: Viscosity vs. shear rate plotted in different temperatures for (A) gelatin 15%, (B) gelatin 15% elastin 2% sodium hyaluronate 0.5%, and (C) gelatin 8% elastin 2% sodium hyaluronate 0.5%

3B.4.2. Morphology, surface roughness and thickness of the membranes

Sample preparation is the main difference between using the 3D Confocal (label-free) Laser Measuring Microscopy and SEM. No sample preparation is needed for the 3D Confocal Laser Measuring Microscopy and the imaging can be performed under room conditions while the membranes are in their original shape. Since the SEM has to be conducted under vacuum

conditions and the samples have to be coated with a conductive material, the samples are slightly deformed, and the images do not represent the exact shape of the construct. Although, the resolution of the SEM is better than the 3D Confocal Laser Measuring Microscope, the latter was good enough for our purpose.

Figure 3B.3(A-C) schematically represents the architecture of the printed membranes. The membrane was printed with gradient structure; i.e. one side had small pores to prevent connective tissue invasion and the other side had larger pores to allow potential epithelial cell/bone growth. Crosslinking helped to keep the structural integrity of the 3D-printed membrane. Based on our visual observations, the handling of non-crosslinked membranes was difficult, and they collapsed easily. The degradation resistance of the hydrogels could be improved significantly by crosslinking.

Regarding the design of the membrane, in a novel configuration, to be able to effectively grow one type of tissue (e.g., epithelial tissue) on one side of the membrane and another type of tissue (e.g., connective tissue/bone) on the other side, we made a gradient membrane with different structures on each side. This model could mimic a real tissue interface which has dissimilar tissues on each side. One side of the membrane had very large pores (400-500 μm) so we could seed cells that could easily grow on the membrane. On the other side, the pore size was smaller (50-150 μm). Our experiments showed that this pore size made a barrier thin layer that prevented keratinocytes from dropping into the other side, which is a necessary feature for the membrane to facilitate guided tissue regeneration (GTR). It is important to note that maintaining the permeability of the membrane is essential since it allows nutrient diffusion and healthy cell growth and differentiation.

Figure 3B.3(D-E) shows the macroscopic images of the prepared 3D-printed membranes. As can be seen in this figure, the membranes were flexible. We also found that they offer easy surgical handling [475]. The thickness of the membrane, based on the measurement with the Electronic Digital Micrometer, was approximately 100-200 μm. Note that if the crosslinking was done immediately after the 3D printing, the thickness was larger (toward 200 μm). Prolonged waiting time after 3D printing and before crosslinking yielded thinner membranes (toward 100 μm).

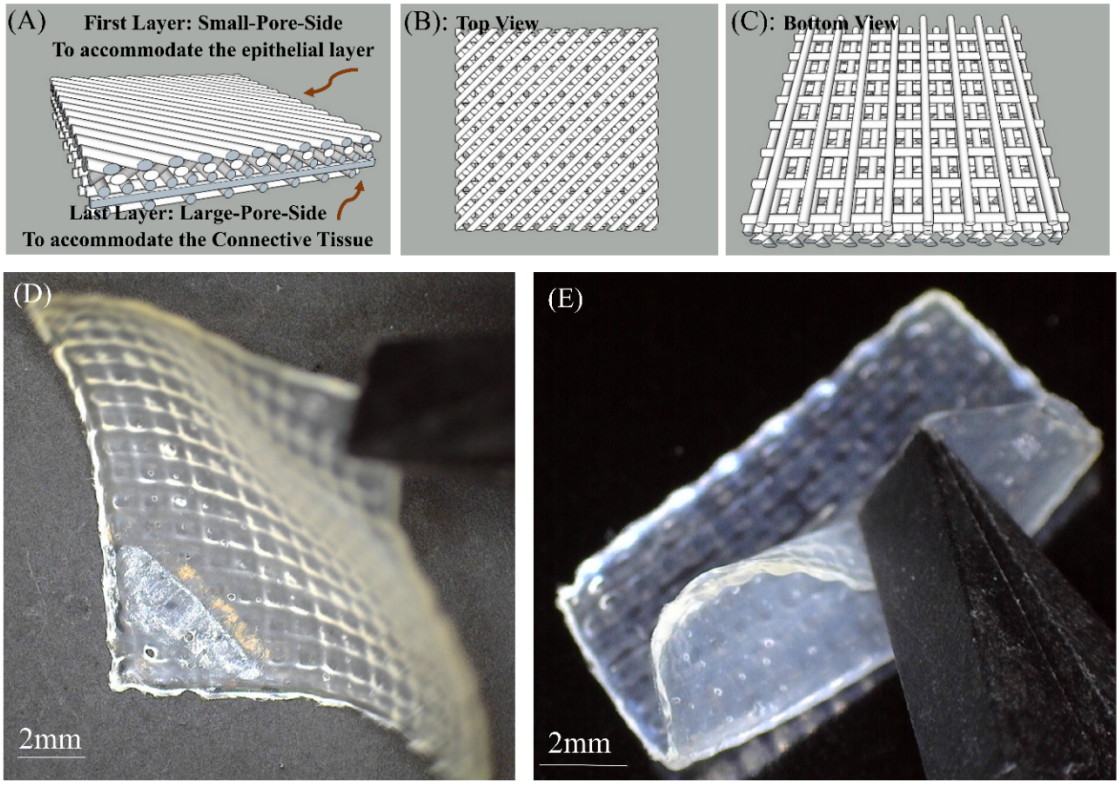

Figure 3B.3: (A-C): Schematic of our design. Each membrane is composed of 6 layers. The strand angels from the first layer to the last layer are: 45, 135, 0, 90, 0, 90°. Distances between strands (from the middle of one strand to the middle of the adjacent one) are set to 0.6 mm for the layers 1-4 and 0.9 mm for layers 5-6. (D-E): The macroscopic view of the 3D-printed gradient membranes of gelatin/elastin/sodium hyaluronate. The membranes are completely flexible and bendable. The surgical handling of the membrane is easy. The thickness is approximately 150 µm.

To store the membrane, having it in 100% ethanol inside a freezer was very effective and it seems the membrane can keep its functionality forever if it is stored this way (we have tried it for several months without seeing any change in the quality of the membrane). In contrast, the membranes were completely hard, fragile and not flexible when kept in ethanol due to the dehydration. Because of the thin structure, by soaking the dehydrated membranes in water, they became flexible in 30 seconds and were the same as the original in terms of shape and quality. We have not seen any visual change in the membranes by soaking them in water for a longer time and it seems that they can be fully swelled in a very short time.

Figure 3B.4 presents high magnification images of the two sides of the membrane taken by the 3D Laser Measuring Microscope. The first layer had small pores and the last layer was designed to contain large pores. The roughness of the two sides were different. The value of the roughness

was not fixed in different membranes, but the small-pore-side was always significantly smoother than the large-pore-side. The average values of the roughness (R_a: Arithmetical mean deviation of the roughness profile) of the small-pore-side and large-pore-side were measured at around 0.30 and 1.19 μm, respectively.

The images in Figure 3B.4(A, B) were taken when the membrane was in the fully swelled state (i.e. just taken out from the water). After about half an hour keeping the membrane under the microscope, the membrane became slightly dry and the pores of both sides can be seen from the top view (from the small-pore-side) under the microscope, as shown in Figure 3B.4(C). As displayed in this figure, the small pores were around 140 μm in this membrane and the large pores were around 440 μm. In different membranes, the sizes of small pores were measured to be between 50-150 μm and the size of the large pores was usually very close to 450 μm.

Figure 3B.5 shows the laser scanning of the edge of the membrane to have more detailed information about the thickness of the membrane. As seen in this figure, although right at the edge, the membrane was thicker; the overall thickness of the membrane was approximately 150 μm, which confirmed the Electronic Digital Micrometer measurement. Having thicker edge is a result of printing a contour for each layer in every printing cycle by the 3D-printer. The contour is a solid printed line that verifies the margins of the printed object in each layer. Printing a contour supports the integrity of the membrane while making the edge thicker as the strands are stacked on top of each other in this region.

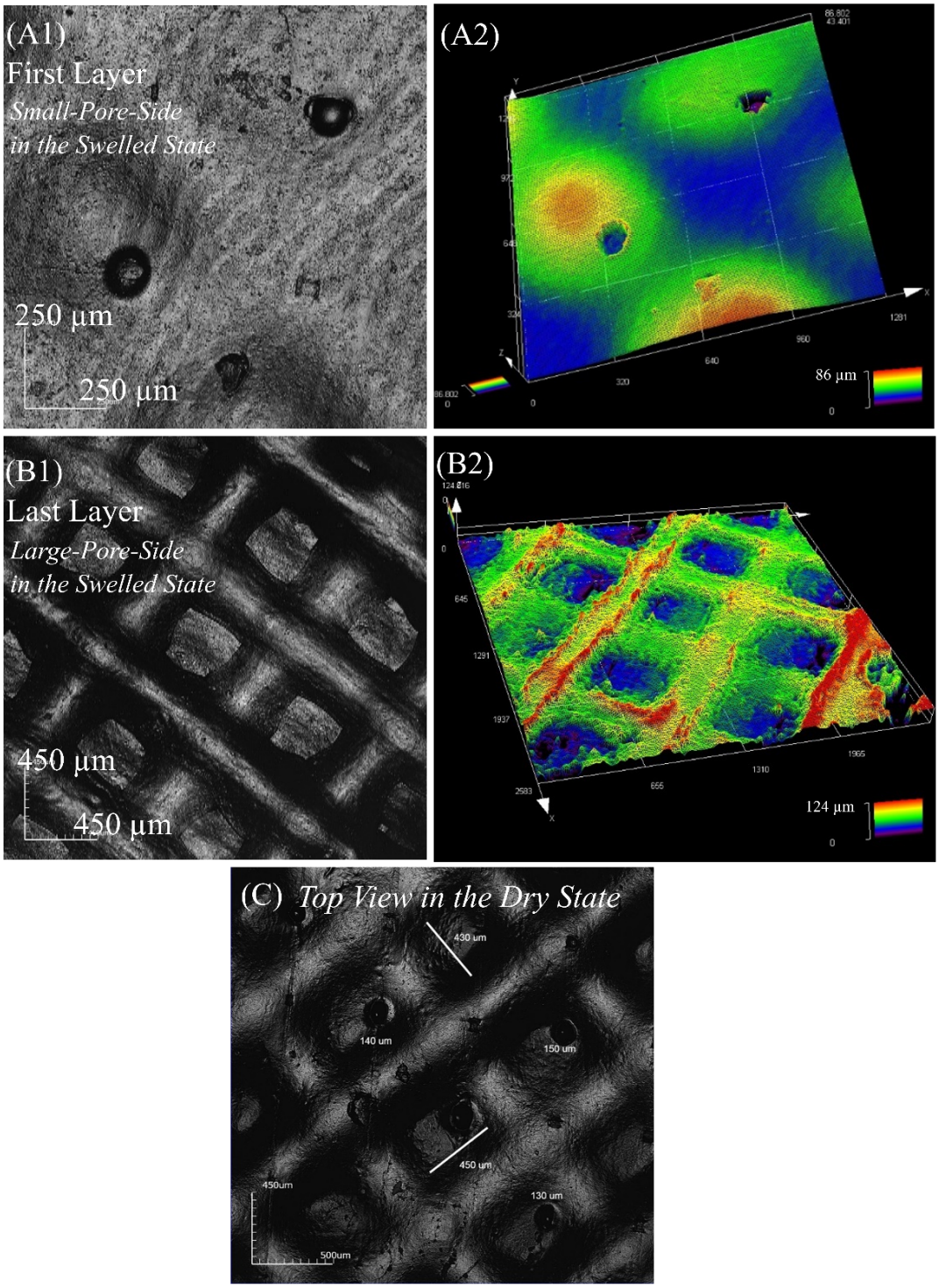

Figure 3B.4: Confocal laser scanning (label-free) of the scaffolds from both sides of the sample composing of gelatin 8%, elastin 2% and sodium hyaluronate 0.5%. (A1, B1): imaging of the small-pore-side and large-pore-side in a completely swelled state. (A2, B2) the height profile and surface morphology of the images in panel A1 and B1. The Red area. Small-pore-side has smoother surface than the large-pore-side. The color coding indicates the height in µm. (C). Both sides of the membrane can be visualized under the 3D Lase Measuring Microscope after drying the sample by 30 minutes keeping a fully swelled membrane under room conditions (C).

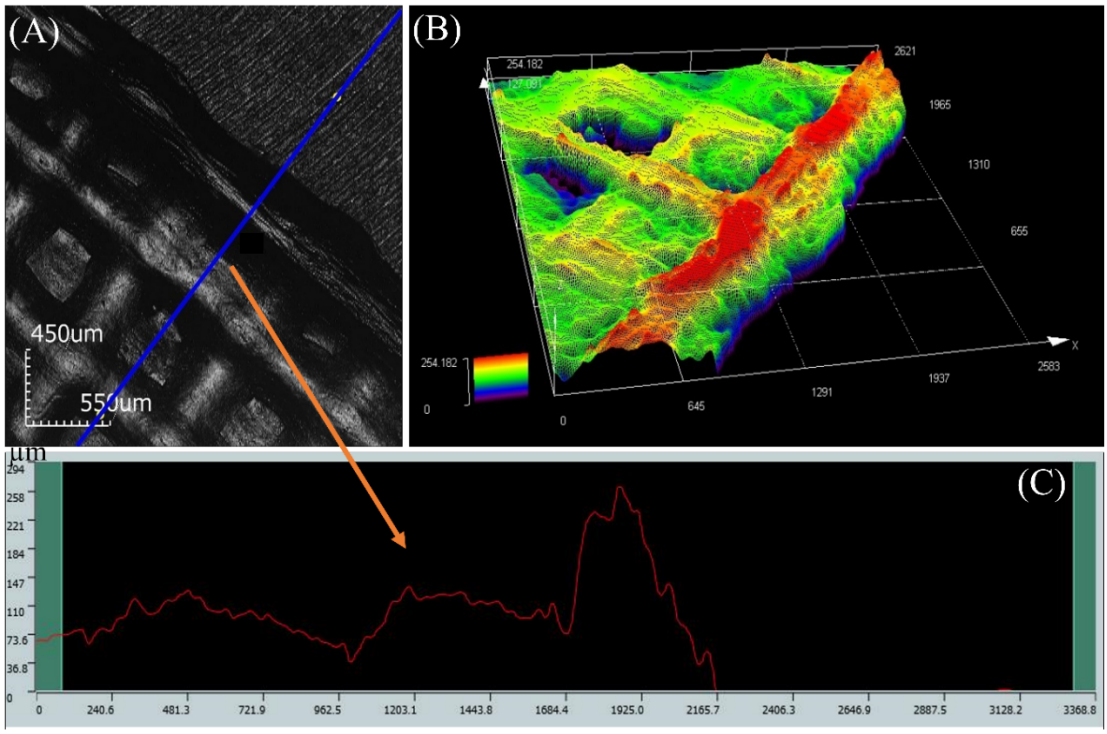

Figure 3B.5: (A) The lable-free 3D confocal laser imaging of the membranes to confirm the thickness of the membranes measured by the Electronic Digital Micrometer. (B) The height profile of the edge of the membrane. (C) The line height scan of the blue line in panel A. The edge of the membrane is a bit higher than the actual surface as the printer was set to do the contouring after each layer of printing.

3B.4.3. Static and dynamic mechanical properties

The tensile static mechanical testing of the membranes (15 mm × 15 mm), cross-linked for 0.5 h revealed a tensile modulus of 1.95 ± 0.55 Mpa (Figure 3B.6) after performing four measurements for four different samples (n=4). Maximum stress of 1.15 ± 0.33 Mpa (n=4) could be applied to them, where the maximum elongation at breaking point was 60 ± 7% (n=4) of the initial length. Figure 3B.6 shows a sample force-displacement graph of the membrane. As can be seen, the membrane exhibited elastic (linear) behavior until it was ripped.

DMA was used to measure the dynamic storage modulus of the printed membrane after crosslinking for 0.5 h. The frequencies in the range of 0-25 Hz were sweeped at room temperature. The results are shown in Figure 3B.6. As can be seen, the storage modulus does not change significantly with frequency change in the scanned range. Note that increasing the temperature to

37 °C did not have a significant impact on the storage modulus. The tensile storage modulus was found to be 314 ± 50 kPa.

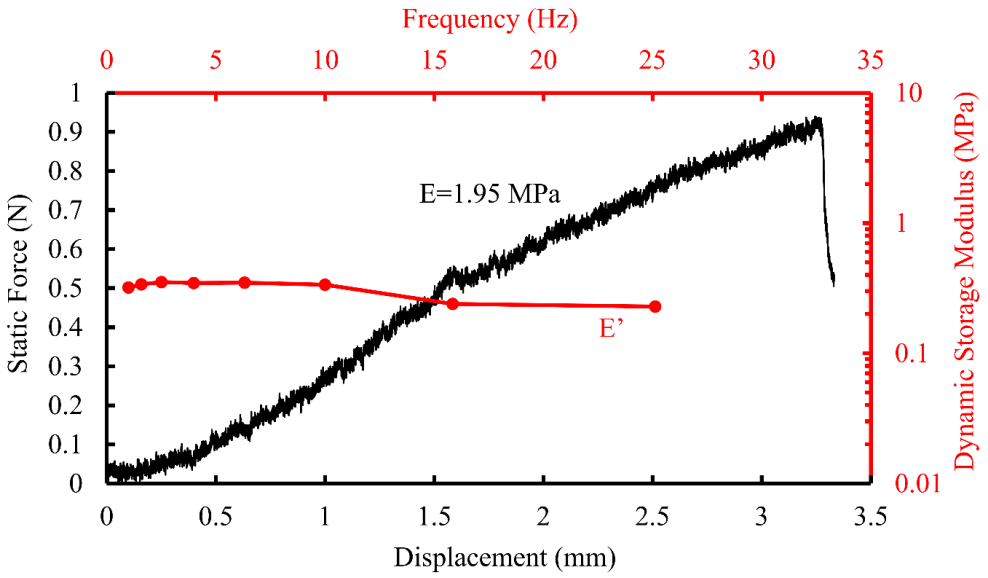

Figure 3B.6: Static mechanical testing revealed elastic modulus of 1.95 ± 0.55 Mpa (black); dynamic storage modulus vs. frequency for printed membranes (red). The measured dynamic storage modulus was 314 ± 50 kPa and had not been significantly altered by increasing the frequency (Although the values presented in the text were obtained out of four measurements from four different samples (n=4), the figure only illustrates the result of the experiment from one sample.).

The values of mechanical properties for one of the widely used GTR/GBR membranes made out of bovine collagen, BioGide®, with the thickness of 440 µm are as follows: 15.7 MPa for tensile modulus, 4.8 MPa maximum stress and maximum elongation at breaking point was 46.8% [476]. Considering the target properties and comparing these values with the properties of our 3D-printed membrane, one may realize that although the maximum elongation in our case is higher than the collagen membrane (due to inclusion of elastin), the tensile modulus and the maximum stress is lower for our membrane. This can be attributed to the lower thickness of our membrane (~150 µm), which is approximately three times thinner than the BioGide® collagen membrane (~440 µm). Thickness and mechanical properties of membranes are known to be directly related to each other [477].

It should be noted that the mechanical properties of hydrogel membranes, and more specifically collagen membranes, are very diverse [478]. Such properties can be easily altered batch-to-batch, and also the unavoidable moistening of the membrane can noticeably change their mechanical properties [478].

3B.4.4. Degradation

Figure 3B.7 shows the degradation profile of the samples in PBS at 37℃. The experiments were performed for four different samples in each condition (n=4). The effect of cross-linking time can be vividly observed in this figure. Increasing the cross-linking time from 0.5 h to 1.5 h, prolonged the degradation resistance for more than 10 days. Longer cross-linking times up to 2 h further increased the degradation time of the samples to more than a month. The membranes kept their integrity and whole weight for a certain period and collapsed suddenly at the next time points. As can be seen, membranes cross-linked for 0.5 h swelled through being immersed in PBS and maintained a portion of their water content up to the end point of the experiment (weight/initial weight > 1). However, increasing the cross-linking time resulted in decreased swelling that was a result of augmentation of cross-linking density. It is worth mentioning that the longer the cross-linking time was, the less flexible the membrane became. The resoprtion rate of the membrane is important since it affects the success of regenration. For example, the membrane should function 4-6 weeks before resorption to allow successful regeneration of the periodontal systems [275]. Monitoring changes in pH of the PBS or the weight of the sample over time is commonly used to track the degradation of biodegradable materials such as PLGA [479], collagen, gelatin and elastin [480] which provide the information about the kinetics of hydrolytic degradation.

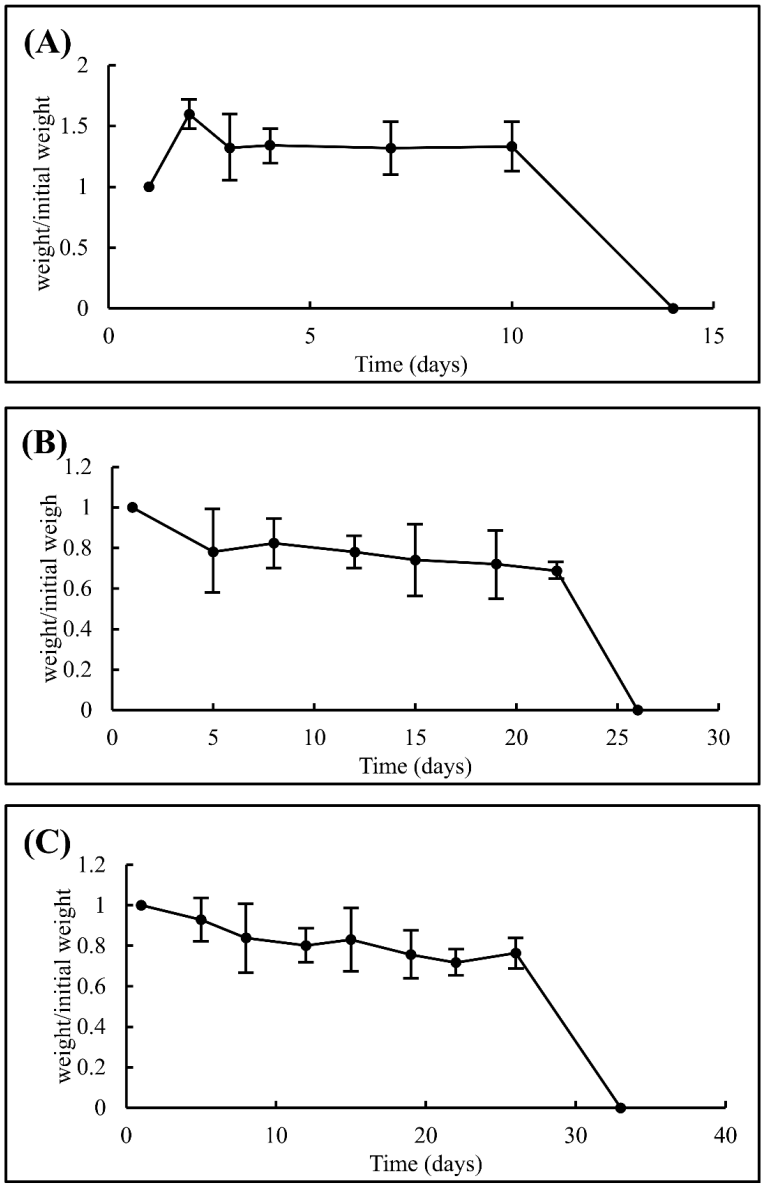

Figure 3B.7: Degradation rate of the membranes crosslinked using EDC/NHS for 0.5 h (A), 1.5 h (B) and 2 h (C). The membranes were soaked in PBS at 37 ℃ for this experiment. Four different samples in each condition were examined (n=4).

Considering the target properties and comparing the degradation of our membrane with collagen membranes, we realized that the values of the degradation time in our membranes with 0.5 h and 1.5 h crosslinking are lower than the GTR collagen membrane. More specifically, the degradation time of BioGide® as a bovine collagen membrane is about 4-8 weeks, and the degradation time of a rat-tail collagen membrane is about 4 weeks [299, 300]. However, the degradation time of our membrane with 2 h crosslinking (about 4 weeks) is still appropriate for GTR application.

3B.4.5. Biological evaluation *in vitro*

Histology allows us to visualize and directly assess any potential toxicity and cell damage on the epithelial cells caused by the materials in the membrane. This can be quantified by using a cell viability assay which has been employed in this study. The ability of the GTR membrane to separate different cells grown on different sides of the membrane can also be assessed using histological evaluation of the constructs.

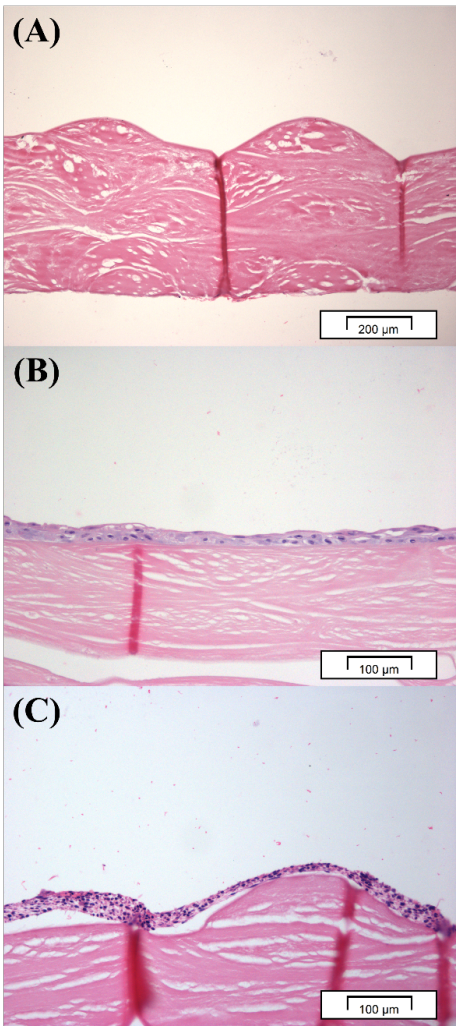

Figure 3B.8: Histological sections of paraffin wax-embedded constructs cultured at submerged condition for 4 days followed by air-liquid interface culture for 12 days. (A) acellular 3D-printed membrane; (B) the epithelial side of the 3D-printed scaffold with cultured NOK forming multilayers at the surface of the membrane without invading deeper into the membrane and (C) the connective tissue side of the scaffold with cultured NOF showing abundance of fibroblast cells nicely separated from the epithelial layer by the GTR membrane. Hematoxylin and Eosin staining, original magnification ×100. Vertical lines are due to folding of the sections.

Figure 3B.8 demonstrates the histological sections of the 3D-printed membrane before and after cell seeding and culture. Oral keratinocytes proliferated and formed an epithelial layer on the

surface of the 3D-printed membrane with no sign of invasion into the deeper layers of the membrane showing the optimal barrier function of the membrane. Oral fibroblasts also proliferated on the other side of the membrane and formed multilayers of cells separated from the epithelial layer by the membrane.

The prestoblue (PB) assay incorporates a fluorometric/colorimetric growth indicator based on detection of metabolic activity. The system incorporates an oxidation–reduction indicator that both fluoresces and changes color in response to chemical reduction of growth medium resulting from cell growth. PB has two advantages: first, its change in color can be detected both spectrophotometrically and fluorometrically, which gives greater sensitivity of detection; second, since it is not toxic to the cells, it is possible to assess cell viability on more than one occasion. The results of the PB tissue viability assay at days 2, 10 and 20 following seeding of the membranes are demonstrated in Figure 3B.9. The cells maintained their vitality throughout the culture period on the 3D-printed membrane. It appears that after day 10 the proliferation rate had reached a plateau which is expected for oral epithelial cells as they start to differentiate at the air-liquid interface culture.

Although cellular vitality persisted *in vitro* for 3 weeks, our quantitative investigations revealed a small decrease in cellularity after 10 days which may indicate reduction in cell proliferation. This may be attributed to the limitations of the static culture condition used in this study as the dominant nutrient exchange within the construct remains by diffusion. Furthermore, mucosal cells have a high proliferation rate and nutritional demands which can result in early deprivation from nutrients and cell death which was noticed in this study towards the end of the culture period.

DAPI is a fluorescent stain that binds strongly to A-T rich regions in DNA and is used extensively in fluorescence microscopy to visualize the cell nuclei. DAPI staining was used in this study to identify any invasion and penetration of the oral keratinocytes into the GTR membrane.

Figure 3B.10 demonstrates DAPI stained cell nuclei on the surface of the 3D-printed membrane. The shiny cell nuclei were only visible on the surface of the membrane and were not detected within the membrane showing an ideal barrier function of the GTR membrane tested in this study.

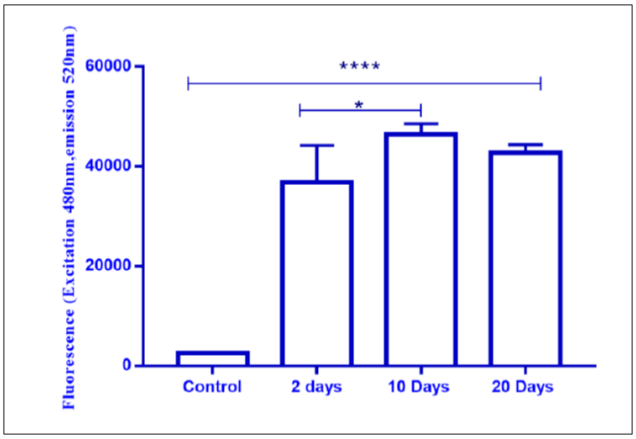

Figure 3B.9: Viability of the membranes seeded with oral fibroblasts and keratinocytes at different culture intervals as assessed by the prestoblue PB assay (assay has been performed after seeding of both cell types i.e. 2 days, 10 days and 20 days). Four different samples in each condition were examined (n=4) and GraphPad Prism 7 was employed to conduct the statistic. The P-value< 0.05 is considered statistically significant difference using the one-way ANOVA test.

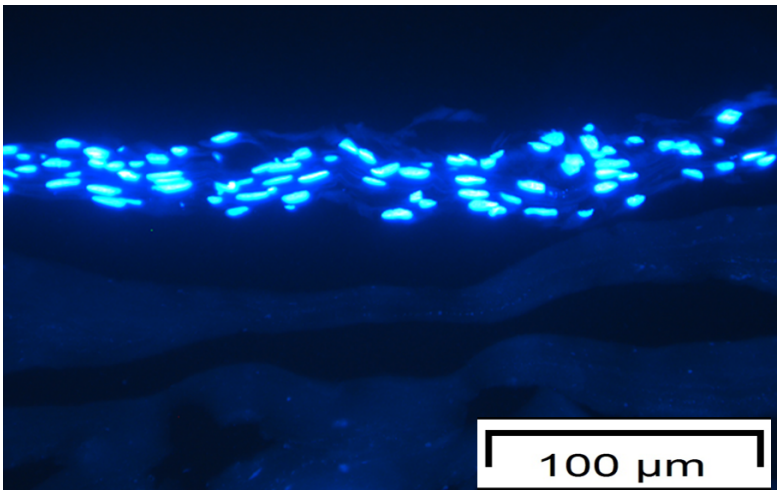

Figure 3B.10: DAPI-stained image of the frozen sectioned construct cultured at submerged condition for 4 days followed by air-liquid interface culture for an additional 12 days showing the nuclei of the cells cultured on the 3D-printed membrane forming multilayers at the surface and absence of any cell nuclei within the membrane confirming its desirable barrier function.

The results of the *in vitro* tests in this study indicated that the 3D-printed membrane had good biocompatibility as assessed by histology and tissue viability assays. Both human oral fibroblasts and keratinocytes were compatible with the membrane and proliferated and attached to the material. The epithelial cells formed a continuous epithelium on the surface of the membrane with no signs of epithelial invasion into the deeper layers of the biomaterial as confirmed by DAPI staining. This suggested that the 3D-printed membrane was able to achieve the desired barrier

function of a GTR membrane *in vitro* by complete separation of the oral epithelial layer from the underlying tissues allowing growth and proliferation of the other cell types under the connective tissue layer. These findings have not previously been reported and this is the first study indicating the suitability of a 3D-printed hybrid scaffold for potential application in guided tissue regeneration. Further *in vivo* studies are underway to assess the *in vivo* biocompatibility and biodegradability of the hybrid material and to optimize the surgical technique for the use of this 3D-printed GTR membrane for different oral soft and hard tissue augmentation procedures.

3B.5. Conclusion

Engaging a 3D-printing method, we manufactured a novel structured soft membrane for GTR application made of gelatin, elastin and sodium hyaluronate. The rationale behind focusing on these three components to make the membrane was the fact that gelatin can act as a fibroblast-attractant, elastin has long-term stability, elasticity and biological activity, and sodium hyaluronate facilitates chemical signaling among cells. After performing the rheology analyses on several different compositions of these three components, we selected a specific composition of 8%w/v gelatin, 2% w/v elastin and 0.5% w/v sodium hyaluronate as the most suitable and printable bioink which resulted in a membrane with appropriate mechanical property. The printed membrane was composed of 6 layers with gradient structure. This design allowed us to have two different sides with large and small pores ideal for different types of cells. 3D Laser Measuring was a useful technique employed for imaging of the membrane to confirm the structures and pores on different sides.

The optimized membrane had the desirable thickness (150 μm), static tensile modules (1.95 ± 0.55 MPa) and dynamic tensile storage modulus (314 ± 50 kPa) to enable easy surgical handling. Moreover, it had optimal *in vitro* biocompatibility and was able to separate two different epithelial and connective tissue cell types resembling the ideal *in vitro* characteristics of a GTR membrane.

Acknowledgements

This work was carried out with support from China Regenerative Medicine International Limited (CRMI).

Statement of Authorship for joint/multi-authored papers for PGR thesis

To appear at the end of each thesis chapter submitted as an article/paper

The statement shall describe the candidate's and co-authors' independent research contributions in the thesis publications. For each publication there should exist a complete statement that is to be filled out and signed by the candidate and supervisor **(only required where there isn't already a statement of contribution within the paper itself).**

Title of Paper	3D-Printed Membrane for Guided Tissue Regeneration
Publication Status	■ Published □ Accepted for Publication □Submitted for Publication □Unpublished and □Unsubmitted work written in a manuscript style
Publication Details	Lobat Tayebi, Morteza Rasoulianboroujeni, Keyvan Moharamzadeh, Thafar KD Almela, Zhanfeng Cui, and Hua Ye. "3D-printed membrane for guided tissue regeneration." Materials Science and Engineering: C 84 (2018): 148-158. https://doi.org/10.1016/j.msec.2017.11.027

Student Confirmation

Student Name:	Lobat Tayebi		
Contribution to the Paper	Contribution in: developing the idea, planning the experiment, performing analysis on samples, interpreting the data, preparing the manuscript		
Signature Lobat Tayebi		Date	16/09/2019

Supervisor Confirmation

By signing the Statement of Authorship, you are certifying that the candidate made a substantial contribution to the publication, and that the description described above is accurate.

Supervisor name and title: Hua Ye, DPhil, Associate Professor, Institute of Biomedical Engineering Department of Engineering Science, University of Oxford Zhanfeng Cui, Professor, Institute of Biomedical Engineering Department of Engineering Science, University of Oxford		
Supervisor comments		
Signature 等青 Cui	Date	25 Sep, 2019

This completed form should be included in the thesis, at the end of the relevant chapter.

Summary of Chapter 3

This chapter began with analyzing the 3D-printing of pure gelatin. Gelatin is a highly biocompatible hydrogel with relatively low-cost, which can make it a reasonable candidate to be used in producing a 3D-printing ink for the generic biomedical application, as desired in this thesis based on Objective 1A&B of Aim 1. However, as shown in Section A of this chapter, pure gelatin did not satisfy the Objective 1C of Aim 1, due to its rheological characteristics leading to challenging printability. More specifically, this section elaborated the complexities in rheological properties of pure gelatin for 3D-printing purpose. Thus, the composition of the ink was modified in Section B of this chapter to overcome such rheological complications. In this section, after examining various compositions, the ink with 8% gelatin, 2% elastin and 0.5% sodium hyaluronate (w/v) was selected as the most appropriate ink with the desired characters described in Objective 1 of Aim 1. This is the ink composition that will be used in the rest of the thesis.

Optimizing the parameters for 3D-printing of this ink, we made a 3D-printed membrane with the thickness of 150 μm to be used for GTR application. Since layer-by-layer deposition of materials in 3D-printing method allows fabrication of different structures in different layers, this membrane was designed in a way to have small pore size (50-150 μm) in one side and large pore size (400-500 μm) in another side. This gradient configuration could facilitate accommodation of different cell types in different sides, assisting the function of the GTR membrane as a barrier construct. More specifically, using histological analysis, this chapter showed that the membrane could nicely separate epithelial layers from the connective tissue. Thus, Objective 1 of Aim 2 of the thesis, “developing the design criteria, fabrication and characterization of a structured membrane to be used for GTR application,” has been achieved in this chapter.

CHAPTER 4. 3D-PRINTED MEMBRANE AND ITS APPLICATION IN OCULAR SURFACE/CONJUNCTIVAL RECONSTRUCTION

4.0. Introduction

This chapter hypothesizes that the membrane 3D-printed by the optimized ink developed in the previous chapter can be used for ocular surface/conjunctival defect reconstruction. Thus, the focus of this chapter is Objective 2 of Aim 2 of the thesis defined as "examining the application of the produced 3D-printed membrane in ocular surface/conjunctival defect reconstruction."

As described in the previous chapter, the ink composed of 8% gelatin, 2% elastin and 0.5% sodium hyaluronate (w/v) has been selected as a generic biocompatible hydrogel ink for production of 3D-printed membranes. This finding has been reconfirmed in this chapter by performing extra rheological analyses and characterization. After 3D-printing of the membrane, it has been fully characterized to ensure its safe application for ocular surface/conjunctival defect reconstruction. The characterizations include *in vitro* analysis using human limbal epithelial cells, examining surgical handling by three surgeons, and exploring other physical and mechanical properties.

AM is known as the conventional membrane used in reconstruction of ocular surface/conjunctival defects. Thus, it has been employed as the control sample in all analyses of this study. An explicit *in vivo* study has been performed using a rabbit model, and promising results have been achieved after clinical observations and histological examinations. The outcomes indicate that the 3D-printed membrane made by the generic ink can be used as a high quality substitute of AM in ocular surface/conjunctival reconstruction, with enhanced surgical handling and degradation pattern, and more importantly, reduced host inflammatory reactions.

To the best of our knowledge, it is the first report of using a cell-free 3D-printed membrane to reconstruct the ocular surface/conjunctival defects, and thus this study is in accordance with Aim

2 to “fill the gaps in using the capacities of 3D-printing technique to fabricate membranes suitable for specific biomedical applications by employing the generic hydrogel ink developed in Aim 1”.

Chapter 4A. 3D-Printed Membrane as an Alternative to Amniotic Membrane for Ocular Surface/Conjunctival Defect Reconstruction: An *In Vitro* & *In Vivo* Study

Attributed paper: Shima Dehghani, Morteza Rasoulianboroujeni, Hamed Ghasemi, Saeed Heidari Keshel, Zohreh Nozarian, Mohammad Naser Hashemian, Mehran Zarei-Ghanavati, Golshan Latifi, Reza Ghaffari, Zhanfeng Cui, Hua Ye, Lobat Tayebi, "3D-Printed membrane as an alternative to amniotic membrane for ocular surface/conjunctival defect reconstruction: An *in vitro* & *in vivo* study". Biomaterials, 174 (2018): 95-112.

4A.1. Abstract

Background: The aim of this study was to evaluate the surgical handling and clinical applicability of a specific 3D-printed membrane design fabricated using a gelatin, elastin and sodium hyaluronate blend for conjunctival reconstruction and compare it with amniotic membrane (AM), which is normally used in such surgeries.

Methods: 3D printing technique was employed to fabricate the membrane based on gradient design. Prior to printing, rheometry was employed to optimize the ink composition. The printed membranes were then fully characterized in terms of physical and mechanical properties. *In vitro* viability, proliferation and adhesion of human limbal epithelial cells were assessed using MTT assay and scanning electron microscopy (SEM), respectively. Prior to *in vivo* experiment, surgical handling of each membrane was evaluated by three surgeons. *In vivo* evaluation was conducted through implanting the gelatin-based membranes and AM on induced conjunctival defects in rabbits (n=8). Clinical observations, including epithelialization, inflammation severity, scar tissue formation and presence of granulation tissue, were recorded from day 1 through day 28. Histological examination was performed on all enucleated eyes on day 28. In addition to H&E staining, specific stains including Periodic Acid Schiff staining, Masson's Trichrome staining and immuno-histochemical staining for α-SMA were further used to assess goblet cell proliferation, healed sub-epithelial stroma and scar tissue formation and the presence of myofibroblasts, respectively.

Results: Among all the examined compositions, a blend of 8% w/v gelatin, 2% w/v elastin and 0.5% w/v sodium hyaluronate was found to be appropriate for printing. The printed membranes had favorable optical characteristics (colorless and transparent), and the surgical handling was significantly easier compared to AM. Epithelial cells cultivated on the membranes indicated

suitable viability and proliferation, and SEM images presented appropriate cell adhesion on the surface of the membranes. Clinical observations suggested similar epithelialization time (approximately 3 weeks) for both the membrane and AM grafted eyes but significantly lower levels of clinical inflammation in the membrane group from day 1 through day 28 ($p = 0.01$), which is a key advantage of using the printed membranes over the AM. Histological examination showed similar qualities in the healed epithelium in terms of cell morphology and cell layers. However, twice the density of goblet cells per 100 cells was observed in the gelatin-based membrane grafted group. Remnant of the degraded implant was seen in only 3 of the membranes, but in 7 of the AM grafted eyes. Inflammation and granulomatous reaction was significantly higher in sections containing the AM compared to membrane ($p < 0.01$ and $p = 0.01$, respectively). α-SMA staining was more evident, but not significantly different from the gelatin-based membrane, for the AM group ($p = 0.25$).

Conclusion: The designed gelatin-based membrane offers the necessary physical and mechanical characteristics needed for successful ocular surface/conjunctival defect construction and may be considered a promising alternative to AM due to a more predictable degradation pattern, higher goblet cell density on the healed epithelium, less inflammation and reduced scar tissue formation.

4A.2. Introduction

Ocular surface damage can occur due to various reasons, such as ocular thermal/chemical burns [338], autoimmune diseases (Steven Johnson's, ocular cicatricial pemphigoid) [336, 337], or due to iatrogenic causes during surgeries where conjunctival excision is necessary, such as Pterygium surgery [339] and conjunctival tumor removal [340]. Repair of the damaged or absent conjunctivae is of utmost importance, as conjunctivae is necessary for proper function of the ocular refractive surface and protection of the cornea. The latter is accomplished through equilibrium of the tear film composition by secreting aqueous, lipid and mucin [334]. The conjunctiva also plays a role in protecting the eye from microbial infections by acting as a mechanical barrier and containing lymphoid tissue (conjunctiva-associated lymphoid tissue—CALT) [335]. Although re-epithelization will occur spontaneously upon conjunctival injury [341-343], several limitations including reduced goblet cell density, scar tissue formation

and contracture hinder the function and anatomy of the healed epithelium that may eventually lead to unfavorable results and even blindness. Goblet cell density and, consequently, the mucin layer thickness of the tear film, that is essential for maintaining the wettability of the ocular surface and clearing it of debris [345], decrease with injury in the healed epithelium [342, 344]. On the other hand, conjunctival contracture and reduced overall surface may lead to fornix foreshortening and eventual symblepharon formation and entropion in the involved eye [346, 347].

Despite favorable results [347-349], autologous tissues have some limitations to replace the absent conjunctiva or modulate the healing process, including unavailability of healthy conjunctiva in autoimmune diseases, cosmetic issues, and absence of goblets [335]. Therefore, allografts such as pericardium [343] and amniotic membrane (AM) have been introduced. AM currently serves amongst the most widespread grafts used in ocular surface reconstruction. It is currently used as a substitute for excised conjunctivae in pterygium surgery, symblepharon lysis, fornix reconstruction, conjunctivochalasis and in tumor resections [354]. AM has been shown to facilitate epithelialization by providing a basement membrane and stroma resembling that of the normal conjunctivae [336, 347, 357, 358]. Studies have also mentioned anti-inflammatory and anti-fibrotic properties, along with lack of immunogenicity for AM [355, 356]. The mentioned characteristics have made AM a favorable tissue for ophthalmic applications [352, 353]. However, there are some studies that challenge the preferential use of AM. For example, histological examinations showed low levels of epithelial stratification (single) and low goblet density (sparse PAS positive cells) on the epithelium grown on cultured AM [365]. Despite favorable results on suppression of inflammation by AM reported in prior studies [336, 338, 347, 356, 357, 362-364], there have been some evidence showing increased inflammatory response in histological sections of wounds grafted with AM [343, 359-361] after conjunctival reconstruction with human AM. Moreover, considering that AM is an allogenic tissue, limitations in the number of diseases that it can be screened for remains a concern [352]. Another complication associated with AM is the considerable likelihood of microbial infections and unwanted host reactions due to lack of standardized and sterile tissue preparations. Post AM transplantation rate of infection

(culture positive) has been reported to be 3.4% in a study on 326 patients [366]. Difficult surgical handling (notably suturing due to the thin structure of AM), prolonged presence in the AM graft site [346, 359, 360], and opacification of the site [367] are among other reported issues associated with AM. Such limitations necessitate development of efficient alternatives like bioengineered scaffolds that can have stroma-like structure similar to AM, promote epithelialization while not transmitting allogenic-related diseases. The results of animal study of several synthetic materials including collagen-glycosaminoglycan (CG) copolymer [342], poly (lactide-co-glycolide) (PLGA) [341], vitrified collagen [344], and cultured membranes [361, 368] have been promising in terms of successful re-epithelialization, decreasing scar formation and fornix foreshortening [346, 357, 358]. However, they still have limitations like undesirable transparency, elasticity, and thickness [341-343]. Also, the ease of surgical handling and the goblet population have not been thoroughly discussed [341, 342, 376]. Among different biomaterials, biodegradability, biocompatibility, ease of processing, and relative inexpensiveness of gelatin-based ones have been the main drivers for further studies, albeit predominantly preclinical, on their ocular applications. Although gelatin-based constructs have been extensively investigated over the last few decades for a multitude of ocular applications [481-488], conjunctival reconstruction has not been reported as a potential application for this group of biomaterials despite their favorable characteristics mentioned above.

This paper is aimed at the development and application of a 3D-printed gelatin/elastin/hyaluronic acid membrane for conjunctival reconstruction and evaluation of epithelialization (time to epithelialization and morphology of the healed epithelium), goblet cell morphology and density, degree and type of inflammation (clinical and histological assessment), quality of healed sub-epithelial stroma and scar tissue formation (gross tissue deformation, collagen deposition pattern from histological data, myofibroblasts by immune histochemical stationing for α-SMA). Additionally, results of the evaluation conducted on the fabricated membrane were compared with corresponding evaluation for the widely used AM graft. Prior to *in vivo* tests conducted on animal models, the membranes were tested for *in vitro* biocompatibility as well.

4A.3. Experimental Procedure

4A.3.1. Ink formulation

The ink used in this study was composed of gelatin (Type A, from porcine skin, Bioreagent grade, Gel strength ~300 g Bloom, Sigma, US), soluble elastin (MW 60KDa, Elastin Products Company, Inc., USA) and sodium hyaluronate (Research Grade, 500KDa-749KDa, Lifecore Biomedical, USA). Gelatin was used as the main component of the ink, while elastin and sodium hyaluronate were employed as additives. Rheological measurements were used to characterize various ink formulations listed in Table 4A.1.

Table 4A.1: Detailed composition of various formulations used for rheological measurements.

Ink ID	Gelatin concentration (%w/v)	Elastin concentration (%w/v)	Sodium hyaluronate concentration(%w/v)
G4	4	-	-
G8	8	-	-
G16	16	-	-
G4E2	4	2	-
G8E2	8	2	-
G16E2	16	2	-
G4E2H0.5	4	2	0.5
G8E2H0.5	8	2	0.5
G16E2H0.5	16	2	0.5

The gelation temperature of each formulation was determined using oscillatory shear measurements. A shear rheometer (Kinexus, Malvern, UK) with a stainless steel parallel-plate geometry of 20 mm in diameter and a Peltier temperature control was used to perform frequency sweep at the gap distance of 0.3 mm for each formulation at temperatures in decreasing 2 °C increments starting from a certain temperature above the formulation gelation temperature. A constant shear strain of 0.1% was applied to each sample during the frequency sweep, where the sample deformation was well within the linear viscoelastic region. The formulation with the sol-gel transition temperature closest to room temperature was selected for printing.

The creep test was run for the selected formulation and the corresponding gelatin solution with no additives. The measurements were conducted at the constant shear stress of 10 Pa using the same parallel-plate geometry and gap distance as the oscillatory measurements at 24-32 °C. Both

creep and recovery phases were monitored for up to 10 min unless the equilibrium condition for steady state was met.

The viscometry of the samples was conducted using the same geometry and gap distance at temperatures in decreasing 2 °C increments ranging from 36 °C to 26 °C. The shear rate varied logarithmically in ramp mode from 0 to 50 s^{-1} and then back to 0 s^{-1}.

4A.3.2. 3D-printing of membranes

The mass flow of the selected ink as a function of actual pneumatic pressure applied by the printer to the ink reservoir was obtained by holding the pressure for 30 s and weighing the dispensed material. Two different needles with inner diameters of 250 (G25) and 410 μm (G22) were examined while the reservoir temperature was set to either 32 or 34 °C. The effect of cooling rate and ultimate temperature on the rheological properties of the selected ink was also investigated. For this purpose, the same parallel-plate geometry with a gap distance of 0.2 or 0.4 μm was employed. The initial temperature was set to 32 °C, and the measurements were conducted in oscillatory mode with a shear strain of 0.1% and a frequency of 1 Hz. The temperature was decreased to 12, 18 or 24 °C, with a cooling rate of 10, 8 or 4 °C/min, respectively, while the oscillatory measurement was current. The variation of complex shear modulus against time was then plotted to evaluate the effect of various temperatures and cooling rates on the kinetics of hardening.

The final membranes were fabricated using a 3D-bioplatter (EnvisionTEC, Germany). Taking the rheology analysis into account, the selected solution was printed at material container temperature of 32 °C, platform temperature of 12 °C, printing pressure of 0.7 bar, and speed of 20 mm/s using a 250 μm-diameter needle. Pre- and post-flow delays were set to zero. Each membrane was composed of 6 layers with strand angles of 45, 135, 0, 90, 0 and 90°. Distances between strands were set to 0.6 mm for the first 4 layers and 0.9 mm for the last 2 layers. Hardening of the ink occurred after being dispensed from the needle and touching the platform through the capability of the solution to form a solid gel at lower temperatures. The samples were cross-linked using 6 mg/ml 1-ethyl-3-(3-dimethylaminopropyl)carbodiimide hydrochloride (EDC, Alfa Aesar, USA)/ 0.75 mg/ml N-hydroxysulfosuccinimide (NHS, Alfa Aesar, USA) in 70% (v/v) ethanol for 1.5 h

(see Supplementary Information 2 (SI2), cross-linking section), washed with a large amount of DI water and stored in pure ethanol (dehydrated state) at -20 °C until use.

4A.3.3. Morphology, line and surface roughness

Morphology, line and surface roughness of the membranes were evaluated using a 3D Confocal Laser Scanning Microscope (LEXT OLS4000, Olympus, Japan). Samples were imaged both in dehydrated (stored in ethanol) and hydrated states. The arithmetic average of the absolute values of the profile height deviations from the mean line (R_a) and the mean surface (S_a) were used to describe line and surface roughness, respectively.

4A.3.4. Human AM preparation and preservation

Cryopreserved human AM (commercialized as *Life Patch* by International Bio Implant (IBI) Company, Tehran, IR) was used in this study. The manufacturer reported that these AMs were partially acellular, DNA diminished, lacking MHC expression, and kept in a solution containing antibiotics (vancomycin, gentamycin, ceftriaxone, streptomycin, glucosulin, and amphotericin B). AMs were stored at -20 ˚C. All donors and AMs processed at IBI were screened against human immunodeficiency virus type 1 and 2, human T-lymphocyte virus type 1 and 2, hepatitis B and C viruses, and syphilis both at delivery and at the time of preparation. Further details pertinent to preparation procedure were not disclosed by the manufacturer due to proprietary concerns. a total of 4 AMs were used in this study. AMs were defrosted in room temperature for 10 minutes prior to use. Then, the plastic paper was peeled off and the AMs were washed in balanced saline solution.

4A.3.5. *In-vitro* cell viability and attachment evaluation

4A.3.5.1. Human limbal epithelial cell isolation and culture

Healthy human limbal tissues (2 mm length and from superior limbus) were transferred immediately to the laboratory using a special media containing Hank's balanced salt solution (HBSS), amphotericin B, and penicillin/streptomycin (all three: Gibco, Massachusetts, USA), at 4 °C. Limbal epithelial progenitor cells (LEPCs) were isolated by using mechanical and enzymatic processes under sterile conditions as follows:

The samples were first cut into smaller pieces and incubated in 10 mM dispase II for 2 hours at 37 °C. Following isolation of the epithelial layer, the limbal samples were incubated in collagenase II for 20 minutes at room temperature and treated with cold trypsin for 10 minutes at 37 °C. The specimens were then centrifuged (400 g at 4 °C). Lastly, the collected cells were suspended in supplemental hormonal epithelial medium (SHEM) and cultured in cell culture plates. To cultivate LEPCs, a mixture of DMEM/F12 (Gibco, Massachusetts, USA; 1:1) was used and supplemented with 10% human serum, 1.05 mM calcium, 5 µg/ml crystalline bovine insulin, 30 ng/ml cholera-toxin, 2 ng/ml epidermal growth factor (EGF), 0.5% dimethyl sulfoxide (DMSO; all from Sigma Chemical Co, St. Louis, USA), 0.5 µg/ml hydrocortisone (Gibco, Massachusetts, USA) , 5 ng/ml sodium selenite (Gibco, Massachusetts, USA), and 5 µg/ml apo-transferrin (Gibco, Massachusetts, USA). Adherent epithelial cells were separated after 3 weeks.

4A.3.5.2. Cell attachment and proliferation assays

MTT assay was used to assess cell viability and proliferation on the proposed membrane. Among the enzyme-based assays, MTT assay is the best-known method for determining mitochondrial dehydrogenase activities in living cells. Enzyme-based methods rely on a reductive coloring reagent and dehydrogenase in a viable cell to determine cell viability with a colorimetric method. These methods are superior to others since they are easy-to-use, safe, highly reproducible, and widely used in both cell viability and cytotoxicity tests.

Human limbal epithelial progenitor cells (LEPCs) at a plating density of 5×10^3 cells/well were seeded onto membranes in 96 well plate cell cultures. For the analysis of proliferation rate and viability after 24, 48, 72 hours of culture, 20 µL of MTT (Sigma, US) substrate (of a 2.5 mg/ml stock solution in phosphate-buffered saline) was added to each well, and then all the plates were returned to standard tissue incubator conditions for an additional 4 hours, after which, the medium was removed, and the cells were solubilized in 100 µL of dimethyl sulfoxide (DMSO, Sigma, US) in preparation for the colorimetric analysis (wavelength, 570 nm, PHOMO microplate reader).

4A.3.6. Mechanical properties, suturability and assessment of surgical handling of the membranes

To quantify the mechanical properties and suturability of the gelatin-based membranes, a universal testing machine (UTM, Shimadzu, Japan) was employed. Membranes were examined in terms of Young's modulus, ultimate strength and the suture retention strength. To do this, membranes were fixed in the lower clamp of the machine; a standard steel wire (D = 0.3 mm) was punctured through the membrane and the two ends were enclosed within the upper clamp to form a ring-like structure. Suture pullout was conducted by moving the upper clamp with the force being monitored. The mechanical tests were conducted using a 1 kN load cell and a crosshead speed of 1 mm/min.

The objectivity of the surgical handling assessment was ensured by assigning three different surgeons with subspecialty in Cornea and Ocular Surface to conduct the operations. Surgeons did not have any prior knowledge about the make and composition of the scaffolds to mitigate the bias in their evaluations. The assessment comprised of suturability, ease of manipulation and cutting with surgical forceps and scissor, and rigidity in terms of how the scaffold lied on the tissue. Surgical operations were recorded (see supplementary data for the videos). Comparative evaluation of the surgical handling of our membrane versus AM was also done by recording and evaluating *in-vivo* operations (details are provided in section 4A.3.7).

4A.3.7. Conjunctival defect induction and AM/gelatin-based membrane implantation in rabbit models

The study included ten male albino rabbits weighing between 3 and 4 kg. The rabbits were all treated according to national guidelines. All investigations conformed to the ARVO Statement for the Use of Animals in Ophthalmic and Vision Research and were approved by Tehran University of Medical Sciences. Eight rabbits were used as the study group. Induced conjunctival defects were transplanted with gelatin-based membrane in one eye and AM in the contralateral eye. The remaining two rabbits served as the control group and were left ungrafted (bare) after conjunctival excision, in only one eye. All surgeries were performed by the same surgeon with the aid of a surgical microscope. The rabbits were first anesthetized by intramuscular injection of

ketamine (15 mg/kg) and xylazine (5 mg/kg). The eyelids were held open during surgery by a speculum.

The defect location was first marked by 8 mm vacuum trephine, colored with surgical ink at the edge, on the supra-temporal conjunctiva of both eyes of each rabbit. The conjunctiva and Tenon were excised with Vannas scissors to the level of bare sclera, ensuring that no Tenon remained. All defects maintained a 2 mm distance from the corneal limbus. Special care was exercised so that the induced defects only involved the bulbar conjunctivae and were not extended into the forniceal area. The use of anchoring sutures, required in surgeries involving fornix reconstruction, was not within the scope of this study.

The gelatin-based membrane and AM were marked with the same vacuum trephine as described above and cut into 8 mm round pieces with Vannas scissors. The AM (epithelium side up) and gelatin-based membrane were secured to episclera with four Nylon 6.0 (Supa, Tehran, IR) sutures (one at the limbal and the other at the forniceal side of the defect) to prevent dislodging, and the remaining surface was adhered to the bare sclera with fibrin glue (Beriplast® P Combi Set, CSL Behring, USA). Both implants covered the bare area completely. The edges of the conjunctivae were slightly pulled to meet the edges of the membranes or AM (Figure 4A.1). Eyes in the control group were left ungrafted, without any further manipulation. Chloramphenicol and betamethasone (Sina Darou, Tehran, IR) eye drops were instilled in the eyes of all rabbits immediately after surgery and then twice a day afterwards for 4 weeks.

4A.3.8. Clinical observations

All rabbits were examined and photographed on days 1, 7, 14, 21 and 28 post-surgery. During examinations, the defect size and epithelialization extent were investigated via fluorescein staining under cobalt blue light. Inflammation severity (rated as mild, moderate, or severe, based on the degree of conjunctival hyperemia and vessel engorgement) and discharge were probed. The scar tissue formation was qualitatively assessed based on gross clinical observations (in terms of conjunctival contracture, vascular pattern alteration, scleral vessel obscuration, and the appearance of fibrous tissue). The presence of granulation tissue or symblepharon were also recorded. Each rabbit was examined by two ophthalmologists independently (i.e. the surgeon and

another ophthalmologist who was blind towards the study groups). All observations were double checked.

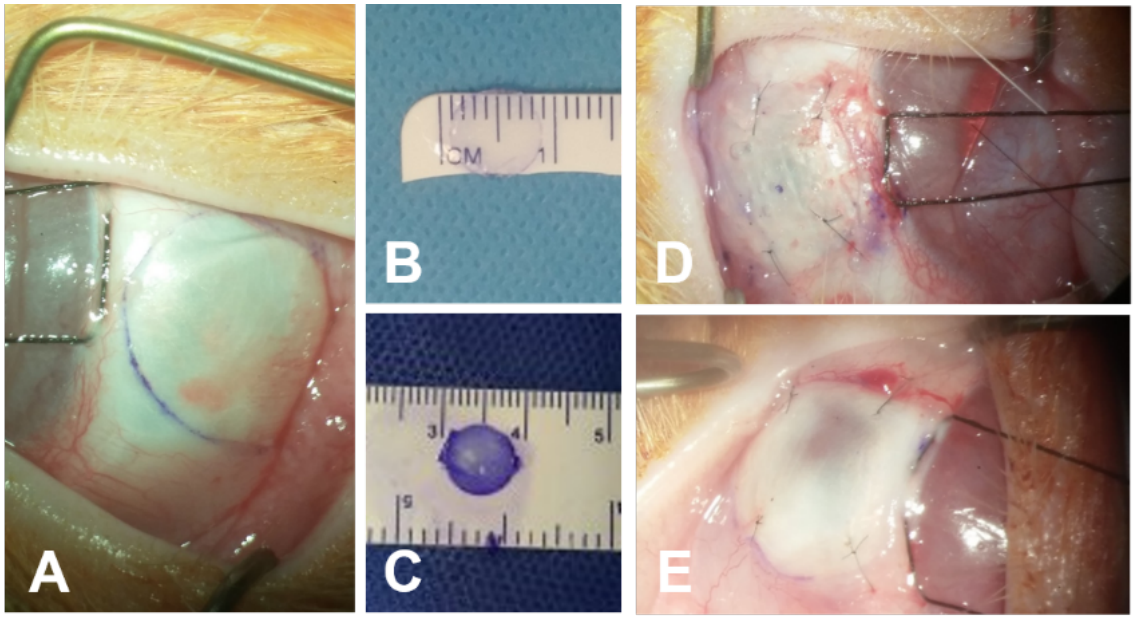

Figure 4A.1: Induction of conjunctival defect and implantation of membranes. (A) The final defect, (B) Gelatin-based membrane, (C) AM cut into an 8-mm round piece, (D) Representative eye implanted with Gelatin-based membrane, (E) Representative eye grafted with AM.

4A.3.9. Histological staining

All 14 rabbits were sacrificed on day 28. Intact eyes, including forniceal and palpebral conjunctivae, were removed via orbital enucleation by the same initial surgeon, and then fixed via immersion in 10% formaldehyde and transferred to the pathology department. Sections were obtained from the center and edges of each healed defect. All dissections were done in the presence of the surgeon to ensure that the exact defective site was included. Sections were then embedded in paraffin, cut into 5 micrometer thick layers using a microtome, and stained with Hematoxylin and Eosin (H&E) for general tissue morphology. Further and more specific staining was performed in order to evaluate goblet cell density and collagen alignment, as discussed in sections 4A.3.9.2 and 4A.3.9.3. Each specimen was observed under 100X and 400X magnifications by a pathologist who was blind towards the treatment groups. All observations were then double checked in the presence of the surgeon.

4A.3.9.1. H&E staining

Epithelialization was recorded as the presence or absence of a continuous layer of epithelium at the defective site. The quality of the healed epithelium was further assessed by recording the number of epithelial layers, representing stratification, and the flattening of epithelial cells while migrating towards the superficial epithelial layers. The inflammation was quantitatively recorded based on the average density of the inflammatory cells observed in each power field. In doing so, the following grading was used: (0) none, (1) mild, (2) moderate, and (3) severe. The inflammation was further classified as granulomatous and non-granulomatous based on the presence of giant cells and histiocytes at the healed defective site or surrounding the transplant.

4A.3.9.2. Periodic Acid Schiff (PAS) staining

All tissue sections were stained with PAS and characterized in terms of goblet cell morphology and density (i.e. goblet cell count in any group of 100 cells within the epithelium). After characterization, the stained tissue sections were divided into two groups, including one with sections with less than 10% goblet cell density and one with those equal to or more than 10% density.

4A.3.9.3. Masson's Trichrome (MT) staining

In order to evaluate the quality of healed sub-epithelial stroma, all sections were additionally stained with MT to observe collagen fibril alignment. The observed quality was rated as follows: (1) randomly aligned and loose collagen deposition, or (2) parallel and packed collagen deposition. Sub-epithelial fibrosis was considered to be present if a packed and parallel collagen alignment, stained blue with MT, was observed in the sub-epithelial area.

4A.3.9.4. Immunohistochemical staining for alpha-Smooth Muscle Actin (α-SMA)

The presence or absence of α-SMA was recorded in each power field. The higher density of myofibroblasts served as an indicator of a higher possibility for tissue contraction in the future.

4A.3.10. Statistical analysis

The raw data was analyzed using Statistical Product and Service Solutions (SPSS) v25.0 software. The normality of data distribution was checked using the Kolmogorov-Smirnov test. The Fisher's exact test was performed to compare categorical data of three groups under investigation. The

continuous data of the groups were compared using Kruskal Wallis analysis. All reported *p*-values were two-sided. The inferences were considered to be statistically significant when the *p*-values were less than 0.01.

4A.4. Results

4A.4.1. Ink formulation and 3D-printing of the membranes

The ink employed in this study was composed of gelatin, elastin and sodium hyaluronate. Figure 4A. 2 presents the important challenges that should be considered when developing the ink formulation and setting printing parameters.

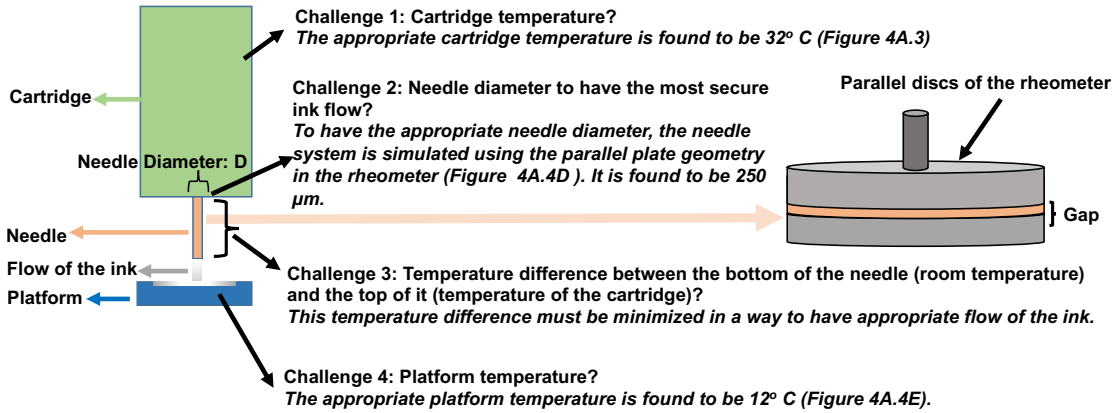

Figure 4A.2: A diagram to explain the ink flow and the thermal model used in this study: For successful 3D-printing, we need to adjust the printing parameters to have appropriate cartridge temperature, needle diameter, temperature difference between the bottom and top of the needle, and the platform temperature as four main challenges.
Challenge 1 (cartridge temperature): Needle obstruction affected by ink gelation can be controlled by adjusting the ink gel point and cartridge temperature. The ink gel point is shown in Figures SI2.1 and SI2.2, and the suitable cartridge temperature are found by creep and recovery test, as explained in Figure 4A.3. 32°C is found to be the suitable temperature for cartridge using the ink of this study.
Challenge 2 (needle diameter): The appropriate needle diameter is found by simulating the needle of the printer using the parallel plates of the rheometer while the "Gap" between the plates is half of the needle dimeter (D) to have the same ratio of surface to volume for two systems (Gap=D/2). The appropriate needle dimeter found in Figure 4A.4 D is 250 µm to have the most secure ink flow.
Challenge 3 (temperature difference between the bottom and top of the needle): The bottom of the needle is at the room temperature, while the temperature of top of the needle is equal to the cartridge temperature. Thus, there is a gradient of temperature between the bottom and top of the needle, which influences the viscosity of the ink. This temperature difference can be minimized by making the ink formulation in a way to have the gel point temperature—and, in turn, the cartridge temperature—closer to room temperature.
Challenge 4 (platform temperature):The proper platform temperature for suitable hardening of the ink is explained and found in figure 4A.4E (12°C).

Gelatin sol-gel transition plays an important role in the printing procedure as it might be both in favor of or against successful printing. While it assists the ink hardening on the platform and shape fidelity of the printed strands, it might cause obstruction of the dispensing needle and interruption of printing. The sol-gel transition temperature of each individual formulation was determined as the frequency-independent value of the damping factor (tan δ) obtained from a multi-frequency plot for a temperature sweep measurement [432] (Figure SI2.1).

The sol-gel transition temperature was found to be around 22, 24 and 28 °C for 4, 8, 16% (w/v) aqueous solution of gelatin (G4, G8 and G16), respectively (Figure. SI2.1). Addition of both elastin and sodium hyaluronate had a minor effect on the gelation temperature, except in the case of G4E2H0.5 where the sol-gel transition could not be detected. In our formulation, gelatin is known to form a thermally reversible physical network when cooled through local assembly of protein coils into triple helices dominated by hydrogen bonding [489]. Our data suggests that there is no significant complexation between sodium hyaluronate and gelatin molecules, which is in agreement with the isothermal microtitration calorimetry results obtained by Picard *et al*. [490]. It has been reported that the extent of triple helix formation in gelatin-hyaluronic acid mixtures is independent of hyaluronic acid concentration, suggesting that unlike some vegetal polysaccharides such as inulin, arabic gum or guar gum [491], hyaluronic acid does not influence network formation in the physical gelatin gel [490].

Amongst all the formulations containing gelatin, elastin and sodium hyaluronate, the sol-gel transition temperature of G8E2H0.5 was found to be close to room temperature. Using such an ink, the obstruction of the dispensing needle that is in contact with ambient temperature can be avoided, while hardening of the ink can be achieved by adjusting the platform temperature well below the room temperature. This formulation was selected to be further characterized and then printed.

In addition to the method proposed by Winter and Chambon [492], the critical gelation point of G8 and G8E2H0.5 samples were determined through plotting the apparent viscoelastic relaxation exponents n' and n" ($G' \propto \omega^{n'}$, $G'' \propto \omega^{n''}$) obtained from the frequency dependence of storage (G') and loss (G") moduli at each temperature (see SI2, Figure. SI2.2(A, B, D, E)) against temperature

to track a crossover where n' = n" = n (as shown in Figure. SI2.2(C, F)). While the two methods of determination of critical gelation temperature delivered very close values (~ 24 °C), the latter suggests a slightly lower gelation temperature for G8E2H0.5 compared to G8.

To further examine the effect of additives and to choose appropriate cartridge temperature, creep and recovery tests at different temperatures were performed. The applied stress was bigger than the yield stress of the gel at the lowest examined temperature. As seen in Figure 4A.3(A), G8 and G8E2H0.5 showed a very similar viscoelastic liquid behavior at 20 °C, which is well below the gelation temperature of both. This finding suggests that the elasticity of the gel determined from the total recoverable deformation is mainly governed by gelatin and, consequently, helices content as discussed before. Despite huge similarity, slight differences can be observed in terms of non-recoverable (J_{NR}) and steady-state compliance (J_e^0), both of which are slightly higher for G8E2H0.5. It is worth mentioning that while a viscoelastic liquid has no equilibrium compliance, for such a material, the creep is the sum of a deformation approaching a constant value (J_e^0), analogous to equilibrium compliance for a viscoelastic solid, plus a viscous flow contribution (t/η_0 where t is the creep time and η_0 is Newtonian viscosity). The steady-state compliance (J_e^0) can be considered as a measure of the elastic deformation during steady flow [493].

At 24 °C (very close to the gelation temperature if not exact), the compliances are one order of magnitude higher than 20 °C and both formulations again displayed viscoelastic liquid behavior (see Figure 4A.3(B)). The relatively high instantaneous compliances (J_0) for both formulations contributed to a big non-recoverable deformation. The higher creep compliance and non-recoverable deformation for G8E2H0.5 compared to G8 support the outcome of gelation temperature determination through apparent viscoelastic relaxation exponents for slightly lower gelation temperature of G8E2H0.5. Despite being around 4 °C above the gelation temperature of both formulations, 28 °C cannot be considered as an ideal temperature for printing, again since the formulation represents a viscoelastic liquid behavior with slight recovery, and the deformation/flow of the material is time-dependent. It can be seen in Figure 4A.3(C) that G8E2H0.5 is more resistant to deformation compared to G8, likely because of higher total

concentration and presence of high molecular weight sodium hyaluronate. It again supports the assumption that at 24 °C, the higher resistance of G8 to deformation compared to G8E2H0.5 could be because of its prompter gelation. Both formulations represented Newtonian behavior at 32 °C, where the presence of sodium hyaluronate acts as a thickener to increase the resistance to flow (see Figure 4A.3(D)). This temperature can be considered as an appropriate temperature or the minimum required temperature for printing. All in all, surrendering the quantitative point of view, the creep behavior of the formulations was very similar, implying the key role of gelatin in the formulation.

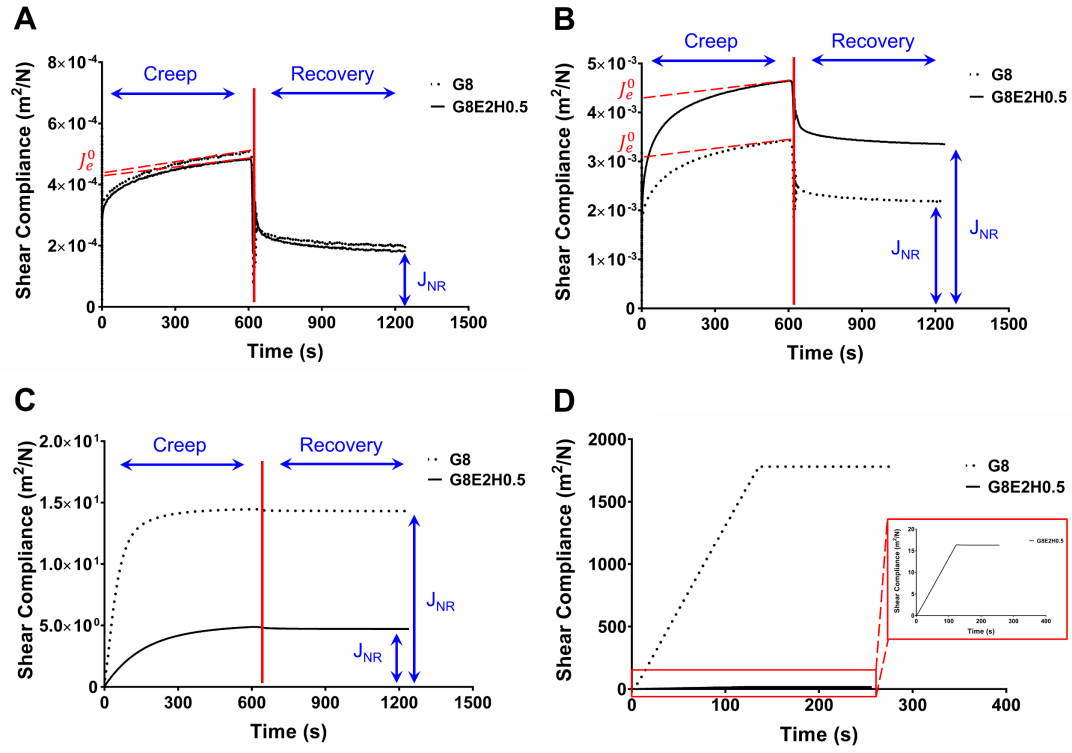

Figure 4A.3: Creep and recovery tests performed at (A) 20 °C, (B) 24 °C, (C) 28 °C and (D) 32 °C for G8 and G8E2H0.5 samples.

Figure 4A.4(A-C) shows the shear viscosity of G4E2H0.5, G8E2H0.5 and G16E2H0.5 as a function of shear rate and temperature. Increasing the gelatin concentration had a remarkable effect on the viscosity, particularly at lower temperatures. The viscosity of all the formulations decreased with increasing temperature, whereas the degree of variation was strongly dependent on gelatin concentration. At lower temperatures (closer to the gelation temperature), the formulations demonstrated shear thinning behavior, whereas at temperatures above 30 °C all

behaved nearly Newtonian. Although hyaluronic acid is known to behave as a non-Newtonian and viscoelastic fluid in aqueous solutions [494], both gelatin and hyaluronic acid solutions with concentrations close to the values in our study have been reported to display a Newtonian behavior at elevated temperatures [490]. It has been suggested that the behavior of gelatin-hyaluronic acid mixtures is dictated by the hyaluronic acid, and gelatin only influences the viscosity from a quantitative point of view. As a result, the shear thinning behavior of such mixtures at high shear rates has been hinted to be a result of alignment of polysaccharidic chains in the direction of the flow [490].

Figure 4A.4(D) illustrates the mass flow rate of G8E2H0.5 formulation as a function of printer actual pressure at 32 or 34 °C, dispensed using standard 25G (250 μm) or 22G (410 μm) needles. The relationship between the mass flow rate and pressure was nearly linear (coefficient of determination, R^2, greater than 0.9) for both dispensing needles and temperatures. Since the ink represents Newtonian behavior at both temperatures, the Hagen-Poiseuille's equation can be used to correlate the applied pressure and the flow rate as follows:

$$Q = \frac{\pi R^4 \Delta P}{8 \mu l} \qquad \text{Eq. 1}$$

where Q is the flow rate, R is the radius of the pipe, ΔP is the applied pressure, μ is dynamic viscosity and l is the length of the pipe. The linear relationship between the pressure and flow rate, as well as the ratio of the slopes of the lines ($(D_2/D_1)^4 = 7.23$, D_2=410 μm, D_1=250 μm vs. average ratio of the slopes = 7.21), suggests that the flow of the ink through the needle is governed by the Hagen-Poiseuille's equation. Using the G25 needle at 32 °C, the mass flow rate fluctuation caused by varying the applied pressure could be minimized, which is beneficial to the printing procedure, as it reduces the system sensitivity.

Needle obstruction due to ink gelation in the dispensing needle and shape fidelity affected by ink hardening speed on the platform were found to be two important challenges that needed to be addressed to enable successful printing of the membranes. The former was addressed through adjusting the gelation temperature close to the room temperature, while the latter was controlled through cooling the platform. Figure 4A.4(E) illustrates the effect of final temperature, cooling

rate and the gap distance on the complex shear modulus of G8E2H0.5 as an indicator for the overall resistance to deformation over time when cooled down from 32 °C using a parallel plate geometry in the rheometer. Indeed, altering the gap distance is expected to affect the heat loss by varying the surface area to volume ratio. Surface area to volume ratio is inversely proportional to the gap distance and diameter of the dispending needle, as halving either one doubles the ratio. As seen in Figure 4A.4(E), the final temperature and cooling rate drastically influence the complex shear modulus, while the effect of gap distance can be neglected.

The minor effect of surface area to volume ratio in the range examined can also be explained by heat transfer equations. As an example, two-dimensional heat conduction equation can be written as:

$$q = kS\Delta T \qquad \text{Eq. 2}$$

where q is the heat flow rate, k is the thermal conductivity, S is the shape factor and ΔT is the temperature difference. For an isothermal cylinder of radius "r" placed in semi-infinite medium, like the dispending needle placed in air, the shape factor is given as [495]:

$$S = \frac{2\pi L}{\ln\frac{2L}{r}}; \quad L \gg r \qquad \text{Eq. 3}$$

where L in the length of the cylinder/needle.

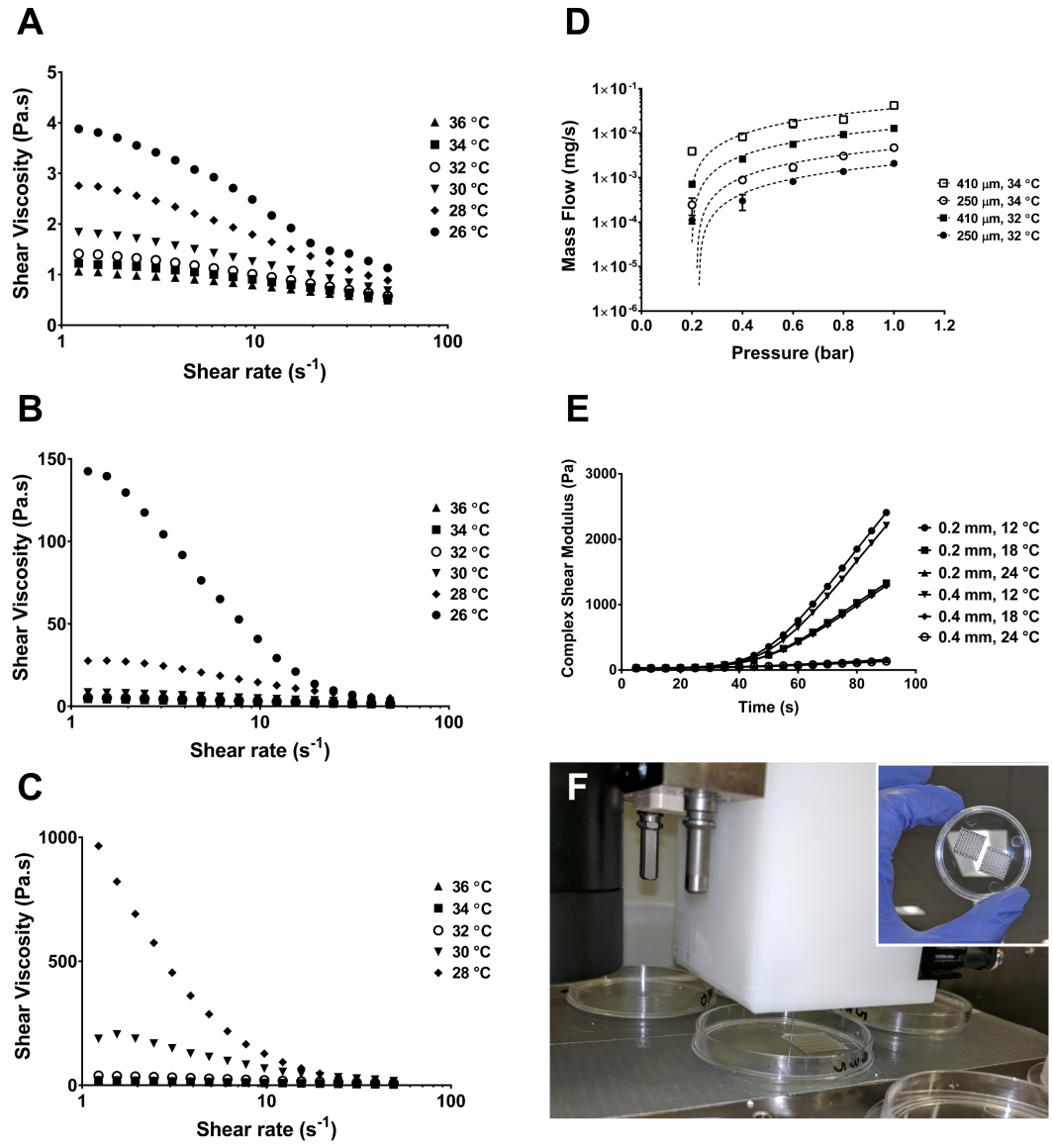

Figure 4A.4: The shear viscosity of (A) G4E2H0.5, (B) G8E2H0.5, (C) G16E2H0.5 as a function of shear rate at different temperatures. (D) The mass flow rate of G8E2H0.5 as a function 3D-printer actual pressure, dispensing needle gauge and temperature. (E) The complex shear modulus of G8E2H0.5 as a function of time, gap distance, final temperature and cooling rate when the formulation is cooled between the rheometer parallel plates; the initial temperature was 32 °C and the material was cooled down to 12, 18 or 24 °C with a cooling rate of 10, 8 or 4 °C/min, respectively. (F) The printing procedure on petri-dishes and the obtained 3D-printed membranes.

The variation of the shape factor by even doubling the radius/diameter while keeping the length constant will be very small:

$$S_r = \frac{2\pi L}{\ln\frac{2L}{r}}\ ; \quad S_{2r} = \frac{2\pi L}{\ln\frac{2L}{2r}} = \frac{2\pi L}{\ln\frac{L}{r}} \quad \rightarrow \quad \frac{S_{2r}}{S_r} = \frac{\ln\frac{2L}{r}}{\ln\frac{L}{r}} = 1 + \frac{\ln 2}{\ln\frac{L}{r}}\ ; \quad \ln\frac{L}{r} \gg \ln 2$$

Considering ln (L/r) >> ln 2, the sensitivity of the shape factor to the variation of the radius is trivial. When the final temperature was set very close to room temperature (i.e. 24 °C), no significant increase in complex shear modulus was observed over time, suggesting the possibility of printing without confronting the needle obstruction. Reaching 12 °C with a high cooling rate resulted in a rapid rise of the complex modulus, which is in favor of shape fidelity. One may suggest to further reduce the platform temperature to achieve better shape fidelity. Such an assumption can be challenged by taking into account the fact that the platform temperature affects the dispensing needle temperature throughout the printing cycle and might drop it below the gelation temperature of the ink. Reflecting all the mentioned challenges, the parameters reported in the "methods" section were used to print the membranes.

4A.4.2. Morphology, line and surface roughness

Figure 4A.5 shows the surface morphology and characteristics of the printed membrane in both dehydrated and hydrated states. The roughness of the membrane surface was found to be in the micrometric range. The membranes had an average pore size of 286 and 374 μm in dehydrated and hydrated states, respectively. Hydration of the samples led to increased roughness (R_a and S_a) and pore size simply because of the swelling. Substrate topography at the micro- and nanoscale has been reported to impact cell attachment behavior [496]. Micrometer-scale surface roughness improves the cell attachment compared to smooth surfaces [497, 498]. It has been suggested that cells tend to maximize the contact area with the surface probably to establish a robust anchorage [496, 499]. The layout of the topographic details might then induce a specific cell alignment as a result [496].

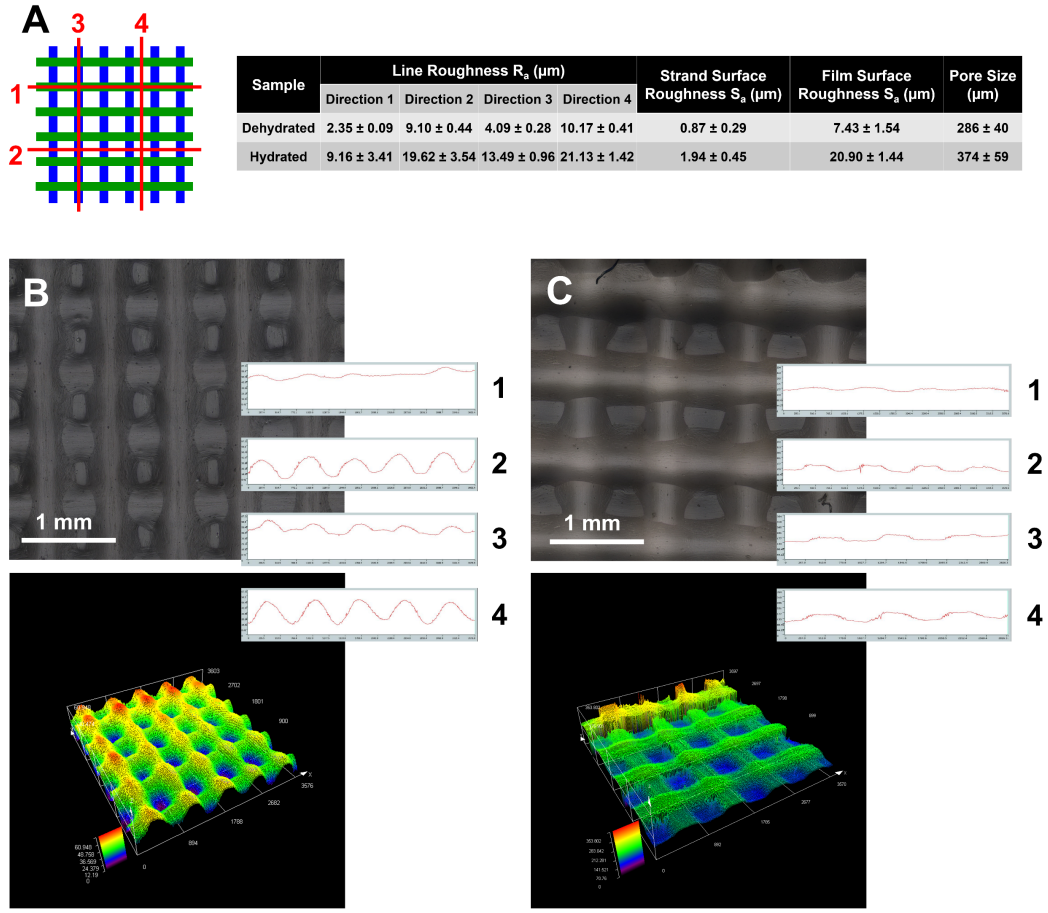

Sample	Line Roughness R_a (µm)				Strand Surface Roughness S_a (µm)	Film Surface Roughness S_a (µm)	Pore Size (µm)
	Direction 1	Direction 2	Direction 3	Direction 4			
Dehydrated	2.35 ± 0.09	9.10 ± 0.44	4.09 ± 0.28	10.17 ± 0.41	0.87 ± 0.29	7.43 ± 1.54	286 ± 40
Hydrated	9.16 ± 3.41	19.62 ± 3.54	13.49 ± 0.96	21.13 ± 1.42	1.94 ± 0.45	20.90 ± 1.44	374 ± 59

Figure 4A.5: (A) Line roughness of the printed membrane measured in 4 different directions, surface roughness of the strands and the whole membrane and the average pore size in both dehydrated and hydrated states along with the morphology and height profile of the surface of the membrane as well as the histograms in all the specified directions for both (B) dehydrated and (C) hydrated states were obtained using laser microscopy.

4A.4.3. *In-vitro* cell attachment and proliferation assays

The results of the *in-vitro* cell viability and proliferation study indicate good biocompatibility. Absorbance values increased from 24 to 72 h and showed values close to the control group (tissue culture plate) (Figure 4A.6). Additionally, SEM images of the membrane surface were obtained 48 h after cultivation. The images showed adhesion of corneal epithelial cells on the membrane surface. The cells kept their normal morphology and malformed cells were not observed. Moreover, signs of degradation were visible. The latter could be a culprit of the observed low count of cells on the membrane surface, since the cells could have migrated to subsurface regions through the intrinsic porous texture and porosity caused by degradation.

It should be noted that while it would be ideal to use conjunctival epithelial cells to conduct *in vitro* tests, a wide range of cell types have been suggested for assessing the efficacy of fabricated scaffolds for ocular surface/conjunctival reconstruction [500-507].

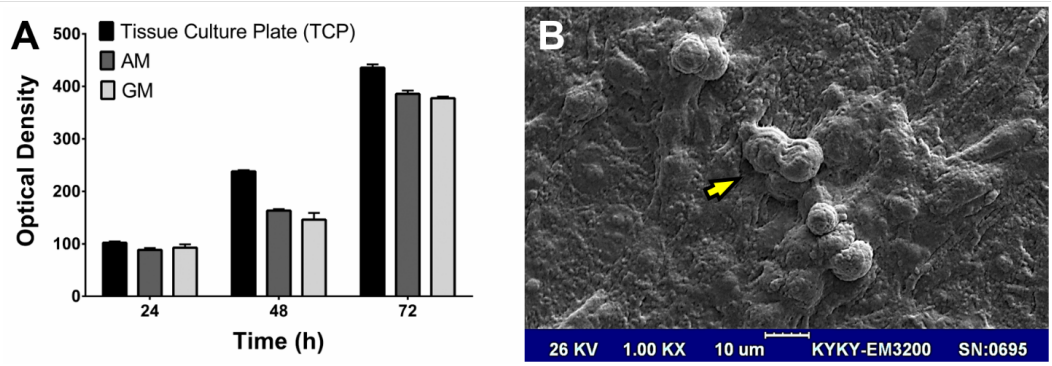

Figure 4A.6: In vitro study of the samples. (A) MTT test absorption values at 24, 48 and 72 h. (B) SEM image illustrating partial gelatin-based membrane degradation and epithelial cell adhesion to the surface, 48 h after cultivation.

4A.4.4. Mechanical properties, suturability and assessment of surgical handling of the membranes

The young's modulus, ultimate strength and suture retention strength of the gelatin-based membranes, were found to be 170.2 ± 36.1 kPa, 95.4 ± 10.1 kPa and 20.4 ± 2.03 g, respectively (Figure SI2.3). Four samples for each experiment were used (n=4), and the reported values are in the form of mean value ± standard deviation (SD).

The pre-operative assessment showed that gelatin-based membranes were suturable, easy to manipulate with surgical forceps and had favorable rigidity. Surgical handling of the gelatin-based membrane appeared to be simpler in terms of cutting ease and placement in the defect (i.e. the membranes did not fold as much as AM did and upside-down placements were easily recognizable). These attributes made suturing easier with gelatin-based membranes (see supplementary videos-suturability). Also, the gelatin-based membranes showed a faster and stronger response to fibrin glue.

In addition to the ease of surgical handling, the gelatin-based membrane studied in this investigation had transparency and (potentially) geometrical conformity. The gelatin-based

membranes can be fabricated in any shape (conforming to a given forniceal area shape), leveraging inherent capability of 3D printing in making complex geometries.

4A.4.5. *In-vivo* conjunctival tissue reconstruction and clinical outcomes

Defects were artificially induced in supralateral bulbar conjunctivae of eighteen eyes using the method detailed in section 4A.3.7. The final defect size had an average diameter of ~9 -10 mm due to retraction of adjacent Tenon. Two eyes (from two different rabbits, one left eye and one right eye) served as the control group and were left untreated. The remaining sixteen eyes (from eight different rabbits) were grafted with either AM or gelatin-based membranes. The number of left eyes grafted with AM was equal to the number of left eyes grafted with gelatin-based membranes. The right eyes had the same count of AM grafts and gelatin-based membranes as well.

4A.4.5.1. Day 12 after surgery (2nd week)

Table 4A.2 captures clinical outcomes for the second week. On day 12 after surgery, the mean defect diameter was 8.6 ± 1.8 mm (3-10 mm), 5.8 ± 1.7 mm (3-10 mm) and 0.0 mm for the gelatin-based membrane, AM and ungrafted eyes, respectively. No significant difference was observed between AM and the gelatin-based membrane groups ($p = 0.42$), while they were both significantly different from the control group ($p < 0.01$). Ungrafted wounds were completely epithelialized. Seven out of eight eyes grafted with AM showed epithelialization and vascularization at the edges of the wound, while one eye had no epithelialization. In the gelatin-based membrane grafted group, two eyes showed epithelialization and vascularization at the wound edges, and six eyes showed no signs of epithelialization. Both eyes in the control group were completely epithelialized. The mean inflammatory response score showed a significant difference between groups ($p < 0.01$), but AM and gelatin-based membrane were not significantly different. The mean score was 0, 2.25 ± 0.48 (range 0-4) and 2.87 ± 0.24 for the control group, eyes grafted with the gelatin-based membranes and AM, respectively. Seven of the eyes in the AM group showed severe inflammation, while only three eyes showed severe inflammation in the gelatin-based membrane group (Table 4A.2). Wounds grafted with either AM or the gelatin-based membrane showed infiltration with white debris that was confirmed to be composed of

acute inflammatory cells in pathology and negative for microbial contamination. The AM-grafted eyes were more strongly infiltrated. The gelatin-based membrane and AM were partially degraded at day 12 after surgery at the peripheral edges, while remaining as a sheath in the defect site (70-80% of the initial defect). All the gelatin-based membranes had maintained their porous structure and showed slight whitening at day twelve. The covering conjunctivae did not show any gross remodeling and scar tissue formation in the control and both study groups except for one rabbit in the AM group, which showed moderate remodeling and contracture in the conjunctivae.

4A.4.5.2. Day 19 after surgery (3rd week)

Table 4A.3 captures clinical outcomes for the third week. On day 19 after the surgery, the mean defect diameter was 0.87 ± 1.45 mm (0-6 mm), 1.62 ± 2.45 mm (0-10 mm), and 0.0 mm for the gelatin-based membrane, AM and ungrafted eyes, respectively ($p = 0.73$). No significant difference was observed between the treated groups ($p = 0.87$). Six out of eight eyes grafted with AM showed complete epithelialization; one had a 3 mm defect, and one eye had no epithelialization. Complete epithelialization was also observed in six out of eight eyes implanted with the gelatin-based membrane, while two other eyes showed defects of 6 and 1 mm in size. The mean inflammation score was 0.0, 1.0 ± 0.9 (range 0-3) and 1.75 ± 0.88 (range 0-3) for the control group, and eyes grafted with the gelatin-based membranes and AM, respectively, which did not show any significant difference between neither all three groups ($p = 0.13$), nor the treated groups ($p = 0.27$). On day 19, three eyes in the AM group showed zero to mild inflammation and three eyes were still showing severe inflammation, while six out of eight eyes grafted with the gelatin-based membrane had zero to mild inflammation and two eyes had severe inflammation (Table 4A.3). In the gelatin-based membrane group, inflammation was mainly seen in the surrounding host conjunctivae. Wounds grafted either with AM or the gelatin-based membrane still showed infiltration with white debris that was again confirmed to be composed of acute inflammatory cells in pathology; microbial tests were again negative. However, AM-grafted eyes were still more strongly infiltrated and the control group showed no inflammatory response. The implanted gelatin-based membrane and AM could not be completely identified in 5 and 6 eyes in each group, respectively, and only 10-20% of the original grafts could be seen in the remaining

eyes of both groups. Covering conjunctivae showed gross remodeling and scar tissue formation in both control eyes and in two AM grafted eyes but not in any of the gelatin-based membrane grafted eyes.

4A.4.5.3. Day 28 (4th week)

Table 4A.4 captures clinical outcomes for the fourth week. On day 28 after the surgery, all grafted and ungrafted wounds had completely epithelialized. The mean inflammatory response score showed a significant difference between all groups ($p < 0.01$) and between the treated groups ($p < 0.01$). The mean score was 0.0, 0.37 ± 0.35 (range 0-1), and 1.5 ± 0.63 (range 0-3) for the control group, eyes grafted with the gelatin-based membranes and AM, respectively. Wounds grafted either with AM or the gelatin-based membrane were still showing infiltration with white debris that was again confirmed to be composed of acute inflammatory cells in pathology and negative for microbial tests. The AM-grafted eyes were still more strongly infiltrated. The gelatin-based membrane and AM were not totally visible under the completely epithelialized surface except in two eyes in the gelatin-based membrane group, wherein the membranes were visible as sub-conjunctival prominences without significant inflammation of the adjacent conjunctivae. The covering conjunctivae showed gross remodeling and scar tissue formation in both of the control eyes, in three of the eight gelatin-based membrane grafted eyes and in six of the eight AM grafted eyes (Figure 4A.7).

Epithelialization rate of conjunctival defects in rabbits has been reported to be approximately 0.2-0.3 mm^2/hr [508]. Given that and considering the average defect size of ~ 63.5-78.5 mm^2 in our study, the epithelization should be completed in ~ 13-16 days. Noting that complete epithelialization was observed by the second week for both eyes in the control group, our planned time of ~ 13-16 days was validated and consistent with prior observations reporting the complete epithelialization between the first and second week in untreated eyes [341, 343]. Early signs of epithelialization were observed in the second week in 25% of the gelatin-based membrane-grafted eyes, compared to 75% in the AM-grafted cases and the mean defect size was approximately 3 mm smaller in the AM-grafted group. However, this difference did not appear to be statistically significant, which could be due to the small sample size (eight rabbits per group). This difference

began to subside and reached about 1 mm (less in gelatin-based membrane grafted eyes) at the end of the third week, wherein 75% of both grafted wounds showed complete epithelialization. Maximum reduction in the defect size was observed during the third week for both grafted groups. Hence, it would be accurate to say that epithelialization began somewhere between the second and third weeks for the gelatin-based membrane grafted group and approximately a week earlier for the AM grafted eyes. Taking into account the degradation profile of gelatin-based membranes (Figure SI2.4), it would be fair to conclude that the gelatin-based membrane met the time requirements of the conjunctival epithelial repair.

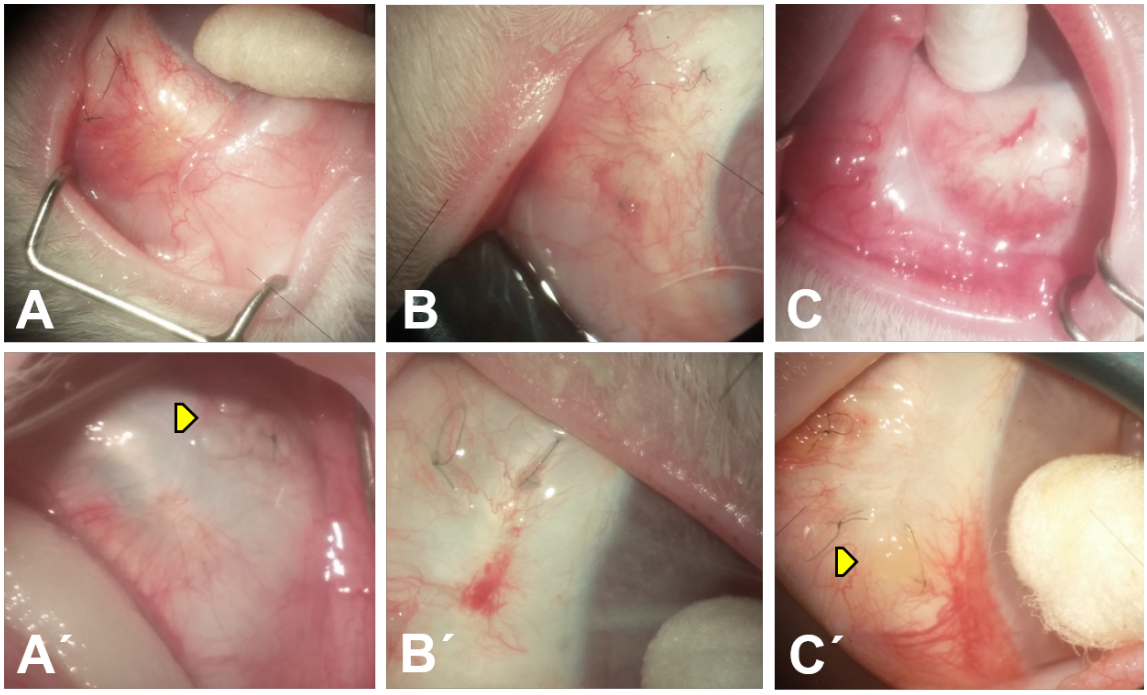

Figure 4A.7: Clinical observation at day 28. (A-C) AM transplanted eyes. Gross conjunctival remodeling and inflammation can be observed. Inflammation is more abundant at the wound edges. (A & B) Non-degraded AM was observed in eyes showing yellowish discoloration under the repaired conjunctivae. (A'-C') Gelatin-based membrane grafted eyes. Less inflammation and conjunctival remodeling was observed compared to AM grafted eyes. (A') Remnant membrane pieces can be seen under the conjunctiva (arrowhead) with no significant adjacent inflammation. (C') White debris clinging onto a suture in a gelatin-based membrane grafted eye. The trend of clinical observations is shown in Figure 4A.8.

In terms of inflammation, the gelatin-based membrane grafted group consistently showed milder degrees of clinically observed inflammation throughout the healing period compared to AM grafted eyes. A stark contrast in inflammation degree existed between the gelatin-based membrane and AM-grafted groups at week one. Severe inflammation was seen in 87.5% (7 out

of 8 eyes) of AM grafted eyes compared to 37.5% (3 out of 8 eyes) of the gelatin-based membrane implanted eyes. This difference subsided at week three, but again became significant at the end of the fourth week, wherein no moderate or severe inflammation remained in the gelatin-based membrane-grafted group while three eyes were still showing moderate degrees of inflammation in the AM group. This observation suggests a plausible likelihood for long-term inflammation in AM-grafted eyes, for which possible mechanisms will be discussed in section 4A.4.6. Early inflammatory responses could also be attributed to a reaction towards the preparation/preservation solutions and antibiotics; however, this factor was attempted to be limited by washing AM in balanced saline solution before transplantation. The trend of clinical observations is shown in Figure 4A.8.

Additionally, gross conjunctival remodeling was seen in both eyes of the control group, which is in agreement with other studies showing increased scar formation in conjunctivae when left untreated [341, 342, 344]. However, fornix foreshortening was an indicator of scar tissue formation in the latter studies, with one having the defect involving the forniceal area [344]. We did not use fornix foreshortening for scar tissue formation evaluation, as the defect was not distended towards the fornix, and anchoring sutures were not applied in the forniceal area. Mild to moderate gross remodeling was seen in 75% of AM-grafted eyes compared to 25% in the gelatin-based membrane grafted group on the fourth week, which can be attributed to prolonged inflammation of the AM-grafted eyes (details in section 4A.4.6).

Table 4A.2: Clinical Outcomes for 2nd Week

	Inflammation Histogram			*Defect Size*			*Tissue Contraction*		
	Bare	*Gelatin-based Membrane*	*AM*	*Bare*	*Gelatin-based Membrane*	*AM*	*Bare*	*Gelatin-based Membrane*	*AM*
Rabbit 1		2.0	3.0		3.0	3.0		*None*	*Moderate*
Rabbit 2		3.0	3.0		10.0	10.0		*None*	*None*
Rabbit 3		2.0	3.0		10.0	3.0		*None*	*None*
Rabbit 4		2.0	3.0		10.0	8.0		*None*	*None*
Rabbit 5		1.0	3.0		10.0	6.0		*None*	*None*

Rabbit 6		3.0	2.0		10.0	4.0		*None*	*None*
Rabbit 7		3.0	3.0		10.0	5.0		*None*	*None*
Rabbit 8		2.0	3.0		6.0	8.0		*None*	*None*
Rabbit 9	*0*			0			*None*		
Rabbit 10	*0*			0			*None*		

Table 4A.3: Clinical Outcomes for 3rd Week

	Inflammation Histogram			*Defect Size*			*Tissue Contraction*		
	Bare	*Gelatin-based Membrane*	*AM*	*Bare*	*Gelatin-based Membrane*	*AM*	*Bare*	*Gelatin-based Membrane*	*AM*
Rabbit 1		*0.0*	*2.0*		*0.0*	*0.0*		*None*	*Moderate*
Rabbit 2		*1.0*	*2.0*		*6.0*	*10.0*		*None*	*None*
Rabbit 3		*0.0*	*0.0*		*0.0*	*0.0*		*None*	*None*
Rabbit 4		*1.0*	*1.0*		*0.0*	*3.0*		*None*	*None*
Rabbit 5		*0.0*	*3.0*		*0.0*	*0.0*		*None*	*None*
Rabbit 6		*3.0*	*0.0*		*0.0*	*0.0*		*None*	*None*
Rabbit 7		*3.0*	*3.0*		*1.0*	*0.0*		*None*	*Moderate*
Rabbit 8		*0.0*	*3.0*		*0.0*	*0.0*		*None*	*None*
Rabbit 9	*0*			*0*			*Mild*		
Rabbit 10	*0*			*0*			*Mild*		

Table 4A.4: Clinical Outcomes for 4th Week

	Inflammation Histogram			*Defect Size*			*Tissue Contraction*		
	Bare	*Gelatin-based Membrane*	*AM*	*Bare*	*Gelatin-based Membrane*	*AM*	*Bare*	*Gelatin-based Membrane*	*AM*
Rabbit 1		*0*	*1*		*0*	*0*		*Moderate (Star Shaped Scar)*	*Moderate (Star Shaped Scar)*
Rabbit2		*0.0*	*1.0*		*0*	*0*		*Mild*	*Moderate*
Rabbit 3		*0.0*	*1.0*		*0*	*0*		*None*	*Mild*

Rabbit 4		*0.0*	*1.0*		*0*	*0*		*None*	*Mild*
Rabbit 5		*1.0*	*2.0*		*0*	*0*		*None*	*Moderate*
Rabbit 6		*1.0*	*2.0*		*0*	*0*		*None*	*None*
Rabbit 7		*1.0*	*0.0*		*0*	*0*		*None*	*None*
Rabbit 8		*0.0*	*2.0*		*0*	*0*		*Mild*	*Moderate*
Rabbit 9	*0*			*0*			*Mild*		
Rabbit 10	*0*			*0*			*Mild*		

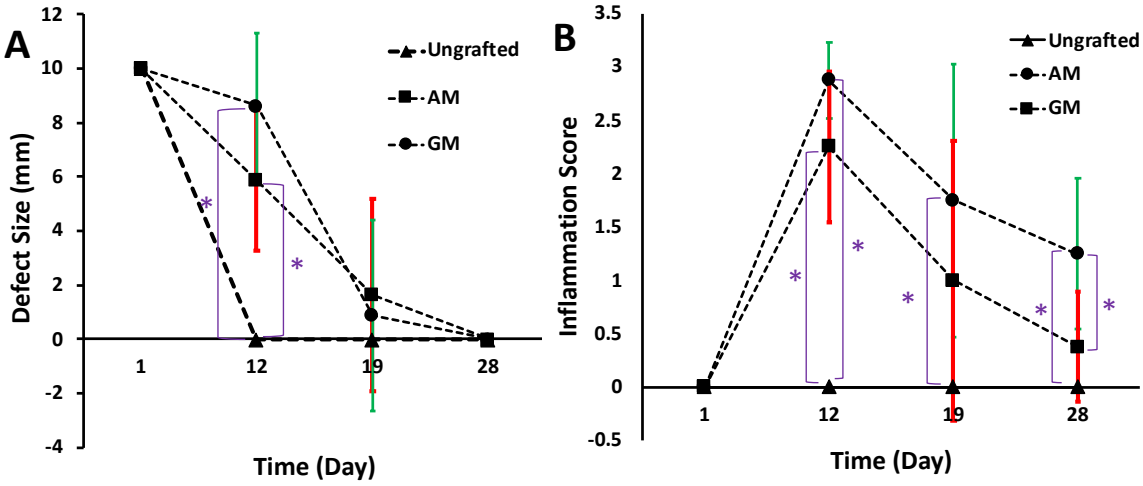

Figure 4A.8: (A) Clinical Observations of the defect size at 1st , 12th , 19th and 28th days post-implantation: GM and AM samples presented significantly higher defect sizes compared to the ungrafted sample (p=0.00078) only at day 12, but not in any other time points. The p-values between other samples in different time points are as follows: p=0.05203 for AM/GM at day 12; p=0.40081 for both Ungrafted/AM and Ungrafted/GM at day 19; p=0.91636 for AM/GM at day 19. The values are same for all samples at day 28 and thus p-value is 1.
(B) the inflammation score at 1st , 12th , 19th and 28th days post-implantation: Significant differences in the inflammation score can be observed between Ungrafted and AM (p=0.00078), and Ungrafted and GM (p=0.00078) at day 12, and between Ungrafted and AM at day 19 (p=0.01172) and day 28 (p=0.00328). Moreover, the inflammation is significantly less in GM samples compared to AM ones at the end of the experiment at day 28 (p=0.03132). The p-values between other samples in different time points are as follows: p=0.08312 for AM/GM at day 12; p=0.09289 for Ungrafted/GM at day 19; p=0.29362 for AM/GM at day 19; p= 0.20758 for Ungrafted/GM at day 28.
Note: Non-parametric ANOVA (Kruskal Wallis) has been used to measure the p-values and the results are considered significant at p <0.05

4A.4.6. Histological assessment of repaired conjunctival tissue

4A.4.6.1. H&E staining

H&E staining was done at the end of week 4 to assess the characteristics of the repaired conjunctivae. Complete epithelialization of the defect was seen in all groups (continuous). The repaired epithelium consisted of 3-5 layers of epithelial cells in eight of the gelatin-based membrane grafted and seven of the AM grafted eyes. All eyes grafted, whether with gelatin-based membrane or AM, showed normal cuboidal basal cells and flattening of the epithelial cells towards the surface. However, less than 3 layers of epithelium were observed in both control eyes with none showing flattening of the epithelial cells towards the surface and normal cuboidal basal cells (Figure 4A.9). Squamous metaplasia was seen in two of the eyes grafted with AM. Goblet cells had normal morphology in all groups (Table 4A.5).

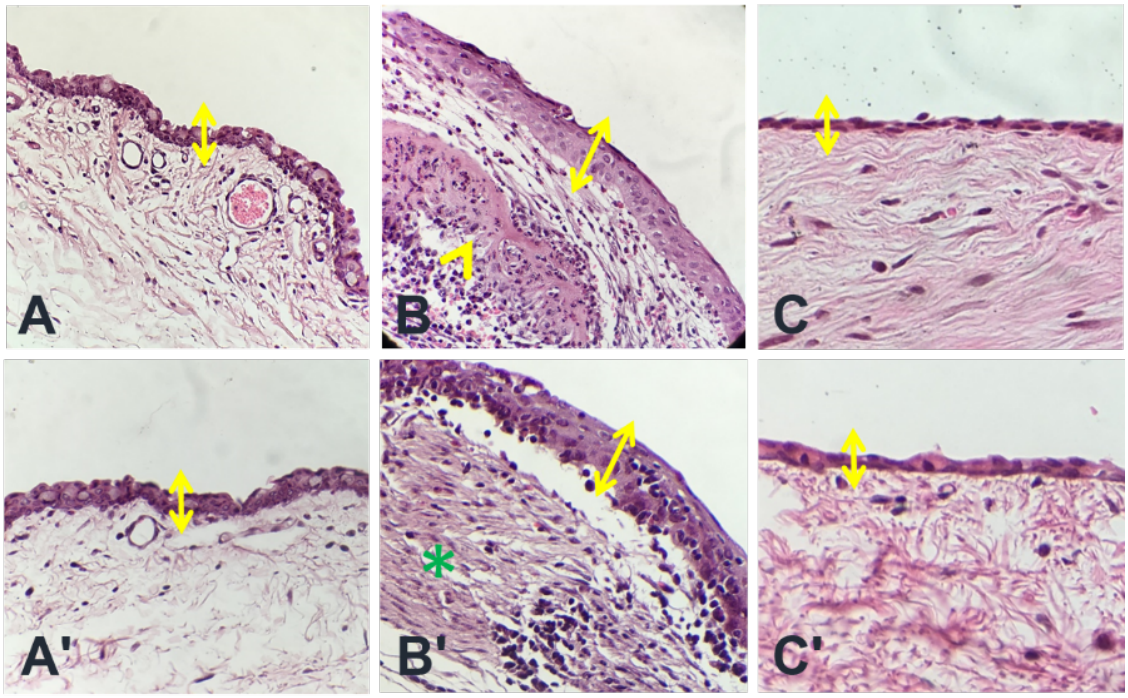

Figure 4A.9: H&E staining; (A & A') gelatin-based membrane grafted eyes: 3-5 layers of epithelial cells (yellow double arrow) are seen in the repaired epithelium with normal cellular morphology. (B & B') Amniotic membrane grafted eyes: 3-5 layers of epithelial cells (yellow double arrow). (B) Squamous metaplasia of epithelium (large cells with increased nuclear to cytoplasmic ratio) and remnant AM can be seen in sub-epithelial stroma (yellow arrowhead) with adjacent inflammatory reaction. (B') Severe inflammatory reaction in site of transplantation. (C & C') Ungrafted eyes: thin epithelium with non-satisfactory flattening of epithelial cells, especially in C'.

The membranes showed complete degradation in six out of eight of gelatin-based membrane grafted eyes and membrane remnants were seen in three eyes, while only one eye in the AM group showed complete degradation and AM remnant was seen in seven out of eight eyes grafted with AM.

The host inflammatory response was compared in the three groups. All eyes implanted with the gelatin-based membranes had inflammatory scores of less than one; four eyes showed no inflammation and the remaining four showed a mild inflammatory response. Of the two eyes in the control group, one showed none, and one showed a mild inflammatory response. In contrast, all eyes in the AM grafted group showed inflammatory responses. The inflammatory response was severe in six eyes and moderate in two eyes ($p < 0.001$ between all three, as well as between the two treated groups). The inflammatory cells consisted of lymphocytes and plasma cells in all groups. Mast cells were seen in the eyes of the AM grafted group. Histiocytes and giant cells, suggestive of granulomatous response, were present in seven out of the eight AM grafted eyes, while being present in only one of the gelatin-based membrane grafted eyes ($p < 0.001$ between all three as well as two treated groups) (Table 4A.6). Figure 4A.10 shows the host's inflammatory response towards the remaining membrane and AM.

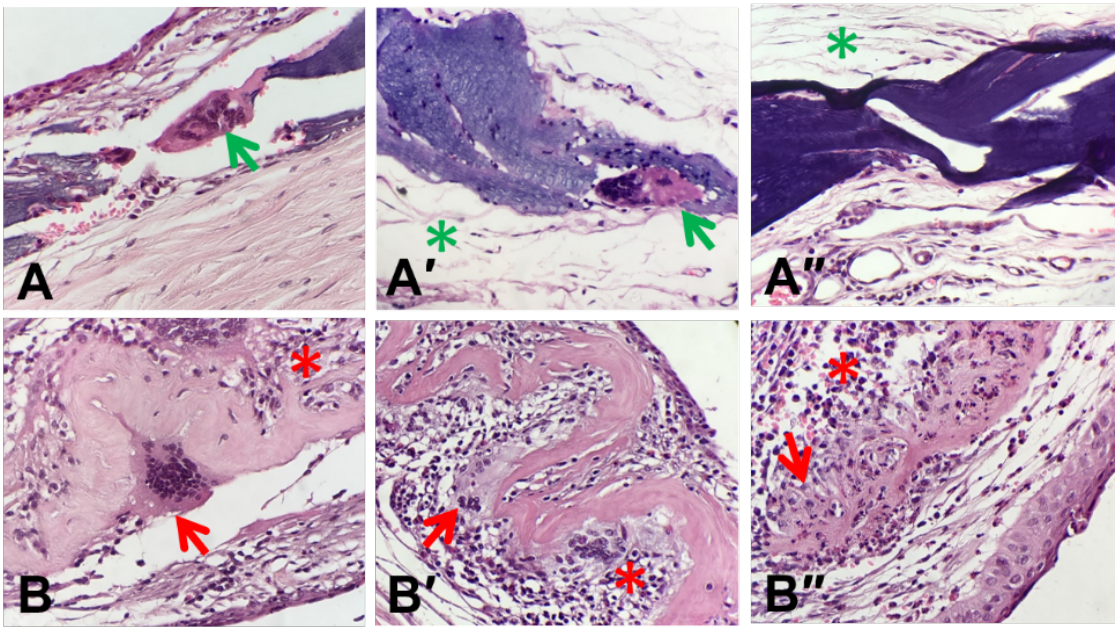

Figure 4A.10: H&E staining; (A & A' & A") Macrophages (green arrow) are digesting the gelatin-based membrane without an adjacent significant inflammatory response (green asterisk). (B & B' & B") Multiple giant cells (red arrow) along with a severe inflammatory response (red asterisk) composed of monocyte, macrophage and mast cells are seen around the remaining AM.

4A.4.6.2. PAS staining

PAS staining was performed to evaluate goblet cell density and compare it between the groups. Goblet cell counts per 100 cells were 2.50 ± 0.97, 10.87 ± 5.17 and 5.37 ± 2.68 in the control, the gelatin-based membrane and the AM grafted groups, respectively ($p = 0.13$ between all three groups and $p = 0.18$ between AM and gelatin-based membrane treated groups). Goblet cell counts of 10 and more were seen in five of the gelatin-based membrane grafted and two of the AM grafted eyes. No goblet cells were observed in eyes of the control group (Fisher's exact: $p = 0.42$ between all three groups, and $p = 0.41$ between AM and gelatin-based membrane treated groups) (Figure 4A.11, Table 4A.5).

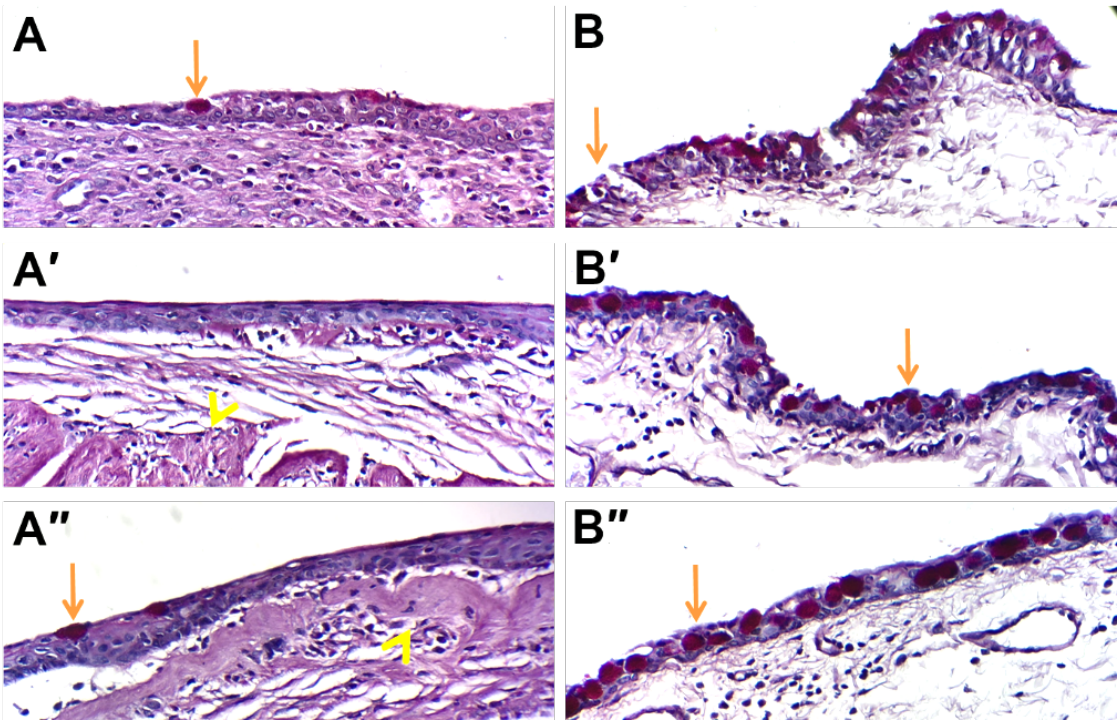

Figure 4A.11: PAS staining: (A&A'&A") Amniotic membrane grafted eyes: Less than 10 goblet cells (orange arrows) per 100 cells are seen along the repaired epithelium. Remnant amniotic membrane (yellow arrowhead) is seen in the sub-epithelial area with adjacent inflammatory cells and fibrosis. (B&B'&B") Gelatin-based membrane grafted eyes: 10 or more goblet cells per 100 cells are seen in the repaired epithelium. The sub-epithelial stoma shows no abundant inflammatory cell infiltration.

4A.4.6.3. Masson trichrome staining

Masson trichrome staining was carried out to evaluate the details of the sub-epithelial regenerated stroma. Comparing collagen alignment between the groups showed that collagen fibrils were aligned irregularly and angled, forming a loose and spongy stroma resembling that of the normal conjunctivae in all (eight) gelatin-based membrane grafted eyes, while composing a dense matrix of parallel and packed collagen fibrils in AM grafted eyes. The latter was especially seen adjacent to AM remnants. The sub-epithelial stroma in both ungrafted eyes showed a dense and thick layer (approximately 3 times thicker that the layer in the AM group) of parallel and densely packed collagen fibers under the thin epithelium (Figure 4A.11). The collagen alignment difference was significant ($p < 0.001$) between all three groups, as well as between the treated groups (Table 4A.6).

4A.4.6.4. Immunohistochemical staining for α-SMA

Immunohistochemical staining for α-SMA was carried out to evaluate and compare the presence of myofibroblasts (cells with contractile potentials) in the study groups. Smooth muscle cells of adjacent extraocular muscles and vascular pericytes are α-SMA-positive. α-SMA-positive cells, which had an elongated and fibroblast like morphology, were considered myofibroblasts (potentially contractile cells). Myofibroblasts were seen in four of the gelatin-based membrane grafted eyes, two contained many α-SMA-positive cells and two showed a moderate infiltration of cells into the stroma. The AM-grafted eyes staining outcome for the latter cell was positive in seven eyes, six of which showed severe infiltration and one showed moderate infiltration of cells in stromal tissue. α-SMA staining did not show any significant difference ($p=0.25$) between gelatin-based membrane and AM-grafted groups (Figure 4A.12 and Table 6).

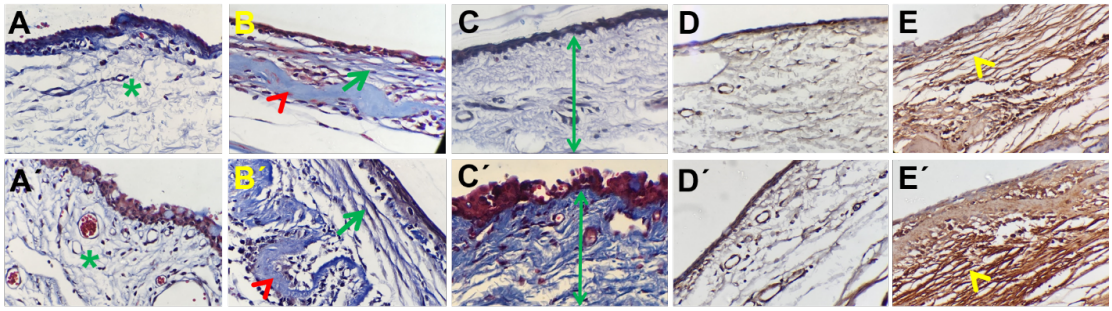

Figure 4A.12: Masson trichrome staining and IHC for α-SMA: (A&A') gelatin-based membrane grafted eyes showed random alignment of collagen fibers (green asterisk) while (B&B') AM grafted eyes showed parallel deposition of collagen (green arrow) along the AM remnant (red arrowhead). (C&C') A thick layer of densely packed collagen fibers was seen in both ungrafted eyes. (D&D') Gelatin-based membrane grafted eyes exhibited no α-SMA-positive cells while (E&E') AM grafted eyes exhibited numerous elongated α-SMA-positive cells.

Table 4A.5: Comparison of healed epithelium characteristics between gelatin-based membrane, AM and ungrafted eyes

Epithelium characteristics	*Bare*	*Gelatin-based Membrane*	*AM*	
				Fisher's exact test
Epithelial layers				
<3	*2*	*0*	*1*	*p = 0.02*
3-5	*0*	*8*	*7*	
>5	*0*	*0*	*0*	
Flattening				
Yes	*0*	*8*	*8*	*p = 0.007*
No	*2*	*0*	*0*	
Goblet count/100 cells				
	2.50 ± 0.97 (2-3)	*10.87 ± 5.17 (2-21)*	*5.37 ± 2.68 (2-12)*	*Kruskal wallis p = 0.13*

Table 4A.6: Comparison of inflammation (severity and type) and characteristics of the healed stroma between gelatin-based membrane, AM and ungrafted eyes (for details about grading criteria, see SI2)

Inflammation	*Bare*	*Gelatin-based Membrane*	*AM*	*Fisher's exact test*
Inflammation				*p < 0.001*
None (0)	*1(50%)*	*4(50%)*	*0*	
Mild (1)	*0*	*4(50%)*	*0*	
Moderate (2)	*1(50%)*	*0*	*2(25%)*	
Severe (3)	*0*	*0*	*6(75%)*	
Granulomatous reaction	*1*	*1*	*7*	*p = 0.01*
Non-granulomatous reaction	*0*	*3*	*1*	
Collagen deposition				
Linear compact	*2*	*1partially*	*8*	*p < 0.001*
Irregular and loose	*2*	*8*	*0*	
α-SMA				
Negative	*NA**	*4*	*1*	*p = 0.25*
Positive	*NA*	*4*	*7*	

**Not assessed*

4A.5. Discussion

The gelatin-based membranes, in this study, offered ease of surgical handling, transparency and potentially geometrical conformity. Conformity is a particularly crucial factor in conjunctival reconstruction within the forniceal area, since placing anchoring sutures would be very difficult, if not impossible, if the membrane does not conform to the shape of the fornix. Conformity is of the utmost importance in diseases that cause forniceal shortening, like ocular burns and autoimmune diseases [346, 358, 509]. Transparency is an advantage in terms of better cosmetic results; materials such as poly(lactic-co-glycolic acid)(PLGA) and Collagen-Glycosaminoglycan (CG) are not transparent, and AM has been reported to result in a blunted conjunctival appearance and decreased clarity until complete degradation [367]. Surgical handling can influence the reconstruction process. As an example, conjunctival reconstruction using CG copolymer matrix scaffolds with 2 mm thickness can lead to unfavorable results due to an increased likelihood of step formation that can hinder epithelial cells migration [342].

Prior studies have reported the completion of epithelialization after two weeks when PLGA or CG copolymers were used [341, 342]. For vitrified collagen cases, it has been reported that

epithelialization started in the first week and complete repair was observed in the fourth week [344]. Given these results, the response of the membranes studied in this investigation were comparable to that of other synthetic materials, albeit somewhat delayed compared to AM-grafted cases. Huang *et al*. has reported the time required for complete epithelialization to be two weeks in a rabbit model grafted with AM [343]. Interestingly, the degradation profile of the gelatin-based membranes is well-matched with the required time for epithelialization. The better quality of the resultant healed conjunctiva for the gelatin-based membrane grafted eyes can be seen in histological examinations. The quality of the repaired epithelium seems to be more promising, in terms of stratification and goblet density, in the gelatin-based membrane implanted eyes, compared to currently used tissue engineered scaffolds. Eyes treated with the gelatin-based membrane showed 3-5 layers of stratification, while Zhou *et al*. reported decreased number of epithelial layers with a flattened epithelial cell morphology in rabbit eyes grafted with collagen virtrigel and eyes left ungrafted [344]. Lee *et al*. [341] and Hsu *et al*. [342] reported 2-3 layers of epithelial cells in modified PLGA and CG copolymer grafted rabbit eyes, respectively.

Goblet cell density was found to be approximately 10 cells per every 100 cells for the gelatin-based membrane grafted eyes, which is the highest density for goblet cells reported between recently evaluated non-seeded bioengineered materials. CG copolymer scaffolds and acellular vitrified collagen material have shown to have very low to absent concentration of goblet cells in the repaired conjunctivae [342, 344]. In the latter study, vitrified collagen seeded with conjunctival epithelial cells obtained 23% goblet density compared to 30% in the normal conjunctivae [344]. Goblet cell density has not been reported in the study on the PLGA [341]. However, NormalGEN, derived from bovine pericardium for conjunctival reconstruction, has been reported to bring about a goblet cell density similar to native conjunctivae, but the epithelium is thin and contains fewer layers. The results with regard to goblet cell density were more promising in the gelatin-based membrane grafted eyes compared to AM grafted eyes. The mean goblet cell count was approximately twice as much in the gelatin-based membrane grafted eyes compared to the AM grafted eyes, with 50% of the eyes having counts higher than 10 per total 100 cells, compared to 25% having more than 10 per total 100 cells in the AM grafted eyes.

However, this difference was not significant, probably due to the small sample size. The relatively more severe and prolonged inflammation in AM grafted eyes may lead to lower goblet cell count in this group. Evaluation of specific mucin secretions, such as MUC5AC and MUC 2 is recommended for future studies, as it can provide additional comparative information on the differences in mucinous secretion regulation on differently repaired conjunctival surfaces.

Additionally, the results of epithelialization for the gelatin-based membrane were comparable to the most widely used substitute (i.e. AM). Both groups showed approximately equal layers of epithelial stratification (3-5), normal epithelial morphology and flattening towards the surface in histological examination.

The results here are consistent with other studies, showing that AM can promote epithelialization [356-358, 364]. Two eyes in the AM grafted groups showed epithelial metaplasia, which did not seem to be a consequence of the inflammation seen in the AM group as both eyes had moderate inflammation with a mean goblet cell count of 10. Metaplasia after AM transplantation was also observed in five out of nine eyes in a study using AM for conjunctival reconstruction after symblepharon removal in OCP patients (by impression cytology) [346]; more studies need to be carried out on this topic.

Studies supporting goblet cell repopulation on AM have been mostly conducted through cultivation of conjunctival epithelial cells on AM. Additionally, most of the studies have not reported the percentage of goblet cells [376, 510, 511]. Three *in vivo* studies on rabbits have also reported goblet cell repopulation after implantation of cryopreserved AM for conjunctival reconstruction, but none have reported the number of cells [343, 510, 512].

In a study conducted on human conjunctival repair using AM after scar tissue and symblepharon removal, restoration of goblet cells was reported in 6 out of 9 eyes (66.7%) in the 4th week of examination. However, only 4 eyes (44.4%) had the normal conjunctival epithelium, with goblet cells restored, in the 28th week of examination. The results were based on impression cytology and no histological data was given. The time to complete epithelialization was similar to our study, i.e. 3 weeks [513]. In another study, goblet cell density was reported to be 10 times as much

in patients receiving AM after iatrogenic conjunctival removal compared to a control group. Again, the data was based on impression cytology and no histological data was given [511].

Our results suggest that both gelatin-based membrane and AM can provide a favorable base for epithelial cell migration and proliferation. The short delay in epithelialization in the gelatin-based membrane group is not clinically important, as the repaired epithelium showed similar quality in both groups eventually. The outcome for ungrafted eyes (i.e. thin epithelium; low stratification) and reduced goblet cell density were consistent with other studies [342-344].

The major difference between the results of the eyes grafted with gelatin-based membrane versus eyes grafted with AM was in the host's inflammatory response seen in histological sections of the graft site. As shown in the results, no inflammatory cells were seen in 50% (4 eyes) of the eyes treated with gelatin-based membranes, and the remaining eyes showed only a mild response that was mostly non-granulomatous. On the other hand, all eight eyes treated with AM continued to show an inflammatory response up to the 28th day, with seven out of eight (87.5%) being granulomatous.

Cryopreserved amniotic membrane has been shown to have anti-inflammatory and, consequently, anti-scarring properties. The anti-inflammatory mechanism of AM is not fully understood yet. In-vitro studies suggest that AM can inhibit expression of pro-inflammatory cytokines such as interleukin (IL) 1a, IL-1b [514] and IL-8 [515]. It contains immunomodulatory substrates, such as heavy chain (HC)-hyaluronan (HA)/pentraxin 3 (PTX3) in its matrix [356]. Anti-scarring effects have been attributed to AM's ability to reduce expression of TGF β-1, β-2, β-3 and TGF receptor, and consequent inhibition of conjunctival fibroblast proliferation [516].

The current study, however, suggests active presence of lymphocytes and lymphoplasma cells around the undegraded AM after 28 days of transplantation, based on histological sections. Histologically confirmed inflammation around the AM has also been reported in a similar study on AM transplantation in rabbits for conjunctival reconstruction, where an increase in severity of monocyte infiltration up until day 28 and eventual decrease in day 58 after transplantation were observed [343]. A similar observation on the 36th and 60th day after filtering surgery has been reported by two other studies, where cryopreserved and dry human AM were used, respectively

[359, 360]. In contrast, the images provided in a study on rhesus monkeys using AM for conjunctival reconstruction did not display any significant inflammatory response two weeks after transplantation [361].

It has been suggested that AM traps and then induces apoptosis in inflammatory cells in damaged ocular surfaces [356, 517]. Considering AM's ability to trap inflammatory cells, prolonged presence of AM in donor tissues, reflecting unpredictable degradation rate, may be the reason for the longstanding mononuclear inflammatory response seen in this study and others [343, 359, 360], as cells are seen to be just surrounding the AM, not distributed in the donor stroma. The remnant has been reported to remain 3-10 weeks after cryopreserved AM transplantation in pemphigoid patient's eyes [346] and 9 weeks after transplantation of dry and cryopreserved AM in rabbit eyes [359, 360]. On the other hand, the ability to induce apoptosis in inflammatory cells and subsequently reduce inflammation, or other anti-inflammatory mechanisms of AM [355, 515, 517, 518], may compensate for certain types of inflammation to certain degrees. However, it becomes less effective when the inflammation is severe [338, 356, 358, 363]. Considering the low inherent immunogenicity of AM and acellularity of the remnants of AM in the histological sections weakens the assumption of xenograft rejection, whereby AM is surrounded by mononuclear cells [359, 360, 519]. Evaluation of the statistics of different inflammatory cells using immunohistochemistry markers, provision of detailed information about their exact composition [520], and the assessment of tear inflammatory factors during the repair process may also be beneficial in classifying and characterizing the reactive/inflammatory processes and conducting further future studies.

Another important group of cells found in this study were histiocytes and giant cells, the hallmarks of chronic inflammation, revealing foreign body reaction towards AM. Such reactions were not seen in the gelatin-based membrane group. Granulomatous reaction towards AM has been observed by others at day 14 after human AM transplantation in rabbits [359]. Granulomatous tissue was observed in the vicinity of suture remnants in all sections. The least possible number of sutures was used in this study to prevent suture reactions from being confounded with the inflammation data. It is also important to note that the strong and rapid

response of gelatin-based membranes to fibrin glue thus serves as another advantage of such biomaterials. Less favorable outcomes using sutures have been reported in clinical studies [521], as sutures themselves induce foreign body reaction.

Both gelatin-based membrane and AM grafted eyes showed less parallel alignment of collagen compared to the control group. The application of porous scaffolds has previously been reported to decrease scar formation. More randomly aligned collagen deposition compared to ungrafted wounds has been suggested as the possible mechanism [341-344]. The obtained results are consistent with the anti-scaring effects reported for AM [516, 522, 523]. However, there was a significant difference between the AM and gelatin-based membrane grafted groups, as near all eyes transplanted with the gelatin-based membrane showed random alignment similar to normal conjunctiva and fewer eyes were positive for ∝-SMA. In contrast, AM transplanted eyes revealed a much thinner layer of collagen deposition compared to control eyes. In addition to parallel and packed deposition of collagen in the vicinity of AM, positive ∝-SMA results in all eyes containing non-degraded AM (equal to 87.5%; i.e. 7 out of 8 eyes) were seen. Observed sub-conjunctival fibrosis (aligned and compact collagen deposition) can mainly be attributed to the prolonged presence of inflammation near the AM [355, 359]. A similar study on AM transplantation in conjunctival defects on rabbits showed that even though it was decreasing by the fourth week following transplantation, the fibroblast count increased on day 58 [343]. It may suggest the reduction of anti-inflammatory or anti-scaring effects of AM over time. Inefficacy or reduction of such effects have been previously observed specifically when the host's baseline inflammation is poorly controlled, such as with ocular cicatricial pemphigoid [346, 358, 521].

The gelatin-based membrane in this study led to similar quality of the healed epithelium in terms of cell morphology, cell layers and alignment of collagen compared to the widely used AM. Similar epithelialization time but significantly lower levels of clinical inflammation in gelatin-based membrane group is a key advantage of using the printed membrane over the AM. The observed similarities and differences can be somewhat explained by looking into the similarities and differences in composition, degradation profile and surface topography. Collagen IV is the major component of the basal lamina of AM used for ocular surface reconstruction [524] while

gelatin is the main element in the printed membranes. Gelatin, as a collagen driven protein, offers comparable bioactivity due to similar functional groups and chemical composition while eliminating immunogenicity due to its denatured structure. Gelatin-based membranes have near complete degradation by day 28 with no histiocytic reaction in the vicinity of the remaining material suggesting biocompatibility and good tolerability by the host's immune cells. In contrast, long-lasting remnants of AM can cause prolonged presence of inflammation and sub-conjunctival fibrosis. Surface roughness outlined by 3D-printing may also affect cell attachment and tissue reconstruction and can be further investigated in future studies.

4A.6. Conclusions

In the current study, a 3D-printed membrane was fabricated using gelatin, elastin and sodium hyaluronate blend and was compared to amniotic membrane (AM) for conjunctival reconstruction. *In-vivo* experiments were conducted on induced conjunctival defects in rabbits. Clinical observations and histological examination suggested that the gelatin-based membranes is a promising synthetic substitute for AM in conjunctival reconstruction due to the following findings: 1) acceptable surgical handling, 2) favorable cell adhesion and proliferation on the membranes, 3) providing a promising stroma for expansion and proliferation of epithelial cells with normal morphology, 4) favorable epithelial cell morphology and acceptable goblet cell density of the repaired epithelium, 5) deterring unfavorable host inflammatory reactions and 6) complete degradation by day 28.

Acknowledgements

This work was carried out with support from China Regenerative Medicine International Limited (CRMI). The stem cell preparation unit (SPU) at Farabi Hospital, particularly Mr. Zarrabi, Mrs. Aghajanpour and Mr. Mohammadnia were very instrumental in conducting the *in-vitro* and *in-vivo* tests.

Statement of Authorship for joint/multi-authored papers for PGR thesis

To appear at the end of each thesis chapter submitted as an article/paper
The statement shall describe the candidate's and co-authors' independent research contributions in the thesis publications. For each publication there should exist a complete statement that is to be filled out and signed by the candidate and supervisor **(only required where there isn't already a statement of contribution within the paper itself).**

Title of Paper	3D-Printed Membrane as an Alternative to Amniotic Membrane for Ocular Surface/Conjunctival Defect Reconstruction: An *In Vitro* & *In Vivo* Study
Publication Status	■ Published □ Accepted for Publication □Submitted for Publication □Unpublished and □Unsubmitted work written in a manuscript style
Publication Details	Shima Dehghani, Morteza Rasoulianboroujeni, Hamed Ghasemi, Saeed Heidari Keshel, Zohreh Nozarian, Mohammad Naser Hashemian, Mehran Zarei-Ghanavati, Golshan Latifi, Reza Ghaffari, Zhanfeng Cui, Hua Ye, Lobat Tayebi 3D-Printed Membrane as an Alternative to Amniotic Membrane for Ocular Surface/Conjunctival Defect Reconstruction: An *In Vitro* & *In Vivo* Study Biomaterials, Volume 174, August 2018, Pages 95-112, https://doi.org/10.1016/j.biomaterials.2018.05.013

Student Confirmation

Student Name:	Lobat Tayebi		
Contribution to the Paper	Contribution in: conceiving the idea of the work, facilitating the project progression, designeinh the experiment with other author, performing some analysis on samples before and after the animal surgery (I have not done the animal surgery), interpreting the data with the help of other authors, preparing the manuscript with the help of other authors		
Signature 		Date	16/09/2019

Supervisor Confirmation

By signing the Statement of Authorship, you are certifying that the candidate made a substantial contribution to the publication, and that the description described above is accurate.

Supervisor name and title: -Hua Ye, DPhil, Associate Professor, Institute of Biomedical Engineering Department of Engineering Science, University of Oxford -Zhanfeng Cui, Professor, Institute of Biomedical Engineering Department of Engineering Science, University of Oxford		
Supervisor comments		
Signature 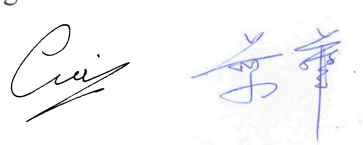	Date	25 Sep, 2019

This completed form should be included in the thesis, at the end of the relevant chapter.

Summary of Chapter 4

This chapter examined the application of the produced 3D-printed membrane in reconstruction of ocular surface/conjunctival defects. First, the physical characteristics of the developed ink in the previous chapter—composed of 8% gelatin, 2% elastin and 0.5% sodium hyaluronate—was further analyzed and compared with other relevant compositions to confirm that the selected composition was indeed the optimized one. Then, the 3D-printed membrane made by this ink went through extensive *in vitro* and *in vivo* (rabbit model) study after assessing the surgical handling and clinical applicability of the membrane. More specifically, the functionality of the membrane to repair the conjunctival defects was compared with AM as a traditional membrane used in clinics for this purpose.

The results indicated that the conjunctival defects treated by the 3D-printed membranes presented less inflammation, higher goblet cell density and reduced scar tissue formation in comparison with the defects treated by AMs. Moreover, the 3D-printed membrane offered better surgical handling and degradation pattern in a way that can be used as a reliable alternative to AM. In sum, the study presented in this chapter, satisfies the Objective 2 of Aim 2, stated as "examining the application of the produced 3D-printed membrane in ocular surface/conjunctival defect reconstruction."

CHAPTER 5. 3D-PRINTED MEMBRANE AND ITS APPLICATION IN CARTILAGE REGENRATION

5.0. Introduction

In this chapter, we hypothesize that a suitable 3D-printed membrane made by the hydrogel ink introduced in this thesis, can facilitate cartilage regeneration. To examine this hypothesis, this chapter is dedicated to conducting the last Objective of Aim 2: "designing and preparing a 3D-printed membrane to be used for cartilage regeneration as part of a newly developed joint plug". For this purpose, a novel joint plug has been designed in Section A of this chapter entitled "design of a new 3D-printed joint plug". This section presents the detailed design criteria of a novel joint plug that can be used to regenerate cartilage tissues in joints of human body such as hips, wrists, elbow, knee and ankle. It discusses the various aspects of the design in terms of the configurational possibilities for implanting the plug in the joint before or during the surgery, along with the cooperative function of different components of the plug.

Section B of this chapter entitled "a tri-component knee plug for the 3rd generation of autologous chondrocyte implantation (ACI)" uses the general design suggested in Section A to make a specific prototype of a knee plug to be used for cartilage regeneration in ACI treatment method. This section presents the fabrication and characterization details of three different parts of the produced plug. In this prototype, the generic ink developed in Aim 1 of the report has been used for 3D-printing of the cartilage part of the plug. This part is a relatively thick 3D-printed membrane with large pores. The membrane includes several knobs for the purpose of interlocking with a bone scaffold at the bottom of the plug. The cartilage part will also be attached to a stitch-able membrane from the top, to assist with the sliding of the knee joint.

The prototype plug fabricated in this chapter is in the size needed for a typical human knee ACI surgery. The *in vitro* study shows promising results regarding growth of chondrocytes into the cartilage part of the plug. The plug is novel (filed for patent), and this work is the first report of using the 3D-printed membrane of gelatin/elastin/sodium hyaluronate to be considered for cartilage regeneration.

Chapter 5A. Design of a New 3D-Printed Joint Plug

Attributed paper: Lobat Tayebi, Zhanfeng Cui, and Hua Ye. "Design of a New 3D-Printed Joint Plug." Asia-Pacific Journal of Chemical Engineering , Editorial e2360, 30 August 2019 https://doi.org/10.1002/apj.2360

5A.1. Abstract

This article introduces a kit of parts as a novel three dimensional (3D)-printed joint plug, in which each of the parts function cooperatively to treat cartilage damage in joints of the human body (e.g. hips, wrists, elbow, knee and ankle). Three required and one optional parts are involved in this plug. The first part is a 3D-printed hard scaffold (Bone Portion) to accommodate bone cells, and the second is a 3D-printed soft scaffold (Cartilage Portion) overlying the Bone Portion to accommodate chondrocytes. The third part of the joint plug is a permeable membrane, termed Film, to cover the entire plug to provide coordinated sliding of the joint during the regeneration of the cartilage. Film is also responsible for retention of the chondrocytes while allowing nutrients to diffuse through the membrane. The plug may further include a fourth part, called Barrier, which is a membrane to assist the Bone Portion in avoiding the loss of chondrocytes from the Cartilage Portion beyond the Barrier. Various engagement means among the parts of the plug are assumed, which are discussed in this paper. Moreover, the detailed design criteria and selection of suitable materials for different parts are elaborated. The 3D-printing practice allows the plug to be personalized and fabricated to fit the shape/size of the target joint and the injured section. Also discussed are the configuration options of the plug to be surgically implanted in a joint. Although the focus of this paper is on the design, a brief overview of a prototype is presented.

5A.2. Introduction

Bones of joints are protected by a thin tissue of cartilage (articular cartilage), which permits the easy slide of the joint tissues [525]. Cartilage lacks neural networks; when it is damaged, the joint exhibits pain, as the nerve system of the bony part underlying the cartilage becomes unprotected and exposed [525, 526]. Damaged cartilage is a widespread occurrence among many people, particularly the elderly [527]. In United States alone, there are reports of over five hundred thousand procedures per year associated with such cartilage disorders [528]. Osteochondral

deficiencies disturb both articular cartilage and the underlying subchondral bone, with the possibility of prompting osteoarthritic degenerative alteration by influencing the mechanical instability of the joint, which indicate the importance of its treatment [378-380].

Due to the limited capacity of cartilage self-restoration, several procedures are applied by surgeons for its treatment [529-531]. In an effective method, surgeons remove the damaged cartilage and sections of the bone underneath, followed by an attempt to stimulate the affected area to produce new tissues by cell therapy [529, 532].

For this purpose, the approach of using basic synthetic implants and tissue grafts is changing toward employing degradable tissue engineering scaffolds with appropriate pore size and configuration, which can be seeded by relevant cells or regenerative agents [533-536]. For example, to regenerate cartilaginous tissues, some investigators studied the use of degradable scaffolds made of polyglycolic acid seeded by mammalian chondrocytes [537, 538], and to regenerate bone tissues, studies indicate the use of bioceramics scaffolds seeded by mesenchymal stem cells (MSCs) [539], or poly(lactic-co-glycolic acid) scaffolds seeded by osteoblasts [540].

Although there are various reports of using bone and cartilage scaffolds, osteochondral scaffolds that aid regeneration of both cartilage and bone together are more appropriate for repair of such articular cartilage (and the underlying bone) [541-543]. For example, it was shown that the repair of osteoarthritis is more effective using tissue engineered osteochondral constructs than cartilage scaffolds [544, 545].

To design appropriate osteochondral scaffolds, the use of biphasic, triphasic and gradient constructs are popular [380, 412, 544, 546, 547]. More specifically, two or more layers of different materials and configurations are assumed for a good osteochondral construct to accommodate both chondrocytes and bone cells. The transitional area from the cartilage to the bony area is usually designed in a way to prevent construct delamination [548, 549]. While usually two or three different compositions and configurations are employed for different layers in biphasic and triphasic osteochondral scaffolds, such constructs can also be made by a single composition, in which the physical properties of different layers are considerably different [546].

During the last decades, many different designs have been suggested for use on osteochondral defects, including monophasic and multiphasic scaffolds [411, 413, 546, 550-552]. Some recent review articles have extensively elaborated the capabilities of different multicomponent constructs to be used for tissue engineering of osteochondral defects and discussed their challenges for clinical applications [411, 550-552]. Fundamentally, a good design must be able to provide a suitable environment for attachment and growth of the relevant cells, bearing in mind that the porosity, pore size, interconnectivity and geometry are extremely important in such an environment [164].

One of the most recent models—which is one of the most similar to the design we are introducing in this paper—is a tri-layered plug in a shape of a simple cylinder with a diameter and height of a few millimeters [553]. While the top layer of the cylinder is made of a nonwoven poly(glycolic acid) (PGA) felt, the mid layer is composed of poly(l- lactic acid) (PLLA) hybrid with a colorant, and the bottom-most layer is made of a porous poly(l-lactic acid)/poly(ε- caprolactone) (PLLA/PCL) structure coated with collagen Type I and calcium phosphate microparticles [553]. This tri-layered plug is produced by molding/salt-leaching technique and implanted *in vivo* without any cell seeding [553]. However, it has been demonstrated that molding/salt-leaching method cannot provide a good control over the pore size, porosity and interconnectivity of the produced constructs [554, 555], which are important factors in osteochondral scaffolds [164]. Therefore, we introduce a design of a joint plug using 3D-printing method, which is an advanced technique that can create fully customized constructs with detailed control over the pore size, porosity, geometry, gradient configurations and interconnectivity of pores [21].

More specifically, in this study, we have designed a new 3D-printed joint plug as a multi-part system with cooperative function to provide suitable support for accommodating the relevant cells in the area of the damaged joint during the cell therapy. The parts, as shown in Figure 5A.1, include two 3D-printed scaffolds and one permeable membrane, which are called Bone Portion, Cartilage Portion and Film, respectively. The fourth optional part, the Barrier, may also be included in the plug to prevent the fall of cells from Cartilage Portion deep into the Bone Portion, while keeping the cells of two Portions in contact (Figure 5A.4). This paper will describe the

design criteria and materials that can be used for each part. Although the paper is mostly focused on the design and its capabilities and possible configurations as a joint plug, a brief outline of a prototype made with specific materials is presented to show the function of the plug in accommodating chondrocytes and osteoblasts.

5A.3. Materials and methods

Sodium Hyaluronate (Research Grade, 500-749 KDa) was purchased from Lifecore Biomedical. Alfa Aesar (USA) was the vendor of caboxymethyle cellulose (CMC), sodium tripolyphosphate (TPP), 1-Ethyl-3-(3-dimethylaminopropyl) carbodiimide (EDC) and N-Hydroxysuccinimide (NHS). Polycaprolactone (PCL) (Mn 80000), β-tricalcium phosphate (TCP), polyethylene glycol (PEG, Mn 2000), gelatin (Type A, from porcine skin, Gel strength ~300 g Bloom) and hydroxyapatite (HA) were obtained from Sigma (USA). Elastin Products Company, Inc. provided the elastin (Elastin-Soluble, No. ES12) with the molecular weight of 60 KDa.

To prepare the paste for 3D-printing of the Bone Portion, 12 g TCP, 3 g HA, 0.5 g TPP, 0.075 g CMC and 5.75 ml water were homogenized in a centrifugal mixer (Thinky, USA) at 2000 rpm for 2 min. A solution of 8% w/v gelatin, 2% w/v elastin and 0.5% w/v sodium-hyaluronate was used as the ink to 3D-print the Cartilage Portion.

Both scaffolds were 3D-printed using a 3D-Bioplotter® system (EnvisionTEC, Germany). The optimized parameters for printing the bone scaffold were pressure of 2 bar, nozzle speed of 4 mm/s, and cartridge and platform temperature of 22 °C. These parameters for printing the cartilage scaffold were pressure of 2 bar, nozzle speed of 15 mm/s, cartridge temperature of 31 °C and platform temperature of 12 °C. The bone scaffold was sintered by keeping it at 600°C for 2 hours (h) to remove the organic additives, and then increasing the temperature to 1100 °C for 4 h.

To make the Film, 1 g PCL, 15 ml 2,2,2-Trifluoroethanol and 1.5 g PEG 2000g/mol were dissolved and then casted. After overnight evaporation of the solvent, the membrane was then waterlogged to eliminate/sacrifice the PEG component. For surface modification of the Film, one side of the membrane was floated on 10% w/v NaOH for at least 8 h. Residual NaOH was washed away using water.

Aminolysis treatment can be used to adhere the PCL Film to the Cartilage Portion. To do the aminolysis treatment of the PCL Film, the Film must be washed with isopropyl alcohol and immersed in 10% (w/w) 1,6-hexanediamine in isopropyl alcohol at 35 °C for 3 h, rinsed with copious amounts of deionized (DI) water followed by drying in a vacuum oven at 30 °C overnight, and then immersed in 2.5 wt% of glutaraldehyde/PBS solution for 24 h at room temperature. Finally, the free glutaraldehyde must be removed by rising with water [556]. Scanning electron microscopy (SEM) of the Film was performed using a JEOL JSM6510 system (Japan) at the accelerating voltage of 3kV after sputter-coating with gold.

Human osteoblasts (HOB, Cell Applications, USA) and normal human chondrocytes (Cell Applications Inc, USA) were cultured under standard aseptic conditions. 2500 cells/mm^2 and 750 cells/mm^2 were used to seed scaffolds of Bone and Cartilage Portions, respectively.

At desired time intervals, the cell culture media was substituted with 10% v/v prestoblue reagent (Life Technologies, USA) in phenol red free DMEM following by 1.5 h incubation at 37°C and 5% CO_2.

5A.4. Result and discussion

As shown in Figure 5A.1, the design is a kit of three parts that form a joint plug as an implant for insertion within an opening of a bone layer in a joint and through a cartilage layer. Part 1 is the Bone Portion and composed of a 3D-printed bone scaffold. Part 2, the Cartilage Portion, is a 3D-printed soft thick membrane (1-3 mm thick), and part 3 is a thin permeable porous membrane, termed Film (0.3-0.7 mm thick).

The joint plug can be implanted in the body as a fully assembled joint plug in order to simplify the surgery (Figure 5A.1(A)). In this case, the desired cells should be seeded into the plug prior to implantation in the body. Other options allow some portions of the plug to be engaged separately. For example, the plug can be implanted in the body while Bone and Cartilage Portions (Figure 5A.1(B)) or the Film and the Cartilage Portion (Figure 5A.1(C)) are already attached. In this case, the third part can be engaged to the plug during the surgery. In another scenario, the components of the kit can be separately implanted, then engaged with each other inside the body

(Figure 5A.1(D)). In such cases, the surgeon has the option of seeding some cells to the accessible parts of the plug during the surgery.

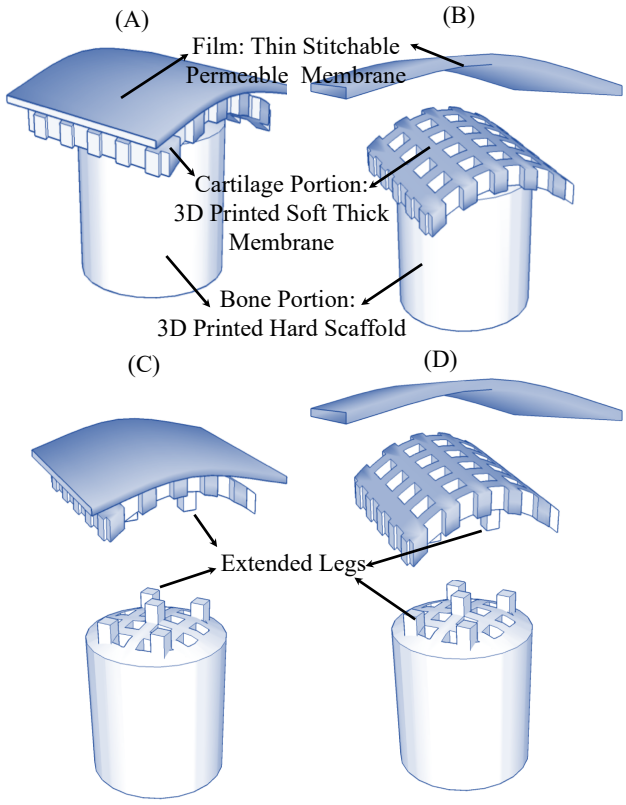

Figure 5A.1: Different designs of the plug that can be used based on the surgery needs: (A) Fully assembled, (B) Adhered Cartilage and Bone Portions, (C) Adhered Film and Cartilage Portion, (D) Unattached form.

5A.4.1. Part 1: Bone portion

The Bone Portion of our design is a 3D-printed hard scaffold made of an appropriate biodegradable material with the size of the removed bone from the patient's specific joint. During the treatment of a joint, a zone of the joint is predictably removed by a surgeon to make an opening in the bone section. 3D-printing technique enables manufacturing of controlled and customizable structures to fit the desired shape and size of the opening in the bone section of an individual joint in which the plug is going to be inserted. Thus, manufacturing of the Bone Portion of the joint plug can be personalized, which allows for easier handling and more efficient treatment of the injured joint.

The materials selected for the scaffold of the Bone Portion must be able to accommodate osteoblasts. Ceramic or composite materials are good options for this purpose. Some examples include bioactive glasses, various calcium phosphates, aluminum oxide, calcium oxide, zirconium oxide, HA, composites of polymers (such as PCL) and calcium phosphates. We have suggested that a combination of TCP and HA (TCP/HA 80:20) is the most suitable material to fabricate the Bone Portion (Figure 5A.2(A,B)). Figure 5A.2(C) shows the attachment of osteoblasts in our bone scaffold.

5A.4.2. Part 2: Cartilage portion

The plug further includes a 3D-printed soft scaffold for accommodating chondrocytes. This middle part, the Cartilage Portion, is configured in a way to be positioned over the Bone Portion. The materials of this part must be a biodegradable biocompatible material, preferably hydrogels, which can accommodate chondrocytes. Examples of the materials that can be used for this purpose include collagen, hyaluronic acid, gelatin, alginate, elastin, poly(amino acids), elastin-like peptides, albumin and fibrin. An example of the Cartilage Portion is demonstrated by the use of a composition of gelatin/elastin/sodium-hyaluronate (8:2:0.5) (Figure 5A.2(A,B)). As seen in Figure 5A.2(D), chondrocytes can robustly attach to this composition. The soft porous scaffold of gelatin/elastin/sodium-hyaluronate not only facilitates the cartilage growth within the cartilage layer but also retains the chondrocytes within the layer by their attachments, enhancing cell differentiation between the bone and cartilage portions.

5A.4.3. Engagement means between the bone and cartilage portions

There are engagement means to mount the Cartilage Portion on the Bone Portion. The engagement means can be in the form of several protrusions or legs/knobs extending from either the bone or cartilage 3D-printed scaffolds, or from both of them (Figure 5A.1(A-D)). This can confine the location of the Bone Portion relative to the Cartilage Portion. Engagement between the Cartilage and Bone Portions can also allow the two portions to be coupled prior to implantation into the joint to simplify the surgical process (Figure 5A.1(A, B)). In the schematic view of the design shown in Figure 5A.1(A-D), legs are fabricated in the Cartilage and Bone

Portions to mechanically interlock them together. Another means of engagements is suturing/stitching between the two portions.

5A.4.4. Part 3: Film

The third component of the plug is a permeable membrane (Film) configured to be placed over the Cartilage Portion. It is located on top of the plug to retain chondrocytes within the Cartilage Portion, while allowing nutrients to diffuse through the Film into the Cartilage Portion to facilitate cell propagation and growth. The Film also eases sliding of the joint during the regeneration and repair procedure of the cartilage tissue. While covering the cartilage portion, the Film may also cover an area of the surrounding joint tissue.

The Film can be composed of hydrogels, biodegradable polymers or a composite material. The material should be selected such that the Film can be attached to the surrounding joint tissue and the Cartilage Portion by suturing/stitching. The pore size of the Film should be less than 15 μm, so the route of cells from the Cartilage Portion out of the joint plug through the Film can be considerably reduced or prevented. In our prototype, we created the Film using PCL with the pore of size of 10 μm using a combination of film casting and sacrificial material leaching methods [557]. The sacrificial material in our case was PEG and the PCL/PEG w/w ratio was 3:2 (Figure 5A.2(A,B,E)).

5A.4.5. Engagement means between film and cartilage portion

Mounting the Film on the Cartilage Portion secures it in place and prevents the migration of the chondrocytes. Retention of the chondrocyte within the Cartilage Portion is an important function of the Film. Such engagement may occur before implantation of the plug into the body (Figure 5A.1(C) or 5A.1(A)), as coupling of Cartilage Portion and Film can simplify the surgery. Alternatively, it can occur after insertion of the components in the joint (Figure 5A.1(B) or 5A.1(D)).

The engagement means can be in the form of suturing/stitching between the Film and Cartilage Portion (Figure 5A.3(A)), and/or can occur through surface modification of the film to provide specific affinity to the Cartilage Portion. Here, we explain two examples of such modifications:

1) *Aminolysis Treatment*: Aminolysis method is an effective method to create amine functional groups on the surface of polyesters where other molecules can be attached. For our case of PCL Film and the scaffold of gelatin/elastin/sodium-hyaluronate of Cartilage Portion, when PCL surface is undergoing the aminolysis treatment, the created anchored $-NH_2$ groups on PCL molecules can react with the $-NH_2$ groups of the gelatin/elastin/sodium-hyaluronate using aldehyde coupling to achieve the strong bonding between PCL Film and Cartilage Portion (Figure 5A.3(B)) [558-560].

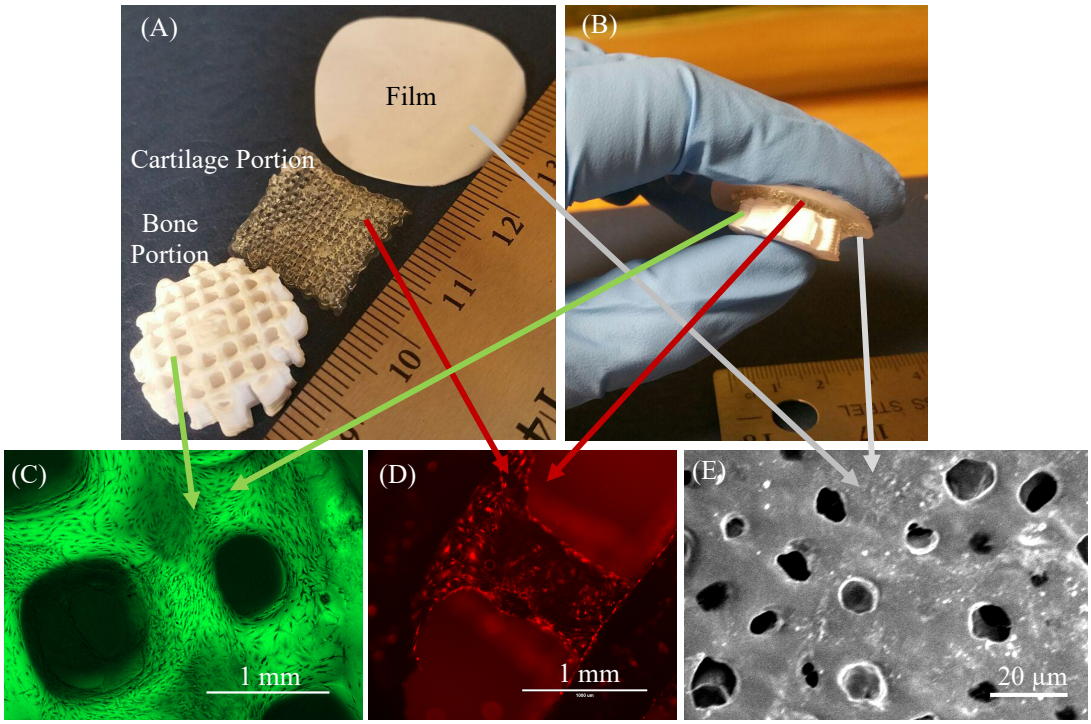

Figure 5A.2: (A) Photographs of the Bone Portion made of TCP/HA (80:20), Cartilage Portion made of gelatin/elastin/sodium-hyaluronate (8:2:0.5) and Film made of PCL and sacrificial material of PEG (PCL/PEG 3:2), (B) Assembled plug with three parts of Film, Cartilage and Bone Portions (C) Florescence image of Bone Portion of the plug with attached human osteoblasts, (D) Fluorescent image of the Cartilage Portion with attached normal human chondrocytes, (E) SEM image of the PCL Film.

Since this method involves a chemical reaction between the Cartilage Portion and the Film, it must be used before seeding the chondrocytes in the Cartilage Portion, and is thus appropriate when the Film and Cartilage Portion are attached prior to the implantation in the joint (Figure 5A.1(A,C)).

2) *Enhancing the Wettability of One Side of the Film*: Cell adhesion is highly influenced by wettability [561, 562]. Creating a Film with hydrophilic/hydrophobic sides can be an effective

technique to engage the Film and Cartilage Portion (from the hydrophilic side), while also preventing the chondrocyte from leaving the plug (from the hydrophobic side) (Figure 5A.3(C)). For example, in the case of the PCL Film, treating one side of the Film with NaOH can significantly increase the wettability of the side facing the Cartilage Portion to facilitate the engagement between the Film and this portion, while keeping the hydrophobicity of the other side to help retain the cells within the plug. More specifically, in our method, treating one side of the film with NaOH decreases the contact angle from 76.7 ± 3.3° to 36.4 ± 3.7°.

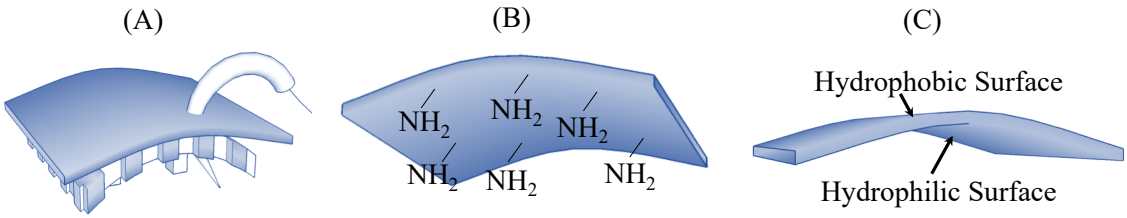

Figure 5A.3: Various engagement means that can be used between the Film and Cartilage Portion: (A) Mechanical engagements, such as suturing/stitching of the two parts, which can be used when the materials of the Film and Cartilage Portion are suturable. (B) Aminolysis treatment of the Film, which usually can be used when the Film is made of some polymers (such as PCL) in which aminolysis can create amine functional groups on the surface of polyesters, which can react with the NH_2 groups of the Cartilage Portion (which is made of hydrogel materials) via aldehyde coupling. (C) Enhancing the wettability of one side of the Film in a way to have the hydrophilic surface facing the Cartilage Portion (to enhance the cell attachment), while the hydrophobic surface faces outside of the plug (to prevent departure of cells). In our case (PCL Film), NaOH treatment could make such hydrophilic/hydrophobic surfaces.

5A.4.5. Gradient configuration

3D-printing offers controllability of the pore sizes within the Bone and Cartilage Portions, which is important for the growth of tissues in different kinds of joints. A gradient in the pore sizes within the Bone and/or Cartilage Portion is also possible using the 3D-printing approach. Generally, a gradient pore size in scaffolds can increase the cell seeding efficiency compared to homogenous scaffolds [563]. Pore size in the scaffolds plays direct role in cell binding, migration and ingrowth, ultimately affecting tissue regeneration. Large pores aid in effective nutrient delivery, gas diffusion and metabolic waste removal, while also offering low cell attachment and intercellular signalling [564-566]. Small pores, on the other hand, allow neither adequate nutrient supply delivery/gas diffusion, nor metabolic waste removal, yet significantly facilitate the cell

attachment and intercellular signalling [564-566]. Thus, having a gradient structure allows acquisition of benefits from both small and large pore sizes.

For example, as shown in Figure 5A.4(A), the size of the pores on top of the Bone Portion (where it is nearest to the Cartilage Portion) may be small (~10-50 µm). This not only facilitates cell attachment and intercellular signalling, but also helps preventing the chondrocytes from potential drop into the Bone Portion. The pore size may grow to 500-900 µm in the bottom of the scaffold in a gradient manner (Figure 5A.4(A)). Since the bottom of the scaffold is close to the surrounding bone, the cells from the adjacent tissue can have smooth ingrowth into the Bone Portion by taking advantage of successful nutrient delivery and waste removal provided by the large pores. After migration of the cells, they can easily attach to the upper areas of the scaffold with small pore size, which results in effective regeneration of the Bone Portion.

Gradient structure for the Cartilage Portion may also start from large pore size (e.g. 500-900 µm) on top, so the chondrocytes can easily migrate when they are seeded into the Cartilage Portion from the top. As shown in Figure 5A.4(A), the gradient configuration continues to the bottom of the Cartilage Portion with the small pore size (e.g. 10-50 µm) so the cells can firmly attach to the scaffold. Having a gradient structure for Bone and Cartilage Portions is not essential in our design, but can be considered as an option to improve the cell seeding efficiency.

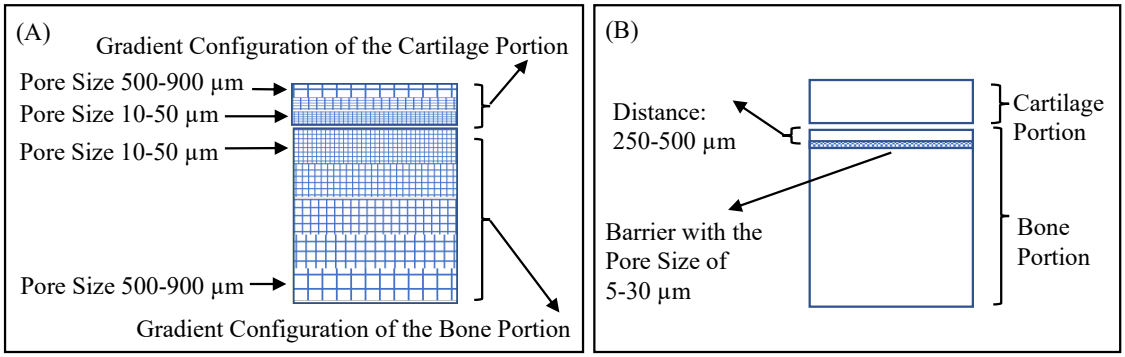

Figure 5A.4: (A) The Cartilage and/or the Bone Portion of the plug may have gradient configuration to enhance the cell seeding efficiency and to prevent the chondrocytes from dropping deep into the Bone Portion, all while maintaining the contact between chondrocytes and osteoblasts. The suggested pore sizes in different areas of the Bone and Cartilage Portions are indicated in this schematic. (B) The Barrier is an optional part of the plug to substantially avoid fall of chondrocytes to the Bone Portion. A distance (250-500 µm) between the Barrier and the bottom of the Cartilage Portion is necessary to provide a space for communication of osteoblasts and chondrocytes to modulate their phenotypic reactions. Barrier and gradient configuration can be used together in a design, as well.

5A.4.6. Optional part: Barrier

The kit of the joint plug may further include a Barrier, which is provided in the Bone Portion to substantially prevent drop of chondrocytes from the Cartilage Portion beyond the Barrier (Figure 5A.4(B)). As described above, the gradient configuration of the Bone/Cartilage Portions can prevent the chondrocytes from a potentially deep fall into the Bone Portion, while maintaining contact between the chondrocytes and osteoblasts. Using a Barrier—a layer with small pore size—in the Bone Portion can provide a similar role but more precisely. It is important to note that communication between osteoblasts and chondrocytes is helpful in regenerating the osteochondral interface on tissue engineered grafts [567]. Basically, investigations show that, under physiological conditions, chondrocytes and osteoblasts may regulate each other's phenotypic reactions and cellular differentiations [567]. Thus, the Barrier must not be designed in a way to block the interaction between the cells in the Bone and Cartilage Portions. More specifically, it should not be placed exactly at the interface of the Bone and Cartilage Portions, because different cell types must be able to still interact with each other. Somewhere inside the Bone Portion and close to the top is a suitable location. As shown in Figure 5A.4(B), the suggested site of the Barrier is 250-500 μm below the interface between the Cartilage and Bone Portions. This 250-500 μm distance can provide the space for possible interaction of bone and cartilage cells to modulate their cellular differentiations.

The Barrier can be integrated with the bone scaffold (integral configuration) or can be a separate part (separate configuration). In the integral configuration, it may be a layer of the 3D-printed construct of the Bone Portion with the same material composition of the bone scaffold (e.g. TCP/HA). This layer should be 3D-printed in a way to have very small pores to avoid easy passage of the chondrocyte beyond the Barrier. In the separate configuration, it can be made of a material different from the material of the Bone Portion (e.g. gelatin/elastin/sodium-hyaluronate or PCL membrane). In this case, the production of the Bone Portion can be divided into 2 steps: 3D-printing of the part above the Barrier and 3D-printing of the part below the Barrier. After obtaining these three sections (Bone Portion above the Barrier, the Barrier and Bone Portion below the Barrier), they should be engaged by a physical engagement means, such as stitching or

a chemical engagement means, depending on their material types. Alternatively, these three sections can be 3D-printed together by using a different ink for the Barrier.

If the plug is planning to be used in a way that the autologous cells are seeded to the Bone Portion before the surgery, the pore size of the Barrier can be designed very small (e.g. 5-15 μm), considering that the cells must be seeded to both sides of Bone Portion. However, if seeding the cells to the both sides is not possible, or the plug is going to be inserted into the joint without seeded cells in the Bone Portion, the pore size of the Barrier should be larger (e.g., 15-30), so it does not completely block the migration of osteoblasts from the bottom of the bone scaffold to the top (does not leave the 250-500 μm with no bone cells). This larger pore size can be considered as a cautionary arrangement for our design, as osteoblasts may always migrate into the Bone Portion from the adjacent bone tissues to the sides of the scaffold.

5A.5. Conclusion

This paper introduces a newly designed joint plug composed of three/four parts: 1) Bone Portion, 2) Cartilage Portion, 3) Film and 4) Barrier (optional). Various aspects of this design were discussed in this manuscript, including the configuration options for surgery and implantation in the body, suggested materials for each part, the cooperative function of the components as a joint plug and options of engagement means between different parts. This paper presents a quick overview of a prototype made as an example of this joint plug.

Acknowledgment

The authors acknowledge the financial support from China Regenerative Medicine International Limited (CRMI). This work could not be performed without the help of late Professor James Richardson from Institute of Orthopaedics, Robert Jones & Agnes Hunt Orthopaedic Hospital (Oswestry, UK).

Author contributions statement

Lobat Tayebi contributes in the design of the work, the acquisition, analysis, interpretation of data and writing of the manuscript.

Zhanfeng Cui contributes in design of the work and interpretation of data

Hua Ye contributes in design of the work, interpretation of data and writing of the manuscript.

All authors have approved the submitted version and have agreed both to be personally accountable for the author's own contributions and to ensure that questions related to the accuracy or integrity of any part of the work, even ones in which the author was not personally involved, are appropriately investigated, resolved, and the resolution documented in the literature.

Competing interests

The authors declare no competing interests

Data availability

Materials, data and associated protocols are available upon request.

Statement of Authorship for joint/multi-authored papers for PGR thesis

To appear at the end of each thesis chapter submitted as an article/paper

The statement shall describe the candidate's and co-authors' independent research contributions in the thesis publications. For each publication there should exist a complete statement that is to be filled out and signed by the candidate and supervisor **(only required where there isn't already a statement of contribution within the paper itself).**

Title of Paper	Design of a New 3D-Printed Joint Plug
Publication Status	■ Published □ Accepted for Publication □Submitted for Publication □Unpublished and □Unsubmitted work written in a manuscript style
Publication Details	Lobat Tayebi, Zhanfeng Cui, and Hua Ye. "Design of a New 3d-Printed Joint Plug." Asia-Pacific Journal of Chemical Engineering , e2360 Editorial, 30 August 2019 https://doi.org/10.1002/apj.2360

Student Confirmation

Student Name:	Lobat Tayebi		
Contribution to the Paper	Contribution in: developing the idea, planning the experiment, performing analysis on samples, interpreting the data, preparing the manuscript		
Signature 		Date	16/09/2019

Supervisor Confirmation

By signing the Statement of Authorship, you are certifying that the candidate made a substantial contribution to the publication, and that the description described above is accurate.

Supervisor name and title: Hua Ye, DPhil, Associate Professor, Institute of Biomedical Engineering Department of Engineering Science, University of Oxford Zhanfeng Cui, Professor, Institute of Biomedical Engineering Department of Engineering Science, University of Oxford		
Supervisor comments		
Signature 	Date	25 Sep, 2019

This completed form should be included in the thesis, at the end of the relevant chapter.

Chapter 5B. A Tri-Component Knee Plug for the 3rd Generation of Autologous Chondrocyte Implantation

Attributed paper: Lobat Tayebi, Zhanfeng Cui, Hua Ye, A Tri-Component Knee Plug for the 3rd Generation of Autologous Chondrocyte Implantation, (Submitted, 2019)

5B.1. Abstract

Here, we report a newly designed knee plug to be used in the 3rd generation of Autologous Chondrocyte Implantation (ACI) in order to heal the damaged knee cartilage. It is composed of three components: The first component (Bone Portion) is a 3D printed hard scaffold with large pores (~850μm), made by hydroxyapatite and β-tricalcium phosphate to accommodate the bony parts underneath the knee cartilage. It is a cylinder with a diameter of 20 mm and height of 7.5 mm, with a slight dome shape on top. The plug also comprises a Cartilage Portion (component 2) which is a 3D printed gelatin/elastin/sodium-hyaluronate soft thick porous membrane with large pores to accommodate chondrocytes. Cartilage Portion is secured on top of the Bone Portion using mechanical interlocking by designing specific knobs in the 3D printed construct of the Cartilage Portion. The third component of the plug (Film) is a stitchable permeable membrane consisting of polycaprolactone on top of the Cartilage Portion to facilitate sliding of the knee joint and to hold the entire plug in place while allowing nutrients delivery to the Cartilage Portion. The PCL Film is prepared using a combination of film casting and sacrificial material leaching with a pore size of 10 μm. It is surface modified to have specific affinity with the Cartilage Portion. The detailed design criteria and production process of this plug is presented in this report. Full *in vitro* analyses have been performed, which indicate the compatibility of the different components of the plug relative to their expected functions.

Keywords: Cartilage, 3D Printing, Knee Plug, Soft/Hard Scaffolds, Tissue Engineering, ACI, Autologous Chondrocyte Implantation

5B.2. Introduction

Bone ends within knee joint is covered with articular cartilage, which is prone to injury. While healthy cartilage is smooth, allowing relaxed sliding of the knee joint, damaged cartilage can be rough—exposing the underlying bone [568, 569]. Articular cartilage injury in knee joints is a

challenging medical problem. A growing number of patients are suffering from symptomatic focal knee cartilage lesions, which can be attributed to the limited self-repairing capacity of articular cartilage [570-574]. Despite development of different medical procedures to provide knee pain relief, there are arguments about the efficacy of current methods in treatment of cartilage defects [393, 575].

The strategies that address knee cartilage problems include:

1) Palliation: Such as arthroscopic chondroplasty and debridement, which are mostly related to minor and moderate cartilage wear. For example, arthroscopic chondroplasty is an outpatient procedure in which the injured tissue is detached to allow healthy cartilage to be developed in its place. This procedure involves using an arthroscope as a specific video camera to help make tiny incisions on the sides of the knee to ultimately repair a small area of damaged cartilage within the knee [382, 383, 576]. In the arthroscopic debridement procedure, a washout or joint lavage eliminates debris around the injured cartilage or bone using specific surgical instruments [384, 385, 577, 578].

2) Repair: Such as microfracture drilling, which is an outpatient and minimally-invasive practice, mostly utilized following sports injuries. In this procedure, the surgeon drills small fractures into the bone at the base of the damaged cartilage in the knee joint to repair the injured area by stimulating the growth of healthy "scar" cartilage, called fibrocartilage. Special care at home may be needed for six to eight weeks after the procedure [386-388].

3) Restoration: Such as osteochondral autograft or allograft, and autologous chondrocyte implantation (ACI), which are applied for serious cartilage injuries.

Osteochondral autografts or allografts are often used to treat knee cartilage injuries that uncover the underlying bone to replace the construct of cartilage/bone by either the patient’s tissue (osteochondral autograft) or a donor’s body (osteochondral allograft) [390-392]. Osteochondral autograft is a good option, yet limited to small defects due to the limitation of tissue supply from the patient’s body [393, 394]. Additionally, osteochondral allograft has the risk for immune rejection [395, 396].

The ACI method, a fairly new and state-of-the-art technique that can be employed for knee cartilage regeneration, is traditionally a two-stage process. In the first-stage, a minor portion of cartilage from the patient's knee is harvested. The biopsy is then enzymatically treated in the laboratory to extract the chondrocytes (cartilage-producing cells). They are expanded for a few weeks and then returned to the patient's knee during an open operative procedure that constitutes the second-stage [398-401].

Among all the above approaches, microfracture and ACI are more popular. However, the formation of fibrocartilage microfracture—instead of natural hyaline cartilage—is problematic, as fibrocartilage is not hard enough and can be deteriorated within a few years [402]. ACI, despite being a more difficult method, replaces the injured cartilage with natural hyaline cartilage, which is a real advantage of this method for severe damages.

ACI has evolved rapidly since its first description in 1994 [397], and has gone through a few generations. In the 1st generation of ACI, cultured chondrocytes were transferred to the injured region as a liquid suspension. Then a strong fibrous tissue, periosteum, was used to cover the area. Due to the use of periosteum, this generation is often called ACI-P, in which 'P' refers to periosteum. However, hypertrophy or ossification of the patched periosteum is known to be challenging [403]. Moreover, harvesting periosteum from the patient is a procedure that has its own complexities and usually causes discomfort for the patients [402]. In the 2nd generation of ACI, a collagen cover was employed as a replacement for periosteum. This generation is usually called ACI-C, in which C refers to collagen. In the 2nd generation, cells were still employed as liquid suspensions, and the collagen cover was stitched in the area [402]. Cell retention was a major challenge in the 1st and 2nd generations of ACI, thus a new generation has been developed (3rd generation), in which the cells are delivered, loaded or seeded to the injured area by the use of a 3-dimensional (3D) matrix, including a scaffold or a membrane (such as collagen membranes), known as the matrix-assisted autologous chondrocyte transplantation (MACT) [402, 404, 579]. Basically, this generation aims to use a 3D object/environment in order to accommodate the cultured chondrocytes to protect the cells, distribute them more homogeneously, facilitate their re-differentiation and aide the surgical implantation [404, 405].

Different scaffolds have been developed for this purpose, with different materials including the scaffolds made of natural materials such as agarose, collagen derivatives, fibrin glue, alginate and hyaluronic acid, and the scaffolds made of synthetic materials such as polylactides like polylactic and polyglycolic acids [404, 580]. The designs of these scaffolds were in different forms of fibers, meshes and gels [404, 580]. One important example of such scaffolds for the 3rd generation of ACI is a solid agarose-alginate hydrogel, which is capable of providing a 3D environment for accommodating chondrocytes (Cartipatch1, Tissue Bank of France, TBF, Lyon, France) [579, 581].

Most of the scaffolds produced for this purpose have only focused on the cartilage tissue and accommodating the chondrocytes [579, 581]. In this paper, we report a new design of a knee plug composed of three components: two components to accommodate the chondrocytes and the bone cells underneath the cartilage, and one component as a membrane that covers the whole construct. The novelty of this work is in the manufacturing of a ready-to-use, highly reproducible 3D printed construct for ACI 3rd generation surgery of damaged knee cartilage, with controlled pore size and structure. The construct has the size of the area that is typically removed from the knee for a damaged cartilage treatment and is made of stitchable materials that can accommodate suitable cells. Utilizing a 3D printing approach to develop this plug provides the controllability over the pore size, which is important for the growth of new tissues. Detailed fabrication procedures of this knee plug, along with the mechanical properties and *in vitro* analyses of different components, are presented in this paper. To the best of our knowledge, such a tri-component 3D printed plug for the knee cartilage repair has not yet been developed.

5B.3. Materials and methods

5B.3.1. Design

As shown in Figure 5B.1, the designed plug is composed of three separate components that can be fixed either by mechanical interlocking or suturing. The bottom part (Component 1, Bone Portion) is a 3D printed hard scaffold made of β-tricalcium phosphate (TCP) and hydroxyapatite (HA) that is sintered to yield sufficient mechanical properties. Once positioned within the

designated area, bioactive TCP and HA can assist growth of osteoblasts within the bone layer, and growing bone secures the joint plug in place.

This scaffold is basically a porous cylinder with a diameter of 20 mm and height of 7.5 mm, with a slight dome shape on top. The size of pores in this 3D printed construct are approximately 850 μm. It is configured for insertion into the opening of the bone layer.

The plug further includes a 3D printed soft scaffold for accommodating chondrocytes. This middle part, (Component 2, Cartilage Portion) is made of gelatin/elastin/sodium hyaluronate. It has a thickness of 2 mm with the approximate pore size of 892 μm and, as shown in the results, is appropriate for the attachment and growth of chondrocytes.

The top part (Component 3, Film) is a porous membrane made of polycaprolactone (PCL), which allows nutrients to diffuse, yet prevents cells from migrating out of the construct. It is fabricated in a way that is stitchable/suturable. The pore size of this membrane is approximately 10 μm.

It is favorable to have engagement means to attach different components. Such engagement may occur before implanting the plug into the body. Alternatively, it can happen after inserting the plug. To engage the Cartilage and Bone Portions, some knobs are designed in the 3D printed construct of the Cartilage Portion that can interlock these two portions and confine their locations. The engagement means between the Film and Cartilage Portion can be in the form of suturing and/or by modifying the surface of the Film so it can have specific affinity to the Cartilage Portion. One effective approach that we follow in this paper, is treating one side of the Film with NaOH. It significantly increases the wettability of the side faced to the Cartilage Portion to facilitate the engagement of the Film to this portion. Hydrophobic surface of the other side of the Film prevents the cells to migrate outside of the plug.

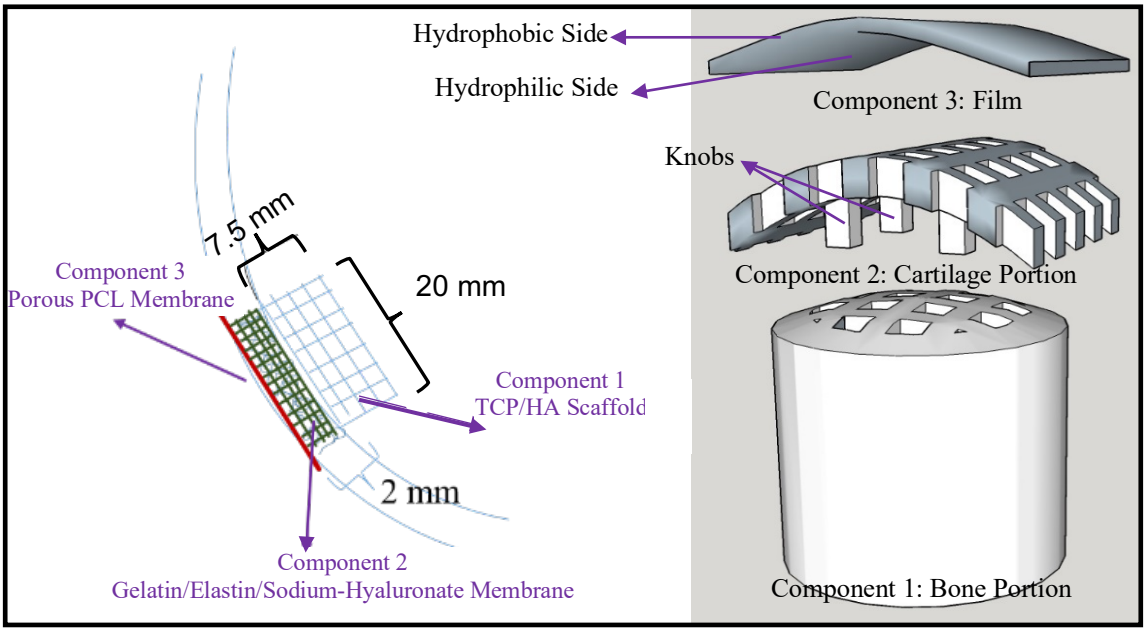

Figure 5B.1: A schematic view of the tri-component knee plug.

5B.3.2. Materials

TCP, HA, PCL (Mn 80000), polyethylene glycol (PEG, Mn 2000) and gelatin (Type A, from porcine skin, Gel strength ~300 g Bloom) were purchased from Sigma (USA). Carboxymethyle cellulose (CMC), sodium tripolyphosphate (TPP), 1-Ethyl-3-(3-dimethylaminopropyl) carbodiimide (EDC) and N-Hydroxysuccinimide (NHS) were purchased from Alfa Aesar (USA). Elastin with a molecular weight of 60 kDa (Elastin-Soluble, No. ES12) was purchased from Elastin Products Company, Inc. Sodium Hyaluronate (Research Grade, 500-749 KDa) was obtained from Lifecore Biomedical. All the solvents were of reagent grade.

5B.3.3. 3D Printing of the Bone and Cartilage Portions

A printable paste composed of TCP, HA, CMC and TPP was used to print the Bone Portion. To prepare the ink, 12 g TCP, 3 g HA, 0.5 g TPP and 0.075 g were added to 5.75 ml water and homogenized at 2000 rpm for 2 minutes(min) using a centrifugal mixer (Thinky, USA). Supplementary Information 3 (SI3) explains in detail the reason of selecting this composition as the ink for printing the scaffold of Bone Portion.

Finally, the ink was loaded into standard Nordson cartridges, and the Bone Portion was printed using a 3D-Bioplotter® system (EnvisionTEC, Germany) by adjusting the printing parameters. The optimized parameters are presented in Table 5B.1.

Table 5B.1: Parameters used in 3D printing of the Bone Portion of the plug.

Parameter	Value
Dimensions	20 mm diameter × 7.5 mm height with a solid rod in the middle (with diameter of 4 mm)
Cartridge Temperature	22°C
Platform Temperature	22°C
Pressure	2 bars
Nozzle Speed	4 mm/s
Distance Between Strands	2 mm
Slicing	300 µm
Nozzle Diameter	410 µm

The resulting constructs were allowed to air-dry overnight before being transferred to a furnace. The samples were heated up to 600°C at the rate of 3°C/min and held at this temperature for 2 hours (h) to eliminate the organic additives. The temperature was then raised to 1100°C at the rate of 5°C/min and kept at this temperature for 4 h to ensure complete sintering of the ceramic scaffolds. Imaging of the scaffolds and measuring their surface roughness were performed using a 3D confocal laser scanning microscope (LEXT, Olympus).

To print the Cartilage Portion, a solution of gelatin/elastin/sodium hyaluronate in deionized (DI) water was prepared and used as the ink. The concentration of gelatin, elastin and sodium hyaluronate was adjusted to 8%, 2% and 0.5% w/v, respectively. The ink was loaded into standard Nordson cartridges and the Cartilage Portion was printed using the parameters listed in Table 5B.2.

Table 5B.2: Applied parameters to 3D print the Cartilage Portion of the plug.

Parameter	Value
Dimensions	20 mm diameter × 2 mm height
Cartridge Temperature	31°C
Platform Temperature	12°C
Pressure	2 bars
Nozzle Speed	15 mm/s
Distance Between Strands	1.5 mm
Total Number of Layers	8
Nozzle Diameter	410 µm

The printed constructs were then cross-linked using a solution of 6 mg/ml EDC and 0.75 mg/ml NHS in 70% v/v ethanol for 4 h. To remove the residual cross-linker, the constructs were washed carefully through soaking in the large amount of DI water. The prepared constructs were stored in pure ethanol inside a -20 °C freezer to be used after rehydration.

5B.3.4. Fabrication and surface treatment of the Film

Porous PCL Film was prepared using the combination of film casting and sacrificial material leaching methods [557]. Briefly, 1 g PCL was dissolved in 15 ml of 2,2,2-Trifluoroethanol, and varying amounts of PEG 2000 g/mol (0, 0.2, 0.4, 1 and 1.5 g) were added to the solution. After complete dissolution, the solution was casted, and the solvent was allowed to evaporate overnight. The obtained membranes were soaked in water to eliminate/sacrifice PEG thereby the porous structures were achieved by sacrificing PEG.

To treat the surface of the Film that faced toward the cells, the prepared membrane was allowed to float on 10% w/v NaOH overnight. The Film was finally rinsed with copious amounts of water to remove residual NaOH.

5B.3.5. Characterization and biological evaluation of the Bone Portion

5B.3.5.1. Mechanical properties

The mechanical properties of the Bone Portion were measured using an Electromechanical Precision Universal Tester (AGS-X 5 kN, Shimadzu, Japan). The samples were tested in compression mode using a 5 kN load cell and crosshead speed of 1 mm/min.

5B.3.5.2. Osteoblast attachment and proliferation

Human osteoblasts (HOB, Cell Applications, USA) were cultured under standard aseptic conditions. The cells were cultured in standard flasks and nourished with Dulbecco Modified Eagle Medium (DMEM) supplemented with 10% v/v fetal bovine serum (FBS), 100 U/mL penicillin, 100 µg/mL streptomycin and 0.25 µg/mL amphotericin every 2 days until a confluency of 90% was reached. The cells were trypsinized using TrypLE (Gibco, US) and sub-cultured. The cells of the third passage were used to seed the scaffolds at a density of 2500 cells per mm^2 of scaffolds (cells/mm^2).

Cell attachment to the scaffolds was evaluated using scanning electron microscopy (SEM, JEOL-JSM6510, Japan). At certain time intervals (i.e. 3, 7, 14 and 21 days), the constructs were taken out, washed with PBS and fixed using Karnovsky's fixative (composed of 2% paraformaldehyde; 2.5% glutaraldehyde in 0.1 M phosphate buffer pH 7.4) for 2 h. The samples were then fixed using 1% w/v Osmium Tetroxide solution, dehydrated using ascending ethanol series (30, 50, 75, 95 and 100% v/v) and left overnight to air dry at room temperature. After being sputter-coated with gold, the samples were imaged using back-scattering and secondary electron modes at different magnifications.

The capability of the prepared scaffolds to induce cell proliferation was evaluated using prestoblue assay. At certain time intervals (i.e. 3, 7, 14 and 21 days), the cell culture media was replaced with 10% v/v prestoblue reagent (life technologies, USA) in phenol red free DMEM and incubated at 37°C and 5% CO_2 for 1.5 h. The fluorescence intensity of the reagent was recorded at the excitation/emission wavelengths of 540/590 nm using a micro-plate reader (Synergy HTX, BioTek, USA).

5B.3.6. Characterization and biological evaluation of the Cartilage Portion

5B.3.6.1. Degradation

Sample degradation rate was measured by monitoring the weight of samples over time. Samples were immersed in phosphate buffered saline (PBS) and kept at 37°C in a shaker incubator (IKA KS 3000) for 60 days. At certain times, from day 0 to day 60, samples were taken out, weighed and returned to the container. The ratio of the recorded weight to the initial weight at each time point was reported as a function of time.

5B.3.6.2. Chondrocyte attachment and proliferation

Normal human chondrocytes (Cell Applications Inc, USA) were cultured and sub-cultured under standard aseptic conditions. At the confluency of 90%, chondrocytes were trypsinized and resuspended in fetal bovine serum (FBS, Sigma-Aldrich, USA) to be seeded to the scaffolds of the Cartilage Portion. Scaffolds were disinfected using 70% ethanol, washed and seeded with a density of 3×10^5 cells/scaffold in 12-well culture plates and allowed 30 min for the initial attachment. The scaffolds were submerged after 30 min and incubated at 37°C and 5% CO_2, using

a chondrocyte growth medium (Cell Applications Inc., USA). The media were changed every other day.

Prestoblue assay was used to measure the proliferation rate of chondrocytes on the Cartilage Portion. At certain time intervals (i.e. 4, 7, 14, 21 days), the media of the wells were replaced with 10% v/v prestoblue reagent. The plates were then incubated for 1.5 h at 37°C and 5% CO_2. The fluorescence intensity was measured at an excitation wavelength of 540 nm and emission wavelength of 590 nm. The same procedure was performed on day 1, after complete attachment of the cells to the scaffolds. The number of cells at each time point (N) to the initial number of the cells (N_0) was calculated by dividing the corresponding intensity value by the absorbance value of the first day.

SEM was used to investigate cell attachment. Scaffold-cell complexes were washed using PBS and immersed in Karnovsky's fixative for 1.5 h. The complexes were then submerged in 1% w/v osmium tetroxide for 1.5 h. Ethanol series (30, 50, 75, 95 and 100% v/v) were used to dehydrate the samples. The samples were then air-dried and sputter-coated with gold. SEM imaging was performed at accelerating voltages between 1-5 kV with different magnifications.

At the mentioned intervals considered for proliferation rate measurement (i.e. 7, 14, 21 days), scaffolds were fixed in formalin solution (10%, neutral buffered) for H&E staining. The cells on the scaffold were fixed overnight and stained using Eosin and Hematoxylin. The color was adjusted using 1% v/v acidic alcohol, ethanol and bluing agent, according to standard histology protocols. 3D confocal laser scanning microscopy (LEXT, Olympus) and fluorescence microscopy (Evos Fl, Life Technologies) were employed for monitoring cell growth on the scaffold and extracellular matrix (ECM) secretion by chondrocytes.

5B.3.7. Characterization of the Film

5B.3.7.1. Scanning Electron Microscopy (SEM)

SEM imaging was employed to investigate the morphology of porous PCL film (SEM, JEOL-JSM6510, Japan). Samples were sputter-coated with gold and imaging was carried out at accelerating voltage of 3 kV at various magnifications.

5B.3.7.2. Mechanical properties and suture retention strength

Tensile strength of the films was examined using an Electromechanical Precision Universal Tester. The samples, fixed into a screw flat tensile grip, underwent the tensile test using a 5 kN load cell and crosshead speed of 1 mm/min. To investigate the effect the addition of PEG and the resulting porosity had on tensile strength, dense PCL films were also prepared using the solvent-casting method and tested under the same conditions.

To measure the suture retention strength, a steel wire of 0.15 mm diameter was used, by which the effects of suture materials on force-displacement curves is minimized. The steel wire was passed through a pinhole created in the Film to form a loop and fixed to the tensile testing machine, such that the distance from the grip was 10 mm. The other edge of the Film was fixed to the inferior screw flat tensile grip. The steel wire was pulled at a rate of 1 mm/min until the Film was completely torn.

5B.3.7.3. Wettability and permeability

The wettability of the Film was evaluated through contact angle measurement. A 5 µl drop of DI water was placed on either side of the samples, and the image was captured using a Dino-lite digital microscope camera. Each image was then processed to determine the contact angle.

Fluorescein sodium salt was selected as the model probe to quantify the permeability of the Film. The Film (D=10 mm) was fixed between two reservoirs filled with 4 mg/ml of solution or pure water. The entire system was fixed in a clamp and placed at 37°C. At certain time intervals, 100 µl of the solution was taken out from the low concentration side, transferred to a 96-well plate and the fluorescence intensity was recorded at excitation/emission wavelengths of 540/590 nm using a micro-plate reader. The diffusion kinetics were reported as the variation in the ratio of concentration at each specific time to the equilibrium concentration over time. Figure 5B.2 displays the setup used for the experiment.

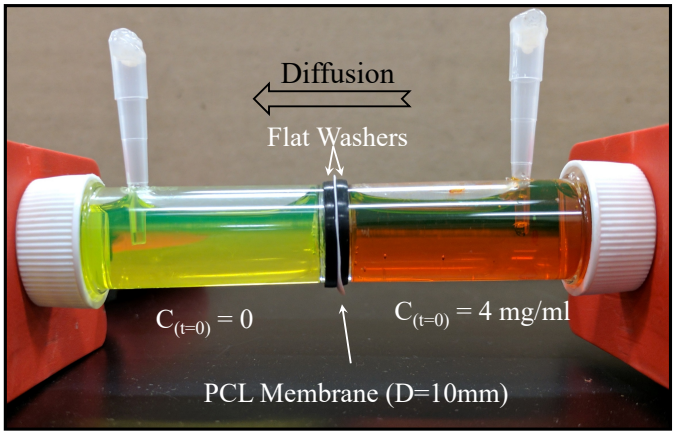

Figure 5B.2: The experimental setup for monitoring the diffusion of the model probe, i.e. fluorescein sodium salt through the PCL Film.

5B.4. Results and discussion

The majority of the inorganic component of natural bone is calcium phosphates, which makes this group of materials very popular in bone tissue engineering [112, 582, 583]. Among all calcium phosphates, HA ($Ca_{10}(PO4)_6(OH)_2$) and TCP ($Ca_3(PO_4)_2$) have been effective elements of many bone substitutes and scaffolds as they are able to effectively facilitate osteogenesis [584-587]. TCP is known as a bioceramic with higher degradability compared to other calcium phosphates [588-591]. The degradation of TCP-based composites can be regulated and slowed down by inclusion of HA. Moreover, HA is known as a bioceramic that can successfully interact with soft tissues (such as cartilage tissue in our case) [592].

Although use of combined TCP and HA, compared to pure TCP and HA, is increasing due to their effectiveness and the tunable degradability [593-599], their ratio in a composition should be selected based on the specific application. In SI3, we have fully examined four ratios of TCP/HA in terms of their printability, degradability, rheological and mechanical properties and selected TCP/HA 80:20 paste as the most suitable ink to be used for printing the Bone Portion of our plug. The results of the TCP/HA 80:20 paste rheologic analysis (SI3, Figure SI3.2 (B1 & B2)) indicates that this ink appears to have a yield flow stress. The shear stress-shear rate curves suggest the Herschel-Bulkley type behavior. Temperature change does not have a significant effect on the rheological properties of the paste. The morphology of the printed and sintered scaffolds is shown in Figure 5B.3(A). The surface roughness of the scaffolds was also measured using the 3D

confocal laser scanning microscope. The arithmetic mean height (S_a) and root mean square height (S_q) were found to be 1.73 ± 0.47 µm and 2.23 ± 0.57 µm, respectively.

The porosity of the scaffolds was 25.5 ± 3.8%. The mechanical testing was performed on the scaffolds made with the structure needed in the plug (i.e., 3D printed cylinder with the diameter of 20 mm, height of 7.5 mm and pore size of 850 µm). The values obtained for Young modulus (E), compressive strength (σ_B) and fracture strain (ε_R), by four repetitions in four separate samples, include E = 218.12 ± 19.10 MPa, σ_B = 39.08 ± 11.74 MPa and ε_R = 16.40 ± 5.66% (n=4). Although the fracture strain of the scaffold is relatively small, the Young modulus and compressive strength are well above the average values reported for trabecular bone [600].

The proliferation rate of osteoblasts on the scaffolds, as well as in the control group (cell culture plate), is shown in Figure 5B.3(B). The results are reported as the variation of N/N_0 over time, which is the ratio of the number of cells at each time point (N) to the initial number of the cells (N_0). The ratio can be obtained by dividing the corresponding intensity values.

As observed, except for the starting point, the number of cells on the scaffold was higher than the control group at all other time points. Furthermore, the cells in the scaffold had improved growth and proliferation compared to the control group.

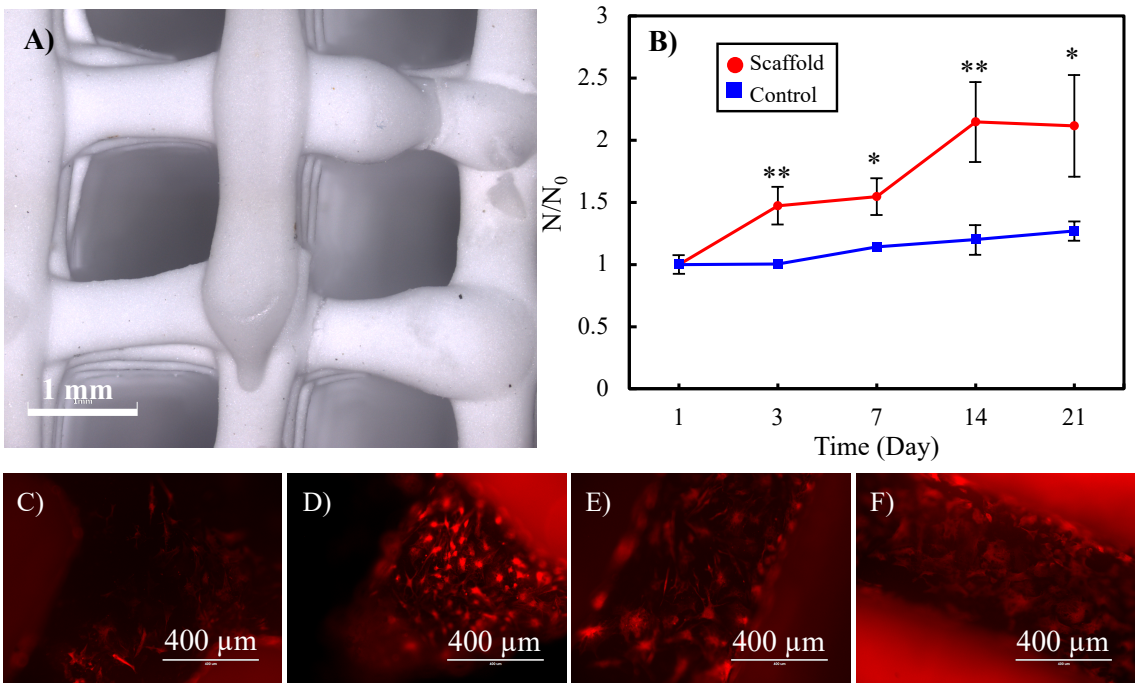

*Figure 5B.3: (A) 3D confocal laser scanning images of a 3D printed hard scaffold (TCP/HA 80:20) to be used for the Bone Portion of the Plug. (B)The proliferation rate of human osteoblasts on the scaffolds, as well as the standard cell culture plate (control group). Four samples were examined at each time point/condition (n=4). N0: Initial number of the cells, N: Number of cells at each time point. Statistical significance *: p<0.05, **: p<0.01, P-values in Day 3: 0.006, Day 7: 0.011, Day 14: 0.006 and Day 21: 0.023. (C-F) The fluorescence images of the attached osteoblasts on the scaffolds after (C) 3, (D) 7, (E) 14 and (F) 21 days.*

Figure 5B.3(C-F) and Figure 5B.4 display the fluorescence and SEM images of the attached osteoblasts on the scaffolds, respectively. The osteoblasts grow within the pores and on the surface of the strands of the 3D printed scaffold, forming an adherent plexus all over the scaffold. It can be vividly seen that osteoblasts have attempted to anchor their cytoskeletal projections, lamellipodia and filopodia, to the surface features, revealing the bioactive characteristics of the scaffolds.

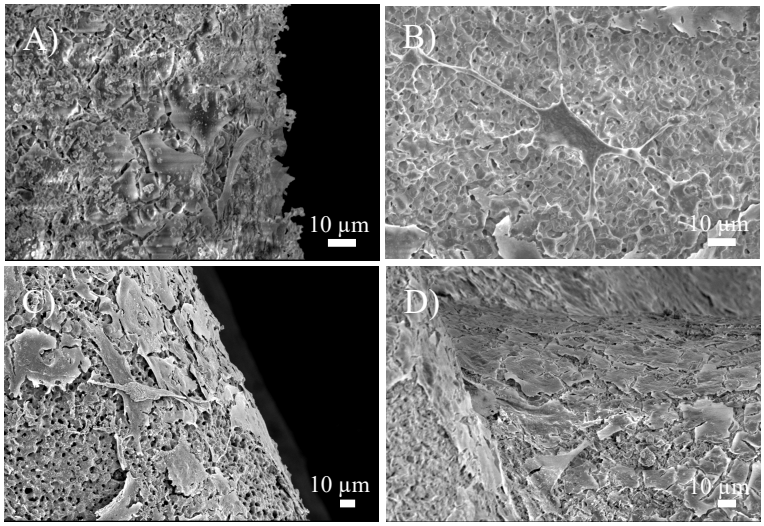

Figure 5B.4: SEM images of the attached osteoblasts on the scaffolds of the Bone Portion after A) 3, (B) 7, (C) 14 and (D) 21 days.

The composition of the scaffold used for cartilage regeneration can have a significant impact on cell behavior. Cartilage Portion in our plug is made of gelatin/elastin/sodium-hyaluronate. Gelatin-based hydrogels have been reported to promote the chondrogenic differentiation of mesenchymal stem cells [601]. The up-regulation of chondrogenic markers—such as SOX9, collagen type II, aggregan and versican—has been shown for gelatin-based scaffolds [602]. Addition of hyaluronic acid to gelatin-based scaffolds may even improve their chondrogenic activity. Chondrocyte proliferation, adhesive activity and new hyaluronic acid production have been shown to significantly increase in hyaluronic acid-treated gelatin scaffold, compared to non-treated groups. Furthermore, higher quality of hyaline-like extracellular matrix production and a higher filling of extracellular matrix in the pore of scaffold have been demonstrated for hyaluronic acid-treated gelatin scaffold via immunohistochemistry and SEM, respectively [603]. Such an effect can be pursued in the mechanism of hyaluronic acid interaction with chondrocytes. Chondrocytes express the glycoprotein CD44 on their cell surface; this has the capacity to function as a hyaluronic acid receptor and, therefore, may be involved in biochemical interactions with chondrocytes [604, 605]. Hyaluronic acid binds to CD44 and acts on intracellular signal transduction via protein kinase C as a result of the transmission of the bound hyaluronic acid to the cytoplasm. Hyaluronic acid increases the synthesis of proteoglycans and collagen by chondrocytes [606]. On the other hand, incorporation of elastin into the formulation might also

influence the chondrogenic activity. According to the study conducted by Betre *et al*. [607], elastin-like polypeptide can promote chondrogenesis for human adipose-derived adult stem cells in the absence of exogenous TGF-β1 and dexamethasone. Significant increases in sulfated glycosaminoglycan (up to 100%) and collagen contents (up to 420%) have been observed by these investigators. Immunolabeling confirms that the matrix formed consists mainly of type II, and not type I, collagen [607].

The morphology of the printed gelatin/elastin/sodium hyaluronate scaffold for the Cartilage Portion of the plug is illustrated in Figure 5B.5(A). A knob that has been designed for interlocking the Bone and Cartilage Portions can be seen in the image. The average pore size was found to be 892 ± 62 μm. The degradation rate of the Cartilage Portion is demonstrated in Figure 5B.5(B). The scaffold weight remained almost constant in the first 30 days, implying the stability of the constructs in this timeframe, but decreased drastically between 30 and 60 days. After 60 days, the scaffolds completely collapsed and disappeared.

As shown in Figure 5B.5(C-F), after one day of cell seeding, chondrocytes attach perfectly to the surface of the gelatin/elastin/sodium-hyaluronate construct.

The proliferation rate of normal human chondrocytes on the scaffolds is illustrated in Figure 5B.6. The results are reported as the variation of N/N_0 over time, which is the ratio of the number of cells at each time point (N) to the initial number of the cells (N_0). The ratio can be obtained by dividing the corresponding intensity values.

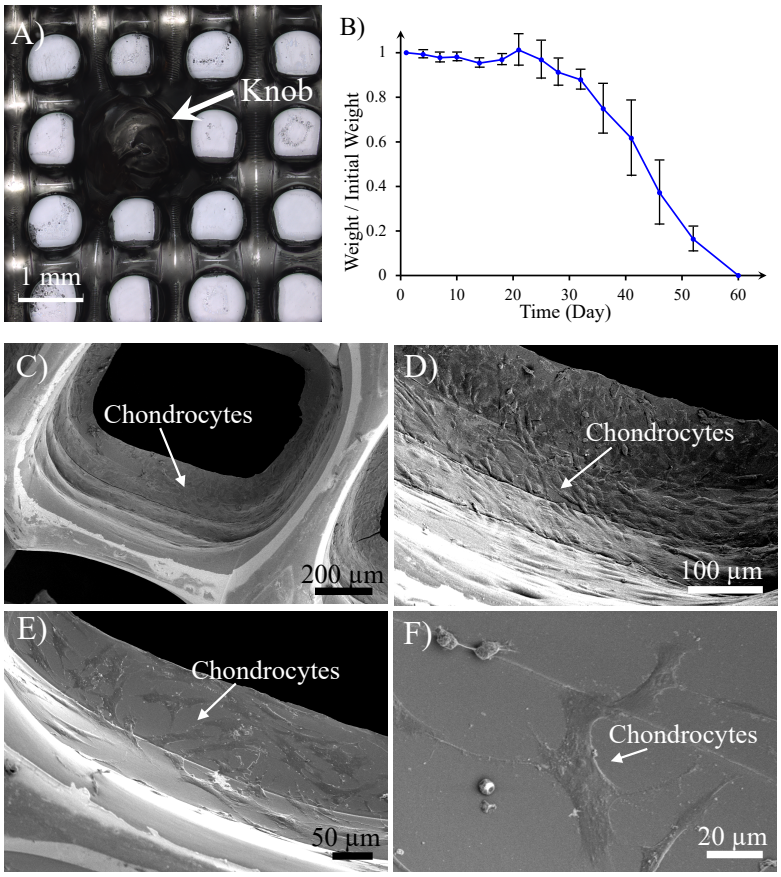

Figure 5B.5: (A) 3D printed construct of the Cartilage Portion (gelatin/elastin/sodium hyaluronate soft membrane). The knobs on the 3D printed membrane are constructed to mechanically interlock the Cartilage Portion to the Bone one. (B) Degradation kinetics of the Cartilage Portion—the weight of the sample at each time point has been normalized to the initial weight of the sample and exploited as an indicator for degradation magnitude. (C-F) Chondrocyte attachment on the gelatin/elastin/sodium-hyaluronate construct one day after seeding. The magnification of SEM images increases from panel C to F.

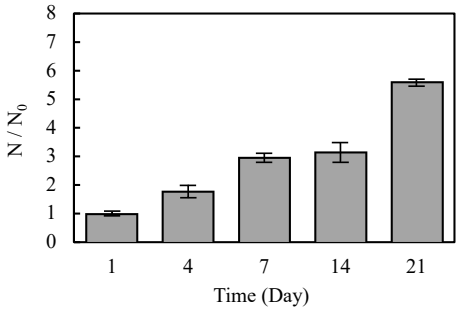

Figure 5B.6: The proliferation rate of normal human chondrocytes on the cartilage (gelatin/elastin/sodium hyaluronate) constructs. The experiments were performed on four samples at each time point (n=4). N: Number of cells at each time point, N_0: Initial number of the cells.

The number of cells on the scaffold persistently increase from day 1 to day 21. After 21 days, the number of cells was more than 5 times that of the initial number seeded on the first day.

Both 3D confocal laser scanning microscopy (label-free) and fluorescence microscopy confirm the attachment, growth, proliferation and ECM secretion over 21 days, as shown in Figure 5B.7.

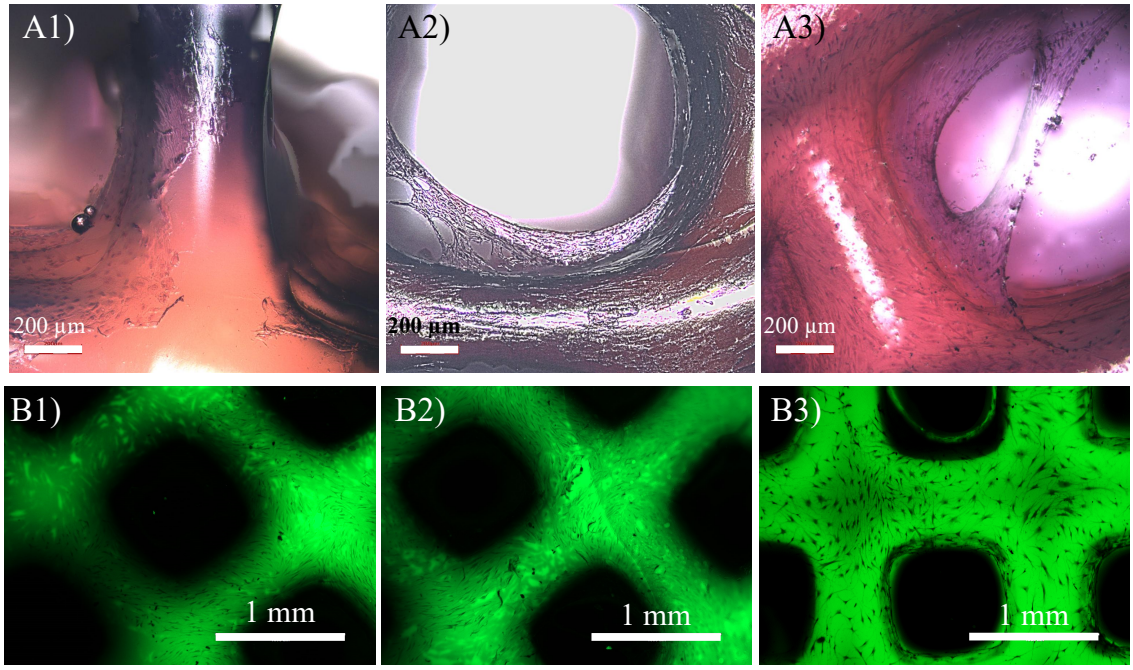

Figure 5B.7: (A1-A3) Chondrocyte attachment, growth and ECM secretion on gelatin/elastin/sodium hyaluronate scaffolds after (A1) 7, (A2) 14 and (A3) 21 days post-seeding. The samples were stained with Eosin/Hematoxylin using standard histology protocols and the images were taken using a 3D confocal laser scanning microscope (label-free). (B1-B3) Fluorescence images of the chondrocytes growing on the gelatin/elastin/sodium-hyaluronate construct after (B1) 7, (B2) 14 and (B3) 21 days.

We observed a "fibroblastic" morphology for chondrocytes on our scaffold. This is in accordance with the study by Awad *et al.* [608], in which chondrogenic differentiation of adipose-derived adult stem cells in gelatin, alginate and agarose scaffolds were investigated. While cells in agarose and alginate scaffolds displayed a spherical morphology that persisted throughout the culture period, the cells in the gelatin scaffolds displayed a distinct "fibroblastic" morphology, proliferating and becoming confluent with notable cell-to-cell contact. However, in general, Awad *et al*. found no significant differences between the chondrogenic differentiation capability of different scaffold materials, despite differences in morphology [608].

A high proliferation rate of chondrocytes was observed in this study. The chondrocyte cell cycle varies according to species and location. The doubling time of human chondrocytes in monolayer cultures ranges between 1.7 to 3.5 days, according to various studies [397, 609, 610]. Our scaffold maintained the typical proliferative activity of the chondrocytes.

For optimization of the permeable PCL membrane to be used as the third component of the knee plug, Film, PCL constructs with various amount of PEG were prepared. Figure 5B.8 illustrates the SEM images of both sides of PCL membrane (top and bottom) made by addition of various amounts of PEG. As shown in this figure, addition of either none or a very small amount of PEG, with the PEG/PCL w/w ratio of 1:5 and 2:5, resulted in none or a very small number of pores per unit of surface area (Figure 5B.8(A-C)). Through employing 1:1 PEG/PCL w/w ratio, more pores were observed on one side (Figure 5B.8(D1)), however, water is unable to pass through the membrane, even when a high vacuum was applied to the other side as a driving force. A possible explanation for this is the formation of no pore at the other side (Figure 5B.8(D2)). While there were adequate pores in one side, they seemed to be close-ended, as the transportation of water molecules was still not possible. However, increasing the ratio to 3:2 w/w resulted in the formation of some pores on the other side, through which the water molecules could permeate by applying a high vacuum based on our observation. We can see the pore on both sides of membrane in Figure 5B.8(E1 and E2). Therefore, this sample was selected as the optimal Film and used for further characterization. As shown in Figure 5B.8(E), the pores on the optimum porous PCL Film were found to be approximately 10 μm. Such pore size allows diffusion of nutrients, like glucose, but prevents cell migration.

Table 5B.3 represents the mechanical properties and suture retention strength of the prepared Films compared to solid PCL membrane fabricated with addition of no PEG. Four samples were used for each experiment and the the values are reported in the form of mean value ± standard deviation (SD). The porous PCL Film was found to have lower modulus and ultimate strength, but higher elongation at break. Having a porous structure, as well as the plasticizing effect of the residual PEG, might account for lower stiffness and strength, along with more flexibility. The suture retention strength was 9.04 ± 0.92 N for the porous PCL Film, which was about half of the corresponding value for solid membrane, but was still strong enough to be sutured to the surrounding tissues or scaffolds as a means of engagement.

The treatment of the surface of the Film with NaOH resulted in improved wettability, as displayed in Figure 5B.9(A). Floating the Film on NaOH solution resulted in a dramatic decrease in the contact angle from 76.7 ± 3.3° to 36.4 ± 3.7°.

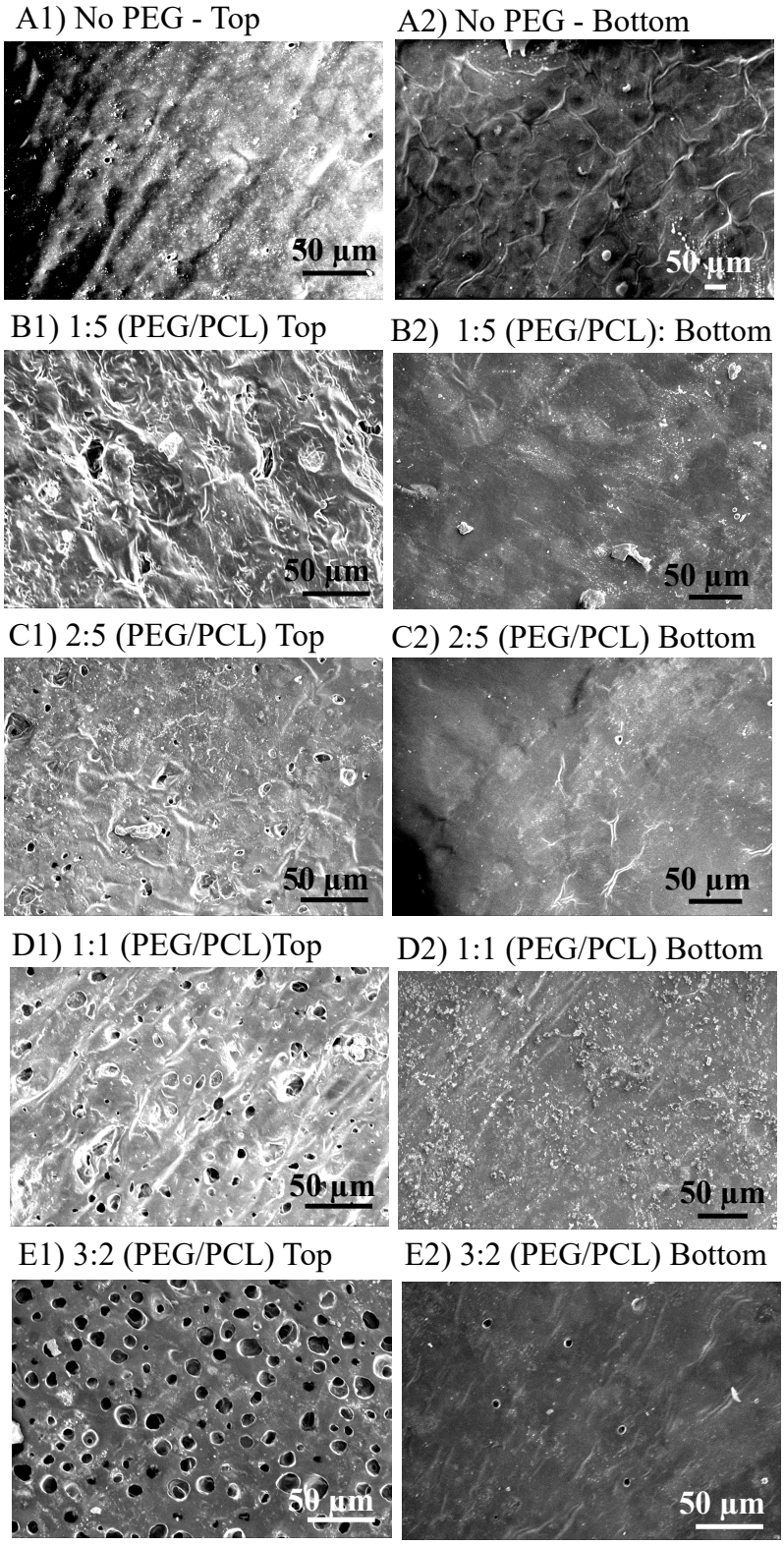

Figure 5B.8: SEM images of both sides (top and bottom) of PCL membranes prepared by addition of different amount of PEG. PEG/PCL w/w ratio is 0(A), 1:5(B), 2:5(C), 1:1(D) and 3:2(E). Only the ratio of 3:2 PEG/PCL formed pores in both sides, which is selected to be used as the Film in the knee plug. The average size of the formed pores in the Film is 10 µm.

Table 5B.3: The mechanical properties and suture retention strength of porous PCL Film compared to a solid PCL membrane.

Parameter	Solid PCL membrane Mean ± SD, n=4	Optimized porous PCL Film Mean ± SD, n=4
Young Modulus (MPa)	112.02 ± 3.62	16.91 ± 2.75
Ultimate Strength (MPa)	12.96 ± 0.99	4.91 ± 1.36
Elongation at Break %	566.83 ± 71.07	973.02 ± 15.35
Suture Retention Strength (N)	18.04 ± 5.28	9.04 ± 0.92

Wettability has been reported to affect protein adsorption and cell adhesion [561, 562]. The number of adhered human umbilical vein endothelial cells (HUVECs) and HeLa cells has been shown to reach a maximum on the surfaces with a water contact angle of 40° and 50°, respectively, and decreases with further increase of water contact angle up to 60–70° [561]. Having the Film on top of the plug is supposed to help retaining the cells within the plug. Having a Film with one hydrophilic (the side facing the Cartilage Portion) and one hydrophobic side, facilitates such retention as cells avoid the hydrophobic sides and attach the hydrophilic side.

The Films was also found to be permeable to the model probe, as shown in Figure 5B.9(B). The diffusion kinetics were faster at the beginning due to a relatively large concentration gradient, but they then decreased over time and eventually reached a plateau after about 100 h. Figure 5B.9(B) illustrates the variation of the model probe concentration in the receiver reservoir normalized to the equilibrium concentration.

Effective permeation of extracellular fluids and nutrients has been listed as one of the important features that a biodegradable polymeric membrane should have to be used for tissue regeneration [611, 612]. The permeability of the PCL Film allows the nutrient delivery and waste removal needed for the healthy growth of the cartilage and bone cells.

The knee plug fabricated in this paper can support both bone and cartilage growth, while keeping favourable cell differentiation between osteoblasts and chondrocytes. One of the functions of this tri-component knee plug is simplifying the surgical procedure employed for the joint repair. Bone and Cartilage Portions may be seeded with cells and then inserted into the designated area of the

body jointly as a unit or separately. They can also be inserted into the joint without cells, and then cells seeded into the relevant components after implantation of each component.

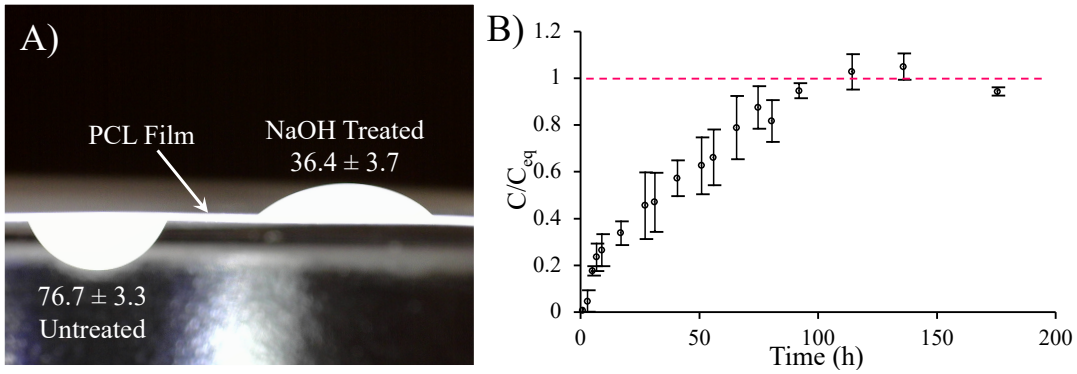

Figure 5B.9: (A) The effect of treatment with NaOH on the wettability and contact angle of the PCL Film. (B) The diffusion kinetics of the model probe (i.e. fluorescein sodium salt) through the Film (C: concentration , C_{eq}: Concentration at equilibrium).

This design considers appropriate accommodation of both osteoblasts and chondrocytes involved in the ACI surgery. Having the large pore size in this design facilitates the nutrient delivery and waste removal and thus assists the cell growth, while resolving the issue of cell retention—a challenge of ACI method.

5B.5. Conclusion

In this paper we presented a new knee plug consisting of 3 components —namely Bone Portion, Cartilage Portion and Film—to be used in the 3rd generation of ACI surgeries with the following advantages : providing a suitable platform for growth of the relevant cells in the area of knee cartilage, simplifying the surgery, control over the pore size and structure, stitchability, use of synthetic materials, possible low cost and less morbidity of other parts of the body during the surgery. The components of this plug are in the size of the tissue normally removed for ACI surgeries in human and can be engaged to each other. The *in vitro* analyses revealed that normal human chondrocytes can perfectly attach to this plug with appropriate proliferation rate.

Acknowledgements

The authors would like to thank the late Professor James Richardson from Institute of Orthopaedics, Robert Jones & Agnes Hunt Orthopaedic Hospital (Oswestry, UK) for the active involvement in this research. The work could not be performed without his insight, guidance and

great discussions. This work was carried out with support from China Regenerative Medicine International Limited (CRMI).

Statement of Authorship for joint/multi-authored papers for PGR thesis

To appear at the end of each thesis chapter submitted as an article/paper

The statement shall describe the candidate's and co-authors' independent research contributions in the thesis publications. For each publication there should exist a complete statement that is to be filled out and signed by the candidate and supervisor **(only required where there isn't already a statement of contribution within the paper itself).**

Title of Paper	A Tri-Component Knee Plug for the 3rd Generation of Autologous Chondrocyte Implantation
Publication Status	□Published □ Accepted for Publication ■ Submitted for Publication □Unpublished and □Unsubmitted work written in a manuscript style
Publication Details	Lobat Tayebi, Zhanfeng Cui, Hua Ye, A Tri-Component Knee Plug for the 3rd Generation of Autologous Chondrocyte Implantation, (Submitted 2019)

Student Confirmation

Student Name:	Lobat Tayebi		
Contribution to the Paper	Contribution in: developing the idea, planning the experiment, performing analysis on samples, interpreting the data, preparing the manuscript		
Signature 		Date	08/12/2019

Supervisor Confirmation

By signing the Statement of Authorship, you are certifying that the candidate made a substantial contribution to the publication, and that the description described above is accurate.

Supervisor name and title: Hua Ye, DPhil, Associate Professor, Institute of Biomedical Engineering Department of Engineering Science, University of Oxford Zhanfeng Cui, Professor, Institute of Biomedical Engineering Department of Engineering Science, University of Oxford		
Supervisor comments		
Signature 	Date	25 Sep, 2019

This completed form should be included in the thesis, at the end of the relevant chapt

Summary of Chapter 5

This chapter examined the application of the 3D-printed membrane for cartilage regeneration. For this purpose, the previously developed ink—with the composition of 8% gelatin, 2% elastin and 0.5% sodium hyaluronate—was used to make a 3D-printed membrane as a part of a new joint plug. It was a tri-component plug, in which the soft cartilage 3D-printed membrane (Cartilage Portion) was placed between a hard TCP/HA 3D-printed scaffold (Bone Portion) and a molded PCL membrane (Film). The physical, mechanical and in vitro characteristics of each component were evaluated and optimized in this chapter. The thickness of the Cartilage Portion was approximately 2 mm composed of large pores with the average size of 892 ± 62 μm. As shown in this chapter, the 3D-printed gelatin/elastin/sodium hyaluronate membrane could effectively accommodate the chondrocyte and, thus, facilitated cartilage regeneration. In sum, this chapter satisfies Objective 3 of Aim 2 of the thesis defined as "designing and preparing a 3D-printed membrane to be used for cartilage regeneration as part of a newly developed joint plug."

CHAPTER 6. DISCUSSION AND CONCLUSION

6.1. Summary of Key Findings

Membranes have diverse set of biomedical and tissue engineering applications. They often require detailed structure in their z-direction for many biomedical applications, which is possible through layer-by-layer deposition of biomaterials promising by 3D-printing method. 3D-printing technique also offers precise control over the pore size, porosity and configuration of each layer, as a key factor for many biomedical applications. Moreover, 3D-printing is the only way of fabricating the complex pore gradient structure.

However, 3D-printing of soft constructs and, more specifically, soft delicate membranes with secure surgical handling, is challenging. With the best our knowledge, no 3D-printed membrane has been yet approved for clinical biomedical applications. The major issue is related to the rheological properties of the hydrogels, that are essential to be employed in synthesis of structured membranes for such applications. The hydrogel inks with relatively good rheological property and acceptable printability often have large amount of alginate [129] which is not a good cell-attractants and cannot be used for versatile applications [430].

To overcome the challenges, this thesis introduces a generic 3D-printing ink composed of hydrogels appropriate for versatile biomedical applications, and a reproducible approach to 3D-print soft membranes with different configurations suitable for the desired application.

For this purpose, an applicable ink with the optimal composition of 8% gelatin, 2% elastin and 0.5% sodium hyaluronate was synthesized with the appropriate rheological properties that make it properly printable in order to fabricate membranes with different structures. This ink was selected after examining the properties of 17 different compositions. In the composition of this ink, gelatin is low-cost and cell-attractant [470], while elastin offers long-term stability, elasticity and biological activity of the produced membranes [25], and sodium hyaluronate improves the chemical signaling among cells [26]. The biomaterials included in this ink are compatible with almost any living cell, offer a cost-effective composition with good mechanical property, along

with secure surgical handing after printing. Thus, we hypothesized that the membranes produced by this ink can be utilized for a diverse set of biomedical and tissue engineering applications. To examine this hypothesis, three different applications—GTR, ocular surface/conjunctival reconstruction and cartilage regeneration—were studied using the 3D-printed membranes made by this ink.

While the printing parameters were similar for each application, the designs of the membrane were adjusted based on the uses. Such adjustment is easily achievable using the 3D-printing capabilities. The design criteria for each application (e.g., pore size, thickness, z-structure and configuration) were determined, the relevant membranes were produced, then biostability, biocompatibility and functionality of the membranes were successfully tested, and promising results were achieved.

In sum, the novelty of this study and its implication for the research field include:

1- Developing a new 3D-printing ink with the characteristics which enable it to be used for diverse biomedical applications.
2- Reporting the first cell-free soft 3D-printed membrane to reconstruct ocular surface/conjunctival defects.
3- Fabrication of a new soft hydrogel GTR 3D-printed membrane.
4- Designing a novel 3D-printed join plug and using the developed generic ink in the plug to facilitate the cartilage regeneration.

6.2. Limitations and Future Works

6.2.1. Modifying and enabling the ink for cell-laden printing

One limitation of our work is the fact that we used a cross-linking method that does not allow us to incorporate cells into the ink prior to printing. More specifically, we have used EDC/NHS as the cross-linker in all membranes produced in this report, although with different concentrations of the EDC/NHS and various exposure time based on the need. EDC has the capability to activate the carboxylic acid residues of the proteins and polysaccharide to react with free amine groups. The activated carboxylic acid groups reacts with NHS and, thus, decreases the possibility of hydrolysis and reorganization of the carboxylic acid groups [613]. This reaction of carboxylic

acid-amine results in creation of amide bonds, which act as a cross-linker amongst the proteins and polysaccharide chains [614]. These reactions are not safe for living cells and must not be performed in the presence of cells in the scaffolds. This imposes an important limitation about the application of our ink for cell-laden printing, in which the cells are incorporated into the ink and printed with it. To avoid this problem, as a future work, it is suggested to replace the gelatin component of the ink with GelMA. Since gelatin is the major component of the ink, using GelMA instead of gelatin provides an opportunity of UV cross-linking instead of chemical cross-linking. When gelatin is chemically functionalized with unsaturated methacryloyl groups to produce GelMA, it forms covalently cross-linked hydrogels by photo-initiated polymerization under mild conditions and enables cell encapsulation with possible good viability [210, 615-617]. For eample, the developed protocol of encapsulation of fibroblast by GelMA indicates good viability of cells after printing, although for limited time [618].

If GelMA is chosen for use in future work instead of gelatin to enable cell-laden printing, its property may need to be adjusted for different applications. The photo cross-linkable hydrogels based on GelMA can be modified to provide desired physicochemical properties. The properties of GelMA hydrogels can be tuned by changing different parameters, including the methacrylation degree, cross-linking density and concentration [619, 620]. Increasing methacrylation degree and/or concentration of the hydrogel can lead to stiffer and more durable hydrogels. The parameters of photo cross-linking including the light exposure duration, initiator concentration and light intensity, may influence the mechanical properties and degradation of the resulting hydrogel [207, 618, 620]. All of these factors must be examined in the membrane fabricated for the specific application. Typically, GelMA with the methacrylation degree of 20-80% is used to design hydrogels with different features [619, 620].

It is worth mentioning that in comparison with the gelatin membrane cross-linked by EDC/NHS, 3D-printed GelMA has less mechanical strength with poor surgical handling, and it may only be selected to prepare the soft scaffold because of its ability to encapsulate live cells for making cell-laden constructs by 3D-printing method [617, 621].

As discussed in the introduction, due to the three major drawbacks of cell-laden printing, including: 1) limitation in the formulations of the hydrogels to meet the certain criteria suitable for cell-laden printing [29], 2) poor cell viability in long term [30], and 3) poor mechanical property [31], we avoided using this approach in this thesis.

Thus, since the vision of this thesis is toward practical applications and prospect of commercialization and clinical use in the field, bioink/cell-laden printing is not the focus of the present study and can be considered for future work.

6.2.2. Loading membranes with drugs/growth factors

It is known that any 3D constructs, including 3D-printed scaffolds and membranes, have the potential to be used for drug delivery purposes [622]. Specific drugs can be loaded in their matrices in a way to be released sustainably and/or locally in the desired area of the body [623]. For example, the inclusion of inflammatory inhibitors and/or antibiotics into specific scaffolds is known as a way to prevent post-surgery infection and other longer-term syndromes [624]. Incorporation of adhesion peptides and growth factors into scaffolds may also be useful in facilitating the signaling among cells, inducing specific differentiation, prompting vascularization or assisting the survival, repair, growth and function of the cells/tissues in the area of body where the scaffolds are implanted [112, 584, 625].

This strategy can be applied in the membrane produced in this thesis as a future work. Depending on the desired function, various drug or growth factor can be used. For example, one may use tacrolimus in the membrane made for ocular surface/conjunctival reconstruction [626], or another may use vascularized endothelial growth factor (VEGF) if vascularization is intended to expand the use of the GTR membranes in critically sized defects [627]. Clinical relevancy of any drug, biological agents and growth factors that are going to be incorporated in the membrane must be fully investigated as the first step of such study.

Drugs or growth factors, with or without carriers—such as micro or nano-particles—may be incorporated into the ink prior to printing [628]. In another approach, they may be immobilized/coated on the surface of the 3D-printed constructs after printing [112]. Numerous applications and approaches can be considered in this path, however, the essential factors that

must be fully studied, engineered and examined are the localized and/or controlled sustained release of the drug and growth factor with the intended dosage [629]. Moreover, after incorporation of drugs/growth factors, a complete bioactivity analysis must be performed to assess the function of the drugs/growths factor [630]. This step is very important for the approach in which the drug/growth factors are incorporated into the ink and gone through the 3D-printing procedure, since the pressure caused during the printing process may result in denaturation and reduced bioactivity of the molecules of drugs/growth factors [631].

6.2.3. Improving the mechanical properties and exploring other applications

Although this thesis attempted to fill some gaps regarding the application of 3D-printed membranes in a few standard applications, there are still many less popular applications that can be examined in future. More specifically, the synthesized ink and the printing parameters set in this thesis can be explored to be used for producing thin or think membranes for other biomedical applications such as treatment of ear tympanic membrane [632, 633], oral mucosa [634] or cleft palates [635]. However, as discussed, the design criteria must be adjusted based on the applications. Some applications may require very strong membranes, for which the mechanical properties of the membrane using solely by this hydrogel ink may not be good enough. In such cases, it can be proposed to use one or two 3D-printed layers of biodegradable polyester (e.g., PCL) in the design of the 3D-printed membrane, in addition to the layers made by the developed ink. These polyester layers may act as a support for the hydrogel membrane. Such non-hydrogel materials, although stronger, may not have the good biocompatibility of hydrogels and cannot be used as a generic material for versatile biomedical applications [636]. However, they can significantly improve the mechanical properties and may be used selectively for some applications that require mechanical strength, such as treatment of cleft palates.

It should be noted that fabrication of hybrid 3D-printed constructs of polyesters and hydrogels is not without serious challenges, which are not within the scope of this thesis and must be considered as a separate study in future. For example, one important challenge associated with such hybrid design is the adhesion of the polyester and hydrogel. If the layers with different types of materials are not adhered together well, the integrity of the construct will be negatively

influenced. For instance, adhesion of PCL layers with gelatin (the major component of our ink) layers is not trivial. One suggested option can be the aminolysis treatment of the PCL layers [637]. When PCL surface is undergoing the aminolysis treatment, the anchored –NH2 groups on PCL molecules can participate in a variety of reactions with other groups. In our case, active amino groups may react with $-NH_2$ groups of the gelatin using hydrogen bonding to achieve a bonding between PCL and gelatin [558-560]. The hydrogel layers are then needed to be printed on top of the aminolysis-treated PCL. This procedure may help the adhesion of the gelatin and PCL, although the strength of such adhesion must be fully evaluated. Moreover, it is important to consider that the aminolysis treatment usually involves the use of glutaraldehyde [637]. Thus, as a post-printing consideration, removal of all free glutaraldehyde from the membrane is necessary, as it is a highly toxic material and not appropriate for biomedical applications [638].

6.2.4. *In vivo* examinations

Another key future work is the *in vivo* examination of the produced membranes for each application.

Although the *in vivo* study using a rabbit model has been performed for ocular surface/conjunctival reconstruction in this thesis (Chapter 4), we have not examined the performance of the produced membranes for cartilage regeneration and GTR *in vivo*, which can be considered as a limitation of our work.

The animal studies to evaluate the membrane for GTR applications may start with a rat calvaria model [639]. It can also be examined in a tibia of a medium size animal (e.g., rabbit) [640], followed by a study on oral cavity of a large animal (e.g., dog) [641].

For the cartilage regeneration, small animal models may not be easily applicable for the case of our knee plug. Based on the previous reports by other investigators, sheep knee model can be a suitable one to implant scaffolds (in our case, the entire structure of the knee plug) and observe the osteochondral reconstruction [642, 643].

Thus, the appropriate animal studies for GTR and cartilage regeneration remain for future work.

In conclusion, the future works that can be considered as continuation of the study performed this thesis include:

1- Modifying the composition of the ink or the cross-linker in a way to enable the ink to be used for cell-laden printing.

2- Loading desired drugs/growth factors into the membranes based on their clinical relevancy.

3- Improving the mechanical properties of the membrane by including layers of 3D-printed polymeric materials—such as PCL—attached to the layers 3D-printed by the produced ink, to be used as a support of the hydrogel membrane.

4- Exploring of other biomedical applications of the present membrane or the membranes enhanced by the above methods.

4- In vivo examinations to evaluate the performance of the membrane for cartilage regeneration and GTR.

APPENDICES

Supplementary Information 1 (SI1): Composition of Initial Solutions (Appendix of Chapter 3B)

Seventeen compositions that have been tested at the beginning of the experiment to select the most suitable ones in term of suturing ability are listed in Table SI1.1. Members with the thickness of approximately 200 μm were made using modeling method, and their ability to be sutured was examined.

Table SI1.1: Initial solution composition. The w/v refers to the weight of the materials in DI water. G: Gelatin, E: Elastin, H: Sodium hyaluronate, CL: Crosslinking Time

Sample Number	Composition (w/v)	CL Time (hour)
1	G(15)	8
2	G(15)	4
3	G(10)	4
4	G(10)/H(0.5)	4
5	G(8)/E(2)	4
6	G(8)/E(2)/H(0.5)	4
7	G(15)	2
8	G(15)/E(2)/H(0.5)	2
9	G(10)	2
10	G(10)/H(0.5)	2
11	G(8)/E(2)	2
12	G(8)/E(2)/H(0.5)	2
13	G(15)	1
14	G(10)	1
15	G(10)/H(0.5)	1
16	G(8)/E(2)	1
17	G(8)/E(2)/H(0.5)	1

Supplementary Information 2 (SI2): Detailed Analyses of the 3D Printed Gelatin/Elastin/Sodium-Hyaluronate Membrane (Appendix of Chapter 4A)

SI2.1. Background

Although conjunctival re-epithelization will occur spontaneously upon conjunctival injury [341-343], there are several limitations that hinder the function and anatomy of the healed epithelium that may eventually lead to unfavorable results and even blindness.

The first limitation is associated with goblet cell density in the presence of injury. Goblet cells are specialized cells that appear as single ovoid cells, extending through the entire thickness of the conjunctival stratified epithelium. The cells are filled with mucin granules that release mucin into the ocular surface. Studies have shown that the goblet-produced mucin is essential for maintaining the wettability of the ocular surface and clearing it of debris [345]. Goblet cell density and, consequently, the mucin layer thickness of the tear film decrease with injury in the healed epithelium [342, 344] or in chronic inflammatory diseases [644, 645]. This is of extreme importance when the damaged surface is large enough to result in significant tear film composition alterations and dry eye. When left untreated, such conditions will compromise the refractive properties and epithelial integrity of the cornea and may eventually lead to blindness as a result of corneal vascularization, as in Steven Johnson's syndrome, ocular cicatricial pemphigoid and extensive ocular burns [345].

The second limitation of self-healing is scar tissue formation and contracture. Studies have shown that the normal process of wound healing is initiated with inflammation and later followed by the migration of fibroblasts. Fibroblasts synthesize collagen to reconstruct the damaged stroma [646]. However, the new, self-healing fibers are laid parallel in the stromal bed compared to the random alignment of collagen in normal stroma; the former results in sub-epithelial fibrosis and scar tissue formation when pathologic [342]. Cells responsible for wound contracture have been suggested to be myofibroblasts, which stain positive for antibodies against alpha-smooth muscle actin (α-SMA) by immunohistochemical staining. Approximation of wound edges, in order to facilitate wound closure, is the primary action of these cells; however, prolonged presence of these cells

may lead to unfavorable wound contracture [342, 353, 646]. Conjunctival contracture and reduced overall surface may lead to fornix foreshortening and eventual symblepharon formation and entropion in the involved eye [346, 347].

Several substitutes have been proposed to replace the absent conjunctiva or modulate the healing process in order to accelerate epithelial healing, increase the goblet density of the healed tissue and reduce inflammation and scarring. Autologous tissues, such as autologous conjunctivae [348], nasal mucosa [349] and oral mucous membrane [347], have been used with favorable results. However, autologous grafts have some limitations, including unavailability of healthy conjunctiva in autoimmune diseases, such as Steven Johnson's, where the entire conjunctival surface is involved. Therefore, not being able to harvest sufficient tissue or donor site morbidity [647] when the defect is large present a problem. Other limitations are cosmetic issues with mucous membranes, as they are thick and not transparent, and absence of goblets in oral mucosal grafts [335]. Therefore, allografts such as pericardium [343] and amniotic membrane (AM) have been introduced.

AM currently serves amongst the most widespread grafts used in ocular surface reconstruction. It is currently used as a substitute for excised conjunctivae in pterygium surgery, symblepharon lysis, fornix reconstruction, conjunctivochalasis and in tumor resections [354]. Some favorable characteristics reported in literature are as follows: AM has been shown to facilitate epithelialization by providing a basement membrane and stroma resembling that of the normal conjunctivae [336, 347, 357, 358]. Studies have also mentioned anti-inflammatory and anti-fibrotic properties, along with lack of immunogenicity for AM [355, 356]. The mentioned characteristics have made AM a favorable tissue for ophthalmic applications [352, 353]. However, studies looking at repopulation of goblet cells on the conjunctival surface repaired by AM have been very limited [337, 346, 648]. All those studies have used impression cytology to document the presence of goblet cells, but have no histological data of the repaired epithelium. Yang *et al*. [365] used a model of rabbits comparing the rabbits grafted with tissue engineered AM (differentiated AM epithelial cells cultured on denuded AM) and simple AM. Histological examinations showed low levels of epithelial stratification (single) and low goblet density (sparse

PAS positive cells) on the epithelium grown on cultured AM [365]. Additionally, despite favorable results on suppression of inflammation by AM reported in prior studies [336, 338, 347, 356, 357, 362-364], there have been some evidence showing increased inflammatory response in histological sections of wounds grafted with AM, three of which were done in rabbits [343, 359, 360], one in monkeys [361] after conjunctival reconstruction with human AM, and the other in rats after transplantation of human AM into the vertebral area. Moreover, considering that AM is an allogenic tissue, limitations in the number of diseases that it can be screened for remains a concern [352]. Another complication associated with AM is the considerable likelihood of microbial infections and unwanted host reactions due to lack of standardized and sterile tissue preparations. Post AM transplantation rate of infection (culture positive) has been reported to be 3.4% in a study on 326 patients [366]. Additionally, since AM lacks viable cells, its efficacy (i.e. ocular surface defect reconstruction) strongly depends on the health of remaining conjunctival host tissue at the borders [354]. The latter is expected to be problematic in situations where the ocular surface is entirely damaged. For such extensively damaged surfaces, it is suggested to transplant healthy epithelial or mesenchymal progenitors with AM [361]. Difficult surgical handling (notably suturing due to the thin structure of AM), prolonged presence in the AM graft site [346, 359, 360], and opacification of the site [367] are among other reported issues associated with AM.

Bioengineered scaffolds can be prepared via standardized procedures yielding repeatable quality, handled with more ease during surgery (since their conformity can be improved by adjusting thickness and structural elasticity), modified with growth factors, and used for drug delivery. However, benefits of synthetic scaffold materials, compared to current accepted substitutes like AM, have not been sufficiently studied, notably in terms of histological data and surgical handling.

Gelatin is a biomaterial, more accurately a biopolymer driven from collagen, that has been extensively investigated over the last few decades for a multitude of ocular applications, including cell-sheet carriers (e.g. growth and delivery of corneal endothelial cells [481, 482], growth of epithelial [483] or limbal cells [484] for corneal surface delivery, etc.), drug delivery [485], bio-

adhesives [486], and bio-artificial grafts (e.g. stromal replacement [487, 488]). Biodegradability, biocompatibility, ease of processing, and relative inexpensiveness of gelatin-based biomaterials have been the main drivers for further studies, albeit predominantly preclinical, on their ocular applications. Adjustable structural stability and mechanical strength are other attractive characteristics that can be achieved via chemical crosslinking. However, conjunctival reconstruction has not been reported as a potential application for this group of biomaterials despite their favorable characteristics mentioned above. Gelatin-based biomaterials possess an additional characteristic that makes them uniquely attractive candidates for conjunctival reconstruction. Gelatin-based biomaterials have a significant similarity to collagen, which is the major protein component of human connective tissue and conjunctival stroma. That similarity, coupled with adjustability of structural stability and mechanical strength, makes gelatin-based biomaterials an exceptionally appealing candidate for conjunctival re-epithelialization. Addition of other components to gelatin-based constructs can further mimic the composition of various tissues and improve different characteristics of these biomaterials. Elastin, for example, is an extracellular matrix protein that provides elasticity to tissues and organs [454]. Hyaluronic acid (HA), as another example to be used as an additive, is a large anionic polysaccharide composed of the repeating disaccharide D-glucuronic acid b-1,3-N-acetyl-D-glucosamine-b1,4 [494]. HA is the major component of synovial liquid and is abundant in solid phases as cartilage and eye vitreous gel. This biomacromolecule participates in organizing extracellular matrix by filling collagen bundles, influences cell proliferation or migration and absorbs elastic shocks [649, 650].

SI2.2. Gelation temperature of various formulations

The sol-gel transition temperature of various formulations was determined using two methods:

1- the method proposed by Winter and Chambon: as the frequency-independent value of the damping factor (tan δ) obtained from a multi-frequency plot for a temperature sweep measurement (Figure SI2.1) [432, 492].

2- through plotting the apparent viscoelastic relaxation exponents n' and n" ($G' \propto \omega n'$, $G'' \propto \omega n''$) obtained from the frequency dependence of storage (G') and loss (G") moduli at each temperature against temperature to track a crossover where $n' = n'' = n$ (Figure SI2.2)

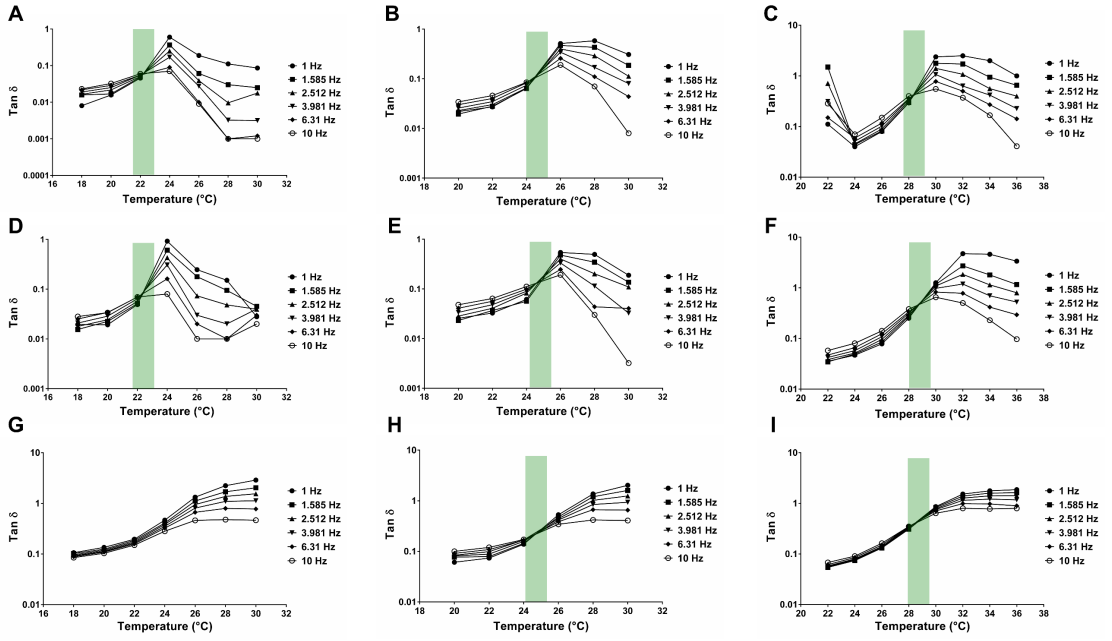

Figure SI2.1: Damping factor (tanδ) as a function of temperature at different oscillation frequencies for (A) G4, (B) G8, (C) G16, (D) G4E2, (E) G8E2, (F) G16E2, (G) G4E2H0.5, (H) G8E2H0.5 and (I) G16E2H0.5 formulations. The green bar displays the estimated gelation temperature for each formulation defined as the frequency-independent value of the damping factor (tanδ).

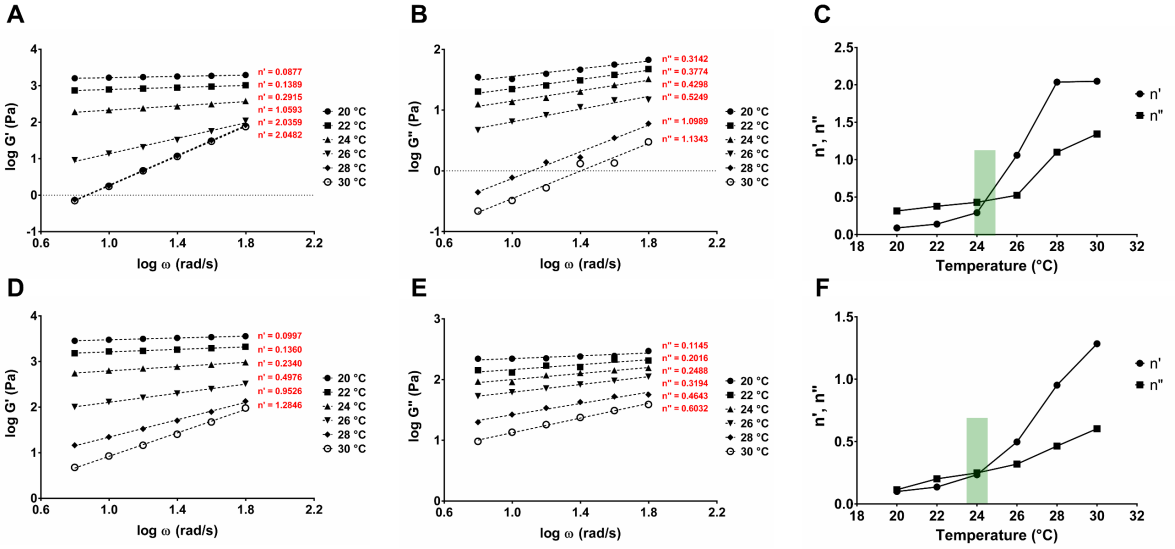

Figure SI2.2: The frequency dependence of G' and G" at different temperatures could be used to calculate the relaxation exponents and, consequently, the critical gelation temperature for (A-C) G8 and (D-F) G8E2H0.5 formulations.

As seen in Figure SI2.2, addition of elastin and sodium hyaluronate affects the gelatin gel's viscoelasticity. The effect has been reported to be correlated with the hyaluronic acid concentration and independent of total concentration in gelatin-hyaluronic acid mixtures [490]. The influence of elastin and sodium hyaluronate on the loss modulus seems to be more significant

compared to the storage modulus, which is in agreement with the results obtained by other authors [490]. It is worth mentioning that the gel elasticity correlates with the helices content in the sample [651].

SI2.3. Cross-linking and mechanical properties of the membranes

EDC/NHS dissolved in 70% (v/v) ethanol was used to cross-link the membranes. Rheological measurements were conducted using parallel-plate geometry and a gap distance of 0.3 mm to investigate the effect of cross-linker concentration on the cross-linking kinetics. Measurements were performed in oscillatory mode at the fixed frequency of 5 Hz and shear strain of 0.1% at 20 °C, which was well below the gelation temperature of the formulation. At t = 20 min, the gel, while being oscillated, was exposed to different concentrations of EDC/NHS, and the variation of storage (G'), loss (G") and complex (G*) moduli was monitored for 1.5 h.

Figure SI2.3A and B display the effect of cross-linker (EDC/NHS) concentration on the storage (G'), loss (G") and complex (G*) moduli representing the kinetics of cross-linking. EDC activates the carboxylic acid residues of the proteins and polysaccharide to react with free amine groups. NHS reacts with the activated carboxylic acid groups and reduces the chance of hydrolysis and rearrangement of the carboxylic acid groups [613]. The carboxylic acid-amine reaction ends up with the formation of amide bonds as chemical cross-links between the proteins and polysaccharide chains [614]. It is worth mentioning that the molar ratio of EDC to NHS for all the concentrations examined was chosen very close to the optimal ratio suggested by Kuijpers *et al.* [652]. As seen in Figure SI2.3, both G' and G" values increased about one order of magnitude upon sample exposure to cross-linker at t = 20 min. The instantaneous increase in moduli was almost the same for all the concentrations examined. While the G" remained almost constant throughout the measurement period, G' and consequently G* increased at different rates for various concentrations as cross-linking proceeded. It was observed that for the first 30 min, medium and high concentrations of EDC/NHS (i.e. 6/0.75 and 12/1.5 mg/ml) advanced the cross-linking reaction very closely while the analogous moduli appeared to be asymptotically heading toward a different direction for the low concentration (i.e. 3/0.375 mg/ml). This phenomenon can be explained by considering the effect of initial concentration of crosslinker on both cross-link

density and diffusion rate. The cross-link density has been shown to be very sensitive to the variation of the EDC/$COOH_{gelatin}$ molar ratio when the ratio is small, while it becomes less sensitive at higher molar ratios [614, 652]. Besides, the diffusion of a specific molecule into a polymer network is governed by the ratio of the correlation length of the polymer network representing the mesh size and the radius of the molecule [653]. It has been reported that the mesh size of the chemical gelatin gels cross-linked by EDC/NHS decreases with cross-link density and is in the order of a few nanometers for all the cross-link densities [614]. Therefore, the cross-linker molecules are expected to diffuse through the structure without any hindrance and with a constant diffusion coefficient during cross-linking. As a result, the diffusion rate is expected to be ruled by the concentration gradient only.

In the first 30 min, both medium and high concentrations act similarly because they are high enough to induce similar cross-link density in a certain period. Furthermore, because of limited diffusion, the regions far from the edges of the rheometer oscillating plate toward the center are not accessible for the cross-linker molecules yet, making the role of chemical gelation in the inner zones inconspicuous. In other words, the measured values of G' and G* represent the properties of a construct composed of a chemically cross-linked part near the borderline and a physical gel at the center. Eventually, the effect of concentration of the cross-linker in the inner regions becomes substantial as the diffusion proceeds, prompting the moduli to diverge over time.

The G' and G* did not reach a plateau within the timescale of the experiment, demonstrating incomplete reaction, likely due to the very limited surface area (equivalent to 0.3 mm gap distance) available for the cross-linker to diffuse into the gel. However, the high surface area of the membrane for cross-linker diffusion significantly shortens the required time to reach the equilibrium.

The tensile modulus and ultimate strength were measured for two membranes cross-linked using 6/0.75 mg/ml solution of EDC/NHS for 0.5 or 1.5 h. The behavior of both materials is schematically shown in Figure SI2.3C. The membranes exhibited elastic behavior until disruption. Longer cross-linking resulted in higher modulus but lower ultimate strength and elongation at break. However, none of the differences were significant ($p > 0.05$).

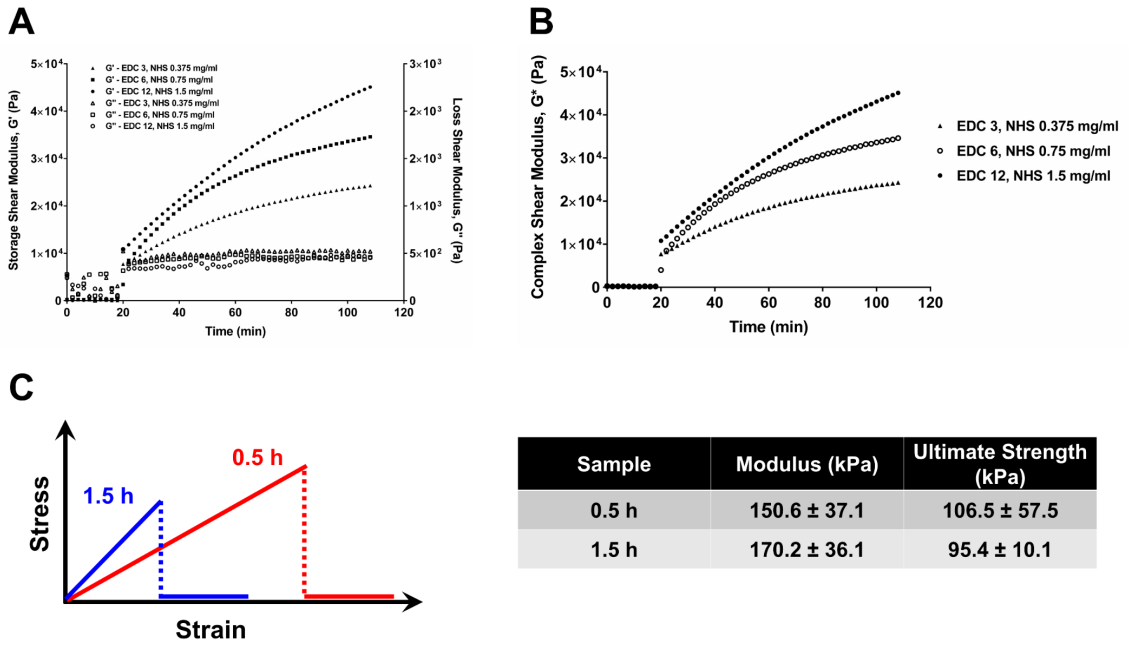

Sample	Modulus (kPa)	Ultimate Strength (kPa)
0.5 h	150.6 ± 37.1	106.5 ± 57.5
1.5 h	170.2 ± 36.1	95.4 ± 10.1

Figure SI2.3: The effect of cross-linker concentration on the cross-linking kinetics of G8E2H0.5 represented by the variation of (A) storage (G') and loss (G") moduli as well as (B) complex modulus (G) measured at 5 Hz and 20 °C. (C) The schematic representation of the effect of cross-linking time on the Young's modulus and ultimate strength of the membranes along with the obtained data for G8E2H0.5 membranes cross-linked by 6 mg/ml EDC and 0.75 mg/ml NHS for 0.5 or 1.5 h.*

SI2.4. Degradation rate of the gelatin-based membranes

The degradation rate of the gelatin-based membranes (15 mm × 15 mm) was measured through immersing the samples in 10 ml Phosphate-Buffered Saline (PBS) while being shaken at 37 °C. Samples were taken out at certain time intervals and their weights were recorded after removing excess water. Figure SI2.4 displays the ratio of the weight at different time point to the initial weight of the sample versus the time of immersion (weight loss). The measurements were performed until complete collapse of the samples.

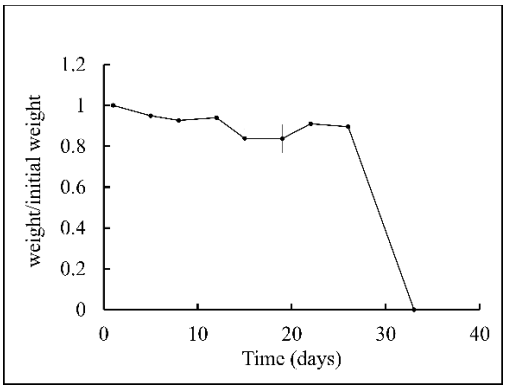

Figure SI2.4: The degradation profile of gelatin-based membranes

SI2.5. *In-vitro* cell culture

It is noteworthy that corneal limbal epithelial cells are amongst the main cells constructing the ocular surface. A well-established isolation, restoration, and characterization protocol was used to prepare corneal limbal epithelial cells that are able to provide a representative assessment of biocompatibility of fabricated scaffolds in ocular surface/conjunctival reconstruction as the primary objective of this study. It should be noted that a wide range of cell types have been used to assess efficacy of fabricated scaffolds for ocular surface/conjunctival reconstruction [500] including cultured corneal equivalents developed from oral mucosal epithelial cells [501, 502], embryonic stem cells [503], bone-marrow-derived mesenchymal stem cells [504], immature dental pulp stem cells [505], hair follicle-derived stem cells [506] and umbilical cord lining stem cells [507]. Additionally, there have been reports of the usage of non-conjunctival derived cells for conjunctival reconstruction for instance epidermal keratinocytes [503], cultured on AM and transplanted in rhesus monkeys, AM epithelial cells [503], cultured to develop a tissue engineered conjunctival equivalent in a study on rabbits, or nasal mucosa [503], suggested to be used for construction of transplants containing goblet cells. In light of that, it appears that there are multiple possible cell sources for developing ocular surface/conjunctival equivalents. Notwithstanding that, a comparative study identifying the optimal choice of donor cells seems missing and further investigation elucidating the interaction of GM and conjunctival epithelial cells is warranted.

SI2.6. Grading criteria for clinical inflammation

The severity of clinical inflammation was rated as mild, moderate or severe based on the degree of conjunctival hyperemia and vessel engorgement. Ratings were made by the same observer. This clinical rating of inflammation has been used previously by ophthalmic surgeons to describe post-operative inflammation in similar conjunctival surgeries [346, 521, 654, 655] and also in another study on rabbits [655]. Also, pathological grading was done based on ordinal method [656], an accepted grading system used by other studies rating the inflammatory response of conjunctivae [657]. In this method the inflammation is quantitatively evaluated based on the average density of inflammatory cells observed in each power field. In doing so, the following

grading is used: 0- none, 1- mild, 2- moderate, and 3- severe to enable. Statistical comparisons were made based on that grading.

SI2.7. Discussion

Surgical handling ease was also studied by other researchers who used PLGA [341], Collagen-Glycosaminoglycan (CG) [342], and vitrified collagen [344] scaffolds/membranes for conjunctival reconstruction. Although PLGA scaffolds/membranes were found to be very soft and flexible, their transparency and extent of suturability haven't been discussed [341]. Conjunctival reconstruction using CG copolymer matrix scaffolds with 2 mm thickness can lead to unfavorable results due to an increased likelihood of step formation that can hinder epithelial cells migration. Additionally, the transparency and extent of suturability of CG copolymer matrix scaffolds have not been discussed [342]. Although vitrified collagen-based scaffolds/membranes have been reported to be transparent, mechanically strong and elastic, their suturability has not been discussed [344]. Biological membranes, such as allogenic (oral and nasal mucous membranes) [335] or xenogeneic grafts (pericardium) [343], have the limitation of being too thick and not being transparent.

Metaplasia is a reversible change that usually occurs in response to chronic irritation and inflammation and allows for substitution of cells that are better able to survive under harsher circumstances [658]. In our study, only two eyes in the AM grafted groups showed epithelial metaplasia to a very limited extent, which did not seem to be a consequence of the inflammation seen in the AM group as both eyes had moderate inflammation with a mean goblet cell count of 10. There are other studies that have reported metaplasia after AM transplantation. For example, metaplasia has been observed in five out of nine eyes in a study using AM for conjunctival reconstruction after symblepharon removal in OCP patients (by impression cytology) [346]. Metaplasia can be caused by the observed chronic inflammatory response of AM grafted eyes. Other factors like exposure of the graft and the poor lubrication of the ocular surface can also contribute.

Three *in vivo* studies on rabbits have also reported goblet cell repopulation after implantation of cryopreserved AM for conjunctival reconstruction, but none have reported the number of cells

[343, 510, 512]. Huang *et al*. reported 4-5 layers of the epithelial stratification and more goblet cells in the AM grafted group compared to the control group based on PAS staining two weeks after AM implantation, again without reporting a number [343]. The second study compared fresh acellular amniotic membrane, with tissue engineered conjunctivae composed of fresh acellular amniotic membrane seeded with epithelial cells induced to differentiate into conjunctival cells. They reported the formation of a single layer of epithelium with few goblet cells on the surface of the AM after 2 weeks, versus acceptable stratification and sporadic PAS positive cells in the tissue engineered group, again without specifying the cell count [512]. The third study also reported the presence of goblet cells in eyes repaired by AM only [510]. Using progenitor cell-derived epidermal sheets on denuded amniotic membrane for conjunctival reconstruction in rhesus monkeys, where the control group was preserved AM, neither groups were positive for goblet cell markers. The test group showed stratification, while the control group showed discontinuity of the epithelium two weeks after transplantation [361].

Goblet cells repopulation in animals or humans, without the use of cultured cells, is not well-examined and needs further study. It should be noted that use of AM cultivated with epithelial cells might not be attractive for routine use in clinical practice due to the cost, time, lack of donors and adverse reactions to the cultivated cells. Promoting epithelialization via AM also depends on the conjunctival status, and AM transplantation might not speed up epithelialization if extensive conjunctival injury exists [356, 358]. On the other hand, gelatin scaffolds have been shown to have the potential to be used for cultivation of ocular epithelial cells and *in-vivo* applications [484, 659, 660].

In-vivo studies of anti-inflammatory effects on AM mostly arrive at conclusions based on clinical observations. Limited studies have provided histological data regarding the type or degree of the host's inflammatory response. They have mostly been confined to impression cytology, mainly because it is difficult to obtain specimens from humans. AM transplantation can significantly reduce ocular surface inflammation in ocular chemical burns [338, 358], autoimmune diseases such as Stevens Johnson's syndrome, toxic epidermolysis and pemphigus[346, 362, 364].

It has been suggested that AM traps and then induces apoptosis in inflammatory cells in damaged ocular surfaces [356, 517]. Histological and immunological data, obtained from explanted AMs used on the ocular surface of patients with an ocular burn for 9 days, showed severe infiltration of macrophages and neutrophils near the undegraded AM with concomitant expression of apoptosis inducing ligands in the infiltration site [356]. This might be a favorable outcome, if short-lived, as infiltration of acute inflammatory cells is necessary in the initial stages of wound healing. However, prolonged presence of infiltration near the AM, even if attributable to the AM's ability to trap cells and induce apoptosis, will result in consequent activation of M1 macrophages and T-lymphocytes leading to autoimmune dysregulation and chronic inflammation. This can result in complications like granulomatous reactions, fibrosis and scarring [355, 359, 521].

The inflammatory reaction towards human AM may also be attributed to xenograft rejection, whereby AM is surrounded by mononuclear cells [359, 360, 519]. In general, AM, especially when cryopreserved, has been suggested to inherently induce low immune response [519, 661]. Among its components, AM epithelial cells have been shown to be possibly immunogenic when used fresh due to expression of MHC-1 [661]. Considering the low inherent immunogenicity of AM and acellularity of the remnants of AM in the histological sections weakens the assumption of xenograft rejection. Additionally, several studies reveal that AM is well-tolerated on a rabbit's ocular surface. Nevertheless, such studies have mostly been conducted through molecular or histological examination of cornea that has immune privilege [519, 662, 663]. Rejection of transplanted cells by the immune system in transplantations for sub-retinal space still remains a problem [664]. The decreased inflammation seen in the previously mentioned study on monkeys [361] might be due to similarity of the species and, therefore, less xenogeneic immune reaction.

Interestingly, despite having a prominent inflammatory reaction depicted through histological sections in 87.5% of eyes transplanted with AM, mild to moderate inflammation with mild gross surface remodeling was clinically observed in those eyes. This can explain why in human studies, AM causes clinically acceptable ocular surface conditions in terms of reducing clinical inflammation. Such studies, however, lack histological data [336, 346, 357, 358, 364].

The anti-angiogenesis properties of AM [352], though are very promising for corneal surface reconstruction, but is considered a shortcoming for reconstruction of conjunctiva, since blood vessel growth into the damaged area is an important step toward wound healing.

Supplementary Information 3 (SI3): Optimizing the Paste to Print the Bone Portion (Appendix of Chapter 5B)

SI3.1. Purpose

To select the most appropriate paste for printing the Bone Portion of the knee plug, this Supplementary Information (SI) aims to examine the four different compositions of pastes in which the β-tricalcium phosphate (TCP) and hydroxyapatite (HA) have the ratios as follows:
Formulation 1) TCP/HA 100:0, Formulation 2) TCP/HA 80:20, Formulation 3) TCP/HA 70:30 Formulation 4) TCP/HA 50:50.

SI3.2. Materials and method

SI3.2.1. Preparation of the Pastes

Starting from formulation 1 (TCP/HA 100:0) the paste was made by mixing 15 g of TCP with 5.75 ml water, 0.5 g sodium tripolyphospahte (TPP, Alfa Aesar) and 75 mg carboxymethyl-cellulose (CMC, Alfa Aesar). This formulation was previously developed as a printable TCP scaffold [665]. We hypothesize that incorporation of HA can improve the mechanical properties. Thus, since sufficient mechanical properties are crucial in bone scaffolds, we replaced some TCP by HA in formulations 2, 3 and 4. For this purpose, the total weight of ceramics (15 g) was held constant but divided between TCP and HA based on their defined ratio in each formulation. More specifically, the amount of TCP and HA are as follows:
Formulation 1) 15 g TCP, Formulation 2) 12 g TCP + 3 g HA, Formulation 3) 10.5 g TCP + 4.5 g HA, and Formulation 4) 7.5 g TCP + 7.5 g HA.
All formulations were homogenized at 2000 rpm for 2 minutes (min) using a centrifugal mixer (Thinky, USA).

SI3.2.2. Rheological analysis

To perform the rheological analysis of each formulation, the viscosity and applied stress were measured as a function of shear rate at different temperatures. For this purpose, a shear rheometer (Kinexus, Malvern, UK) with a stainless steel parallel-plate geometry of 20 mm in diameter and a Peltier temperature control was used. The viscometry of the samples was conducted, applying

a gap distance of 0.5 mm at temperatures increasing in 2°C increments, ranging from 20°C up to 26°C. The shear rate varied logarithmically in ramp mode from 0 to 50 s^{-1} and then back to 0 s^{-1}.

SI3.2.3. 3D-Printing and sintering

The scaffolds were fabricated using a 3D-Bioplotter® system (EnvisionTEC, Germany). By applying the optimized parameters (air pressure of 1-1.5 bar at a speed of 4-7 mm/s), the pastes were extruded from a cartridge through a plotting needle with a diameter of 250 μm (Nordson, USA). The printer head deposited strands of the pastes in a layer-by-layer fashion on the platform, forming a disc with 6 mm diameter and 3 mm thickness. Scaffolds were air-dried overnight and then sintered. For sintering, temperature of the furnace was raised to 600°C at the constant rate of 3°C/min, held for 1 hour (h) in 600°C, then raised from 600°C to 1100°C at a rate of 5°C/min and remained at 1100°C for 4 h.

SI3.2.4. Mechanical testing and degradation analysis

The Young modulus and compressive strength of the scaffolds were measured using a mechanical testing machine (Shimadzu, Japan), with a 5kN load cell and a cross-head speed of 1.0 mm/min.

To evaluate the degradation behavior of the samples, they were immersed in PBS for 12 weeks. Since their weight were not changed noticeably during this time (especially for the samples with higher percentage of HA), we have evaluated their degradation behavior by measuring their mechanical properties. At certain times, samples were taken out, and their Young modulus and compressive strength were measured using a 5 kN load cell and crosshead speed of 1 mm/min.

SI3.3. Results and discussion

All four formulations were 3D printed in the form of disc with a diameter of 6 mm and thickness of 3 mm. Figure SI3.1 presents their structures. During the printing procedure, it was determined that formulations 1 and 2 are the most robust pastes for printing. More specifically, only about 5% of the constructs made with these pastes had uneven strands. This number is about 30% for formulation 3, due to the clogging of the dispenser. Printing of formulation 4 failed very frequently; 7 out of 10 constructs (70%) made with this formulation were composed of uneven strands due to frequent blockage during the printing procedure.

Please note that HA particles were sieved using a 45-micron mesh prior to be mixed in the formulation. Considering the use of a much larger nozzle size (250 µm diameter) for the printing procedure, the frequent clogging of formulations 3 and 4 cannot be attributed to the HA particle size, but might mostly be relevant to the fact that HA particles were prone to agglomeration. Thus, we concluded that their amount in the formulations must be limited and not exceed the 20% of the ceramic content.

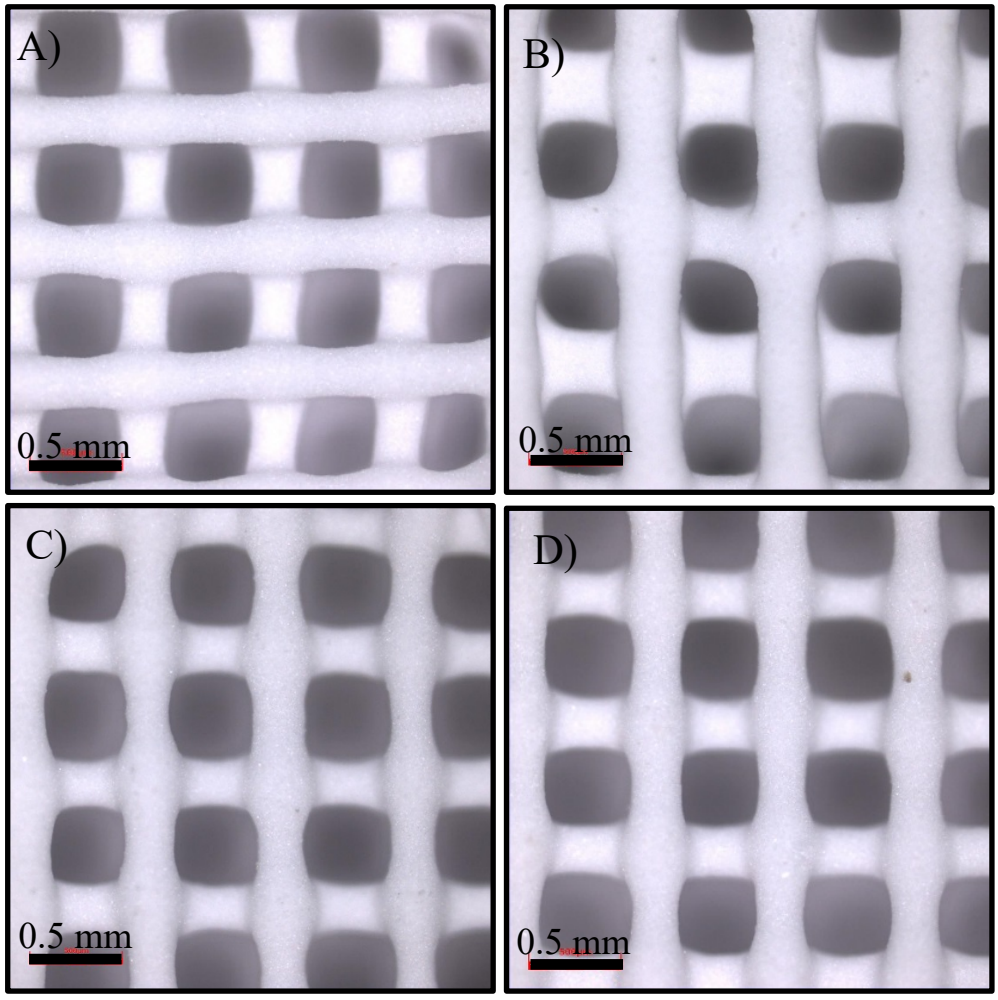

Figure SI3.1: Microscopic images of the 3D printed scaffolds with the TCP/HA ratio of: (A) 100:0 [formulation 1], (B) 80:20 [formulation 2], (C) 70:30 [formulation 3] and (D) 50:50 [formulation 4].

The rheologic properties of these four pastes may also help explaining the encountered difficulties in the printability of formulations 3 and 4. More specifically, analyzing Figure SI3.2, one may realize two considerations that aid in understanding the behavior of the pastes during the printing procedure:

1) Formulations 3 and 4 are more temperature sensitive compared to formulations 1 and 2 at lower temperatures. It is especially important because lower temperatures (20-22°C) are more favorable for printing due to reduced evaporation which in turn improves consistency. The room temperature, in which the printing was performed, was also around 20-22°C. Formulation 2 appears to be the least sensitive paste to temperature which makes it reliable during the printing procedure.

2) For most of the compositions/situations, the viscosity is increasing with increasing HA. This can be generalized to all the ratios at low temperatures (20°C). The viscosity values of formulations 3 and 4 are very high, which make them difficult to be handled for smooth 3D printing.

Please note that the shear stress versus shear rate is typically ascending and the fluctuating seen in formulation 4 at some temperatures can be considered as an artefact, or irregular behaviour of this formulation.

Considering the above facts about the printability and rheological properties of all formulations, we realized that formulations 3 and 4 were definitely not suitable for printing.

We further studied the formulations by analyzing the mechanical and degradation properties of the scaffolds made by these compositions.

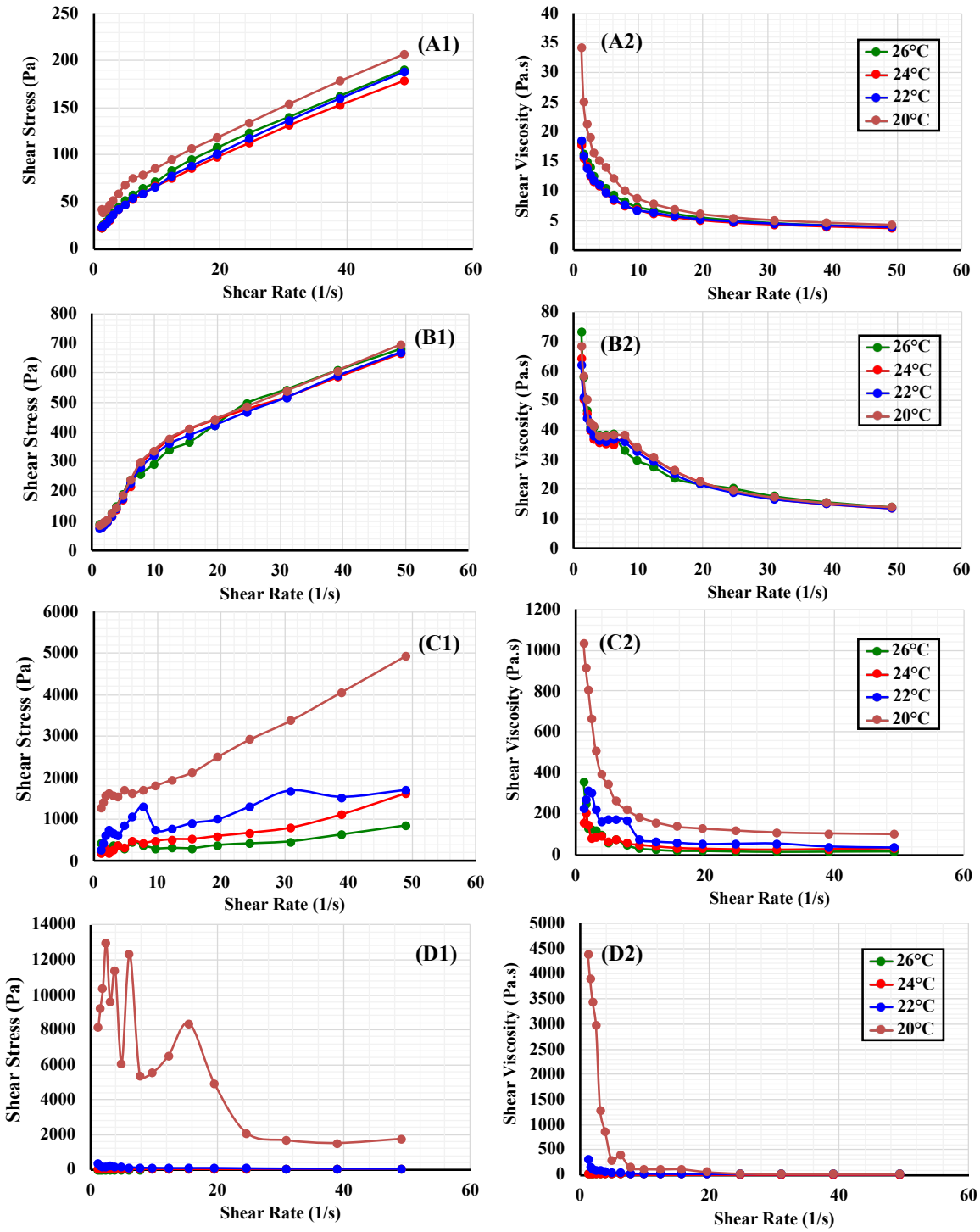

Figure SI3.2: Shear stress versus shear rate and shear viscosity versus shear rate at various temperatures for the pates with the TCP/HA ratio of: (A1,A2) 100:0 [formulation 1], (B1,B2) 80:20 [formulation 2], (C1,C2) 70:30 [formulation 3] and (D1,D2) 50:50 [formulation 4].

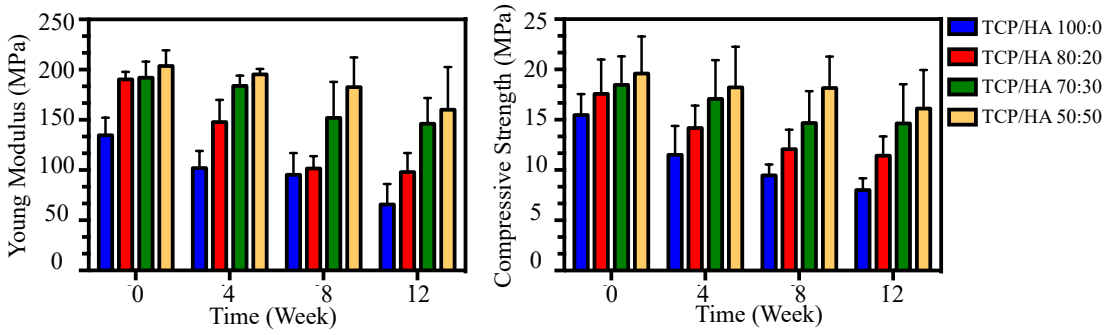

Figure SI3.3: Mechanical properties (Young modulus and compressive strength) and degradation of the printed scaffolds using the ink composed of TCP/HA ratio of: 1) 100:0, 2) 80:20, 3) 70:30 and 4) 50:50 were measured immediately after preparation and storage in SBF for 4, 8 and 12 weeks. The values of Young modulus and compressive strength are obtained after three repetitions on three separate samples. All scaffolds were in the shape of a disc with 6 mm diameter, 3 mm thickness, porosity of 41.9 ± 2.5% and the inner structure as shown in Figure SI3.2.

The mechanical properties of the printed scaffolds were measured immediately after preparation and storage in PBS for 4, 8 and 12 weeks. Young modulus and compressive strength of the scaffolds are presented in Figure SI3.3. The values of Young modulus and compressive strength are extracted after three replications on three separate samples.

In general, the values of Young modulus and compressive strength increased by increasing the HA content in the compositions. Also, the mechanical properties declined by increasing storage time in PBS, which is indicative of scaffold degradation. However, many of these changes in the values of Young modulus and compressive strength from one composition to another and from one week to another are not significant, and thus, not conclusive in determining the best formulation. However, the two considerations below, along with the previously mentioned points about the printability and rheological properties of TCP/HA 80:20, are convincing that formulation 2 can be an optimized choice:

1) Young modulus is significantly increased in formulation 2 compared to formulation 1 by addition of 20% HA—from TCP/HA 100:0 to 80:20—in most of the weeks. However, this increase is not significant when the addition of HA continued to 30 and 50% in formulations 3 and 4. Thus, having 20% HA seems to be sufficient, and it is not necessary to increase the amount of HA further, as it does not significantly improve the mechanical properties after 20%, at least in the printed samples under the mentioned circumstances.

2) As shown in Figure SI3.3, although scaffolds with all formulations demonstrate a continuous decrease in mechanical properties after storage in PBS solution over time, this decrease for formulations 3 and 4 is very slow, which indicates the exceedingly slow degradation property of them. During the experimental procedure, no noticeable change in the morphology of these scaffolds was observed after period of 12 weeks. This result is in agreement with the reported property of HA regarding the slow degradation of this material (in the order of 10^{-3} g per two weeks storage in PBS) [666, 667]. Since we are seeking a degradable scaffold in which the degraded materials can be replaced by the growing cells, such a slow degradation is not favourable.

Considering the two above points, which favour formulation 2 over formulation 1, along with the facts about the difficulty in printability and rheological properties of formulation 3 and 4, formulation 2 is selected as the optimized paste to be used in fabrication of the scaffold for the Bone Portion.

Note that we observed a slight increase in the Young modulus and compressive strength of the scaffold made specifically for the Bone Portion of the plug (cylinder with the diameter of 20 mm, height of 6-8 mm and pore size of 850 μm), compared to the scaffold made for studying the various formulation in this study (disc with 6 mm diameter, 3 mm thickness and pore size of 250 μm). This difference can be attributed to the different distance between strands as well as use of different nozzles during printing (250 μm versus 410 μm), which resulted in different porosities. More specifically, the porosity of the discs made in this SM was 41.9 ± 2.5%, while the porosity of the scaffolds made for the Bone Portion was 25.5 ± 3.8%.

SI3.4. Conclusion

To find the most appropriate scaffold for the Bone Portion of the plug, four formulations of pastes with the TCP/HA ratio of : A)100:0, B) 80:20, C)70:30 and D) 50:50 were examined. After studying of the printability, rheological, mechanical and degradation properties of all formulations, the paste with the TCP/HA ratio of 80:20 was ultimately selected as the most optimized paste for 3D printing of the Bone Portion.

BIBLIOGRAPHY

1. Michalski, M.H. and J.S. Ross, *The shape of things to come: 3D printing in medicine.* Jama, 2014. **312**(21): p. 2213-2214.
2. Trombetta, R., et al., *3D printing of calcium phosphate ceramics for bone tissue engineering and drug delivery.* Annals of biomedical engineering, 2017. **45**(1): p. 23-44.
3. Duda, T. and L.V. Raghavan, *3D metal printing technology.* IFAC-PapersOnLine, 2016. **49**(29): p. 103-110.
4. Zhu, C., et al., *Highly compressible 3D periodic graphene aerogel microlattices.* Nature communications, 2015. **6**: p. 6962.
5. Wang, X., et al., *3D printing of polymer matrix composites: A review and prospective.* Composites Part B: Engineering, 2017. **110**: p. 442-458.
6. Murphy, S.V., A. Skardal, and A. Atala, *Evaluation of hydrogels for bio-printing applications.* Journal of Biomedical Materials Research Part A, 2013. **101**(1): p. 272-284.
7. Séquin, C.H., *Rapid prototyping: a 3d visualization tool takes on sculpture and mathematical forms.* Communications of the ACM, 2005. **48**(6): p. 66-73.
8. Kostakis, V., V. Niaros, and C. Giotitsas, *Open source 3D printing as a means of learning: An educational experiment in two high schools in Greece.* Telematics and informatics, 2015. **32**(1): p. 118-128.
9. Gonzalez-Gomez, J., et al., *A new open source 3d-printable mobile robotic platform for education*, in *Advances in autonomous mini robots*. 2012, Springer. p. 49-62.
10. Tseng, P., et al., *Research highlights: printing the future of microfabrication.* Lab on a Chip, 2014. **14**(9): p. 1491-1495.
11. Kim, K., et al., *3D optical printing of piezoelectric nanoparticle–polymer composite materials.* ACS nano, 2014. **8**(10): p. 9799-9806.
12. Femmer, T., A.J. Kuehne, and M. Wessling, *Print your own membrane: direct rapid prototyping of polydimethylsiloxane.* Lab on a Chip, 2014. **14**(15): p. 2610-2613.
13. Philamore, H., et al., *Cast and 3D printed ion exchange membranes for monolithic microbial fuel cell fabrication.* Journal of Power Sources, 2015. **289**: p. 91-99.
14. Low, Z.-X., et al., *Perspective on 3D printing of separation membranes and comparison to related unconventional fabrication techniques.* Journal of Membrane Science, 2017. **523**: p. 596-613.
15. Maruf, S.H., et al., *Fabrication and characterization of a surface-patterned thin film composite membrane.* Journal of membrane science, 2014. **452**: p. 11-19.
16. Porter Jr, L.A., C.A. Chapman, and J.A. Alaniz, *Simple and inexpensive 3D printed filter fluorometer designs: User-friendly instrument models for laboratory learning and outreach activities*. 2016, ACS Publications.
17. Zhang, B. and H. Zirath, *3D printed iris bandpass filters for millimetre-wave applications.* Electronics Letters, 2015. **51**(22): p. 1791-1793.
18. Singh, D., D. Singh, and S. Han, *3D printing of scaffold for cells delivery: Advances in skin tissue engineering.* Polymers, 2016. **8**(1): p. 19.
19. Muwaffak, Z., et al., *Patient-specific 3D scanned and 3D printed antimicrobial polycaprolactone wound dressings.* International journal of pharmaceutics, 2017. **527**(1-2): p. 161-170.
20. Webster, M., *Merriam-Webster online dictionary.* Retrieved June, 2006. **20**: p. 2013.
21. Chia, H.N. and B.M. Wu, *Recent advances in 3D printing of biomaterials.* Journal of biological engineering, 2015. **9**(1): p. 4.
22. Billiet, T., et al., *A review of trends and limitations in hydrogel-rapid prototyping for tissue engineering.* Biomaterials, 2012. **33**(26): p. 6020-6041.

23. Highley, C.B., C.B. Rodell, and J.A. Burdick, *Direct 3D printing of shear-thinning hydrogels into self-healing hydrogels.* Advanced Materials, 2015. **27**(34): p. 5075-5079.
24. Su, K. and C. Wang, *Recent advances in the use of gelatin in biomedical research.* Biotechnology letters, 2015. **37**(11): p. 2139-2145.
25. Lee, A.Y., et al., *Effects of elastin degradation and surrounding matrix support on artery stability.* American Journal of Physiology-Heart and Circulatory Physiology, 2011. **302**(4): p. H873-H884.
26. Entwistle, J., C.L. Hall, and E.A. Turley, *HA receptors: regulators of signalling to the cytoskeleton.* Journal of cellular biochemistry, 1996. **61**(4): p. 569-577.
27. Murphy, S.V. and A. Atala, *3D bioprinting of tissues and organs.* Nature biotechnology, 2014. **32**(8): p. 773.
28. Mironov, V., N. Reis, and B. Derby, *Bioprinting: A beginning.* Tissue engineering, 2006. **12**(4): p. 631-634.
29. Skardal, A. and A. Atala, *Biomaterials for integration with 3-D bioprinting.* Annals of biomedical engineering, 2015. **43**(3): p. 730-746.
30. Mironov, V., et al., *Organ printing: tissue spheroids as building blocks.* Biomaterials, 2009. **30**(12): p. 2164-2174.
31. Schuurman, W., et al., *Bioprinting of hybrid tissue constructs with tailorable mechanical properties.* Biofabrication, 2011. **3**(2): p. 021001.
32. Lanza, R., R. Langer, and J.P. Vacanti, *Principles of tissue engineering*. 2011: Academic press.
33. Chen, G., T. Ushida, and T. Tateishi, *Scaffold design for tissue engineering.* Macromolecular Bioscience, 2002. **2**(2): p. 67-77.
34. O'Brien, F.J., et al., *Influence of freezing rate on pore structure in freeze-dried collagen-GAG scaffolds.* Biomaterials, 2004. **25**(6): p. 1077-1086.
35. Deville, S., E. Saiz, and A.P. Tomsia, *Freeze casting of hydroxyapatite scaffolds for bone tissue engineering.* Biomaterials, 2006. **27**(32): p. 5480-5489.
36. Lee, S.B., et al., *Study of gelatin-containing artificial skin V: fabrication of gelatin scaffolds using a salt-leaching method.* Biomaterials, 2005. **26**(14): p. 1961-1968.
37. Gouma, P.-I. and D. Han, *Electrospun Bioscaffolds That Mimic the Topology of Extracellular Matrix*, in *Nanomedicine in Cancer*. 2017, Pan Stanford. p. 185-196.
38. Poursamar, S.A., et al., *Gelatin porous scaffolds fabricated using a modified gas foaming technique: Characterisation and cytotoxicity assessment.* Materials Science and engineering: C, 2015. **48**: p. 63-70.
39. Sezer, N., et al., *Review of magnesium-based biomaterials and their applications.* Journal of magnesium and alloys, 2018. **6**(1): p. 23-43.
40. Rasoulianboroujeni, M., et al., *From solvent-free microspheres to bioactive gradient scaffolds.* Nanomedicine: Nanotechnology, Biology and Medicine, 2017. **13**(3): p. 1157-1169.
41. Do, A.V., et al., *3D printing of scaffolds for tissue regeneration applications.* Advanced healthcare materials, 2015. **4**(12): p. 1742-1762.
42. Sachs, E.M., et al., *Three-dimensional printing techniques*. 1993, Google Patents.
43. Campbell, P.G. and L.E. Weiss, *Tissue engineering with the aid of inkjet printers.* Expert opinion on biological therapy, 2007. **7**(8): p. 1123-1127.
44. Tan, Y., et al., *3D printing facilitated scaffold-free tissue unit fabrication.* Biofabrication, 2014. **6**(2): p. 024111.
45. Chavanne, P., et al., *3D printed chitosan/hydroxyapatite scaffolds for potential use in regenerative medicine.* Biomedical Engineering/Biomedizinische Technik, 2013.
46. Cima, M., et al., *Three-dimensional printing techniques*. 1995, Google Patents.
47. Cui, X., et al., *Thermal inkjet printing in tissue engineering and regenerative medicine.* Recent patents on drug delivery & formulation, 2012. **6**(2): p. 149-155.

48. Xu, T., et al., *High-throughput production of single-cell microparticles using an inkjet printing technology.* Journal of Manufacturing Science and Engineering, 2008. **130**(2): p. 021017.
49. Okamoto, T., T. Suzuki, and N. Yamamoto, *Microarray fabrication with covalent attachment of DNA using bubble jet technology.* Nature biotechnology, 2000. **18**(4): p. 438.
50. Goldmann, T. and J.S. Gonzalez, *DNA-printing: utilization of a standard inkjet printer for the transfer of nucleic acids to solid supports.* Journal of Biochemical and Biophysical Methods, 2000. **42**(3): p. 105-110.
51. Saunders, R., et al., *Selective cell delivery for 3D tissue culture and engineering.* Eur Cells Mater, 2004. **7**(Suppl 1): p. 84-5.
52. Saunders, R.E., J.E. Gough, and B. Derby, *Delivery of human fibroblast cells by piezoelectric drop-on-demand inkjet printing.* Biomaterials, 2008. **29**(2): p. 193-203.
53. Nakamura, M., et al., *Biocompatible inkjet printing technique for designed seeding of individual living cells.* Tissue engineering, 2005. **11**(11-12): p. 1658-1666.
54. Demirci, U. and G. Montesano, *Single cell epitaxy by acoustic picolitre droplets.* Lab on a Chip, 2007. **7**(9): p. 1139-1145.
55. Xu, T., et al., *Inkjet printing of viable mammalian cells.* Biomaterials, 2005. **26**(1): p. 93-99.
56. Khalil, S. and W. Sun, *Biopolymer deposition for freeform fabrication of hydrogel tissue constructs.* Materials Science and Engineering: C, 2007. **27**(3): p. 469-478.
57. Skardal, A., et al., *Bioprinted amniotic fluid-derived stem cells accelerate healing of large skin wounds.* Stem cells translational medicine, 2012. **1**(11): p. 792-802.
58. Xu, T., et al., *Hybrid printing of mechanically and biologically improved constructs for cartilage tissue engineering applications.* Biofabrication, 2012. **5**(1): p. 015001.
59. Hong, J.M., et al., *Enhancement of bone regeneration through facile surface functionalization of solid freeform fabrication-based three-dimensional scaffolds using mussel adhesive proteins.* Acta Biomaterialia, 2012. **8**(7): p. 2578-2586.
60. Wong, K.V. and A. Hernandez, *A review of additive manufacturing.* ISRN Mechanical Engineering, 2012. **2012**.
61. Zein, I., et al., *Fused deposition modeling of novel scaffold architectures for tissue engineering applications.* Biomaterials, 2002. **23**(4): p. 1169-1185.
62. Rai, B., et al., *Differences between in vitro viability and differentiation and in vivo bone-forming efficacy of human mesenchymal stem cells cultured on PCL–TCP scaffolds.* Biomaterials, 2010. **31**(31): p. 7960-7970.
63. Khojasteh, A., et al., *The effect of PCL-TCP scaffold loaded with mesenchymal stem cells on vertical bone augmentation in dog mandible: A preliminary report.* Journal of Biomedical Materials Research Part B: Applied Biomaterials, 2013. **101**(5): p. 848-854.
64. Xu, N., et al., *3D artificial bones for bone repair prepared by computed tomography-guided fused deposition modeling for bone repair.* ACS applied materials & interfaces, 2014. **6**(17): p. 14952-14963.
65. Liu, F.-H., *Synthesis of biomedical composite scaffolds by laser sintering: Mechanical properties and in vitro bioactivity evaluation.* Applied Surface Science, 2014. **297**: p. 1-8.
66. Kruth, J.-P., et al., *Consolidation phenomena in laser and powder-bed based layered manufacturing.* CIRP annals, 2007. **56**(2): p. 730-759.
67. Kim, K., et al., *Stereolithographic bone scaffold design parameters: osteogenic differentiation and signal expression.* Tissue Engineering Part B: Reviews, 2010. **16**(5): p. 523-539.
68. Nguyen, K.T. and J.L. West, *Photopolymerizable hydrogels for tissue engineering applications.* Biomaterials, 2002. **23**(22): p. 4307-4314.

69. Fazel-Rezai, R., *Biomedical Engineering: Frontiers and Challenges*. 2011: BoD–Books on Demand.
70. Cooke, M.N., et al., *Use of stereolithography to manufacture critical-sized 3D biodegradable scaffolds for bone ingrowth.* Journal of Biomedical Materials Research Part B: Applied Biomaterials: An Official Journal of The Society for Biomaterials, The Japanese Society for Biomaterials, and The Australian Society for Biomaterials and the Korean Society for Biomaterials, 2003. **64**(2): p. 65-69.
71. Elomaa, L., et al., *Preparation of poly (ε-caprolactone)-based tissue engineering scaffolds by stereolithography.* Acta biomaterialia, 2011. **7**(11): p. 3850-3856.
72. Tumbleston, J.R., et al., *Continuous liquid interface production of 3D objects.* Science, 2015. **347**(6228): p. 1349-1352.
73. Ozbolat, I.T., H. Chen, and Y. Yu, *Development of 'Multi-arm Bioprinter'for hybrid biofabrication of tissue engineering constructs.* Robotics and Computer-Integrated Manufacturing, 2014. **30**(3): p. 295-304.
74. Peltola, S.M., et al., *A review of rapid prototyping techniques for tissue engineering purposes.* Annals of medicine, 2008. **40**(4): p. 268-280.
75. Yousefi, A.M., et al., *Design and fabrication of 3D-plotted polymeric scaffolds in functional tissue engineering.* Polymer Engineering & Science, 2007. **47**(5): p. 608-618.
76. Costa, P.F., et al., *Advanced tissue engineering scaffold design for regeneration of the complex hierarchical periodontal structure.* Journal of clinical periodontology, 2014. **41**(3): p. 283-294.
77. Fina, F., et al., *Selective laser sintering (SLS) 3D printing of medicines.* International journal of pharmaceutics, 2017. **529**(1-2): p. 285-293.
78. Williams, J.M., et al., *Bone tissue engineering using polycaprolactone scaffolds fabricated via selective laser sintering.* Biomaterials, 2005. **26**(23): p. 4817-4827.
79. Eosoly, S., S. Lohfeld, and D. Brabazon. *Effect of hydroxyapatite on biodegradable scaffolds fabricated by SLS*. in *Key Engineering Materials*. 2009. Trans Tech Publ.
80. Duan, B., W.L. Cheung, and M. Wang, *Optimized fabrication of Ca–P/PHBV nanocomposite scaffolds via selective laser sintering for bone tissue engineering.* Biofabrication, 2011. **3**(1): p. 015001.
81. Gibson, I. and D. Shi, *Material properties and fabrication parameters in selective laser sintering process.* Rapid prototyping journal, 1997. **3**(4): p. 129-136.
82. Landers, R. and R. Mülhaupt, *Desktop manufacturing of complex objects, prototypes and biomedical scaffolds by means of computer-assisted design combined with computer-guided 3D plotting of polymers and reactive oligomers.* Macromolecular Materials and Engineering, 2000. **282**(1): p. 17-21.
83. Poldervaart, M.T., et al., *Prolonged presence of VEGF promotes vascularization in 3D bioprinted scaffolds with defined architecture.* Journal of controlled release, 2014. **184**: p. 58-66.
84. Pataky, K., et al., *Microdrop printing of hydrogel bioinks into 3D tissue-like geometries.* Advanced Materials, 2012. **24**(3): p. 391-396.
85. Bertassoni, L.E., et al., *Direct-write bioprinting of cell-laden methacrylated gelatin hydrogels.* Biofabrication, 2014. **6**(2): p. 024105.
86. Serra, T., et al., *Relevance of PEG in PLA-based blends for tissue engineering 3D-printed scaffolds.* Materials Science and Engineering: C, 2014. **38**: p. 55-62.
87. Zhao, S., et al., *Three dimensionally printed mesoporous bioactive glass and poly (3-hydroxybutyrate-co-3-hydroxyhexanoate) composite scaffolds for bone regeneration.* Journal of Materials Chemistry B, 2014. **2**(36): p. 6106-6118.
88. Neufurth, M., et al., *Engineering a morphogenetically active hydrogel for bioprinting of bioartificial tissue derived from human osteoblast-like SaOS-2 cells.* Biomaterials, 2014. **35**(31): p. 8810-8819.

89. Wang, M.-D., et al., *Novel crosslinked alginate/hyaluronic acid hydrogels for nerve tissue engineering.* Frontiers of Materials Science, 2013. **7**(3): p. 269-284.
90. Dutta Roy, T., et al., *Performance of hydroxyapatite bone repair scaffolds created via three-dimensional fabrication techniques.* Journal of Biomedical Materials Research Part A: An Official Journal of The Society for Biomaterials, The Japanese Society for Biomaterials, and The Australian Society for Biomaterials and the Korean Society for Biomaterials, 2003. **67**(4): p. 1228-1237.
91. Vorndran, E., et al., *3D powder printing of β-tricalcium phosphate ceramics using different strategies.* Advanced Engineering Materials, 2008. **10**(12): p. B67-B71.
92. Serra, T., J.A. Planell, and M. Navarro, *High-resolution PLA-based composite scaffolds via 3-D printing technology.* Acta biomaterialia, 2013. **9**(3): p. 5521-5530.
93. Lee, J.-S., et al., *3D printing of composite tissue with complex shape applied to ear regeneration.* Biofabrication, 2014. **6**(2): p. 024103.
94. Guo, T., et al., *3D printing PLGA: a quantitative examination of the effects of polymer composition and printing parameters on print resolution.* Biofabrication, 2017. **9**(2): p. 024101.
95. Schmidt, M., D. Pohle, and T. Rechtenwald, *Selective laser sintering of PEEK.* CIRP annals, 2007. **56**(1): p. 205-208.
96. Rosenzweig, D., et al., *3D-printed ABS and PLA scaffolds for cartilage and nucleus pulposus tissue regeneration.* International journal of molecular sciences, 2015. **16**(7): p. 15118-15135.
97. Tellis, B., et al., *Trabecular scaffolds created using micro CT guided fused deposition modeling.* Materials Science and Engineering: C, 2008. **28**(1): p. 171-178.
98. Heo, E.Y., et al., *Novel 3D printed alginate–BFP1 hybrid scaffolds for enhanced bone regeneration.* Journal of Industrial and Engineering Chemistry, 2017. **45**: p. 61-67.
99. Lewis, P.L., R.M. Green, and R.N. Shah, *3D-printed gelatin scaffolds of differing pore geometry modulate hepatocyte function and gene expression.* Acta biomaterialia, 2018. **69**: p. 63-70.
100. Billiet, T., et al., *The 3D printing of gelatin methacrylamide cell-laden tissue-engineered constructs with high cell viability.* Biomaterials, 2014. **35**(1): p. 49-62.
101. Ouyang, L., et al., *3D printing of shear-thinning hyaluronic acid hydrogels with secondary cross-linking.* ACS Biomaterials Science & Engineering, 2016. **2**(10): p. 1743-1751.
102. Liu, C., et al., *Novel 3D collagen scaffolds fabricated by indirect printing technique for tissue engineering.* Journal of Biomedical Materials Research Part B: Applied Biomaterials: An Official Journal of The Society for Biomaterials, The Japanese Society for Biomaterials, and The Australian Society for Biomaterials and the Korean Society for Biomaterials, 2008. **85**(2): p. 519-528.
103. Ghosh, S., et al., *Direct-write assembly of microperiodic silk fibroin scaffolds for tissue engineering applications.* Advanced Functional Materials, 2008. **18**(13): p. 1883-1889.
104. Pati, F., et al., *Printing three-dimensional tissue analogues with decellularized extracellular matrix bioink.* Nature communications, 2014. **5**: p. 3935.
105. Snyder, J., et al., *Bioprinting cell-laden matrigel for radioprotection study of liver by pro-drug conversion in a dual-tissue microfluidic chip.* Biofabrication, 2011. **3**(3): p. 034112.
106. Tayebi, L., et al., *3D-printed membrane for guided tissue regeneration.* Materials Science and Engineering: C, 2018. **84**: p. 148-158.
107. Pati, F., et al., *Biomimetic 3D tissue printing for soft tissue regeneration.* Biomaterials, 2015. **62**: p. 164-175.
108. Chevalier, J. and L. Gremillard, *Ceramics for medical applications: A picture for the next 20 years.* Journal of the European Ceramic Society, 2009. **29**(7): p. 1245-1255.

109. Kim, H.-M., *Ceramic bioactivity and related biomimetic strategy.* Current opinion in solid state and materials science, 2003. **7**(4-5): p. 289-299.
110. Yang, S., et al., *Rapid prototyping of ceramic lattices for hard tissue scaffolds.* Materials & Design, 2008. **29**(9): p. 1802-1809.
111. Will, J., et al., *Porous ceramic bone scaffolds for vascularized bone tissue regeneration.* Journal of Materials Science: materials in medicine, 2008. **19**(8): p. 2781-2790.
112. Fahimipour, F., et al., *3D printed TCP-based scaffold incorporating VEGF-loaded PLGA microspheres for craniofacial tissue engineering.* Dental Materials, 2017. **33**(11): p. 1205-1216.
113. Seitz, H., et al., *Three-dimensional printing of porous ceramic scaffolds for bone tissue engineering.* Journal of Biomedical Materials Research Part B: Applied Biomaterials: An Official Journal of The Society for Biomaterials, The Japanese Society for Biomaterials, and The Australian Society for Biomaterials and the Korean Society for Biomaterials, 2005. **74**(2): p. 782-788.
114. Ahn, E.S., *Tricalcium phosphates, their composites, implants incorporating them, and method for their production*. 2011, Google Patents.
115. Tarafder, S., et al., *SrO-and MgO-doped microwave sintered 3D printed tricalcium phosphate scaffolds: Mechanical properties and in vivo osteogenesis in a rabbit model.* Journal of Biomedical Materials Research Part B: Applied Biomaterials, 2015. **103**(3): p. 679-690.
116. Cox, S.C., et al., *3D printing of porous hydroxyapatite scaffolds intended for use in bone tissue engineering applications.* Materials Science and Engineering: C, 2015. **47**: p. 237-247.
117. Leukers, B., et al., *Hydroxyapatite scaffolds for bone tissue engineering made by 3D printing.* Journal of Materials Science: Materials in Medicine, 2005. **16**(12): p. 1121-1124.
118. Michna, S., W. Wu, and J.A. Lewis, *Concentrated hydroxyapatite inks for direct-write assembly of 3-D periodic scaffolds.* Biomaterials, 2005. **26**(28): p. 5632-5639.
119. Bergmann, C., et al., *3D printing of bone substitute implants using calcium phosphate and bioactive glasses.* Journal of the European Ceramic Society, 2010. **30**(12): p. 2563-2567.
120. LeGeros, R.Z., *Properties of osteoconductive biomaterials: calcium phosphates.* Clinical Orthopaedics and Related Research (1976-2007), 2002. **395**: p. 81-98.
121. Shanjani, Y., et al., *Solid freeform fabrication and characterization of porous calcium polyphosphate structures for tissue engineering purposes.* Journal of Biomedical Materials Research Part B: Applied Biomaterials, 2010. **93**(2): p. 510-519.
122. Tarafder, S. and S. Bose, *Polycaprolactone-coated 3D printed tricalcium phosphate scaffolds for bone tissue engineering: in vitro alendronate release behavior and local delivery effect on in vivo osteogenesis.* ACS applied materials & interfaces, 2014. **6**(13): p. 9955-9965.
123. Dávila, J., et al., *Fabrication of PCL/β-TCP scaffolds by 3D mini-screw extrusion printing.* Journal of Applied Polymer Science, 2016. **133**(15).
124. Castilho, M., et al., *Fabrication of individual alginate-TCP scaffolds for bone tissue engineering by means of powder printing.* Biofabrication, 2015. **7**(1): p. 015004.
125. Bian, W., et al., *Fabrication of a bio-inspired beta-Tricalcium phosphate/collagen scaffold based on ceramic stereolithography and gel casting for osteochondral tissue engineering.* Rapid Prototyping Journal, 2012. **18**(1): p. 68-80.
126. Wei, Q., et al., *Synthetic polymers for biomedical applications.* International journal of biomaterials, 2018. **2018**.
127. Ligon, S.C., et al., *Polymers for 3D printing and customized additive manufacturing.* Chemical reviews, 2017. **117**(15): p. 10212-10290.

128. Stansbury, J.W. and M.J. Idacavage, *3D printing with polymers: Challenges among expanding options and opportunities.* Dental Materials, 2016. **32**(1): p. 54-64.
129. Guvendiren, M., et al., *Designing biomaterials for 3D printing.* ACS biomaterials science & engineering, 2016. **2**(10): p. 1679-1693.
130. Suganuma, J. and H. Alexander, *Biological response of intramedullary bone to poly-L-lactic acid.* Journal of applied biomaterials, 1993. **4**(1): p. 13-27.
131. Woodruff, M.A. and D.W. Hutmacher, *The return of a forgotten polymer—Polycaprolactone in the 21st century.* Progress in polymer science, 2010. **35**(10): p. 1217-1256.
132. Shor, L., et al., *Precision extruding deposition (PED) fabrication of polycaprolactone (PCL) scaffolds for bone tissue engineering.* Biofabrication, 2009. **1**(1): p. 015003.
133. Haq, R.H.A., et al. *Fabrication process of polymer nano-composite filament for fused deposition modeling*. in *Applied Mechanics and Materials*. 2014. Trans Tech Publ.
134. Yeong, W., et al., *Porous polycaprolactone scaffold for cardiac tissue engineering fabricated by selective laser sintering.* Acta biomaterialia, 2010. **6**(6): p. 2028-2034.
135. Temple, J.P., et al., *Engineering anatomically shaped vascularized bone grafts with hASCs and 3D-printed PCL scaffolds.* Journal of biomedical materials research Part A, 2014. **102**(12): p. 4317-4325.
136. Bose, S., S. Vahabzadeh, and A. Bandyopadhyay, *Bone tissue engineering using 3D printing.* Materials today, 2013. **16**(12): p. 496-504.
137. Konopnicki, S., et al., *Tissue-engineered bone with 3-dimensionally printed β-tricalcium phosphate and polycaprolactone scaffolds and early implantation: An in vivo pilot study in a porcine mandible model.* Journal of Oral and Maxillofacial Surgery, 2015. **73**(5): p. 1016. e1-1016. e11.
138. Zhu, Y., C. Gao, and J. Shen, *Surface modification of polycaprolactone with poly (methacrylic acid) and gelatin covalent immobilization for promoting its cytocompatibility.* Biomaterials, 2002. **23**(24): p. 4889-4895.
139. Causa, F., et al., *Surface investigation on biomimetic materials to control cell adhesion: the case of RGD conjugation on PCL.* Langmuir, 2010. **26**(12): p. 9875-9884.
140. Chen, M., et al., *Self-assembled composite matrix in a hierarchical 3-D scaffold for bone tissue engineering.* Acta Biomaterialia, 2011. **7**(5): p. 2244-2255.
141. Bauermeister, A.J., A. Zuriarrain, and M.I. Newman, *Three-dimensional printing in plastic and reconstructive surgery: a systematic review.* Annals of plastic surgery, 2016. **77**(5): p. 569-576.
142. Makadia, H.K. and S.J. Siegel, *Poly lactic-co-glycolic acid (PLGA) as biodegradable controlled drug delivery carrier.* Polymers, 2011. **3**(3): p. 1377-1397.
143. Park, T.G., *Degradation of poly (lactic-co-glycolic acid) microspheres: effect of copolymer composition.* Biomaterials, 1995. **16**(15): p. 1123-1130.
144. Vozzi, G., et al., *Fabrication of PLGA scaffolds using soft lithography and microsyringe deposition.* Biomaterials, 2003. **24**(14): p. 2533-2540.
145. Ge, Z., et al., *Histological evaluation of osteogenesis of 3D-printed poly-lactic-co-glycolic acid (PLGA) scaffolds in a rabbit model.* Biomedical materials, 2009. **4**(2): p. 021001.
146. Mironov, A.V., et al., *3D printing of PLGA scaffolds for tissue engineering.* Journal of Biomedical Materials Research Part A, 2017. **105**(1): p. 104-109.
147. Intra, J., et al., *Pulsatile release of biomolecules from polydimethylsiloxane (PDMS) chips with hydrolytically degradable seals.* Journal of Controlled Release, 2008. **127**(3): p. 280-287.
148. Mountziaris, P.M., et al., *Harnessing and modulating inflammation in strategies for bone regeneration.* Tissue Engineering Part B: Reviews, 2011. **17**(6): p. 393-402.

149. Rajan, V. and R. Murray, *The duplicitous nature of inflammation in wound repair.* Wound Practice & Research: Journal of the Australian Wound Management Association, 2008. **16**(3): p. 122.
150. Talbott, M.F., G.S. Springer, and L.A. Berglund, *The effects of crystallinity on the mechanical properties of PEEK polymer and graphite fiber reinforced PEEK.* Journal of Composite Materials, 1987. **21**(11): p. 1056-1081.
151. Parthasarathy, J., *3D modeling, custom implants and its future perspectives in craniofacial surgery.* Annals of maxillofacial surgery, 2014. **4**(1): p. 9.
152. Kurtz, S.M., *PEEK biomaterials handbook*. 2019: William Andrew.
153. Hoskins, T., K. Dearn, and S. Kukureka, *Mechanical performance of PEEK produced by additive manufacturing.* Polymer Testing, 2018. **70**: p. 511-519.
154. El Halabi, F., et al., *Mechanical characterization and numerical simulation of polyether–ether–ketone (PEEK) cranial implants.* Journal of the mechanical behavior of biomedical materials, 2011. **4**(8): p. 1819-1832.
155. Berretta, S., et al., *Fused Deposition Modelling of high temperature polymers: Exploring CNT PEEK composites.* Polymer Testing, 2017. **63**: p. 251-262.
156. Rahman, K.M., T. Letcher, and R. Reese. *Mechanical properties of additively manufactured PEEK components using fused filament fabrication*. in *ASME 2015 International Mechanical Engineering Congress and Exposition*. 2016. American Society of Mechanical Engineers Digital Collection.
157. Kurtz, S.M., *Chemical and radiation stability of PEEK*, in *PEEK biomaterials handbook*. 2012, Elsevier. p. 75-79.
158. Rodríguez, J.F., J.P. Thomas, and J.E. Renaud, *Mechanical behavior of acrylonitrile butadiene styrene (ABS) fused deposition materials. Experimental investigation.* Rapid prototyping journal, 2001. **7**(3): p. 148-158.
159. Rodriguez, J.F., J.P. Thomas, and J.E. Renaud, *Characterization of the mesostructure of fused-deposition acrylonitrile-butadiene-styrene materials.* Rapid Prototyping Journal, 2000. **6**(3): p. 175-186.
160. Li, Y. and H. Shimizu, *Improvement in toughness of poly (l-lactide)(PLLA) through reactive blending with acrylonitrile–butadiene–styrene copolymer (ABS): Morphology and properties.* European Polymer Journal, 2009. **45**(3): p. 738-746.
161. Dawoud, M., I. Taha, and S.J. Ebeid, *Mechanical behaviour of ABS: An experimental study using FDM and injection moulding techniques.* Journal of Manufacturing Processes, 2016. **21**: p. 39-45.
162. Szykiedans, K. and W. Credo, *Mechanical properties of FDM and SLA low-cost 3-D prints.* Procedia Engineering, 2016. **136**: p. 257-262.
163. Li, X., et al., *3D-printed biopolymers for tissue engineering application.* International Journal of Polymer Science, 2014. **2014**.
164. Hutmacher, D.W., *Scaffolds in tissue engineering bone and cartilage*, in *The biomaterials: Silver jubilee compendium*. 2000, Elsevier. p. 175-189.
165. Szivek, J., et al., *213 POROUS POLYBUTYLENE TEREPHTHALATE IMPLANTS ALLOW FOR BONE INGROWTH AND PROVIDE A WELL-ANCHORED SCAFFOLD THAT CAN BE USED TO DELIVER TISSUE-ENGINEERED CARTILAGE*. 2006, BMJ Publishing Group Limited.
166. Radder, A., H. Leenders, and C. Van Blitterswijk, *Bone-bonding behaviour of poly (ethylene oxide)-polybutylene terephthalate copolymer coatings and bulk implants: a comparative study.* Biomaterials, 1995. **16**(7): p. 507-513.
167. Ullah, F., et al., *Classification, processing and application of hydrogels: A review.* Materials Science and Engineering: C, 2015. **57**: p. 414-433.
168. Buwalda, S.J., et al., *Hydrogels in a historical perspective: From simple networks to smart materials.* Journal of controlled release, 2014. **190**: p. 254-273.
169. Draget, K.I., *Alginates*, in *Handbook of hydrocolloids*. 2009, Elsevier. p. 807-828.

170. ANDRESEN, I.-L., et al., *Some biological functions of matrix components in benthic algae in relation to their chemistry and the composition of seawater*. 1977, ACS Publications.
171. Shi, W., R. He, and Y. Liu, *3D printing scaffolds with hydrogel materials for biomedical applications.* European Journal of BioMedical Research, 2015. **1**(3): p. 3-8.
172. Mørch, Y.A., et al., *Binding and leakage of barium in alginate microbeads.* Journal of Biomedical Materials Research Part A, 2012. **100**(11): p. 2939-2947.
173. Topuz, F., et al., *Magnesium ions and alginate do form hydrogels: a rheological study.* Soft Matter, 2012. **8**(18): p. 4877-4881.
174. Lee, S.-J., J.-W. Rhie, and D.-W. Cho, *Development of three-dimensional alginate encapsulated chondrocyte hybrid scaffold using microstereolithography.* Journal of Manufacturing Science and Engineering, 2008. **130**(2): p. 021007.
175. Lee, S., et al., *Development of Three-Dimensional Hybrid Scaffold Using Chondrocyte-Encapsulated Alginate Hydroge (S & M 0695).* Sensors and Materials, 2007. **19**(8): p. 445.
176. Lee, S.-J., et al., *Application of microstereolithography in the development of three-dimensional cartilage regeneration scaffolds.* Biomedical microdevices, 2008. **10**(2): p. 233-241.
177. Axpe, E. and M. Oyen, *Applications of alginate-based bioinks in 3D bioprinting.* International journal of molecular sciences, 2016. **17**(12): p. 1976.
178. Xu, C., et al., *Scaffold-free inkjet printing of three-dimensional zigzag cellular tubes.* Biotechnology and bioengineering, 2012. **109**(12): p. 3152-3160.
179. Yu, Y., et al., *Evaluation of cell viability and functionality in vessel-like bioprintable cell-laden tubular channels.* Journal of biomechanical engineering, 2013. **135**(9): p. 091011.
180. Hockaday, L., et al., *Rapid 3D printing of anatomically accurate and mechanically heterogeneous aortic valve hydrogel scaffolds.* Biofabrication, 2012. **4**(3): p. 035005.
181. Duan, B., et al., *3D bioprinting of heterogeneous aortic valve conduits with alginate/gelatin hydrogels.* Journal of biomedical materials research Part A, 2013. **101**(5): p. 1255-1264.
182. Pourchet, L.J., et al., *Human skin 3D bioprinting using scaffold-free approach.* Advanced healthcare materials, 2017. **6**(4): p. 1601101.
183. Markstedt, K., et al., *3D bioprinting human chondrocytes with nanocellulose–alginate bioink for cartilage tissue engineering applications.* Biomacromolecules, 2015. **16**(5): p. 1489-1496.
184. Alsberg, E., et al., *Cell-interactive alginate hydrogels for bone tissue engineering.* Journal of dental research, 2001. **80**(11): p. 2025-2029.
185. Lee, K.Y. and D.J. Mooney, *Hydrogels for tissue engineering.* Chemical reviews, 2001. **101**(7): p. 1869-1880.
186. Elzoghby, A.O., W.M. Samy, and N.A. Elgindy, *Protein-based nanocarriers as promising drug and gene delivery systems.* Journal of controlled release, 2012. **161**(1): p. 38-49.
187. Wang, H., et al., *Comparison of micro-vs. nanostructured colloidal gelatin gels for sustained delivery of osteogenic proteins: Bone morphogenetic protein-2 and alkaline phosphatase.* Biomaterials, 2012. **33**(33): p. 8695-8703.
188. Cheng, N.C., et al., *Efficient transfer of human adipose-derived stem cells by chitosan/gelatin blend films.* Journal of Biomedical Materials Research Part B: Applied Biomaterials, 2012. **100**(5): p. 1369-1377.
189. Ruggeri, R.R., et al., *Derivation and culture of putative parthenogenetic embryonic stem cells in new gelatin substrates modified with galactomannan.* Macromolecular Research, 2014. **22**(10): p. 1053-1058.

190. Tang, G., et al., *Preparation of PLGA scaffolds with graded pores by using a gelatin-microsphere template as porogen.* Journal of Biomaterials Science, Polymer Edition, 2012. **23**(17): p. 2241-2257.
191. Young, S., et al., *Gelatin as a delivery vehicle for the controlled release of bioactive molecules.* Journal of controlled release, 2005. **109**(1-3): p. 256-274.
192. Wang, X., et al., *Generation of three-dimensional hepatocyte/gelatin structures with rapid prototyping system.* Tissue engineering, 2006. **12**(1): p. 83-90.
193. Wu, Z., et al., *Bioprinting three-dimensional cell-laden tissue constructs with controllable degradation.* Scientific reports, 2016. **6**.
194. Laronda, M.M., et al., *A bioprosthetic ovary created using 3D printed microporous scaffolds restores ovarian function in sterilized mice.* Nature communications, 2017. **8**: p. 15261.
195. Irvine, S.A., et al., *Printing cell-laden gelatin constructs by free-form fabrication and enzymatic protein crosslinking.* Biomedical microdevices, 2015. **17**(1): p. 16.
196. Zhang, L.-M., *Cellulosic associative thickeners.* Carbohydrate Polymers, 2001. **45**(1): p. 1-10.
197. Utech, S. and A.R. Boccaccini, *A review of hydrogel-based composites for biomedical applications: enhancement of hydrogel properties by addition of rigid inorganic fillers.* Journal of materials science, 2016. **51**(1): p. 271-310.
198. Blokhuis, T.J., et al., *Properties of calcium phosphate ceramics in relation to their in vivo behavior.* Journal of trauma and acute care surgery, 2000. **48**(1): p. 179.
199. Song, W., et al., *The study on the degradation and mineralization mechanism of ion-doped calcium polyphosphate in vitro.* Journal of Biomedical Materials Research Part B: Applied Biomaterials: An Official Journal of The Society for Biomaterials, The Japanese Society for Biomaterials, and The Australian Society for Biomaterials and the Korean Society for Biomaterials, 2009. **89**(2): p. 430-438.
200. Khanarian, N.T., et al., *A hydrogel-mineral composite scaffold for osteochondral interface tissue engineering.* Tissue Engineering Part A, 2011. **18**(5-6): p. 533-545.
201. Gobin, A.S. and J.L. West, *Val-ala-pro-gly, an elastin-derived non-integrin ligand: Smooth muscle cell adhesion and specificity.* Journal of Biomedical Materials Research Part A: An Official Journal of The Society for Biomaterials, The Japanese Society for Biomaterials, and The Australian Society for Biomaterials and the Korean Society for Biomaterials, 2003. **67**(1): p. 255-259.
202. Dehghani, S., et al., *3D-Printed membrane as an alternative to amniotic membrane for ocular surface/conjunctival defect reconstruction: An in vitro & in vivo study.* Biomaterials, 2018. **174**: p. 95-112.
203. Shi, W., et al., *Structurally and functionally optimized silk-fibroin–gelatin scaffold using 3D printing to repair cartilage injury in vitro and in vivo.* Advanced materials, 2017. **29**(29): p. 1701089.
204. Ng, W.L., W.Y. Yeong, and M.W. Naing, *Polyelectrolyte gelatin-chitosan hydrogel optimized for 3D bioprinting in skin tissue engineering.* International Journal of Bioprinting, 2016. **2**(1).
205. Malafaya, P.B., G.A. Silva, and R.L. Reis, *Natural–origin polymers as carriers and scaffolds for biomolecules and cell delivery in tissue engineering applications.* Advanced drug delivery reviews, 2007. **59**(4-5): p. 207-233.
206. Van Den Bulcke, A.I., et al., *Structural and rheological properties of methacrylamide modified gelatin hydrogels.* Biomacromolecules, 2000. **1**(1): p. 31-38.
207. Koshy, S.T., et al., *Injectable, porous, and cell-responsive gelatin cryogels.* Biomaterials, 2014. **35**(8): p. 2477-2487.
208. Burdick, J.A. and G.D. Prestwich, *Hyaluronic acid hydrogels for biomedical applications.* Advanced materials, 2011. **23**(12): p. H41-H56.

209. Kogan, G., et al., *Hyaluronic acid: a natural biopolymer with a broad range of biomedical and industrial applications.* Biotechnology letters, 2007. **29**(1): p. 17-25.
210. Schuurman, W., et al., *Gelatin-methacrylamide hydrogels as potential biomaterials for fabrication of tissue-engineered cartilage constructs.* Macromolecular bioscience, 2013. **13**(5): p. 551-561.
211. Pescosolido, L., et al., *Hyaluronic acid and dextran-based semi-IPN hydrogels as biomaterials for bioprinting.* Biomacromolecules, 2011. **12**(5): p. 1831-1838.
212. Skardal, A., et al., *A hydrogel bioink toolkit for mimicking native tissue biochemical and mechanical properties in bioprinted tissue constructs.* Acta biomaterialia, 2015. **25**: p. 24-34.
213. Highley, C.B., G.D. Prestwich, and J.A. Burdick, *Recent advances in hyaluronic acid hydrogels for biomedical applications.* Current opinion in biotechnology, 2016. **40**: p. 35-40.
214. Kesti, M., et al., *A versatile bioink for three-dimensional printing of cellular scaffolds based on thermally and photo-triggered tandem gelation.* Acta biomaterialia, 2015. **11**: p. 162-172.
215. Müller, M., et al., *Nanostructured Pluronic hydrogels as bioinks for 3D bioprinting.* Biofabrication, 2015. **7**(3): p. 035006.
216. Skardal, A., et al., *Photocrosslinkable hyaluronan-gelatin hydrogels for two-step bioprinting.* Tissue Engineering Part A, 2010. **16**(8): p. 2675-2685.
217. Skardal, A., J. Zhang, and G.D. Prestwich, *Bioprinting vessel-like constructs using hyaluronan hydrogels crosslinked with tetrahedral polyethylene glycol tetracrylates.* Biomaterials, 2010. **31**(24): p. 6173-6181.
218. Skardal, A., et al., *Dynamically crosslinked gold nanoparticle–hyaluronan hydrogels.* Advanced Materials, 2010. **22**(42): p. 4736-4740.
219. Parenteau-Bareil, R., R. Gauvin, and F. Berthod, *Collagen-based biomaterials for tissue engineering applications.* Materials, 2010. **3**(3): p. 1863-1887.
220. Silvipriya, K., et al., *Collagen: Animal sources and biomedical application.* J Appl Pharm Sci, 2015. **5**(3): p. 123-127.
221. Chevallay, B. and D. Herbage, *Collagen-based biomaterials as 3D scaffold for cell cultures: applications for tissue engineering and gene therapy.* Medical and Biological Engineering and Computing, 2000. **38**(2): p. 211-218.
222. Yang, Y.-l., L.M. Leone, and L.J. Kaufman, *Elastic moduli of collagen gels can be predicted from two-dimensional confocal microscopy.* Biophysical journal, 2009. **97**(7): p. 2051-2060.
223. Glowacki, J. and S. Mizuno, *Collagen scaffolds for tissue engineering.* Biopolymers: Original Research on Biomolecules, 2008. **89**(5): p. 338-344.
224. Loo, Y., et al., *Peptide bioink: self-assembling nanofibrous scaffolds for three-dimensional organotypic cultures.* Nano letters, 2015. **15**(10): p. 6919-6925.
225. Helary, C., et al., *Concentrated collagen hydrogels as dermal substitutes.* Biomaterials, 2010. **31**(3): p. 481-490.
226. Nöth, U., et al., *Chondrogenic differentiation of human mesenchymal stem cells in collagen type I hydrogels.* Journal of Biomedical Materials Research Part A: An Official Journal of The Society for Biomaterials, The Japanese Society for Biomaterials, and The Australian Society for Biomaterials and the Korean Society for Biomaterials, 2007. **83**(3): p. 626-635.
227. Park, J.Y., et al., *A comparative study on collagen type I and hyaluronic acid dependent cell behavior for osteochondral tissue bioprinting.* Biofabrication, 2014. **6**(3): p. 035004.

228. Lee, W., et al., *On-demand three-dimensional freeform fabrication of multi-layered hydrogel scaffold with fluidic channels.* Biotechnology and bioengineering, 2010. **105**(6): p. 1178-1186.
229. Lee, W., et al., *Multi-layered culture of human skin fibroblasts and keratinocytes through three-dimensional freeform fabrication.* Biomaterials, 2009. **30**(8): p. 1587-1595.
230. Lee, W., et al., *Three-dimensional bioprinting of rat embryonic neural cells.* Neuroreport, 2009. **20**(8): p. 798-803.
231. Zhao, L., et al., *The integration of 3-D cell printing and mesoscopic fluorescence molecular tomography of vascular constructs within thick hydrogel scaffolds.* Biomaterials, 2012. **33**(21): p. 5325-5332.
232. Lee, V., et al., *Design and fabrication of human skin by three-dimensional bioprinting.* Tissue Engineering Part C: Methods, 2013. **20**(6): p. 473-484.
233. Lee, Y.-B., et al., *Bio-printing of collagen and VEGF-releasing fibrin gel scaffolds for neural stem cell culture.* Experimental neurology, 2010. **223**(2): p. 645-652.
234. Hinton, T.J., et al., *Three-dimensional printing of complex biological structures by freeform reversible embedding of suspended hydrogels.* Science advances, 2015. **1**(9): p. e1500758.
235. Shim, J.-H., et al., *Three-dimensional bioprinting of multilayered constructs containing human mesenchymal stromal cells for osteochondral tissue regeneration in the rabbit knee joint.* Biofabrication, 2016. **8**(1): p. 014102.
236. Wu, Z., et al., *Bioprinting three-dimensional cell-laden tissue constructs with controllable degradation.* Scientific reports, 2016. **6**: p. 24474.
237. Lee, H.J., et al., *A new approach for fabricating collagen/ECM-based bioinks using preosteoblasts and human adipose stem cells.* Advanced healthcare materials, 2015. **4**(9): p. 1359-1368.
238. Duarte Campos, D.F., et al., *The stiffness and structure of three-dimensional printed hydrogels direct the differentiation of mesenchymal stromal cells toward adipogenic and osteogenic lineages.* Tissue Engineering Part A, 2014. **21**(3-4): p. 740-756.
239. Duarte Campos, D.F., et al., *Bioprinting organotypic hydrogels with improved mesenchymal stem cell remodeling and mineralization properties for bone tissue engineering.* Advanced healthcare materials, 2016. **5**(11): p. 1336-1345.
240. Sanjana, N.E. and S.B. Fuller, *A fast flexible ink-jet printing method for patterning dissociated neurons in culture.* Journal of neuroscience methods, 2004. **136**(2): p. 151-163.
241. Rutz, A.L., et al., *A multimaterial bioink method for 3D printing tunable, cell-compatible hydrogels.* Advanced Materials, 2015. **27**(9): p. 1607-1614.
242. Inzana, J.A., et al., *3D printing of composite calcium phosphate and collagen scaffolds for bone regeneration.* Biomaterials, 2014. **35**(13): p. 4026-4034.
243. Xu, T., et al., *Viability and electrophysiology of neural cell structures generated by the inkjet printing method.* Biomaterials, 2006. **27**(19): p. 3580-3588.
244. Xu, F., et al. *Cell bioprinting as a potential high-throughput method for fabricating cell-based biosensors (CBBs)*. in *SENSORS, 2009 IEEE*. 2009. IEEE.
245. Smith, C.M., et al., *Three-dimensional bioassembly tool for generating viable tissue-engineered constructs.* Tissue engineering, 2004. **10**(9-10): p. 1566-1576.
246. Roth, E.A., et al., *Inkjet printing for high-throughput cell patterning.* Biomaterials, 2004. **25**(17): p. 3707-3715.
247. Yeo, M., et al., *An innovative collagen-based cell-printing method for obtaining human adipose stem cell-laden structures consisting of core–sheath structures for tissue engineering.* Biomacromolecules, 2016. **17**(4): p. 1365-1375.

248. Alberts, B., et al., *The extracellular matrix of animals*, in *Molecular Biology of the Cell. 4th edition*. 2002, Garland Science.
249. Miranda-Nieves, D. and E.L. Chaikof, *Collagen and elastin biomaterials for the fabrication of engineered living tissues.* ACS Biomaterials Science & Engineering, 2016. **3**(5): p. 694-711.
250. Włodarczyk-Biegun, M.K. and A. del Campo, *3D bioprinting of structural proteins.* Biomaterials, 2017. **134**: p. 180-201.
251. Suntivich, R., et al., *Inkjet printing of silk nest arrays for cell hosting.* Biomacromolecules, 2014. **15**(4): p. 1428-1435.
252. DeSimone, E., et al., *Biofabrication of 3D constructs: Fabrication technologies and spider silk proteins as bioinks.* Pure and Applied Chemistry, 2015. **87**(8): p. 737-749.
253. Jose, R.R., et al., *Polyol-silk bioink formulations as two-part room-temperature curable materials for 3D printing.* ACS Biomaterials Science & Engineering, 2015. **1**(9): p. 780-788.
254. Das, S., et al., *Enhanced redifferentiation of chondrocytes on microperiodic silk/gelatin scaffolds: toward tailor-made tissue engineering.* Biomacromolecules, 2013. **14**(2): p. 311-321.
255. Das, S., et al., *Bioprintable, cell-laden silk fibroin–gelatin hydrogel supporting multilineage differentiation of stem cells for fabrication of three-dimensional tissue constructs.* Acta biomaterialia, 2015. **11**: p. 233-246.
256. Parker, S.T., et al., *Biocompatible silk printed optical waveguides.* Advanced Materials, 2009. **21**(23): p. 2411-2415.
257. Schacht, K., et al., *Biofabrication of cell-loaded 3D spider silk constructs.* Angewandte Chemie International Edition, 2015. **54**(9): p. 2816-2820.
258. Gregory, D.A., et al., *Reactive Inkjet Printing of Biocompatible Enzyme Powered Silk Micro-Rockets.* Small, 2016. **12**(30): p. 4048-4055.
259. Ling, S., et al., *Printing of stretchable silk membranes for strain measurements.* Lab on a Chip, 2016. **16**(13): p. 2459-2466.
260. Tao, H., et al., *Inkjet printing of regenerated silk fibroin: From printable forms to printable functions.* Advanced materials, 2015. **27**(29): p. 4273-4279.
261. Xu, W., et al., *Rapid prototyping three-dimensional cell/gelatin/fibrinogen constructs for medical regeneration.* Journal of bioactive and compatible polymers, 2007. **22**(4): p. 363-377.
262. Li, S., et al., *Direct fabrication of a hybrid cell/hydrogel construct by a double-nozzle assembling technology.* Journal of bioactive and compatible polymers, 2009. **24**(3): p. 249-265.
263. Zhao, Y., et al., *Three-dimensional printing of Hela cells for cervical tumor model in vitro.* Biofabrication, 2014. **6**(3): p. 035001.
264. Dai, X., et al., *3D bioprinted glioma stem cells for brain tumor model and applications of drug susceptibility.* Biofabrication, 2016. **8**(4): p. 045005.
265. Hughes, C.S., L.M. Postovit, and G.A. Lajoie, *Matrigel: a complex protein mixture required for optimal growth of cell culture.* Proteomics, 2010. **10**(9): p. 1886-1890.
266. Crapo, P.M., T.W. Gilbert, and S.F. Badylak, *An overview of tissue and whole organ decellularization processes.* Biomaterials, 2011. **32**(12): p. 3233-3243.
267. ; Available from: https://www.thermofisher.com/us/en/home/life-science/protein-biology/protein-biology-learning-center/protein-biology-resource-library/pierce-protein-methods/carbodiimide-crosslinker-chemistry.html.
268. Grabarek, Z. and J. Gergely, *Zero-length crosslinking procedure with the use of active esters.* Analytical biochemistry, 1990. **185**(1): p. 131-135.

269. Hwang, Y.-J., J. Granelli, and J. Lyubovitsky, *Effects of zero-length and non-zero-length cross-linking reagents on the optical spectral properties and structures of collagen hydrogels.* ACS applied materials & interfaces, 2011. **4**(1): p. 261-267.
270. Hurley, L.A., et al., *The role of soft tissues in osteogenesis: An experimental study of canine spine fusions.* JBJS, 1959. **41**(7): p. 1243-1266.
271. Gottlow, J., et al., *New attachment formation as the result of controlled tissue regeneration.* Journal of clinical periodontology, 1984. **11**(8): p. 494-503.
272. Villar, C.C. and D.L. Cochran, *Regeneration of periodontal tissues: guided tissue regeneration.* Dental Clinics, 2010. **54**(1): p. 73-92.
273. Retzepi, M. and N. Donos, *Guided bone regeneration: biological principle and therapeutic applications.* Clinical oral implants research, 2010. **21**(6): p. 567-576.
274. Buser, D., C. Dahlin, and R. Schenk, *Guided bone regeneration.* Chicago Quintessence, 1994.
275. Bottino, M.C., et al., *Recent advances in the development of GTR/GBR membranes for periodontal regeneration—a materials perspective.* Dental materials, 2012. **28**(7): p. 703-721.
276. Caballé-Serrano, J., et al., *On the search of the ideal barrier membrane for guided bone regeneration.* Journal of clinical and experimental dentistry, 2018. **10**(5): p. e477.
277. Wang, J., et al., *Biodegradable polymer membranes applied in guided bone/tissue regeneration: a review.* Polymers, 2016. **8**(4): p. 115.
278. Bartee, C.M. and B.K. Bartee, *PTFE composite multi-layer material*. 2010, Google Patents.
279. Williams, D.F., et al., *Implants in surgery*. 1973: Saunders London.
280. Aurer, A. and K. Jorgić-Srdjak, *Membranes for periodontal regeneration.* Acta Stomatologica Croatica, 2005. **39**(1): p. 107-112.
281. Schliephake, H., et al., *Guided bone regeneration around endosseous implants using a resorbable membrane vs a PTFE membrane.* Clinical Oral Implants Research, 2000. **11**(3): p. 230-241.
282. Scantlebury, T.V., *1982-1992: A decade of technology development for guided tissue regeneration.* Journal of periodontology, 1993. **64**: p. 1129-1137.
283. Becker, W. and B.E. Becker, *Periodontal regeneration: A contemporary re-evaluation.* Periodontology 2000, 1999. **19**(1): p. 104-114.
284. Buser, D., et al., *Localized ridge augmentation with autografts and barrier membranes.* Periodontology 2000, 1999. **19**(1): p. 151-163.
285. Trombelli, L., *Periodontal regeneration in gingival recession defects.* Periodontology 2000, 1999. **19**: p. 138-150.
286. Ratka-Krüger, P., E. Neukranz, and P. Raetzke, *Guided tissue regeneration procedure with bioresorbable membranes versus conventional flap surgery in the treatment of infrabony periodontal defects.* Journal of clinical periodontology, 2000. **27**(2): p. 120-127.
287. Gottlow, J., et al., *New attachment formation in the human periodontium by guided tissue regeneration Case reports.* Journal of clinical periodontology, 1986. **13**(6): p. 604-616.
288. Cortellini, P., G.P. Prato, and M.S. Tonetti, *Periodontal regeneration of human intrabony defects with titanium reinforced membranes. A controlled clinical trial.* Journal of Periodontology, 1995. **66**(9): p. 797-803.
289. Murphy, K.G., *Postoperative Healing Complications Associated With Gore-Tex Periodontal Material. Part I. Incidence and Characterization.* International Journal of Periodontics & Restorative Dentistry, 1995. **15**(4).
290. Hardwick, R., B.K. Hayes, and C. Flynn, *Devices for dentoalveolar regeneration: an up-to-date literature review.* Journal of periodontology, 1995. **66**(6): p. 495-505.

291. Rakhmatia, Y.D., et al., *Current barrier membranes: titanium mesh and other membranes for guided bone regeneration in dental applications.* Journal of prosthodontic research, 2013. **57**(1): p. 3-14.
292. Barber, H.D., et al., *Using a dense PTFE membrane without primary closure to achieve bone and tissue regeneration.* Journal of Oral and Maxillofacial Surgery, 2007. **65**(4): p. 748-752.
293. Sheikh, Z., et al., *Protein adsorption capability on polyurethane and modified-polyurethane membrane for periodontal guided tissue regeneration applications.* Materials Science and Engineering: C, 2016. **68**: p. 267-275.
294. Simion, M., et al., *Guided bone regeneration using resorbable and nonresorbable membranes: a comparative histologic study in humans.* International Journal of Oral & Maxillofacial Implants, 1996. **11**(6).
295. Bunyaratavej, P. and H.L. Wang, *Collagen membranes: a review.* Journal of periodontology, 2001. **72**(2): p. 215-229.
296. Patino, M.G., et al., *Collagen as an implantable material in medicine and dentistry.* Journal of Oral Implantology, 2002. **28**(5): p. 220-225.
297. Locci, P., et al., *Phenotype expression of gingival fibroblasts cultured on membranes used in guided tissue regeneration.* Journal of periodontology, 1997. **68**(9): p. 857-863.
298. Wang, H.L., M. Miyauchi, and T. Takata, *Initial attachment of osteoblasts to various guided bone regeneration membranes: an in vitro study.* Journal of periodontal research, 2002. **37**(5): p. 340-344.
299. Blumenthal, N.M., *The use of collagen membranes to guide regeneration of new connective tissue attachment in dogs.* Journal of periodontology, 1988. **59**(12): p. 830-836.
300. Pitaru, S., et al., *Partial regeneration of periodontal tissues using collagen barriers.* Journal of Periodontology, 1988. **59**(6): p. 380-386.
301. Li, S.-T., et al., *A Comparative study of Zimmer BioMend® and BioMend® Extend™ membranes made at two different manufacturing facilities.* Zimmer Dental White Paper, 2013: p. 1-5.
302. Shieh, A.T., et al., *Development and clinical evaluation of a root coverage procedure using a collagen barrier membrane.* Journal of periodontology, 1997. **68**(8): p. 770-778.
303. Wang, H.L., et al., *Evaluation of an absorbable collagen membrane in treating Class II furcation defects.* Journal of periodontology, 1994. **65**(11): p. 1029-1036.
304. Yukna, C. and R. Yukna, *Multi-center evaluation of bioabsorbable collagen membrane for guided tissue regeneration in human Class II furcations.* Journal of periodontology, 1996. **67**(7): p. 650-657.
305. Tanner, M.G., C.W. Solt, and S. Vuddhakanok, *An Evaluation of New Attachment Formation Using a Microfibhllar Collagen Barrier.* Journal of Periodontology, 1988. **59**(8): p. 524-530.
306. Paul, B.F., et al., *Use of a collagen barrier to enhance healing in human periodontal furcation defects.* International Journal of Periodontics & Restorative Dentistry, 1992. **12**(2).
307. Kuo, S.M., et al., *Guided tissue regeneration for using a chitosan membrane: an experimental study in rats.* Journal of Biomedical Materials Research Part A: An Official Journal of The Society for Biomaterials, The Japanese Society for Biomaterials, and The Australian Society for Biomaterials and the Korean Society for Biomaterials, 2006. **76**(2): p. 408-415.
308. Kim, H.W., J.H. Song, and H.E. Kim, *Nanofiber generation of gelatin–hydroxyapatite biomimetics for guided tissue regeneration.* Advanced functional materials, 2005. **15**(12): p. 1988-1994.

309. Ling, L.J., et al., *The influence of membrane exposure on the outcomes of guided tissue regeneration: clinical and microbiological aspects.* Journal of periodontal research, 2003. **38**(1): p. 57-63.
310. Garrett, S., M. Martin, and J. Egelberg, *Treatment of periodontal furcation defects Coronally positioned flaps versus dura mater membranes in class II defects.* Journal of clinical periodontology, 1990. **17**(3): p. 179-185.
311. Yukna, R.A., *Clinical human comparison of expanded polytetrafluoroethylene barrier membrane and freeze-dried dura mater allografts for guided tissue regeneration of lost periodontal support. I. Mandibular molar Class II furcations.* Journal of periodontology, 1992. **63**(5): p. 431-442.
312. Scott, T.A., et al., *Comparison of bioabsorbable laminar bone membrane and non-resorbable ePTFE membrane in mandibular furcations.* Journal of periodontology, 1997. **68**(7): p. 679-686.
313. Von Arx, T., et al., *Evaluation of a prototype trilayer membrane (PTLM) for lateral ridge augmentation: an experimental study in the canine mandible.* International journal of oral and maxillofacial surgery, 2002. **31**(2): p. 190-199.
314. Simion, M., et al., *Treatment of dehiscences and fenestrations around dental implants using resorbable and nonresorbable membranes associated with bone autografts: a comparative clinical study.* International Journal of Oral & Maxillofacial Implants, 1997. **12**(2).
315. Lorenzoni, M., et al., *Treatment of peri-implant defects with guided bone regeneration: a comparative clinical study with various membranes and bone grafts.* International Journal of Oral & Maxillofacial Implants, 1998. **13**(5).
316. Nair, L.S. and C.T. Laurencin, *Biodegradable polymers as biomaterials.* Progress in polymer science, 2007. **32**(8-9): p. 762-798.
317. Haidar, Z.S., *Bio-inspired/-functional colloidal core-shell polymeric-based nanosystems: Technology promise in tissue engineering, bioimaging and nanomedicine.* Polymers, 2010. **2**(3): p. 323-352.
318. Donos, N., L. Kostopoulos, and T. Karring, *Alveolar ridge augmentation using a resorbable copolymer membrane and autogenous bone grafts.* Clinical Oral Implants Research, 2002. **13**(2): p. 203-213.
319. Stavropoulos, F., et al., *A comparative study of barrier membranes as graft protectors in the treatment of localized bone defects: An experimental study in a canine model.* Clinical oral implants research, 2004. **15**(4): p. 435-442.
320. Lundgren, D., T. Mathisen, and J. Gottlow, *The development of a bioresorbable barrier for guided tissue regeneration.* Swed Dent J, 1994. **86**: p. 741-756.
321. Tengan, K.S., *Prospective, comparative assessment of alveolar ridge preservation using Guidor® Easy-Graft® Classic in atrumatic extraction socket.* 2017.
322. Shim, J.-H., et al., *Efficacy of rhBMP-2 loaded PCL/PLGA/β-TCP guided bone regeneration membrane fabricated by 3D printing technology for reconstruction of calvaria defects in rabbit.* Biomedical materials, 2014. **9**(6): p. 065006.
323. Won, J., et al., *Evaluation of 3D printed PCL/PLGA/β-TCP versus collagen membranes for guided bone regeneration in a beagle implant model.* Biomedical Materials, 2016. **11**(5): p. 055013.
324. Wadhawan, A., T.M. Gowda, and D.S. Mehta, *Gore-tex® versus resolut adapt® GTR membranes with perioglas® in periodontal regeneration.* Contemporary clinical dentistry, 2012. **3**(4): p. 406.
325. Labate, G.D.U. and G. Catapano, *Membranes for Regenerative Medicine in Clinical Applications.* Biomedical Membranes And (Bio) artificial Organs, 2017. **2**: p. 263.

326. Haghighat, A., et al., *Histologic, Histomorphometric, and Osteogenesis Comparative Study of a Novel Fabricated Nanocomposite Membrane Versus Cytoplast Membrane.* Journal of Oral and Maxillofacial Surgery, 2019.
327. Li, S.-T., et al., *A Comparative Study of a New Porcine Collagen Membrane to Bio-Gide®.* Science, Technology, Innovation, 2015: p. 1-5.
328. Wu, S.-Y., et al., *Comparison of clinical outcomes following guided tissue regeneration treatment with a polylactic acid barrier or a collagen membrane.* International Journal of Periodontics & Restorative Dentistry, 2010. **30**(2).
329. Sheikh, Z., et al., *Collagen based barrier membranes for periodontal guided bone regeneration applications.* Odontology, 2017. **105**(1): p. 1-12.
330. Seciu, A.-M., et al., *RIBOFLAVIN CROSS-LINKING OF COLLAGEN POROUS SCAFFOLDS FOR PERIODONTAL REGENERATION.* Studia Universitatis Vasile Goldis Seria Stiintele Vietii (Life Sciences Series), 2016. **26**(2).
331. Gentile, P., et al., *Polymeric membranes for guided bone regeneration.* Biotechnology Journal, 2011. **6**(10): p. 1187-1197.
332. Gielkens, P.F., et al., *Vivosorb®, Bio-Gide®, and Gore-Tex® as barrier membranes in rat mandibular defects: an evaluation by microradiography and micro-CT.* Clinical oral implants research, 2008. **19**(5): p. 516-521.
333. Lee, W.B. and M.J. Mannis, *Historical Concepts of Ocular Surface Disease*, in *Ocular Surface Disease: Cornea, Conjunctiva and Tear Film*. 2013, Elsevier Inc. p. 3-10.
334. Dartt, D.A. and M.D.P. Willcox, *Complexity of the tear film: Importance in homeostasis and dysfunction during disease.* Experimental eye research, 2013. **117**: p. 1-3.
335. Schrader, S., et al., *Tissue engineering for conjunctival reconstruction: established methods and future outlooks.* Curr Eye Res, 2009. **34**(11): p. 913-24.
336. Gregory, D.G., *The ophthalmologic management of acute Stevens-Johnson syndrome.* Ocul Surf, 2008. **6**(2): p. 87-95.
337. Stefano Barabino, M., 1 Maurizio Rolando, MD,1 Giorgio Bentivoglio, MD,2 Cristina Mingari, MD,3 Sabrina Zanardi, PhD,4 Rosa Bellomo, PhD,5 Giovanni Calabria, MD,PhD, *Role of Amniotic Membrane Transplantation for Conjunctival Reconstruction in Ocular-Cicatricial Pemphigoid.* ophthalmology, 2003(110): p. 110:474–480.
338. Meller, D., et al., *Amniotic membrane transplantation for acute chemical or thermal burns.* Ophthalmology. **107**(5): p. 980-989.
339. Li, M., et al., *Comparison of conjunctival autograft transplantation and amniotic membrane transplantation for pterygium: a meta-analysis.* Graefe's Archive for Clinical and Experimental Ophthalmology, 2012. **250**(3): p. 375-381.
340. Lim, L.-A., M.C. Madigan, and R.M. Conway, *Conjunctival melanoma: a review of conceptual and treatment advances.* Clinical Ophthalmology (Auckland, N.Z.), 2013. **7**: p. 521-531.
341. Lee, S.Y., et al., *In vivo conjunctival reconstruction using modified PLGA grafts for decreased scar formation and contraction.* Biomaterials, 2003. **24**(27): p. 5049-59.
342. Hsu, W.C., et al., *Inhibition of conjunctival scarring and contraction by a porous collagen-glycosaminoglycan implant.* Invest Ophthalmol Vis Sci, 2000. **41**(9): p. 2404-11.
343. Huang, D., et al., *Conjunctival structural and functional reconstruction using acellular bovine pericardium graft (Normal GEN(R)) in rabbits.* Graefes Arch Clin Exp Ophthalmol, 2016. **254**(4): p. 773-83.
344. Zhou, H., et al., *Vitrified collagen-based conjunctival equivalent for ocular surface reconstruction.* Biomaterials, 2014. **35**(26): p. 7398-406.
345. Gipson, I.K., *Goblet cells of the conjunctiva: A review of recent findings.* Prog Retin Eye Res, 2016. **54**: p. 49-63.

346. Barabino, S., et al., *Role of amniotic membrane transplantation for conjunctival reconstruction in ocular-cicatricial pemphigoid.* Ophthalmology, 2003. **110**(3): p. 474-80.
347. Kheirkhah, A., et al., *A Combined Approach of Amniotic Membrane and Oral Mucosa Transplantation for Fornix Reconstruction in Severe Symblepharon.* Cornea, 2013. **32**(2): p. 155-160.
348. Clearfield, E., et al., *Conjunctival autograft for pterygium.* Cochrane Database Syst Rev, 2016. **2**: p. Cd011349.
349. Morgan, P.V., J.D. Suh, and C.J. Hwang, *Nasal Floor Mucosa: New Donor Site for Mucous Membrane Grafts.* Ophthalmic Plastic and Reconstructive Surgery, 2016. **32**(3): p. 174-177.
350. Nakamura, T., et al., *Transplantation of cultivated autologous oral mucosal epithelial cells in patients with severe ocular surface disorders.* British Journal of Ophthalmology, 2004. **88**(10): p. 1280-1284.
351. Morgan, P.V., J.D. Suh, and C.J. Hwang, *Nasal Floor Mucosa: New Donor Site for Mucous Membrane Grafts.* Ophthalmic Plastic & Reconstructive Surgery, 2016. **32**(3): p. 174-177.
352. Chintan Malhotra, A.K.J., *Human amniotic membrane transplantation: Different modalities of its use in ophthalmology.* World J Transplant 2014: p. 4(2): 111-121.
353. Manuelpillai, U., et al., *Amniotic membrane and amniotic cells: potential therapeutic tools to combat tissue inflammation and fibrosis?* Placenta, 2011. **32 Suppl 4**: p. S320-5.
354. Jingbo Liu1, Hosam Sheha1,3, Yao Fu1,4, Lingyi Liang5, and Scheffer CG Tseng, *Update on amniotic membrane transplantation.* Expert Rev Ophthalmol 2010: p. 5(5): 645–661.
355. Tseng, S.C., *HC-HA/PTX3 Purified From Amniotic Membrane as Novel Regenerative Matrix: Insight Into Relationship Between Inflammation and Regeneration.* Invest Ophthalmol Vis Sci, 2016. **57**(5): p. ORSFh1-8.
356. Liu, T., et al., *Amniotic membrane traps and induces apoptosis of inflammatory cells in ocular surface chemical burn.* Mol Vis, 2012. **18**: p. 2137-46.
357. Muqit, M.M., R.B. Ellingham, and C. Daniel, *Technique of amniotic membrane transplant dressing in the management of acute Stevens-Johnson syndrome.* Br J Ophthalmol, 2007. **91**(11): p. 1536.
358. Tamhane, A., et al., *Evaluation of amniotic membrane transplantation as an adjunct to medical therapy as compared with medical therapy alone in acute ocular burns.* Ophthalmology, 2005. **112**(11): p. 1963-9.
359. Barton, K., et al., *Glaucoma filtration surgery using amniotic membrane transplantation.* Invest Ophthalmol Vis Sci, 2001. **42**(8): p. 1762-8.
360. Lee, J.W., et al., *Tissue response to implanted Ahmed glaucoma valve with adjunctive amniotic membrane in rabbit eyes.* Ophthalmic Res, 2014. **51**(3): p. 129-39.
361. Lu, R., et al., *Conjunctival Reconstruction with Progenitor Cell-Derived Autologous Epidermal Sheets in Rhesus Monkey.* PLOS ONE, 2011. **6**(11): p. e25713.
362. Lopez-Garcia, J.S., et al., *Amniotic membrane transplantation in acute toxic epidermal necrolysis: histopathologic changes and ocular surface features after 1-year follow-up.* Eur J Ophthalmol, 2014. **24**(5): p. 667-75.
363. Shammas, M.C., et al., *Management of acute Stevens-Johnson syndrome and toxic epidermal necrolysis utilizing amniotic membrane and topical corticosteroids.* Am J Ophthalmol, 2010. **149**(2): p. 203-213.e2.
364. Shay, E., et al., *Amniotic membrane transplantation as a new therapy for the acute ocular manifestations of Stevens-Johnson syndrome and toxic epidermal necrolysis.* Surv Ophthalmol, 2009. **54**(6): p. 686-96.

365. Yang, S., X. Yang, and G. Cao, *Conjunctiva reconstruction by induced differentiation of human amniotic epithelial cells.* Genet. Mol. Res, 2015. **14**(4): p. 13823-13834.
366. Marangon, F.B., et al., *Incidence of Microbial Infection After Amniotic Membrane Transplantation.* Cornea, 2004. **23**(3): p. 264-269.
367. Lee, J.E., et al., *Corneal tattooing to mask subsequent opacification after amniotic membrane grafting for stromal corneal ulcer.* Acta Ophthalmol Scand, 2006. **84**(5): p. 696-8.
368. S.P. Yang1, X.Z.Y.a.G.P.C., *Conjunctiva reconstruction by induced differentiation of human amniotic epithelial cellsS.P. Yang1, X.Z. Yang1 and G.P. Ca.* brGenetics and Molecular Research 14 (4): 13823-13834 2015: p. 14 (4): 13823-13834
369. Hsu, W.-C., et al., *Inhibition of conjunctival scarring and contraction by a porous collagen-glycosaminoglycan implant.* Investigative ophthalmology & visual science, 2000. **41**(9): p. 2404-2411.
370. Yannas, I., et al., *Design of an artificial skin. II. Control of chemical composition.* Journal of biomedical materials research, 1980. **14**(2): p. 107-132.
371. Yannas, I., et al., *Synthesis and characterization of a model extracellular matrix that induces partial regeneration of adult mammalian skin.* Proceedings of the National Academy of Sciences, 1989. **86**(3): p. 933-937.
372. Lee, S.Y., et al., *In vivo conjunctival reconstruction using modified PLGA grafts for decreased scar formation and contraction.* Biomaterials, 2003. **24**(27): p. 5049-5059.
373. Zhou, H., et al., *Vitrified collagen-based conjunctival equivalent for ocular surface reconstruction.* Biomaterials, 2014. **35**(26): p. 7398-7406.
374. Takezawa, T., et al., *Collagen vitrigel: a novel scaffold that can facilitate a three-dimensional culture for reconstructing organoids.* Cell transplantation, 2004. **13**(4): p. 463-474.
375. McIntosh Ambrose, W., et al., *Collagen Vitrigel membranes for the in vitro reconstruction of separate corneal epithelial, stromal, and endothelial cell layers.* Journal of Biomedical Materials Research Part B: Applied Biomaterials: An Official Journal of The Society for Biomaterials, The Japanese Society for Biomaterials, and The Australian Society for Biomaterials and the Korean Society for Biomaterials, 2009. **90**(2): p. 818-831.
376. Eidet, J.R., D.A. Dartt, and T.P. Utheim, *Concise Review: Comparison of Culture Membranes Used for Tissue Engineered Conjunctival Epithelial Equivalents.* J Funct Biomater, 2015. **6**(4): p. 1064-84.
377. Yan, L.-P., et al., *Current concepts and challenges in osteochondral tissue engineering and regenerative medicine.* ACS Biomaterials Science & Engineering, 2015. **1**(4): p. 183-200.
378. Dhollander, A.A., et al., *The use of scaffolds in the treatment of osteochondral lesions in the knee: current concepts and future trends.* The journal of knee surgery, 2012. **25**(03): p. 179-186.
379. Martin, I., et al., *Osteochondral tissue engineering.* Journal of biomechanics, 2007. **40**(4): p. 750-765.
380. Temenoff, J.S. and A.G. Mikos, *Tissue engineering for regeneration of articular cartilage.* Biomaterials, 2000. **21**(5): p. 431-440.
381. McNickle, A.G., M.T. Provencher, and B.J. Cole, *Overview of existing cartilage repair technology.* Sports medicine and arthroscopy review, 2008. **16**(4): p. 196-201.
382. Kosy, J.D., et al., *The use of radiofrequency energy for arthroscopic chondroplasty in the knee.* Arthroscopy: The Journal of Arthroscopic & Related Surgery, 2011. **27**(5): p. 695-703.

383. Cetik, O., et al., *Risk of osteonecrosis of the femoral condyle after arthroscopic chondroplasty using radiofrequency: a prospective clinical series.* Knee Surgery, Sports Traumatology, Arthroscopy, 2009. **17**(1): p. 24-29.
384. Aaron, R.K., et al., *Arthroscopic debridement for osteoarthritis of the knee.* JBJS, 2006. **88**(5): p. 936-943.
385. Sauerland, S., et al., *Letter regarding" The effects of arthroscopic joint debridement in the knee osteoarthritis: results of a meta-analysis".* Knee surgery, sports traumatology, arthroscopy, 2015. **23**(4): p. 1259.
386. Mithoefer, K., et al., *Clinical efficacy of the microfracture technique for articular cartilage repair in the knee: an evidence-based systematic analysis.* The American journal of sports medicine, 2009. **37**(10): p. 2053-2063.
387. Gracitelli, G.C., et al., *Surgical interventions (microfracture, drilling, mosaicplasty, and allograft transplantation) for treating isolated cartilage defects of the knee in adults.* The Cochrane Library, 2016.
388. Bert, J.M., *Abandoning microfracture of the knee: Has the time come?* Arthroscopy: The Journal of Arthroscopic & Related Surgery, 2015. **31**(3): p. 501-505.
389. Farr, J., et al., *Clinical cartilage restoration: evolution and overview.* Clinical Orthopaedics and Related Research®, 2011. **469**(10): p. 2696-2705.
390. Krych, A.J., et al., *Return to athletic activity after osteochondral allograft transplantation in the knee.* The American journal of sports medicine, 2012. **40**(5): p. 1053-1059.
391. Bentley, G., et al., *A prospective, randomised comparison of autologous chondrocyte implantation versus mosaicplasty for osteochondral defects in the knee.* Bone & Joint Journal, 2003. **85**(2): p. 223-230.
392. Horas, U., et al., *Autologous chondrocyte implantation and osteochondral cylinder transplantation in cartilage repair of the knee joint: a prospective, comparative trial.* JBJS, 2003. **85**(2): p. 185-192.
393. Vavken, P. and D. Samartzis, *Effectiveness of autologous chondrocyte implantation in cartilage repair of the knee: a systematic review of controlled trials.* Osteoarthritis and Cartilage, 2010. **18**(6): p. 857-863.
394. Intzoglou, K., et al., *Synthetic or autologous plugs for the repair of osteochondral rabbit knee defects: a comparative study.* Journal of Experimental and Applied Animal Sciences, 2014. **1**(2): p. 229-240.
395. Bugbee, W., M. Cavallo, and S. Giannini, *Osteochondral allograft transplantation in the knee.* The journal of knee surgery, 2012. **25**(02): p. 109-116.
396. Chahal, J., et al., *Outcomes of osteochondral allograft transplantation in the knee.* Arthroscopy: The Journal of Arthroscopic & Related Surgery, 2013. **29**(3): p. 575-588.
397. Brittberg, M., et al., *Treatment of deep cartilage defects in the knee with autologous chondrocyte transplantation.* New england journal of medicine, 1994. **331**(14): p. 889-895.
398. Basad, E., et al., *Matrix-induced autologous chondrocyte implantation versus microfracture in the treatment of cartilage defects of the knee: a 2-year randomised study.* Knee surgery, sports traumatology, arthroscopy, 2010. **18**(4): p. 519-527.
399. Peterson, L., et al., *Autologous chondrocyte implantation: a long-term follow-up.* The American journal of sports medicine, 2010. **38**(6): p. 1117-1124.
400. Vasiliadis, H.S., et al., *Autologous chondrocyte implantation in cartilage lesions of the knee: long-term evaluation with magnetic resonance imaging and delayed gadolinium-enhanced magnetic resonance imaging technique.* The American journal of sports medicine, 2010. **38**(5): p. 943-949.
401. Harris, J.D., et al., *Autologous chondrocyte implantation: a systematic review.* JBJS, 2010. **92**(12): p. 2220-2233.

402. Mistry, H., et al., *Autologous chondrocyte implantation in the knee: systematic review and economic evaluation.* 2017.
403. Kuroda, T., et al., *Therapeutic strategy of third-generation autologous chondrocyte implantation for osteoarthritis.* Upsala journal of medical sciences, 2011. **116**(2): p. 107-114.
404. Kon, E., et al., *Scaffold-based cartilage treatments: with or without cells? A systematic review of preclinical and clinical evidence.* Arthroscopy: The Journal of Arthroscopic & Related Surgery, 2015. **31**(4): p. 767-775.
405. Stoddart, M.J., et al., *Cells and biomaterials in cartilage tissue engineering.* 2009.
406. Longley, R., A. Ferreira, and P. Gentile, *Recent approaches to the manufacturing of biomimetic multi-phasic scaffolds for osteochondral regeneration.* International journal of molecular sciences, 2018. **19**(6): p. 1755.
407. Benders, K.E., et al., *Extracellular matrix scaffolds for cartilage and bone regeneration.* Trends in biotechnology, 2013. **31**(3): p. 169-176.
408. Gillette, B.M., et al., *Engineering extracellular matrix structure in 3D multiphase tissues.* Biomaterials, 2011. **32**(32): p. 8067-8076.
409. Kim, B.-S., et al., *Design of artificial extracellular matrices for tissue engineering.* Progress in Polymer Science, 2011. **36**(2): p. 238-268.
410. Fuentes-Mera, L., et al., *Therapeutic Potential of Articular Cartilage Regeneration using Tissue Engineering Based on Multiphase Designs*, in *Cartilage Tissue Engineering and Regeneration Techniques*. 2019, IntechOpen.
411. Castro, N.J., S.A. Hacking, and L.G. Zhang, *Recent progress in interfacial tissue engineering approaches for osteochondral defects.* Annals of biomedical engineering, 2012. **40**(8): p. 1628-1640.
412. Swieszkowski, W., et al., *Repair and regeneration of osteochondral defects in the articular joints.* Biomolecular engineering, 2007. **24**(5): p. 489-495.
413. Yousefi, A.M., et al., *Current strategies in multiphasic scaffold design for osteochondral tissue engineering: a review.* Journal of biomedical materials research Part A, 2015. **103**(7): p. 2460-2481.
414. Grayson, W.L., et al., *Spatial regulation of human mesenchymal stem cell differentiation in engineered osteochondral constructs: effects of pre-differentiation, soluble factors and medium perfusion.* Osteoarthritis and cartilage, 2010. **18**(5): p. 714-723.
415. Lee, M. and B.M. Wu, *Recent advances in 3D printing of tissue engineering scaffolds*, in *Computer-Aided Tissue Engineering*. 2012, Springer. p. 257-267.
416. Mauck, R.L., et al., *Functional tissue engineering of articular cartilage through dynamic loading of chondrocyte-seeded agarose gels.* Journal of biomechanical engineering, 2000. **122**(3): p. 252-260.
417. Harley, B.A., et al., *Design of a multiphase osteochondral scaffold III: Fabrication of layered scaffolds with continuous interfaces.* Journal of Biomedical Materials Research Part A: An Official Journal of The Society for Biomaterials, The Japanese Society for Biomaterials, and The Australian Society for Biomaterials and the Korean Society for Biomaterials, 2010. **92**(3): p. 1078-1093.
418. Harley, B.A., et al., *Design of a multiphase osteochondral scaffold. II. Fabrication of a mineralized collagen–glycosaminoglycan scaffold.* Journal of Biomedical Materials Research Part A: An Official Journal of The Society for Biomaterials, The Japanese Society for Biomaterials, and The Australian Society for Biomaterials and the Korean Society for Biomaterials, 2010. **92**(3): p. 1066-1077.
419. Wang, Y., et al., *Fabrication and in vitro evaluation of an articular cartilage extracellular matrix-hydroxyapatite bilayered scaffold with low permeability for interface tissue engineering.* Biomedical engineering online, 2014. **13**(1): p. 80.

420. Miyagi, S., et al., *Construction of an osteochondral-like tissue graft combining β-tricalcium phosphate block and scaffold-free mesenchymal stem cell sheet.* Journal of Orthopaedic Science, 2013. **18**(3): p. 471-477.
421. Niyama, K., et al., *Construction of osteochondral-like tissue graft combining β-tricalcium phosphate block and scaffold-free centrifuged chondrocyte cell sheet.* Journal of Orthopaedic Science, 2011. **16**(5): p. 613-621.
422. TUAN, H.S., *Tissue engineering of an osteochondral transplant by using a cell/scaffold construct*. 2009.
423. Jeon, J.E., et al., *Multiphasic construct studied in an ectopic osteochondral defect model.* Journal of The Royal Society Interface, 2014. **11**(95): p. 20140184.
424. Liu, X.-g. and H.-k. Jiang, *Preparation of an osteochondral composite with mesenchymal stem cells as the single-cell source in a double-chamber bioreactor.* Biotechnology letters, 2013. **35**(10): p. 1645-1653.
425. Shim, J.-H., et al., *Bioprinting of a mechanically enhanced three-dimensional dual cell-laden construct for osteochondral tissue engineering using a multi-head tissue/organ building system.* Journal of Micromechanics and Microengineering, 2012. **22**(8): p. 085014.
426. Nguyen, L.H., et al., *Engineering articular cartilage with spatially-varying matrix composition and mechanical properties from a single stem cell population using a multi-layered hydrogel.* Biomaterials, 2011. **32**(29): p. 6946-6952.
427. Chen, J., et al., *Simultaneous regeneration of articular cartilage and subchondral bone in vivo using MSCs induced by a spatially controlled gene delivery system in bilayered integrated scaffolds.* Biomaterials, 2011. **32**(21): p. 4793-4805.
428. Collins, S.F., *Bioprinting Is Changing Regenerative Medicine Forever.* Stem cells and development, 2014. **23**(S1): p. 79-82.
429. B Starly , R.S., *3D Bioprinting and Nanotechnology in Tissue Engineering and Regenerative Medicine.* , in *Three-dimensional (3D) Bioprinting*, J.F. L Zhang, K Leong , MA Waltham, Editor. 2015, Academic Press.
430. Sarker, B., et al., *Evaluation of fibroblasts adhesion and proliferation on alginate-gelatin crosslinked hydrogel.* PLoS One, 2014. **9**(9): p. e107952.
431. Chillari, S., S. Guccione, and G. Muscato. *An experimental comparison between several pneumatic position control methods*. in *Proceedings of the 40th IEEE Conference on Decision and Control (Cat. No. 01CH37228)*. 2001. IEEE.
432. Winter, H., *Can the gel point of a cross-linking polymer be detected by the G'–G "crossover?* Polymer Engineering & Science, 1987. **27**(22): p. 1698-1702.
433. Sam, G. and B.R. Pillai, *Evolution of Barrier Membranes in Periodontal Regeneration-"Are the third Generation Membranes really here?".* J Clin Diagn Res, 2014. **8**(12): p. ZE14-7.
434. Bottino, M.C. and V. Thomas, *Membranes for Periodontal Regeneration--A Materials Perspective.* Front Oral Biol, 2015. **17**: p. 90-100.
435. Kim, H.N., et al., *Nanotopography-guided tissue engineering and regenerative medicine.* Advanced drug delivery reviews, 2013. **65**(4): p. 536-558.
436. Hutmacher, D., M.B. Hürzeler, and H. Schliephake, *A review of material properties of biodegradable and bioresorbable polymers and devices for GTR and GBR applications.* International Journal of Oral & Maxillofacial Implants, 1996. **11**(5).
437. Needleman, I.G., et al., *Guided tissue regeneration for periodontal infra-bony defects.* Cochrane Database Syst Rev, 2006(2): p. CD001724.
438. Rispoli, L., et al., *Surgery Guidelines for Barrier Membranes in Guided Bone Regeneration (GBR).* Journal of Otolaryngology and Rhinology, 2015. **1**: p. 008.

439. Dimitriou, R., et al., *The role of barrier membranes for guided bone regeneration and restoration of large bone defects: current experimental and clinical evidence.* BMC medicine, 2012. **10**(1): p. 81.
440. Matsuo, A., et al., *Clinical application of a custom-made bioresorbable raw particulate hydroxyapatite/poly-L-lactide mesh tray for mandibular reconstruction.* Odontology, 2010. **98**(1): p. 85-88.
441. Ducheyne, P., et al., *Influence of a functional dynamic loading on bone ingrowth into surface pores of orthopedic implants.* Journal of biomedical materials research, 1977. **11**(6): p. 811-838.
442. Heck, D., et al., *The effect of load alteration on the biological and biomechanical performance of a titanium fiber-metal segmental prosthesis.* J Bone Joint Surg Am, 1986. **68**(1): p. 118-126.
443. Amano, Y., et al., *Evaluation of a poly-l-lactic acid membrane and membrane fixing pin for guided tissue regeneration on bone defects in dogs.* Oral Surgery, Oral Medicine, Oral Pathology, Oral Radiology, and Endodontology, 2004. **97**(2): p. 155-163.
444. O'Brien, F.J., et al., *The effect of pore size on cell adhesion in collagen-GAG scaffolds.* Biomaterials, 2005. **26**(4): p. 433-441.
445. Murphy, C.M., M.G. Haugh, and F.J. O'Brien, *The effect of mean pore size on cell attachment, proliferation and migration in collagen–glycosaminoglycan scaffolds for bone tissue engineering.* Biomaterials, 2010. **31**(3): p. 461-466.
446. Grinnell, F., *Cellular adhesiveness and extracellular substrata.* International review of cytology, 1978. **53**: p. 65-144.
447. Machtei, E.E., et al., *Clinical, microbiological, and histological factors which influence the success of regenerative periodontal therapy.* Journal of periodontology, 1994. **65**(2): p. 154-161.
448. Wikesjö, U., et al., *Dynamics of wound healing in periodontal regenerative therapy.* Journal of the California Dental Association, 1995. **23**(12): p. 30-35.
449. Takata, T., H.L. Wang, and M. Miyauchi, *Attachment, proliferation and differentiation of periodontal ligament cells on various guided tissue regeneration membranes.* Journal of periodontal research, 2001. **36**(5): p. 322-327.
450. Marouf, H.A. and H.M. El-Guindi, *Efficacy of high-density versus semipermeable PTFE membranes in an elderly experimental model.* Oral Surgery, Oral Medicine, Oral Pathology, Oral Radiology, and Endodontology, 2000. **89**(2): p. 164-170.
451. Dimitriou, R., et al., *The role of barrier membranes for guided bone regeneration and restoration of large bone defects: current experimental and clinical evidence.* BMC medicine, 2012. **10**(1): p. 1.
452. Sam, G. and B.R.M. Pillai, *Evolution of Barrier Membranes in Periodontal Regeneration-"Are the third Generation Membranes really here?* Journal of clinical and diagnostic research: JCDR, 2014. **8**(12): p. ZE14.
453. Chiara, G., et al., *Nanostructured biomaterials for tissue engineered bone tissue reconstruction.* International journal of molecular sciences, 2012. **13**(1): p. 737-757.
454. Daamen, W.F., et al., *Elastin as a biomaterial for tissue engineering.* Biomaterials, 2007. **28**(30): p. 4378-4398.
455. Burdick, J.A. and G.D. Prestwich, *Hyaluronic acid hydrogels for biomedical applications.* Advanced materials, 2011. **23**(12).
456. Omidi, M., A. Yadegari, and L. Tayebi, *Wound dressing application of pH-sensitive carbon dots/chitosan hydrogel.* RSC Advances, 2017. **7**(18): p. 10638-10649.
457. Rasoulianboroujeni, M., S. Pitcher, and L. Tayebi, *Fabrication of gradient scaffolds for bone and dental tissue engineering.* Dental Materials, 2016. **32**: p. e47-e48.
458. Jacobs, P.F., *Rapid prototyping & manufacturing: fundamentals of stereolithography*. 1992: Society of Manufacturing Engineers.

459. Agarwala, M., et al., *Direct selective laser sintering of metals.* Rapid Prototyping Journal, 1995. **1**(1): p. 26-36.
460. Yeong, W.-Y., et al., *Rapid prototyping in tissue engineering: challenges and potential.* TRENDS in Biotechnology, 2004. **22**(12): p. 643-652.
461. Boland, T. and V. Mironov, *How to Define Biofabrication? Review of the Book Biofabrication: Micro-and Nano-Fabrication, Printing, Patterning, and Assemblies, Edited by Gabor Forgacs and Wei Sun (William Andrew, 2013, 265 Pages).* 3D Printing and Additive Manufacturing, 2014. **1**(1): p. 52-54.
462. Melchels, F.P., et al., *Additive manufacturing of tissues and organs.* Progress in Polymer Science, 2012. **37**(8): p. 1079-1104.
463. Skardal, A. and A. Atala, *Biomaterials for Integration with 3-D Bioprinting.* Annals of biomedical engineering, 2014: p. 1-17.
464. Skardal, A., et al., *Bioprinted amniotic fluid-derived stem cells accelerate healing of large skin wounds.* Stem cells translational medicine, 2012. **1**(11): p. 792-802.
465. Seol, Y.-J., et al., *Bioprinting technology and its applications.* European Journal of Cardio-Thoracic Surgery, 2014: p. ezu148.
466. Binder, K.W., et al., *In situ bioprinting of the skin for burns.* Journal of the American College of Surgeons, 2010. **211**(3): p. 7.
467. Xu, T., et al. *Bio-printing of living organized tissues using an inkjet technology*. in *NIP & Digital Fabrication Conference*. 2006. Society for Imaging Science and Technology.
468. Xu, T., et al., *Complex heterogeneous tissue constructs containing multiple cell types prepared by inkjet printing technology.* Biomaterials, 2013. **34**(1): p. 130-139.
469. Mironov, V., V. Kasyanov, and R.R. Markwald, *Organ printing: from bioprinter to organ biofabrication line.* Current opinion in biotechnology, 2011. **22**(5): p. 667-673.
470. Hoffman, A.S., *Hydrogels for biomedical applications.* Advanced drug delivery reviews, 2012. **64**: p. 18-23.
471. *Biomaterials for Oral and Dental Tissue Engineering*. 1st Edition ed. 2017: Elsevier-Woodhead Publishing. 562.
472. Shabafrooz, V., et al., *The effect of hyaluronic acid on biofunctionality of gelatin–collagen intestine tissue engineering scaffolds.* Journal of Biomedical Materials Research Part A, 2014. **102**(9): p. 3130-3139.
473. Moharamzadeh, K., et al., *Development, optimization and characterization of a full-thickness tissue engineered human oral mucosal model for biological assessment of dental biomaterials.* Journal of Materials Science: Materials in Medicine, 2008. **19**(4): p. 1793-1801.
474. Rheinwald, J.G. and H. Green, *Formation of a keratinizing epithelium in culture by a cloned cell line derived from a teratoma.* Cell, 1975. **6**(3): p. 317-330.
475. Shima Dehghani, M.R., Saeed Heidari Keshel, Hamed GHasemi, Lobat Tayebi, *Gelatin Scaffold for Conjunctival Tissue Engineering*, in *The 6th Annual Meeting of the Iranian Research Association for Vision And Ophthalmology*. March 3-4, 2016, The Iranian Society of Ophthalmology: Tehran, Iran.
476. Ortolani, E., et al., *Mechanical qualification of collagen membranes used in dentistry.* Annali dell'Istituto superiore di sanita, 2015. **51**: p. 229-235.
477. Lee, Y.-J., et al., *The effect of thickness of resorbable bacterial cellulose membrane on guided bone regeneration.* Materials, 2017. **10**(3): p. 320.
478. Coïc, M., et al., *Mechanical properties of collagen membranes used in guided bone regeneration: a comparative study of three models.* Revue de Stomatologie et de Chirurgie Maxillo-faciale, 2010. **111**(5-6): p. 286-290.
479. Buchanan, F.J., *Degradation rate of bioresorbable materials: Prediction and evaluation*. 2008: Elsevier.

480. Grover, C.N., R.E. Cameron, and S.M. Best, *Investigating the morphological, mechanical and degradation properties of scaffolds comprising collagen, gelatin and elastin for use in soft tissue engineering.* Journal of the mechanical behavior of biomedical materials, 2012. **10**: p. 62-74.
481. Hsiue, G.H., et al., *A novel strategy for corneal endothelial reconstruction with a bioengineered cell sheet.* Transplantation, 2006. **81**(3): p. 473-6.
482. Lai, J.Y., K.H. Chen, and G.H. Hsiue, *Tissue-engineered human corneal endothelial cell sheet transplantation in a rabbit model using functional biomaterials.* Transplantation, 2007. **84**(10): p. 1222-32.
483. Yan, J., et al., *Effect of fiber alignment in electrospun scaffolds on keratocytes and corneal epithelial cells behavior.* J Biomed Mater Res A, 2012. **100**(2): p. 527-35.
484. de la Mata, A., et al., *Chitosan-gelatin biopolymers as carrier substrata for limbal epithelial stem cells.* J Mater Sci Mater Med, 2013. **24**(12): p. 2819-29.
485. Sung, B., et al., *Alternating Magnetic Field-Responsive Hybrid Gelatin Microgels for Controlled Drug Release.* J Vis Exp, 2016(108): p. 53680.
486. Li, Y., et al., *Gelatin Microgel Incorporated Poly(ethylene glycol)-Based Bioadhesive with Enhanced Adhesive Property and Bioactivity.* ACS Appl Mater Interfaces, 2016. **8**(19): p. 11980-9.
487. Lai, J.Y., *Corneal stromal cell growth on gelatin/chondroitin sulfate scaffolds modified at different NHS/EDC molar ratios.* Int J Mol Sci, 2013. **14**(1): p. 2036-55.
488. Lai, J.Y., et al., *Nanoscale modification of porous gelatin scaffolds with chondroitin sulfate for corneal stromal tissue engineering.* Int J Nanomedicine, 2012. **7**: p. 1101-14.
489. Djabourov, M., *Architecture of gelatin gels.* Contemporary Physics, 1988. **29**(3): p. 273-297.
490. Picard, J., S. Giraudier, and V. Larreta-Garde, *Controlled remodeling of a protein-polysaccharide mixed gel: examples of gelatin-hyaluronic acid mixtures.* Soft Matter, 2009. **5**(21): p. 4198-4205.
491. Harrington, J.C. and E.R. Morris, *Conformational ordering and gelation of gelatin in mixtures with soluble polysaccharides.* Food Hydrocolloids, 2009. **23**(2): p. 327-336.
492. Winter, H.H. and F. Chambon, *Analysis of linear viscoelasticity of a crosslinking polymer at the gel point.* Journal of rheology, 1986. **30**(2): p. 367-382.
493. Ferry, J.D., *Viscoelastic properties of polymers*. 1980: John Wiley & Sons.
494. Hyun, K., et al., *Large amplitude oscillatory shear as a way to classify the complex fluids.* Journal of Non-Newtonian Fluid Mechanics, 2002. **107**(1): p. 51-65.
495. Rohsenow, W.M., J.P. Hartnett, and Y.I. Cho, *Handbook of heat transfer*. Vol. 3. 1998: McGraw-Hill New York.
496. Hsu, L.C., et al., *Effect of micro-and nanoscale topography on the adhesion of bacterial cells to solid surfaces.* Applied and environmental microbiology, 2013. **79**(8): p. 2703-2712.
497. Sammons, R.L., et al., *Comparison of osteoblast spreading on microstructured dental implant surfaces and cell behaviour in an explant model of osseointegration.* Clinical oral implants research, 2005. **16**(6): p. 657-666.
498. Huang, H.-H., et al., *Effect of surface roughness of ground titanium on initial cell adhesion.* Biomolecular engineering, 2004. **21**(3): p. 93-97.
499. Whitehead, K.A., J. Colligon, and J. Verran, *Retention of microbial cells in substratum surface features of micrometer and sub-micrometer dimensions.* Colloids and Surfaces B: Biointerfaces, 2005. **41**(2): p. 129-138.
500. Wenkel, H., V. Rummelt, and G.O. Naumann, *Long term results after autologous nasal mucosal transplantation in severe mucus deficiency syndromes.* Br J Ophthalmol, 2000. **84**(3): p. 279-84.

501. Nakamura, T., et al., *Phenotypic investigation of human eyes with transplanted autologous cultivated oral mucosal epithelial sheets for severe ocular surface diseases.* Ophthalmology, 2007. **114**(6): p. 1080-8.
502. Burillon, C., et al., *Cultured autologous oral mucosal epithelial cell sheet (CAOMECS) transplantation for the treatment of corneal limbal epithelial stem cell deficiency.* Invest Ophthalmol Vis Sci, 2012. **53**(3): p. 1325-31.
503. Homma, R., et al., *Induction of epithelial progenitors in vitro from mouse embryonic stem cells and application for reconstruction of damaged cornea in mice.* Invest Ophthalmol Vis Sci, 2004. **45**(12): p. 4320-6.
504. Reinshagen, H., et al., *Corneal surface reconstruction using adult mesenchymal stem cells in experimental limbal stem cell deficiency in rabbits.* Acta Ophthalmol, 2011. **89**(8): p. 741-8.
505. Gomes, J.A., et al., *Corneal reconstruction with tissue-engineered cell sheets composed of human immature dental pulp stem cells.* Invest Ophthalmol Vis Sci, 2010. **51**(3): p. 1408-14.
506. Meyer-Blazejewska, E.A., et al., *From hair to cornea: toward the therapeutic use of hair follicle-derived stem cells in the treatment of limbal stem cell deficiency.* Stem Cells, 2011. **29**(1): p. 57-66.
507. Reza, H.M., et al., *Umbilical cord lining stem cells as a novel and promising source for ocular surface regeneration.* Stem Cell Rev, 2011. **7**(4): p. 935-47.
508. Geggel, H.S., J. Friend, and R.A. Thoft, *Conjunctival epithelial wound healing.* Invest Ophthalmol Vis Sci, 1984. **25**(7): p. 860-3.
509. Radford, C.F., et al., *Incidence, presenting features, and diagnosis of cicatrising conjunctivitis in the United Kingdom.* Eye, 2012. **26**(9): p. 1199-1208.
510. Safinaz, M.K., et al., *The use of autologous fibrin as a scaffold for cultivating autologous conjunctiva in the treatment of conjunctival defect.* Cell Tissue Bank, 2014. **15**(4): p. 619-26.
511. Prabhasawat, P. and S.C. Tseng, *Impression cytology study of epithelial phenotype of ocular surface reconstructed by preserved human amniotic membrane.* Arch Ophthalmol, 1997. **115**(11): p. 1360-7.
512. Yang, S.P., X.Z. Yang, and G.P. Cao, *Conjunctiva reconstruction by induced differentiation of human amniotic epithelial cells.* Genet Mol Res, 2015. **14**(4): p. 13823-34.
513. Ahmed Tamer S S, M.O.A.K., Waleed M M., *Role of Amniotic Membrane Transplantation in Symblepharon. .* JOJ Ophthal., 2016. **1**(3): p. 555565.
514. Solomon, A., et al., *Suppression of interleukin 1alpha and interleukin 1beta in human limbal epithelial cells cultured on the amniotic membrane stromal matrix.* Br J Ophthalmol, 2001. **85**(4): p. 444-9.
515. Lee, H.-N., et al., *Human Amniotic Membrane Extracts have Anti-Inflammatory Effects on Damaged Human Corneal Epithelial Cells In Vitro.* Journal of Hard Tissue Biology, 2016. **25**(3): p. 282-287.
516. Lee, S.B., et al., *Suppression of TGF-beta signaling in both normal conjunctival fibroblasts and pterygial body fibroblasts by amniotic membrane.* Curr Eye Res, 2000. **20**(4): p. 325-34.
517. Shimmura, S., et al., *Antiinflammatory Effects of Amniotic Membrane Transplantation in Ocular Surface Disorders.* Cornea, 2001. **20**(4): p. 408-413.
518. Magatti, M., et al., *Human Amniotic Membrane-Derived Mesenchymal and Epithelial Cells Exert Different Effects on Monocyte-Derived Dendritic Cell Differentiation and Function.* Cell Transplant, 2015. **24**(9): p. 1733-52.
519. Kubo, M., et al., *Immunogenicity of human amniotic membrane in experimental xenotransplantation.* Invest Ophthalmol Vis Sci, 2001. **42**(7): p. 1539-46.

520. Rehg, J.E., D. Bush, and J.M. Ward, *The Utility of Immunohistochemistry for the Identification of Hematopoietic and Lymphoid Cells in Normal Tissues and Interpretation of Proliferative and Inflammatory Lesions of Mice and Rats.* Toxicologic Pathology, 2012. **40**(2): p. 345-374.
521. Kheirkhah, A., et al., *Role of conjunctival inflammation in surgical outcome after amniotic membrane transplantation with or without fibrin glue for pterygium.* Cornea, 2008. **27**(1): p. 56-63.
522. Li, W., et al., *Reversal of myofibroblasts by amniotic membrane stromal extract.* J Cell Physiol, 2008. **215**(3): p. 657-64.
523. Tseng, S.C., D.Q. Li, and X. Ma, *Suppression of transforming growth factor-beta isoforms, TGF-beta receptor type II, and myofibroblast differentiation in cultured human corneal and limbal fibroblasts by amniotic membrane matrix.* J Cell Physiol, 1999. **179**(3): p. 325-35.
524. Cooper, L.J., et al., *An investigation into the composition of amniotic membrane used for ocular surface reconstruction.* Cornea, 2005. **24**(6): p. 722-729.
525. Sophia Fox, A.J., A. Bedi, and S.A. Rodeo, *The basic science of articular cartilage: structure, composition, and function.* Sports health, 2009. **1**(6): p. 461-468.
526. Logerstedt, D.S., et al., *Knee Pain and Mobility Impairments: Meniscal and Articular Cartilage Lesions Revision 2018: Clinical Practice Guidelines Linked to the International Classification of Functioning, Disability and Health From the Orthopaedic Section of the American Physical Therapy Association.* Journal of Orthopaedic & Sports Physical Therapy, 2018. **48**(2): p. A1-A50.
527. Simon, T.M. and D.W. Jackson, *Articular cartilage: injury pathways and treatment options.* Sports medicine and arthroscopy review, 2018. **26**(1): p. 31-39.
528. Vahdati, A. and D.R. Wagner, *Implant size and mechanical properties influence the failure of the adhesive bond between cartilage implants and native tissue in a finite element analysis.* Journal of biomechanics, 2013. **46**(9): p. 1554-1560.
529. Vaishya, R., *The journey of articular cartilage repair.* Journal of clinical orthopaedics and trauma, 2016. **7**(3): p. 135.
530. Magill, P., et al., *Osteochondral reconstruction and grafting.* Journal of orthopaedic surgery, 2011. **19**(1): p. 93-98.
531. Kon, E., et al., *How to Treat Osteochondritis Dissecans of the Knee: Surgical Techniques and New TrendsAAOS Exhibit Selection.* JBJS, 2012. **94**(1): p. e1.
532. Gobbi, A., et al., *Tissue Engineering for the Cartilage Repair of the Ankle*, in *Sports Injuries of the Foot and Ankle*. 2019, Springer. p. 119-124.
533. Vacanti, J.P. and R. Langer, *Tissue engineering: the design and fabrication of living replacement devices for surgical reconstruction and transplantation.* The lancet, 1999. **354**: p. S32-S34.
534. Hutmacher, D. and S. Cool, *Concepts of scaffold-based tissue engineering—the rationale to use solid free-form fabrication techniques.* Journal of cellular and molecular medicine, 2007. **11**(4): p. 654-669.
535. Reichert, J.C., et al., *Custom-made composite scaffolds for segmental defect repair in long bones.* International orthopaedics, 2011. **35**(8): p. 1229-1236.
536. Cheng, A., et al., *Advances in porous scaffold Design for Bone and Cartilage Tissue Engineering and regeneration.* Tissue Engineering Part B: Reviews, 2019. **25**(1): p. 14-29.
537. Vacanti, C., *Tissue-engineered growth of bone and cartilage.* Transplant Proc, 1993. **25**(1): p. 1019-1021.
538. Vunjak-Novakovic, G., et al., *Bioreactor cultivation conditions modulate the composition and mechanical properties of tissue-engineered cartilage.* Journal of Orthopaedic Research, 1999. **17**(1): p. 130-138.

539. Fahimipour, F., et al., *Enhancing cell seeding and osteogenesis of MSCs on 3D printed scaffolds through injectable BMP2 immobilized ECM-Mimetic gel.* Dental Materials, 2019.
540. Rasoulianboroujeni, M., et al., *Development of 3D-printed PLGA/TiO2 nanocomposite scaffolds for bone tissue engineering applications.* Materials Science and Engineering: C, 2019. **96**: p. 105-113.
541. Liu, C. *Bionics engineering of osteochondral scaffold: grand challenge*. 2016. The 5th International Conference of Bionic Engineering (ICBE).
542. Zhou, X., et al., *3D Printed scaffolds with hierarchical biomimetic structure for osteochondral regeneration.* Nanomedicine: Nanotechnology, Biology and Medicine, 2019. **19**: p. 58-70.
543. Liu, J., et al., *3D printing of biomimetic multi-layered GelMA/nHA scaffold for osteochondral defect repair.* Materials & Design, 2019. **171**: p. 107708.
544. Schaefer, D., et al., *Tissue-engineered composites for the repair of large osteochondral defects.* Arthritis & Rheumatism, 2002. **46**(9): p. 2524-2534.
545. Cui, W., et al., *Repair of articular cartilage defects with tissue-engineered osteochondral composites in pigs.* Journal of bioscience and bioengineering, 2011. **111**(4): p. 493-500.
546. Jeon, J.E., et al., *Perspectives in multiphasic osteochondral tissue engineering.* The Anatomical Record, 2014. **297**(1): p. 26-35.
547. Gao, T.-J., et al., *Morphological and biomechanical difference in healing in segmental tibial defects implanted with Biocoral® or tricalcium phosphate cylinders.* Biomaterials, 1997. **18**(3): p. 219-223.
548. Heinegård, D. and T. Saxne, *The role of the cartilage matrix in osteoarthritis.* Nature Reviews Rheumatology, 2011. **7**(1): p. 50.
549. Chua, C., et al., *Selective laser sintering of functionally graded tissue scaffolds.* MRS bulletin, 2011. **36**(12): p. 1006-1014.
550. Nukavarapu, S.P. and D.L. Dorcemus, *Osteochondral tissue engineering: current strategies and challenges.* Biotechnology advances, 2013. **31**(5): p. 706-721.
551. Keeney, M. and A. Pandit, *The osteochondral junction and its repair via bi-phasic tissue engineering scaffolds.* Tissue Engineering Part B: Reviews, 2009. **15**(1): p. 55-73.
552. Romandini, I., et al., *Cell-Free Scaffolds for the Treatment of Chondral and Osteochondral Lesions*, in *Cartilage Restoration*. 2018, Springer. p. 297-305.
553. Yucekul, A., et al., *Tri-layered composite plug for the repair of osteochondral defects: in vivo study in sheep.* Journal of tissue engineering, 2017. **8**: p. 2041731417697500.
554. Zhu, N. and X. Chen, *Biofabrication of tissue scaffolds*, in *Advances in biomaterials science and biomedical applications*. 2013, IntechOpen.
555. Sefat, F., M. Mozafari, and A. Atala, *Introduction to tissue engineering scaffolds*, in *Handbook of Tissue Engineering Scaffolds: Volume One*. 2019, Elsevier. p. 3-22.
556. Yuan, S., et al., *Immobilization of gelatin onto poly (glycidyl methacrylate)-grafted polycaprolactone substrates for improved cell–material interactions.* Biointerphases, 2012. **7**(1): p. 30.
557. Nyitray, C.E., et al., *Polycaprolactone thin-film micro-and nanoporous cell-encapsulation devices.* ACS nano, 2015. **9**(6): p. 5675-5682.
558. Khoshroo, K., et al., *Development of 3D PCL microsphere/TiO2 nanotube composite scaffolds for bone tissue engineering.* Materials Science and Engineering: C, 2017. **70**: p. 586-598.
559. Tayebi, L., et al., *3D-printed thick structured gelatin membrane for engineering of heterogeneous tissues.* Materials Letters, 2018. **217**: p. 39-43.

560. Yuan, S., et al., *Surface modification of polycaprolactone substrates using collagen-conjugated poly (methacrylic acid) brushes for the regulation of cell proliferation and endothelialisation.* Journal of Materials Chemistry, 2012. **22**(26): p. 13039-13049.
561. Arima, Y. and H. Iwata, *Effect of wettability and surface functional groups on protein adsorption and cell adhesion using well-defined mixed self-assembled monolayers.* Biomaterials, 2007. **28**(20): p. 3074-3082.
562. Dowling, D.P., et al., *Effect of surface wettability and topography on the adhesion of osteosarcoma cells on plasma-modified polystyrene.* Journal of biomaterials applications, 2011. **26**(3): p. 327-347.
563. Sobral, J.M., et al., *Three-dimensional plotted scaffolds with controlled pore size gradients: effect of scaffold geometry on mechanical performance and cell seeding efficiency.* Acta biomaterialia, 2011. **7**(3): p. 1009-1018.
564. Vaquette, C. and J.J. Cooper-White, *Increasing electrospun scaffold pore size with tailored collectors for improved cell penetration.* Acta biomaterialia, 2011. **7**(6): p. 2544-2557.
565. Lee, H. and G. Kim, *Cryogenically fabricated three-dimensional chitosan scaffolds with pore size-controlled structures for biomedical applications.* Carbohydrate polymers, 2011. **85**(4): p. 817-823.
566. Cai, S. and J. Xi, *A control approach for pore size distribution in the bone scaffold based on the hexahedral mesh refinement.* Computer-Aided Design, 2008. **40**(10-11): p. 1040-1050.
567. Jiang, J., S.B. Nicoll, and H.H. Lu, *Co-culture of osteoblasts and chondrocytes modulates cellular differentiation in vitro.* Biochemical and biophysical research communications, 2005. **338**(2): p. 762-770.
568. Pool, R., *Bone and cartilage*. 1978: University of California Press Berkeley.
569. Fung, Y.-C., *Bone and cartilage*, in *Biomechanics*. 1993, Springer. p. 500-544.
570. Curl, W.W., et al., *Cartilage injuries: a review of 31,516 knee arthroscopies.* Arthroscopy: The Journal of Arthroscopic & Related Surgery, 1997. **13**(4): p. 456-460.
571. Widuchowski, W., J. Widuchowski, and T. Trzaska, *Articular cartilage defects: study of 25,124 knee arthroscopies.* The Knee, 2007. **14**(3): p. 177-182.
572. Roos, E.M., *Joint injury causes knee osteoarthritis in young adults.* Current opinion in rheumatology, 2005. **17**(2): p. 195-200.
573. Vaquero-Picado, A. and E.C. Rodríguez-Merchán, *Cartilage Injuries of the Knee*, in *Joint Preservation in the Adult Knee*. 2017, Springer. p. 127-141.
574. Tuan, R.S., *A second-generation autologous chondrocyte implantation approach to the treatment of focal articular cartilage defects.* Arthritis research & therapy, 2007. **9**(5): p. 109.
575. Benthien, J.P., M. Schwaninger, and P. Behrens, *We do not have evidence based methods for the treatment of cartilage defects in the knee.* Knee Surgery, Sports Traumatology, Arthroscopy, 2011. **19**(4): p. 543-552.
576. DeFalco, R.A., A.R. Ricci, and F.C. Balduini, *Osteonecrosis of the Knee after Arthroscopic Meniscectomy and Chondroplasty.* The American journal of sports medicine, 2003. **31**(6): p. 1013-1016.
577. Silva, M., R. Tharani, and T.P. Schmalzried, *Results of direct exchange or debridement of the infected total knee arthroplasty.* Clinical orthopaedics and related research, 2002. **404**: p. 125-131.
578. Dervin, G.F., et al., *Effect of arthroscopic debridement for osteoarthritis of the knee on health-related quality of life.* JBJS, 2003. **85**(1): p. 10-19.
579. Clavé, A., et al., *Third-generation autologous chondrocyte implantation versus mosaicplasty for knee cartilage injury: 2-year randomized trial.* Journal of Orthopaedic Research, 2016. **34**(4): p. 658-665.

580. Kon, E., et al., *Matrix assisted autologous chondrocyte transplantation for cartilage treatment: a systematic review.* Bone & joint research, 2013. **2**(2): p. 18-25.
581. Selmi, T.A.S., et al., *Autologous chondrocyte implantation in a novel alginate-agarose hydrogel: outcome at two years.* The Journal of bone and joint surgery. British volume, 2008. **90**(5): p. 597-604.
582. Hutmacher, D.W., et al., *State of the art and future directions of scaffold-based bone engineering from a biomaterials perspective.* Journal of tissue engineering and regenerative medicine, 2007. **1**(4): p. 245-260.
583. Jazayeri, H.E., et al., *The cross-disciplinary emergence of 3D printed bioceramic scaffolds in Orthopedic bioengineering.* Ceramics International, 2018. **44**(1): p. 1-9.
584. Khojasteh, A., et al., *Development of PLGA-coated β-TCP scaffolds containing VEGF for bone tissue engineering.* Materials Science and Engineering: C, 2016. **69**: p. 780-788.
585. Masaeli, R., et al., *Efficacy of calcium phosphate cement enhanced with 3wt%-nanostrontium-hydroxyapatite, and nanostrontium-CPC-incorporated simvastatin-loaded poly (lactic-co-glycolic-acid) microspheres in bone formation: an explorative multi-phase experimental in-vitro/in-vivo study.* Mater. Sci. Eng. C, 2016.
586. Heidari, F., et al., *Mechanical properties of natural chitosan/hydroxyapatite/magnetite nanocomposites for tissue engineering applications.* Materials Science and Engineering: C, 2016. **65**: p. 338-344.
587. Heidari, F., et al., *Evaluation of the mechanical properties, in vitro biodegradability and cytocompatibility of natural chitosan/hydroxyapatite/nano-Fe3O4 composite.* Ceramics International, 2018. **44**(1): p. 275-281.
588. Tas, A.C., et al., *An investigation of the chemical synthesis and high-temperature sintering behaviour of calcium hydroxyapatite (HA) and tricalcium phosphate (TCP) bioceramics.* Journal of Materials Science: Materials in Medicine, 1997. **8**(2): p. 91-96.
589. Klein, C.P., et al., *Studies of the solubility of different calcium phosphate ceramic particles in vitro.* Biomaterials, 1990. **11**(7): p. 509-512.
590. Klein, C., A. Driessen, and K. De Groot, *Relationship between the degradation behaviour of calcium phosphate ceramics and their physical-chemical characteristics and ultrastructural geometry.* Biomaterials, 1984. **5**(3): p. 157-160.
591. Jarcho, M., *Calcium phosphate ceramics as hard tissue prosthetics.* Clinical Orthopaedics and Related Research®, 1981. **157**: p. 259-278.
592. Zhou, H. and J. Lee, *Nanoscale hydroxyapatite particles for bone tissue engineering.* Acta biomaterialia, 2011. **7**(7): p. 2769-2781.
593. Kwon, S.-H., et al., *Synthesis and dissolution behavior of β-TCP and HA/β-TCP composite powders.* Journal of the European Ceramic Society, 2003. **23**(7): p. 1039-1045.
594. Harada, Y., *Experimental studies of healing process on compound blocks of hydroxyapatite (HAP) particles and tricalcium phosphate (TCP) powder implantation in rabbit mandible--comparison of HAP/TCP ratios and plastic methods.* Shika gakuho. Dental science reports, 1989. **89**(2): p. 263-297.
595. Ryu, H.-S., et al., *An improvement in sintering property of β-tricalcium phosphate by addition of calcium pyrophosphate.* Biomaterials, 2002. **23**(3): p. 909-914.
596. Ramay, H.R. and M. Zhang, *Biphasic calcium phosphate nanocomposite porous scaffolds for load-bearing bone tissue engineering.* Biomaterials, 2004. **25**(21): p. 5171-5180.
597. Wang, J., et al., *Biological evaluation of biphasic calcium phosphate ceramic vertebral laminae.* Biomaterials, 1998. **19**(15): p. 1387-1392.
598. Bouler, J.-M., et al., *Biphasic calcium phosphate ceramics for bone reconstruction: A review of biological response.* Acta biomaterialia, 2017. **53**: p. 1-12.

599. Miron, R.J., et al., *Osteoinductive potential of a novel biphasic calcium phosphate bone graft in comparison with autographs, xenografts, and DFDBA.* Clinical oral implants research, 2016. **27**(6): p. 668-675.
600. Brunski, J.B., *Mechanical properties of trabecular bone in the human mandible: implications for dental implant treatment planning and surgical placement.* Journal of Oral and Maxillofacial Surgery, 1999. **57**(6): p. 706-708.
601. Salamon, A., et al., *Gelatin-based hydrogels promote chondrogenic differentiation of human adipose tissue-derived mesenchymal stem cells in vitro.* Materials, 2014. **7**(2): p. 1342-1359.
602. Focaroli, S., et al., *Influence of a biomimetic gelatin porous scaffold in chondrogenic and osteogenic differentiation of mesenchymal stem cells.* Italian Journal of Anatomy and Embryology, 2014. **119**(1): p. 89.
603. Pruksakorn, D., et al., *Chondrogenic properties of primary human chondrocytes culture in hyaluronic acid treated gelatin scaffold.* Medical journal of the Medical Association of Thailand, 2009. **92**(4): p. 483.
604. Chow, G., et al., *Increased expression of CD44 in bovine articular chondrocytes by catabolic cellular mediators.* Journal of Biological Chemistry, 1995. **270**(46): p. 27734-27741.
605. Knudson, W., et al., *Hyaluronan oligosaccharides perturb cartilage matrix homeostasis and induce chondrocytic chondrolysis.* Arthritis & Rheumatism, 2000. **43**(5): p. 1165-1174.
606. Aibe, K., J. Ryu, and S. Sano, *Effects of hyaluronic acid on cartilage metabolism in free chondrocytes.* Journal of Orthopaedic Science, 1996. **1**(4): p. 268-276.
607. Betre, H., et al., *Chondrocytic differentiation of human adipose-derived adult stem cells in elastin-like polypeptide.* Biomaterials, 2006. **27**(1): p. 91-99.
608. Awad, H.A., et al., *Chondrogenic differentiation of adipose-derived adult stem cells in agarose, alginate, and gelatin scaffolds.* Biomaterials, 2004. **25**(16): p. 3211-3222.
609. Jakob, M., et al., *Specific growth factors during the expansion and redifferentiation of adult human articular chondrocytes enhance chondrogenesis and cartilaginous tissue formation in vitro.* Journal of cellular biochemistry, 2001. **81**(2): p. 368-377.
610. Jakob, M., et al., *Chondrogenesis of expanded adult human articular chondrocytes is enhanced by specific prostaglandins.* Rheumatology, 2004. **43**(7): p. 852-857.
611. Kim, E.J., et al., *Preparation of biodegradable PLA/PLGA membranes with PGA mesh and their application for periodontal guided tissue regeneration.* Biomedical Materials, 2009. **4**(5): p. 055001.
612. Cho, W., et al. *PCL Electrospun Sheet-Embedded Microporous PLGA Membrane For Effective Guided Bone Regeneration*. in *3rd Kuala Lumpur International Conference on Biomedical Engineering 2006*. 2007. Springer.
613. Timkovich, R., *Detection of the stable addition of carbodiimide to proteins.* Analytical biochemistry, 1977. **79**(1-2): p. 135-143.
614. Kuijpers, A., et al., *Characterization of the network structure of carbodiimide cross-linked gelatin gels.* Macromolecules, 1999. **32**(10): p. 3325-3333.
615. Kaemmerer, E., et al., *Gelatine methacrylamide-based hydrogels: an alternative three-dimensional cancer cell culture system.* Acta biomaterialia, 2014. **10**(6): p. 2551-2562.
616. Chen, Y.C., et al., *Functional human vascular network generated in photocrosslinkable gelatin methacrylate hydrogels.* Advanced functional materials, 2012. **22**(10): p. 2027-2039.
617. Yue, K., et al., *Synthesis, properties, and biomedical applications of gelatin methacryloyl (GelMA) hydrogels.* Biomaterials, 2015. **73**: p. 254-271.
618. Nichol, J.W., et al., *Cell-laden microengineered gelatin methacrylate hydrogels.* Biomaterials, 2010. **31**(21): p. 5536-5544.

619. Jung, J. and J. Oh, *Swelling characterization of photo-cross-linked gelatin methacrylate spherical microgels for bioencapsulation.* e-Polymers, 2014. **14**(3): p. 161-168.
620. Zhao, X., et al., *Photocrosslinkable gelatin hydrogel for epidermal tissue engineering.* Advanced healthcare materials, 2016. **5**(1): p. 108-118.
621. Kolesky, D.B., et al., *3D bioprinting of vascularized, heterogeneous cell-laden tissue constructs.* Advanced materials, 2014. **26**(19): p. 3124-3130.
622. Garg, T., et al., *Scaffold: a novel carrier for cell and drug delivery.* Critical Reviews™ in Therapeutic Drug Carrier Systems, 2012. **29**(1).
623. Cushnie, E.K., Y.M. Khan, and C.T. Laurencin, *Tissue-engineered matrices as functional delivery systems: Adsorption and release of bioactive proteins from degradable composite scaffolds.* Journal of Biomedical Materials Research Part A, 2010. **94**(2): p. 568-575.
624. Zhang, Y. and M. Zhang, *Calcium phosphate/chitosan composite scaffolds for controlled in vitro antibiotic drug release.* Journal of Biomedical Materials Research: An Official Journal of The Society for Biomaterials, The Japanese Society for Biomaterials, and The Australian Society for Biomaterials and the Korean Society for Biomaterials, 2002. **62**(3): p. 378-386.
625. Fahimipour, F., et al., *Enhancing cell seeding and osteogenesis of MSCs on 3D printed scaffolds through injectable BMP2 immobilized ECM-Mimetic gel.* Dental Materials, 2019. **35**(7): p. 990-1006.
626. Miyazaki, D., et al., *Therapeutic effects of tacrolimus ointment for refractory ocular surface inflammatory diseases.* Ophthalmology, 2008. **115**(6): p. 988-992. e5.
627. Novosel, E.C., C. Kleinhans, and P.J. Kluger, *Vascularization is the key challenge in tissue engineering.* Advanced drug delivery reviews, 2011. **63**(4-5): p. 300-311.
628. Prasad, L.K. and H. Smyth, *3D Printing technologies for drug delivery: a review.* Drug development and industrial pharmacy, 2016. **42**(7): p. 1019-1031.
629. Allen, T.M. and P.R. Cullis, *Drug delivery systems: entering the mainstream.* Science, 2004. **303**(5665): p. 1818-1822.
630. Lipworth, B., *New perspectives on inhaled drug delivery and systemic bioactivity.* Thorax, 1995. **50**(2): p. 105.
631. Goole, J. and K. Amighi, *3D printing in pharmaceutics: A new tool for designing customized drug delivery systems.* International journal of pharmaceutics, 2016. **499**(1-2): p. 376-394.
632. Teh, B.M., et al., *Tissue engineering of the tympanic membrane.* Tissue Engineering Part B: Reviews, 2012. **19**(2): p. 116-132.
633. Shen, Y., et al., *Scaffolds for tympanic membrane regeneration in rats.* Tissue Engineering Part A, 2012. **19**(5-6): p. 657-668.
634. Moharamzadeh, K., *Oral mucosa tissue engineering*, in *Biomaterials for Oral and Dental Tissue Engineering*. 2017, Elsevier. p. 223-244.
635. Moreau, J.L., et al., *Tissue engineering solutions for cleft palates.* Journal of Oral and Maxillofacial Surgery, 2007. **65**(12): p. 2503-2511.
636. Malikmammadov, E., et al., *PCL and PCL-based materials in biomedical applications.* Journal of Biomaterials science, Polymer edition, 2018. **29**(7-9): p. 863-893.
637. Zhu, Y., Z. Mao, and C. Gao, *Aminolysis-based surface modification of polyesters for biomedical applications.* RSC advances, 2013. **3**(8): p. 2509-2519.
638. Zeiger, E., B. Gollapudi, and P. Spencer, *Genetic toxicity and carcinogenicity studies of glutaraldehyde—a review.* Mutation Research/Reviews in Mutation Research, 2005. **589**(2): p. 136-151.
639. Bohning, B.P., W.D. Davenport, and B.G. Jeansonne, *The effect of guided tissue regeneration on the healing of osseous defects in rat calvaria.* Journal of endodontics, 1999. **25**(2): p. 81-84.

640. Aaboe, M., et al., *Guided tissue regeneration using degradable and nondegradable membranes in rabbit tibia.* Clinical Oral Implants Research, 1993. **4**(4): p. 172-176.
641. Owens, K.W. and R.A. Yukna, *Collagen membrane resorption in dogs: a comparative study.* Implant dentistry, 2001. **10**(1): p. 49-58.
642. Kandel, R., et al., *Repair of osteochondral defects with biphasic cartilage-calcium polyphosphate constructs in a sheep model.* Biomaterials, 2006. **27**(22): p. 4120-4131.
643. Schagemann, J.C., et al., *Cell-laden and cell-free biopolymer hydrogel for the treatment of osteochondral defects in a sheep model.* Tissue Engineering Part A, 2008. **15**(1): p. 75-82.
644. Le, Q.H., et al., *An in vivo confocal microscopy and impression cytology analysis of goblet cells in patients with chemical burns.* Invest Ophthalmol Vis Sci, 2010. **51**(3): p. 1397-400.
645. Nelson, J. and J.C. Wright, *COnjunctival goblet cell densities in ocular surface disease.* Archives of Ophthalmology, 1984. **102**(7): p. 1049-1051.
646. Diegelmann, R.F. and M.C. Evans, *Wound healing: an overview of acute, fibrotic and delayed healing.* Front Biosci, 2004. **9**: p. 283-9.
647. Syam, P.P., H. Eleftheriadis, and C.S. Liu, *Inferior conjunctival autograft for primary pterygia.* Ophthalmology, 2003. **110**(4): p. 806-10.
648. Prabhasawat P, T.S., *Impression cytology study of epithelial phenotype of ocular surface reconstructed by preserved human amniotic membrane.* Arch Ophthalmol 1997: p. 115:1360–7.
649. Ambrosio, L., et al., *Rheological study on hyaluronic acid and its derivative solutions.* Journal of Macromolecular Science—Pure and Applied Chemistry, 1999. **36**(7-8): p. 991-1000.
650. Terbojevich, M., et al., *Structural properties of hyaluronic acid in moderately concentrated solutions.* Carbohydrate research, 1986. **149**(2): p. 363-377.
651. Joly-Duhamel, C., et al., *All gelatin networks: 2. The master curve for elasticity.* Langmuir, 2002. **18**(19): p. 7158-7166.
652. Kuijpers, A.J., et al., *Cross-linking and characterisation of gelatin matrices for biomedical applications.* Journal of Biomaterials Science, Polymer Edition, 2000. **11**(3): p. 225-243.
653. Tokita, M., *Transport Phenomena in Gel.* Gels, 2016. **2**(2): p. 17.
654. Kheirkhah, A., et al., *Postoperative conjunctival inflammation after pterygium surgery with amniotic membrane transplantation versus conjunctival autograft.* Am J Ophthalmol, 2011. **152**(5): p. 733-8.
655. Ronkko, S., et al., *Histopathology of the three implanted degradable biopolymers in rabbit eye.* J Biomed Mater Res A, 2009. **88**(3): p. 717-24.
656. Gibson-Corley, K.N., A.K. Olivier, and D.K. Meyerholz, *Principles for valid histopathologic scoring in research.* Vet Pathol, 2013. **50**(6): p. 1007-15.
657. Cook, N., et al., *Chronic tarsal conjunctivitis.* BMC Ophthalmol, 2016. **16**: p. 130.
658. Slack, J.M., *Metaplasia and transdifferentiation: from pure biology to the clinic.* Nat Rev Mol Cell Biol, 2007. **8**(5): p. 369-78.
659. Mimura, T., et al., *Tissue engineering of corneal stroma with rabbit fibroblast precursors and gelatin hydrogels.* Mol Vis, 2008. **14**: p. 1819-28.
660. Rose, J., et al., *Gelatin-Based Materials in Ocular Tissue Engineering.* Materials, 2014. **7**(4): p. 3106.
661. Hori, J., et al., *Immunological Characteristics of Amniotic Epithelium.* Cornea, 2006. **25**: p. S53-S58.
662. Mimura, T., et al., *Cultured Human Corneal Endothelial Cell Transplantation with a Collagen Sheet in a Rabbit Model.* Investigative Ophthalmology & Visual Science, 2004. **45**(9): p. 2992-2997.

663. Avila, M., et al., *Reconstruction of Ocular Surface With Heterologous Limbal Epithelium and Amniotic Membrane in a Rabbit Model.* Cornea, 2001. **20**(4): p. 414-420.
664. Enzmann, V., et al., *Immunological problems of transplantation into the subretinal space.* Acta Anat (Basel), 1998. **162**(2-3): p. 178-83.
665. Fahimipour, F., et al., *Collagenous matrix supported by a 3D-printed scaffold for osteogenic differentiation of dental pulp cells.* Dental Materials, 2018. **34**(2): p. 209-220.
666. Wang, H., et al., *Ca/P ratio effects on the degradation of hydroxyapatite in vitro.* Journal of Biomedical Materials Research Part A: An Official Journal of The Society for Biomaterials, The Japanese Society for Biomaterials, and The Australian Society for Biomaterials and the Korean Society for Biomaterials, 2003. **67**(2): p. 599-608.
667. Wang, H., *Hydroxyapatite degradation and biocompatibility*. 2004, The Ohio State University.